MECHANICS OF PRESTRESSED AND INHOMOGENEOUS BODIES

A Dissertation

by

SARAVANAN UMAKANTHAN

Submitted to the Office of Graduate Studies of
Texas A&M University
in partial fulfillment of the requirements for the degree of

DOCTOR OF PHILOSOPHY

August 2005

Major Subject: Mechanical Engineering

MECHANICS OF PRESTRESSED AND INHOMOGENEOUS BODIES

A Dissertation

by

SARAVANAN UMAKANTHAN

Submitted to the Office of Graduate Studies of
Texas A&M University
in partial fulfillment of the requirements for the degree of

DOCTOR OF PHILOSOPHY

Approved by:

Co-Chairs of Committee,	K. R. Rajagopal
	Jay D Humphrey
Committee Members,	John C Criscione
	Jay R Walton
	Joseph E Pasciak
Head of Department,	Dennis O'Neal

August 2005

Major Subject: Mechanical Engineering

ABSTRACT

Mechanics of Prestressed and Inhomogeneous Bodies. (August 2005)

Saravanan Umakanthan, B.Tech, Indian Institute of Technology-Madras;

M.S., Texas A&M University

Co–Chairs of Advisory Committee: Dr. K. R. Rajagopal
Dr. J. D. Humphrey

In finite elasticity, while developing representation for stress, it is customary to require the reference configuration to be stress free. This study relaxes this requirement and develops representations for stress from a stressed reference configuration. Using the fact that the value of Cauchy stress in the current configuration is independent of the choice of the reference configuration, even though the formula used to compute it depends on the choice of the reference configuration, the sought representation is obtained. It is then assumed that there exists a piecewise smooth mapping between a configuration with prestresses and a configuration that is stress free, and the representation obtained above is used to study the mechanical response of prestressed bodies. The prestress fields are obtained by directly integrating the balance of linear momentum along with the traction free boundary condition. Then, different classes of boundary value problems for the type of inhomogeneous and prestressed bodies of interest are formulated and studied. For the cases studied, it is found that even the global measures like axial-load required to engender a given stretch ratio for a prestressed body vary from the homogeneous stress free bodies, though not significantly. The local measures - stress and deformation - in a prestressed body differ considerably from their homogeneous stress free counterparts. The above gained knowledge is applied to understand the mechanics of circumflex arteries obtained from normotensive

and hypertensive micro-mini pigs. It is found that the deformation of these arteries when subjected to inflation and axial extension is not of the form $r = r(R)$, $\theta = \Theta$, $z = \lambda Z$. Comparison is also made between the response of an artery at various levels of smooth muscle activation and stretch ratio, λ, as well as normotensive and hypertensive specimens, using statistical methods.

To my Grandparents

ACKNOWLEDGMENTS

I take this opportunity to thank Prof. Rajagopal for going out of his way to help me during some trying times during the course of this work. I am indebted to Prof. Humphrey for his support and permission to use the facilities in his lab to conduct some experiments. I also record my appreciation for some of the discussions I had with Jin-Jia Hu, which helped to make a better presentation of the experimental results. Also, I am thankful to Dr. Baek for conducting some of the experiments and sharing the data with me.

I am also grateful to my parents and sister for standing by me and providing support and encouragement for the successful completion of this work.

TABLE OF CONTENTS

CHAPTER Page

CHAPTER Page

LIST OF TABLES

LIST OF FIGURES

FIGURE Page

FIGURE Page

FIGURE Page

FIGURE Page

FIGURE Page

FIGURE Page

FIGURE Page

FIGURE Page

FIGURE Page

FIGURE Page

CHAPTER I

INTRODUCTION

Let us begin by defining what we mean by a body being inhomogeneous. Merriam Webster dictionary defines inhomogeneous as "the condition of not being homogeneous" and as "a part that is not homogeneous with the larger uniform mass in which it occurs". It also defines homogeneous as being "of the same or a similar kind or nature" and as possessing "uniform structure or composition throughout". Thus, if the abstract body is considered to be made up of material points and if these material points are not of the same kind or nature then the abstract body is said to be inhomogeneous. We call a body that is inhomogeneous to be an inhomogeneous body and a homogeneous body, otherwise. Now, we have to define what we mean by the material points being of the same kind or nature. Towards this, the one to one onto mapping of these material points that constitute the abstract body, $\mathcal{B}$, to the points in the Euclidean space, $\mathcal{E}$, is called a placer. Two material points - P_1, $P_2 \in \mathcal{B}$ - are said to be materially uniform, if there exist two placers, κ_1 and κ_2 such that there exist neighborhoods $N_{\mathbf{X}_1}$ of $\mathbf{X}_1 = \kappa_1(P_1)$ and $N_{\mathbf{X}_2}$ of $\mathbf{X}_2 = \kappa_2(P_2)$ which are indistinguishable with respect to their thermomechanical response, when attention is restricted to thermomechanical processes; since here we do not consider the body's electro-magnetic or other responses. If the two material points are materially uniform with respect to the same placer then they are considered to be of the same type or kind. Alternatively, material points are not of the same kind if there exist no common placer in which they are in the same state and from which they have same constitutive relations.

The journal model is *Mathematics and Mechanics of Solids*.

Next, let us define what we mean by a prestressed body. The Merriam Webster dictionary defines prestress as, "the stresses introduced in prestressing", "the process of prestressing", "the condition of being prestressed" when it is used as a noun and as "to introduce internal stresses into a body to counteract the stresses that will result from applied load" when it is used as a transitive verb. Thus, from the above we garner that prestressed body is a body with internal stresses to counteract the stresses that will result from applied load. However, in this study, we call a body with internal stresses a prestressed body; the prestress can counteract or synergize with the applied load. Internal stresses are stresses within the body that is free of traction on the boundary. Here internal is used in the sense of something existing only inside the surface or boundary. It is pertinent to point out that, in many cases and in this study as well, one has to neglect the gravity and atmospheric pressure for the body to be free of traction on the boundary. Since, a body is subjected to some manufacturing process, at the end of which on the removal of the traction on the boundary, the body develops internal stresses, it is also called residual stress. Here residual refers to the state after the manufacturing process and is used to emphasize that the internal stresses are an internal aftereffect that influences later behavior. While this study recognizes the presence of internal stresses, it does not concern how they were introduced nor does allow the internal stresses to evolve during the processes studied here. Hence, it is appropriate to use the term prestresses instead of residual stress. It is pertinent to point out that in biological bodies, studied here in some detail, the chemical process that causes the development of internal stresses is not known, at this point in time.

Now, let us consider a couple of examples of prestressed and inhomogeneous bodies. Consider two homogeneous bodies, an annular right circular cylinder and a solid right circular cylinder, made of the same material, such that the inner radius of the

annular cylinder is slightly smaller than the solid cylinder at the room temperature. Then, let us cool the solid cylinder so that it just fits into the annular cylinder. This compound body is called a shrink fit shaft. Now, when the shrink fit shaft returns to the room temperature, the solid cylinder is in a state of radial compression and the annular cylinder is in a state of radial tension. Thus, the compound body develops internal stresses and is therefore a prestressed body. Also, while shrink fit shaft is materially uniform, it is inhomogeneous since there exist no placer for the compound body, in Euclidean space in which all the material points are in the same state. The next example is an everted cylindrical shell. This is a section of an annular right circular homogeneous cylinder, turned inside out. Theoretical calculations [1] and experimental observations [2] show that the everted homogeneous cylindrical shell is prestressed. Thus, certain prestressed bodies are homogeneous and others inhomogeneous.

A. Origin of prestresses

Most prestresses are believed to arise from misfits between different regions of the body[1]. In components that are engineered, misfits can arise, at least, in four different ways. One, through the interaction between misfitting parts within the assembly, as in shrink fit shaft, prestressed concrete. Two, by chemical process such as nitriding where nitrates form on the surface of the steel along with an associated volume increase, resulting in the development of compressive stresses on the surface and tensile stresses in the interior. The process of depositing thin films and coatings also results in the development of prestresses. While chemical vapor deposition gives rise to compressive or tensile coating stresses depending on the conditions, plasma deposition

[1]This section is adapted from Withers and Bhadeshia [3]

always gives rise to tensile deposit stresses. Thus, the third way of introducing misfits is through thermal processes. For example, rapid cooling of glass introduces compressive stresses near the surface and tensile stresses in the interior and such a glass is called thermally toughened glass. Welding results in large thermal stress gradients in the vicinity of welded joints due to localized heating and subsequent cooling of the weld zone. The fourth way of introducing misfits is through plastic deformations. Bending of the bar beyond the elastic limit, introduces internal stresses which vary over the thickness of the bar. Industrial examples include autofrettaging of cylinders and gun barrels, forging, extruding, drawing, shot-peening, over speeding of rotating discs, prestressing of springs and overloading to reduce weld stresses in pressure vessels. Finally, changes in crystal structure of a body undergoing a phase change gives raise to transformation strains that contribute to the development of prestresses.

Furthermore, in natural or artificial multiphase materials, prestresses arise due to differences in the material properties like thermal expansivity or Young's modulus. For example, internal stresses arise during the fabrication of the composites because the composite use temperature is rarely the fabrication temperature and the different constituents seldom have the same coefficient of thermal expansion. Biological bodies, a natural multiphase material, are also known to be prestressed ([4],[5]). In this case, incompatible growth is considered to be responsible for the development of the internal stresses ([6],[7]).

Prestresses also arise when a body is held in equilibrium under the mutual gravitation of its parts [8]. The rationale for neglecting them, on numerous occasions, while studying the mechanical response of traditional engineering bodies is the assumption that the magnitude of these stresses is negligible. However, earth is an example of a body which must be considered as being prestressed, as the internal stresses that arise due to mutual gravitation of its parts are not negligible [8].

B. Uses and problems of prestresses

Above we have briefly reviewed the processes which result in the development of the prestresses. While compressive prestresses are beneficial tensile prestresses pose problems. However, since prestresses are self equilibrating, when body forces and atmospheric pressure are neglected, both compressive and tensile prestresses would be present in the same body. This necessitates intelligent use of the prestresses. Prestressed concrete and thermally toughened glass are examples where the compressive prestresses are used beneficially. In the thermally toughened glass, the compressive stresses near the surface causes the surface flaws to experience in-plane compression delaying their propagation. However, when the flaws reach the interior, which initially is relatively free of flaws, they propagate rapidly and catastrophically to give the characteristic shattered 'mosaic' pattern [9]. Since, free surfaces are often a preferred site for the initiation of a fatigue crack, compressive stresses near the surface increases the fatigue life [9]. Thus, processes like peening, autofrettage, cold hole expansion, case hardening increases fatigue life. On the other hand, the prestresses that develop during the fabrication of composites can cause cracks to develop in the material even before it enters the service and hence a reduction in the fatigue life [10]. In any case, the largest gain in fatigue life, due to the presence of prestresses, are experienced in low amplitude high cycle fatigue, the least in large strain controlled low cycle fatigue [9]. According to Krawietz et. al. [11], in thin film technology prestresses are a key tool to adjust the functionality of the devices. For example, band bending by prestresses is used to tailor the excitation spectrum of semiconductor dots or stripes in optoelectronic materials. On the other hand, prestresses are also known to cause delamination and cracking which degrade the stability of microelectronic devices [12]. In biological bodies, like blood vessels the prestresses are believed to reduce the stress

gradient [5].

As the design of engineering components becomes less conservative there is increasing interest in how prestresses affects the mechanical response [3]. This is because in many cases where unexpected failure occurred, this was due to the presence of prestresses which have combined with the service stresses to considerably shorten the component life [9]. Since, in practice it is not likely that any manufactured component would be entirely free from prestresses introduced during processing [3], considerable effort is currently being devoted to the development of a basic framework within which prestresses can be incorporated into the design of components [9]. Moreover, prestresses are conjectured ([6],[7],[13]) to play a key role in the growth and remodelling of biological bodies. These technological relevance has motivated the present study.

C. Measurement of prestresses

Before looking at the frameworks available to model prestressed bodies and their drawbacks, we would like to explore, how we know that prestresses exist in a given configuration which is free of traction on the boundary? Given that stresses are not directly amenable to experimental measurement, the above is a relevant question.

The tendency of the light to propagate with different speeds along different directions in a transparent birefringent body subjected to mechanical stress is called photoelastic effect. This gives rise to interference fringe patterns when a birefringent body is viewed in monochromatic light between crossed polars. The interaction of stresses with electromagnetic fields has been investigated to some extent, see for example Smith and Rivlin [14], Boulanger and Hayes [15], Ieşan [16]. Thus, this provides an unequivocal evidence to the presence of prestresses albeit in birefringent

bodies.

The speed of propagation of ultrasonic waves is found to depend on the stresses along its direction of propagation. Thus, we infer the prestresses by observing the changes in the speed of propagation of ultrasonic waves (see [17] for details). This too provides an unequivocal evidence of the presence of prestresses.

One of the popular ways of inferring prestresses is by observing the changes in the spacing of the crystallographic planes between a stress free body and a prestressed body, as inferred from diffraction experiments. Briefly, here the surface of the body is irradiated with a monochromatic beam of X-rays which is constructively scattered when it meets lattice planes spaced and oriented to fulfill Bragg's law, resulting in diffraction peaks. By observing, the shift in these diffraction peaks we infer the changes in the lattice spacing and hence the strain and the stress. For more details on this procedure refer to Lu [17]. Here one could use electron beams or neutron beams instead of the X-rays to infer the changes in the lattice spacing and hence the prestresses. However, using this method only prestresses close to the surface can be determined and one requires a good estimate of the spacing of the crystallographic planes in a stress free body, which is difficult to obtain.

Other techniques like magnetic methods (see [17],[9]), piezospectroscopic effects [9] are also used to infer the prestresses. In the techniques considered so far the internal stresses are deduced by nondestructive testing procedures. These stresses are also obtained from destructive testing procedures like hole drilling and ring core methods, layer removal method, sectioning methods. In these methods additional traction free surfaces are introduced and the subsequent deformation of the body measured, from which the prestresses in the intact body is computed (see [17] for details). However, it should be emphasized that introduction of additional traction free surfaces is a dissipative process, which itself will alter the prestress fields.

Let us consider sectioning methods used popularly in the study of the mechanics of blood vessels in some detail. Here a radial cut is introduced in a segment of the blood vessel that is free of boundary traction and the "opening angle" used as a single measure of the resulting deformation (see Chuong and Fung [18]). In most cases, a single radial cut is assumed to relieve the internal stresses and the resulting configuration is considered to be stress free. However, Vossoughi et. al. [19] showed that if one cuts the arterial ring into outer and inner rings, the opening angle associated with each radially cut part will be different, suggesting that one radial cut may not be sufficient to relieve all the internal stresses. Greenwald et al. [20] confirmed the above observation. As rightly pointed out by Humphrey [5], since prestresses are self equilibrating, removing portions of a body requires the prestresses in the remaining body to change and hence the differences in the opening angle. Therefore, as suggested by Humphrey [5], prestresses ought to be considered within the context of a boundary value problem rather than basing them on empirical observations from destructive testing techniques. This study aims to develop a framework in which the prestresses could be considered within the context of a boundary value problem.

D. Modelling of prestressed bodies

Given the technological relevance and the wide variety of scenarios in which prestresses arise significant effort has been devoted to model them. In fact, according to Love [8], the first model that accounts for prestresses was developed by Cauchy. Even though his derivation was not based on the hypothesis of continuum, it was for infinitesimal strain superposed on finite deformation. Numerous alternative derivations of the same equations within the framework of continuum mechanics are available (see for example Green et. al. [21], Truesdell and Noll [22], Biot [23], Ieşan [16]). However,

here our aim is to obtain general constitutive representations for finite deformation from a stressed reference configuration. This problem has been studied by Johnson and Hoger [24] and Hoger [25]. To obtain the sought representation, they seek to invert the constitutive relation between the stress and left Cauchy Green stretch tensor, from a stress free reference configuration. Apart from the inherent difficulties in inverting a non-linear relation, inversion would not be possible, in general, when the algebraic multiplicity of the eigen values of the left Cauchy Green stretch tensor is two or three. This is because in those cases the relationship between the stress and left Cauchy Green stretch tensor is not one to one (shown in appendix A). Further, as they point out, they require all the components of the prestresses and material properties to be smooth functions which is not the case for many prestressed bodies like shrink fit shaft. Also, they a priori require the constitutive relation for stress from stress free configuration, which may not be available in some cases of interest. The representation for stress from stressed reference configuration, developed here, does not suffer from the above limitations.

A related issue of developing representations from stressed reference configurations is the symmetry of the body in the stressed reference configuration and its influence on the resulting representations. Wineman et. al. [26] show that the symmetry group of an uniaxially or equibiaxially stretched body that is isotropic in the stress free state, contains unimodular but nonorthogonal elements for the deformed configuration. Thus, uniaxially or equibiaxially stretched body in this stressed configuration is not just transversely isotropic; the symmetry group just contains transversely isotropic group as its subgroup. As they point out, this, suggest an inherent distinction between a body that is transversely isotropic in the stress free state and one that is uniaxially or equibiaxially stretched. Therefore, the representations for the constitutive functions for a transversely isotropic body in the stress free state

would be different from a uniaxially or equibiaxially stretched body that is isotropic in the stress free state. The representations that we obtain here does reflect these differences.

Many practical models for prestressed bodies, within the context of linearized elasticity, appeal to the superposition principle. They simply get an estimate of the prestresses and superpose them on the stresses developed due to the service loads on the body to get the total stress in the body. Estimate of the prestresses is obtained experimentally or by modelling the process that causes the development of the misfits and hence the prestresses (see Dennis et. al. [27] and the references there in). The success of these approaches strongly owe to the fact that the gradient of displacement is small both in the processes that induce prestresses and in the processes studied from the prestressed state. Here we investigate the status of these models by linearizing the representation obtained for finite deformations from a stressed reference configuration. Even though the linearized equation does not capture the change in the material symmetry between a unstressed reference configuration and stressed reference configuration, it is robust, within the limits of its applicability, albeit in some cases for which the value of the shear modulus can change with the magnitude of prestresses in the reference configuration.

E. Mechanics of blood vessels

As an application of the theoretical framework developed to study prestressed body, we try to understand the mechanical response of circumflex artery from micro-mini pigs which is believed to be inhomogeneous and prestressed. With cardiovascular diseases being the leading cause for mortality in the developed countries (American Heart Association) understanding the mechanical response of the vasculature will provide

insight to prevention or mitigation of the disease. The response of arteries to mechanical stress plays a key role in formation, development and rupture of an aneurysm and in modelling the rupture of aorta in automobile accidents [28]. It is believed that mechanical factors may be important in triggering the onset of atherosclerosis [29]. Also, mechanical stress is one of the important factors modulating the prognosis of cardiovascular diseases like hypertension ([4],[30]) and in improving the mechanical properties of engineered vascular constructs [31]. Moreover, several clinical treatments like percutaneous transluminal angioplasty can only be studied in detail if a reliable constitutive model of the arterial wall is available [29]. This study is a step towards obtaining a reliable constitutive model for the blood vessels within the framework of continuum mechanics.

The general characteristics of the response of healthy "passive"[2] arterial segments is known. They exhibit hysteresis under cyclic loading, stress relax under constant extensions, creep under constant loads and are relatively insensitive to strain rate, therefore, their response is viscoelastic [5]. Increased axial extension tend to circumferentially "stiffen" cyclically pressurized vessels while axial force length behavior is less sensitive to changes in constant diameter indicating a complex coupling between the axial and circumferential directions [5]. Further, the axial load required to maintain a constant length during increased inflation (1) increases when the length at which the artery is held constant is greater than the in vivo length (2) decreases when the length at which the artery is held constant is less than the in vivo length (3) remains nearly a constant when the length at which the artery is held constant is near the in vivo value [5]. Moreover, the temperature of the arteries increases un-

[2]The passive state is defined differently by different authors see Humphrey [5] for a discussion on this issue. Here, it is defined as the state of the blood vessel in which it is isolated from natural hormonal and neural stimuli and its smooth muscle cells are relaxed; not necessarily fully relaxed.

der tension and decreases under compression [32] as does rubber and in contrast to metals.

Next, let us consider the response of healthy blood vessels in "active"[3] state. As commented by Humphrey [5], because muscle contraction is length-dependent, physiologically meaningful data are those obtained by pressure[4]-diameter and axial force-length tests on intact cylindrical segments. 1D tests on arterial rings or helical strips, relieves or modifies the prestresses in the arteries there by altering the state of the smooth muscle cells and hence their response. As a result of activation, the diameter of the blood vessel decreases when the radial component of the normal stress at the boundary is held constant along with the length of the vessel. The pressure-outer diameter response shows that the blood vessel in active state requires greater pressure to engender the same outer diameter than in passive state (See Cox ([33],[34], [35]), Zulliger et. al. [36], Fridez et. al. ([37],[38],[39]). It is also known that in vitro the tone of the vascular smooth muscle depends on the concentration of the agonist, temperature and the mechanical state of the blood vessel [5]. Zulliger et. al. [36] show that increasing the axial stretch of the vessel causes the smooth muscle cells to contract even though the cells are oriented circumferentially. Moreover, the "opening angle" increased with the activation of smooth muscle cells when care is taken to control the temperature, in rat aorta and carotid arteries ([40], [41]). Also, Zeller and Skalak [42] report that the "opening angle" of rat saphenous artery increased with relaxation of the smooth muscle cell. These variations in the "opening angle" suggests a change in the prestresses when the smooth muscle tone is altered.

---

[3]The state of the blood vessel in which its smooth muscle cells are in (maximally) contracted state.

[4]Henceforth, by pressure we mean the radial component of the normal stress at the inner surface of the blood vessel.

Having delineated general characteristics of the response of a blood vessel of interest, we next turn our attention to the theoretical framework available for their quantification. Since arteries exhibit a nearly repeatable response to cyclic loading once they have been preconditioned their behavior is regarded as pseudoelastic. In these models, different constitutive relations are used to describe the loading and unloading portions of the plot of the radial component of the normal stress at the inner surface required to engender a given outer diameter versus outer diameter. Popular models are presented in Humphrey [5], they are critically reviewed in [29] and in the review articles [43], [44]. In some cases, the blood vessel is viewed as a biphasic material, a fluid saturated porous medium. This approach is useful to study the transport phenomena across the wall of the blood vessel [43]. Holzapfel et. al [45] has developed a model for blood vessels as viscoelastic solid. However, a major lacuna in these models is their inability to capture the changes in mechanical response of the blood vessels with various levels of smooth muscle cell activation. This issue has been addressed by Rachev and Hayashi [46] and more recently by Zulliger et. al. [47]. However, these models are 1D and hence 3D mathematical models are needed. The present study develops a general framework from which models for blood vessels incorporating prestresses, inhomogeneity and smooth muscle tone can be obtained.

While developing models with the postulates of field theories one is confronted by the question, based on what observations should a given body be modelled as inhomogeneous? This is a pertinent question especially since all bodies are inhomogeneous at some scale. This study outlines a procedure to verify if a given body is inhomogeneous and prestressed by observing its motion due to applied mechanical loads. This procedure also, in many cases, help identify the nature of inhomogeneity i.e., if a given body is radially inhomogeneous or radially and circumferentially inhomogeneous and so on. As an application of this procedure we investigate the motion

of the circumflex artery subjected to inflation at constant length and axial extension at constant pressure. We find that the motion of the circumflex artery is not given by $r = r(R)$, $\theta = \Theta$, $z = \lambda Z$[5] to the applied mechanical loads and hence it could belong to a special class of compressible bodies or be radially and circumferentially inhomogeneous and/or its prestresses vary radially and circumferentially or it could not be idealized as an annular right circular cylinder. In any case, all the existing models, even those that account for the inhomogeneity ([29],[31],[45],[48],[49],[50], [51]) is still inadequate to describe the motion of the circumflex artery. However, at this moment we could not propose constitutive relation that adequately describes the circumflex artery because of the limitation in our experimental setup in inferring a motion different from the above assumed form.

1. Changes in blood vessels due to experimental hypertension

General characteristics of the mechanical response of healthy blood vessels was outlined above. Now, we study the changes in the blood vessels due to experimental hypertension. It seems that the response to the experimental hypertension depends on the animal model [5]. For example, the response to Goldblatt models are characterized by two phases of development while aortic coarctation models have three phases of development despite tapping into the same system, i.e., autoregulation of renin. On the other hand spontaneously hypertensive rats do not have any distinct phases of development. We record the salient changes in the blood vessels as reported in the literature (Olivetti et. al. [52], Owens and Reidy [53], Liu and Fung [54], Fung and Liu [13], Fridez et. al. ([37], [38], [39])) for aortic coarctation model, since this

[5]Here λ is a constant and (R, Θ, Z) are coordinates of a typical material point in the reference configuration in cylindrical polar coordinates and (r, θ, z) coordinates of a typical material point in the current configuration in cylindrical polar coordinates.

is the model we use.

Elevated blood pressure is associated with geometrical, structural and functional changes in the blood vessels [5]. First let us consider the geometrical changes. The internal radius and the thickness of the arteries increases with age of the animal. In response to elevated blood pressure the wall thickness of the arteries increases, over and above that due to increase in age. It is conjectured that the increase in wall thickness is to help restore the wall stresses to their haemostatic values. On the other hand the inner radius of the arteries from hypertensive rats is slightly less than that of the age matched controls. The "opening angle" increases initially and then asymptotically reaches a steady state value. Similarly, the in vivo stretch ratio, defined as the axial length of the artery in vivo to the axial length of the artery at zero axial load increases during the 8 days post induction of hypertension in rats. Data for longer duration of hypertension is unavailable. This suggest an alteration in the prestress fields during the remodelling of arteries due to experimentally introduced hypertension.

Next, let us consider the structural changes in the arteries due to hypertension when it is induced by aortic coarctation. Consistent with the commonly held perception that hypertension is a disease of the media, most changes due to hypertension are found to occur in media. While the thickness of the elastic lamellar units increases, the number of units remains unchanged. The lamellar units thicken due to increases in the amount of collagen, elastin and hypertrophy or/and hyperplasia of the smooth muscle cells. Fridez et. al. [39] observed that the collagen content increases rapidly in the acute phase and then levels down, during which phase the vascular smooth muscle content raises. They also found that the vascular smooth muscle cells initially undergo apoptosis followed by hyperplasia as well as hypertrophy. In the long term, the elastin content increases sightly. They also report that the innermost lamellar

units thicken first followed by outer layers.

Finally, let us consider the mechanical response of hypertensive and normotensive arteries subjected to inflation at constant length. Here one finds reports that the arterial stiffness increases, decreases or remains the same with hypertension. As Humphrey [5] points out, many of the conflicting observations are simply due to the use of different definitions of the stiffness, including material versus structural stiffness. Thus, since the thickness of the arteries changes due to hypertension, the radial component of the normal stresses at the inner surface of the artery required to realize a given outer diameter changes, even if the newly deposited material is of the same type as the old. However, now due to the altered geometry of the artery, the prestress field will be different, a fact corroborated by experiments ([13],[37],[54]). A similar problem arises while comparing the radial component of the normal stress required at the inner surface of the artery to engender a given outer diameter, for various smooth muscle tone, because in this case the inner and outer radius of the blood vessel changes with the vascular smooth muscle tone. This change in the geometry of the blood vessel is a result of a change in the prestress field. Hence, there is a pressing need for the development of a theoretical framework to interpret the mechanical response of these arteries. Here we present such a framework and highlight the difficulties in interpreting the pressure-outer diameter data, for it is insufficient to characterize the mechanical response of the arteries which are inhomogeneous and prestressed.

The arrangement of this thesis is as follows. In the next chapter we introduce the notation to be used and record the standard balance laws and general restrictions on the constitutive relations. A general representation for stress from stress free reference configuration, satisfying the appropriate restrictions, is derived and issues related to the material symmetry are also discussed. In chapter III representations

for stress and Helmoltz potential from a stressed configuration is obtained. Then, we linearize the obtained representation to examine the status of the models developed within the framework of linearized elasticity. The chapter concludes with developing representations for prestress fields in three different geometries of the body. Chapter IV concerns with the general formulation of the boundary value problems and its solution. The techniques developed is illustrated by the studying in detail inflation of a spherical shell and outlining the procedure for many other classes of deformation. In chapter V we study inflation, extension and torsion of right circular cylinder using the same techniques developed in the previous chapter. In the next chapter, we concern ourselves with understanding the mechanics of the circumflex arteries, as an application of the above theoretical developments. The thesis concludes with a summary of the results obtained and directions for future developments.

CHAPTER II

PRELIMINARIES

In this chapter, the notation and terminology that is used in this thesis is introduced. Then, the balance laws as applicable to a thermo-mechanical process is recorded. Next, the restrictions on the constitutive relations due to invariance with respect to the choice of basis vectors and material symmetry is recorded along with the 2^{nd} law of thermodynamics. This is followed by the derivation of a representation for stress from a stress free reference configuration for an isotropic body undergoing elastic deformation. Then, a few constitutive relations for stress, popular in the literature, is recorded for later reference. Finally, we discuss certain issues with determining the material symmetry.

A. Notation

According to Truesdell and Noll [22], a body, $\mathcal{B}$ is a three dimensional differential manifold, the elements of which are called material particles (or material points) P. This manifold may be referred to a system of coordinates which establishes a one-to-one correspondence between particles and triples (A_1, A_2, A_3) of real numbers:

$$P = \hat{P}(A_1, A_2, A_3), \qquad A_i = \hat{A}_i(P), \quad i = 1, 2, 3. \tag{2.1}$$

In general, no particular geometric structure is imputed to a body.

A one-to-one mapping $\hat{\boldsymbol{\chi}} : \mathcal{B} \times \mathcal{I} \to \mathcal{E}$ written as

$$\mathbf{x} = \hat{\boldsymbol{\chi}}(P, t), \tag{2.2}$$

is called a motion of the body[1]. Here $\mathcal{I} \in (-\infty, t_o)$ for some t_o, $\mathcal{E}$ denotes the three dimensional Euclidean space, t is the time and $\mathbf{x}$ is a place in the Euclidean space. The value of $\hat{\boldsymbol{\chi}}$ is the place $\mathbf{x}$ that the particle P occupies at time t. We shall consider only motions that are smooth in the sense that $\hat{\boldsymbol{\chi}}$ is differentiable with respect to P and t as many times as needed.

Often it is convenient to select one particular configuration[2] and refer everything concerning the body to that configuration and call it the reference configuration. Let $\boldsymbol{\kappa}$ be a mapping of the abstract body $\mathcal{B}$ onto three dimensional Euclidean space, called the placement. Then the mapping

$$\mathbf{Y} = \boldsymbol{\kappa}(P), \tag{2.3}$$

gives the place $\mathbf{Y}$ occupied by the particle P in the configuration $\boldsymbol{\chi}(\mathcal{B}, t)$. Since, we assume the mapping to be bijective,

$$P = \boldsymbol{\kappa}^{-1}(\mathbf{Y}). \tag{2.4}$$

Hence the motion (2.2) may be written as

$$\mathbf{x} = \hat{\boldsymbol{\chi}}(\boldsymbol{\kappa}^{-1}(\mathbf{Y}), t) \equiv \hat{\boldsymbol{\chi}}_{\kappa}(\mathbf{Y}, t). \tag{2.5}$$

Thus, the motion is a sequence of mappings of the reference configuration $\boldsymbol{\kappa}(\mathcal{B})$ onto the actual configuration and is visualized as mappings parts of space onto parts of space.

Introduction of the reference configuration just allows us to use the apparatus of

[1]As in the case of elastic response of bodies, when the dependence of $\hat{\boldsymbol{\chi}}$ on time need not be emphasized we call $\hat{\boldsymbol{\chi}}$, deformation field.

[2]A smooth homeomorphism of the body, $\mathcal{B}$ onto a region of three-dimensional Euclidean space is called the configuration of the body.

Euclidean geometry. The choice of reference configuration, like the choice of coordinate system, is arbitrary. In particular, it need not even be a configuration occupied by the body in the course of its motion. For each different choice of reference configuration, there results a different function of $\hat{\boldsymbol{\chi}}_{\kappa}$. Thus one motion of the body is represented by infinitely many different motions of parts of space, one for each choice of $\boldsymbol{\kappa}$. For some choice of $\boldsymbol{\kappa}$, we may get a particularly simple description, just as in geometry one choice of coordinates lead to a simple equation for a particular figure, but the reference configuration itself has nothing to do with such motions as it may be used to describe, just as coordinate system has nothing to do with geometric figures themselves. Reference configurations are introduced just to allow the use of mathematical apparatus familiar in other contexts. Emphasizing again that the choice of reference configuration $\boldsymbol{\kappa}(\mathcal{B})$ is ours, any physically significant result must be independent of the choice of the reference configuration. Note that the above discussion on reference configuration is adapted from Truesdell and Rajagopal [55].

Here we study the motion of the body with respect to two different configurations as reference. The first configuration that we use as reference is a configuration occupied by the body at some time t_o. This configuration need not be stress free[3] or even free of traction on the boundary. However, this is the configuration that is realizable, to say, an experimentalist. Let $\boldsymbol{\kappa}_o$ denote this mapping of the abstract body on to the Euclidean space, i.e.,

$$\mathbf{P} = \boldsymbol{\kappa}_o(P), \tag{2.6}$$

[3]A body in a particular configuration, $\boldsymbol{\kappa}_p$ is said to be stress free if

$$\mathbf{T}(\mathbf{x}) = \mathbf{0}, \qquad \forall \quad \mathbf{x} \in \boldsymbol{\kappa}_p.$$

and traction free if

$$\mathbf{t}_{(\mathbf{n})}(\mathbf{x}) = \mathbf{T}\mathbf{n} = \mathbf{0}, \qquad \forall \quad \mathbf{x} \in \partial\boldsymbol{\kappa}_p,$$

where $\mathbf{n}$ is outward unit normal field on $\partial\kappa_p$ and $\mathbf{T}$ is the Cauchy stress.

Hence, from (2.5)

$$\mathbf{x} = \hat{\boldsymbol{\chi}}(\boldsymbol{\kappa}_o^{-1}(\mathbf{P}), t) \equiv \widetilde{\boldsymbol{\chi}}(\mathbf{P}, t). \tag{2.7}$$

The second configuration that we use as reference is a stress free configuration. This need not be a configuration actually occupied by the body during the process under study. Let $\boldsymbol{\kappa}_{sf}$ denote this mapping of the abstract body on to the Euclidean space, i.e.,

$$\mathbf{X} = \boldsymbol{\kappa}_{sf}(P), \tag{2.8}$$

Hence, from (2.5)

$$\mathbf{x} = \hat{\boldsymbol{\chi}}(\boldsymbol{\kappa}_{sf}^{-1}(\mathbf{X}), t) \equiv \boldsymbol{\chi}(\mathbf{X}, t). \tag{2.9}$$

Then, we define the gradient of motion

$$\mathbf{F}_t = \nabla(\boldsymbol{\chi}) \quad (= \frac{\partial \boldsymbol{\chi}}{\partial \mathbf{X}}), \qquad \mathbf{H}_t = \widetilde{\nabla}(\widetilde{\boldsymbol{\chi}}) \quad (= \frac{\partial \widetilde{\boldsymbol{\chi}}}{\partial \mathbf{P}}). \tag{2.10}$$

The assumption that the body not penetrate itself is expressed by the requirement that $\boldsymbol{\chi}$ (and $\widetilde{\boldsymbol{\chi}}$) be one to one. Further, $det(\mathbf{F}_t) \neq 0$ since it represents the volume after deformation per unit volume in the reference configuration. Consequently, a motion with $det(\mathbf{F}_t) \leq 0$ cannot be reached by a continuous process starting from the reference configuration in which $\mathbf{F}_t$ is identity and hence $det(\mathbf{F}_t) = 1$. Hence, $\mathbf{F}_t \in Lin^+$ i.e., the set of all tensors such that $det(\mathbf{F}_t) > 0$. For the same reasons, $\mathbf{H}_t \in Lin^+$

If the stress free configuration is realizable then

$$\mathbf{P} = \boldsymbol{\chi}(\mathbf{X}, t_o), \qquad \mathbf{X} = \widetilde{\boldsymbol{\chi}}(\mathbf{P}, t_{sf}). \tag{2.11}$$

Here we assume that the motion field $\boldsymbol{\chi}(\mathbf{X}, t_o)$ is smooth and bijective. We note that if the configuration κ_o is prestressed, with prestresses arising from misfit of subparts of the body, the smoothness requirement does not hold for the entire body. They

hold at most to subparts of a given body. Thus, when the reference configuration has prestresses we can not assume the existence of a stress free configuration for the entire body, they exist only for the subparts of the body.

Now,

$$\mathbf{F}_o = \nabla(\boldsymbol{\chi}(\mathbf{X}, t_o)), \qquad \mathbf{H}_{sf} = \widetilde{\nabla}(\widetilde{\boldsymbol{\chi}}(\mathbf{P}, t_{sf})). \tag{2.12}$$

Also, it follows that $\mathbf{F}_o = \mathbf{H}_{sf}^{-1}$ and

$$\mathbf{F}_t = \mathbf{H}_t \mathbf{F}_o. \tag{2.13}$$

Next, we record the expressions for the left and right Cauchy-Green stretch tensors

$$\mathbf{B} = \mathbf{F}_t \mathbf{F}_t^t, \qquad \mathbf{C} = \mathbf{F}_t^t \mathbf{F}_t, \tag{2.14}$$

$$\widetilde{\mathbf{B}} = \mathbf{H}_t \mathbf{H}_t^t, \qquad \widetilde{\mathbf{C}} = \mathbf{H}_t^t \mathbf{H}_t, \tag{2.15}$$

with respect to the stress free reference configuration and stressed reference configuration respectively. While $\mathbf{C}$ carries the information on the change in the length and angles of line segments in the stress free reference configuration, $\widetilde{\mathbf{C}}$ carries the same information for segments in the stressed reference configuration. In addition, we define

$$\mathbf{B}_o = \mathbf{F}_o \mathbf{F}_o^t, \qquad \mathbf{C}_o = \mathbf{F}_o^t \mathbf{F}_o. \tag{2.16}$$

According to the polar decomposition theorem, the gradient of motion can be uniquely decomposed as

$$\mathbf{F}_t = \mathbf{R}\mathbf{U} = \mathbf{V}\mathbf{R}, \qquad \mathbf{H}_t = \widetilde{\mathbf{R}}\widetilde{\mathbf{U}} = \widetilde{\mathbf{V}}\widetilde{\mathbf{R}}, \tag{2.17}$$

where $\mathbf{U}$, $\mathbf{V}$, $\widetilde{\mathbf{U}}$, $\widetilde{\mathbf{V}}$ are positive definite symmetric tensors and $\mathbf{R}$, $\widetilde{\mathbf{R}}$ are rotations. See Gurtin [56] for proof.

Given a second order tensor, say $\mathbf{A}$, the determinant of $(\mathbf{A} - \lambda\mathbf{1})$ admits a representation

$$det(\mathbf{A} - \lambda\mathbf{1}) = -\lambda^3 + I_1\lambda^2 - I_2\lambda + I_3 \tag{2.18}$$

for every $\lambda \in \mathcal{R}$, set of real numbers, where

$$I_1 = tr\mathbf{A}, \qquad I_2 = \frac{1}{2}[(tr\mathbf{A})^2 - tr\mathbf{A}^2], \qquad I_3 = det\mathbf{A}, \tag{2.19}$$

called the principal invariants of $\mathbf{A}$. When $\mathbf{A}$ is positive definite, it is convenient to use the following set of invariants

$$J_1 = \mathbf{1} \cdot \mathbf{A}, \qquad J_2 = \frac{I_2}{I_3} = \mathbf{1} \cdot \mathbf{A}^{-1}, \qquad J_3 = I_3^{1/2}. \tag{2.20}$$

Here (J_1, J_2, J_3), denotes the invariants of $\mathbf{B}$ and $(\widetilde{J}_1, \widetilde{J}_2, \widetilde{J}_3)$ the invariants of $\widetilde{\mathbf{C}}$. It is pertinent to note that the value of invariants of left stretch tensor is same as that of the right stretch tensor.

Finally, it follows from Cayley-Hamilton theorem[4] that every tensor $\mathbf{A}$ satisfies its own characteristic equation, i.e.

$$\mathbf{A}^3 - I_1\mathbf{A}^2 + I_2\mathbf{A} - I_3\mathbf{1} = \mathbf{0}. \tag{2.21}$$

Here it is postulated that the state of the body is determined by

1. density (ρ)
2. stress ($\mathbf{T}$)
3. internal energy per unit mass (ϵ)
4. entropy per unit mass (η)
5. temperature (ϑ)

and that, for our purposes, i.e., thermo-mechanical response, the value of these state variables depend only on the gradient of motion ($\mathbf{H}_t$), temperature (ϑ) and the value of these state variables themselves in the reference configuration. We specify, the

[4]See Halmos [57] section 58 for proof

equation of state which establishes the above relation, after recording the conservation laws.

B. Balance laws

In general, while equation of state is for the specific material that the body is made up of, balance laws hold for all materials. However, the form of the balance laws depends on the process being studied as does the equation of state. For concreteness, in what follows, use shall be made of the stressed reference configuration, understanding the same equations are valid for stress free reference configuration on making the obvious changes.

1. Balance of mass

For our purposes here, this law states that the rate of change of mass is zero. Mathematically, this law can be expressed as

$$\frac{d}{dt}\int_{\kappa_t} \rho dv = 0. \tag{2.22}$$

If the above equation holds for any arbitrary bounded regular[5] subsets of κ_t then[6]

$$\frac{d\rho}{dt} + \rho div(\mathbf{v}) = 0, \tag{2.23}$$

$$\frac{\partial\rho}{\partial t} + div(\rho\mathbf{v}) = 0, \tag{2.24}$$

$$\rho = \frac{\rho_o}{\widetilde{J}_3}, \tag{2.25}$$

[5]See Kellogg [58] for definition of a regular region.

[6]Here, $\frac{d(\cdot)}{dt}$ denotes derivative w.r.t. t holding $\mathbf{P}$ a constant and $\frac{\partial(\cdot)}{\partial t}$ denotes derivative w.r.t. t holding $\mathbf{x}$ a constant. Hence, $\frac{d\rho}{dt} = \frac{\partial\rho}{\partial t} + \mathbf{v}\cdot grad(\rho)$

where ρ_o denotes the density in the reference configuration, $\widetilde{J}_3 = det(\mathbf{H}_t)$, $\mathbf{v} = \frac{d\widetilde{\boldsymbol{\chi}}}{dt}$ and $div(\mathbf{v}) = tr(grad(\mathbf{v}))$[7]. Here we have assumed that there is no diffusion of mass[8] or transformation of mass into energy or vice versa and hence (2.25) is also the equation of state for density.

2. Balance of linear momentum

This law states that the rate of change of momentum is equal to the applied force in both direction and magnitude. Mathematically,

$$\frac{d}{dt}\int_{\kappa_t} \rho \frac{d\widetilde{\boldsymbol{\chi}}}{dt} dv = \int_{\partial\kappa_t} \mathbf{T}\mathbf{n} da + \int_{\kappa_t} \rho \mathbf{b} dv, \tag{2.26}$$

where $\mathbf{b}$ is the body force per unit mass, $\mathbf{n}$ is the outward unit normal field on $\partial\kappa_t$. If the above holds for arbitrary bounded regular subsets of κ_t and using (2.23) and divergence theorem we obtain

$$\rho \frac{d^2\widetilde{\boldsymbol{\chi}}}{dt^2} = div(\mathbf{T}) + \rho \mathbf{b}, \tag{2.27}$$

when $\mathbf{T}$ is a smooth field over κ_t.

Equation (2.26) could equally be expressed as

$$\frac{d}{dt}\int_{\kappa_o} \widetilde{J}_3 \rho \frac{d\widetilde{\boldsymbol{\chi}}}{dt} dV = \int_{\partial\kappa_o} \widetilde{\mathbf{S}}\mathbf{N} dA + \int_{\kappa_o} \widetilde{J}_3 \rho \mathbf{b} dV, \tag{2.28}$$

where $\widetilde{\mathbf{S}} = \widetilde{J}_3 \mathbf{T}\mathbf{H}_t^{-t}$ and $\mathbf{N}$ is the outward unit normal field on $\partial\kappa_o$. Using same

[7]Here, we use $\widetilde{Grad}(\cdot)$ for gradient w.r.t. $\mathbf{P}$, $Grad(\cdot)$ for gradient w.r.t $\mathbf{X}$ and $grad(\cdot)$ for gradient w.r.t. $\mathbf{x}$

[8]It is well known [59] that the above form of the balance of mass does not hold for chemically reacting inhomogeneous bodies. In theories of chemical reaction, the balance of mass holds only for sufficiently large bodies, among the parts of which the mass is generally exchanged i.e. there is diffusion of mass.

arguments as before

$$\widetilde{J}_3\rho\frac{d^2\widetilde{\boldsymbol{\chi}}}{dt^2} = \widetilde{Div}(\widetilde{\mathbf{S}}) + \widetilde{J}_3\rho\mathbf{b}, \tag{2.29}$$

where $\widetilde{Div}(\widetilde{\mathbf{S}})\cdot\mathbf{a} = tr(\widetilde{Grad}(\widetilde{\mathbf{S}}^t\mathbf{a}))$, for every vector $\mathbf{a}$.

3. Balance of energy

This law asserts that energy can neither be created nor destroyed but transformed from one form to another. Mathematically this translates as

$$\begin{aligned}\frac{d}{dt}\int_{\kappa_t}\frac{\rho}{2}\frac{d\boldsymbol{\chi}}{dt}\cdot\frac{d\boldsymbol{\chi}}{dt}dv \;&+\; \frac{d}{dt}\int_{\kappa_t}\rho\epsilon dv \\ &= \int_{\partial\kappa_t}\mathbf{n}\cdot\left[\mathbf{T}^t\frac{d\boldsymbol{\chi}}{dt}-\mathbf{q}\right]da + \int_{\kappa_t}\rho\left[\mathbf{b}\cdot\frac{d\boldsymbol{\chi}}{dt}+g\right]dv,\end{aligned} \tag{2.30}$$

Assuming the above equation holds for arbitrary bounded regular subsets of κ_t and using (2.23) and (2.27) and divergence theorem we obtain

$$\rho\frac{d\epsilon}{dt} = \mathbf{T}\cdot\mathbf{L} - div(\mathbf{q}) + \rho g, \tag{2.31}$$

where, $\mathbf{L} = grad(\mathbf{v})$, $\mathbf{q}$ is the heat flux and g is volumetric heating. We assume that the heat flux, $\mathbf{q}$ is a smooth field over κ_t.

Equation (2.30) could equally be expressed as

$$\begin{aligned}&\frac{d}{dt}\int_{\kappa_o}\widetilde{J}_3\frac{\rho}{2}\frac{d\boldsymbol{\chi}}{dt}\cdot\frac{d\boldsymbol{\chi}}{dt}dV + \frac{d}{dt}\int_{\kappa_o}\widetilde{J}_3\rho\epsilon dV \\ &= \int_{\partial\kappa_o}\mathbf{N}\cdot\left[\widetilde{\mathbf{S}}^t\frac{d\boldsymbol{\chi}}{dt}-\widetilde{J}_3\mathbf{H}_t^{-1}\mathbf{q}\right]dA + \int_{\kappa_o}\widetilde{J}_3\rho\left[\mathbf{b}\cdot\frac{d\boldsymbol{\chi}}{dt}+g\right]dV,\end{aligned} \tag{2.32}$$

which using arguments as before and $\widetilde{\mathbf{S}}\cdot\widetilde{Grad}(\mathbf{v}) = \widetilde{J}_3\mathbf{T}\cdot\mathbf{L}$ yields

$$\widetilde{J}_3\rho\frac{d\epsilon}{dt} = \widetilde{J}_3\mathbf{T}\cdot\mathbf{L} - Div(\widetilde{J}_3\mathbf{H}_t^{-1}\mathbf{q}) + \widetilde{J}_3\rho g. \tag{2.33}$$

4. Balance of angular momentum

According to this law, the rate of change of angular momentum must equal the applied torque in both magnitude and direction. Mathematically, taking momentum about the origin, this transforms as

$$\frac{d}{dt}\int_{\kappa_t}\mathbf{x}\wedge\rho\frac{d\boldsymbol{\chi}}{dt}dv=\int_{\partial\kappa_t}\mathbf{x}\wedge\mathbf{T}\mathbf{n}da+\int_{\kappa_t}\rho\mathbf{x}\wedge\mathbf{b}dv, \tag{2.34}$$

which yields

$$tr(\mathbf{T}\mathbf{A}_a)=0, \tag{2.35}$$

for any skew-symmetric tensor, $\mathbf{A}_a$, on assuming that (2.34) holds for arbitrary bounded regular subsets of κ_t and using (2.23), (2.27) and the identities

$$\int_{\partial\kappa_t}\mathbf{x}\wedge\mathbf{T}\mathbf{n}da = \int_{\kappa_t}div(\mathbf{X}_x\mathbf{T})dv, \tag{2.36}$$

$$div(\mathbf{X}_x\mathbf{T})\cdot\mathbf{a} = \mathbf{a}\cdot(\mathbf{x}\wedge div(\mathbf{T}))+\mathbf{T}\cdot\mathbf{A}_a, \tag{2.37}$$

where, $\mathbf{X}_x$ is the skew symmetric tensor with $\mathbf{x}$ as its axial vector, $\mathbf{a}$ is a constant but arbitrary vector and $\mathbf{A}_a$ is the skew symmetric tensor with $\mathbf{a}$ as its axial vector. It then follows from (2.35) that $\mathbf{T}$ is a symmetric tensor.

C. General restrictions on constitutive relations

In this section, the restrictions on constitutive relation for state variables due to 2^{nd} law of thermodynamics, coordinate frame indifference and material symmetry is discussed. Of course, there are other restrictions on the constitutive relations but they would not be considered at this point, especially because they are not universal as those considered here.

1. 2^{nd} law of thermodynamics

This law states that the rate of entropy production is nonnegative. Mathematically, this requires

$$\frac{d}{dt}\int_{\kappa_t}\rho\eta dv \geq \int_{\kappa_t}\rho\frac{g}{\vartheta}dv - \int_{\partial\kappa_t}\frac{\mathbf{q}}{\vartheta}\cdot\mathbf{n}da, \tag{2.38}$$

which yields

$$\rho\vartheta\frac{d\eta}{dt} - \frac{1}{\vartheta}\mathbf{q}\cdot grad(\vartheta) \geq \rho\frac{d\epsilon}{dt} - \mathbf{T}\cdot\mathbf{L}, \tag{2.39}$$

on assuming that (2.38) holds for arbitrary regular subsets of κ_t and using (2.23) and (2.31)

For ease in computation we introduce, free energy (or Helmoltz potential) per unit volume in the current configuration defined as[9]

$$\psi = \rho(\epsilon - \eta\vartheta), \tag{2.40}$$

Substituting the above in (2.39) and using (2.23) we obtain

$$\frac{1}{\vartheta}\mathbf{q}\cdot grad(\vartheta) + \frac{d\psi}{dt} + \rho\eta\frac{d\vartheta}{dt} + (\psi\mathbf{1} - \mathbf{T})\cdot\mathbf{D} \leq 0. \tag{2.41}$$

2. Coordinate frame indifference

Certain mathematical quantities (or state variables), like density, internal energy, entropy, Helmoltz potential describes the state of the body. Since these quantities represent the state of the body we require that the value of these scalars[10] be inde-

[9]The reason for defining free energy per unit volume instead of per unit mass will become evident in the next chapter.

[10]The value of the components of a tensor of order greater than zero do depend on the coordinate basis. Given a tensor $\mathbf{T}$, the representations that can be obtained for this; by changing coordinate basis could be imagined to form one or more closed curves or surfaces in the n-dimensional space of components of $\mathbf{T}$, called orbit. Then, two representations are different only if their orbits do not coincide.

pendent of the choice of basis[11] required to represent the components of a tensor. In other words, for a given observer the value of the scalar quantities that describe the state of the body cannot change unless there is a causative process in (or on or from) the body. Hence, the value of the Helmoltz potential of a particle $P \in \mathcal{B}$ should not depend on the particular choice of basis used to represent the components of a tensor and moreover the formula used to compute Helmoltz potential should also not depend on the choice of basis used to represent the components of a tensor. This is based on the requirement that the value of material parameters, say shear modulus, has to be independent of the choice of the basis used to represent the components of a tensor.

Let $\mathbf{Q} \in \mathcal{O}$, the set of orthogonal transformations. Then, for a change of basis in the current configuration such that $\mathbf{e}_l^* = \mathbf{Q}\mathbf{e}_l$

$$\psi = \psi_{sf}(\mathbf{F}_t, \vartheta) = \psi_{sf}(\mathbf{Q}\mathbf{F}_t, \vartheta), \tag{2.42}$$

$$\mathbf{T} = \mathbf{f}(\mathbf{F}_t, \vartheta) = \mathbf{Q}\mathbf{f}(\mathbf{Q}\mathbf{F}_t, \vartheta)\mathbf{Q}^t, \tag{2.43}$$

$\forall\ \mathbf{Q} \in \mathcal{O}$ and $\forall\ (\mathbf{F}_t, \vartheta) \in \mathcal{D}_{sf} \subseteq Lin^+ \times \mathcal{R}^+$, where $\mathcal{D}_{sf}$ denotes the domain of ψ_{sf} and $\mathcal{R}^+$ the set of non-negative reals and

$$\psi = \psi_o(\mathbf{H}_t, \mathbf{T}^o, \vartheta) = \psi_o(\mathbf{Q}\mathbf{H}_t, \mathbf{T}^o, \vartheta), \tag{2.44}$$

$$\mathbf{T} = \mathbf{h}(\mathbf{H}_t, \mathbf{T}^o, \vartheta) = \mathbf{Q}\mathbf{h}(\mathbf{Q}\mathbf{H}_t, \mathbf{T}^o, \vartheta)\mathbf{Q}^t, \tag{2.45}$$

$\forall\ \mathbf{Q} \in \mathcal{O}$ and $\forall\ (\mathbf{H}_t, \mathbf{T}^o, \vartheta) \in \mathcal{D}_o \subseteq (Lin^+ \times Lin \times \mathcal{R}^+)$, where $\mathcal{D}_o$ denotes the domain of ψ_o and $\mathbf{T}^o$ the stress field in the reference configuration.

[11] For those who regard (2.9) (or (2.7)) as coordinate transformation, this will cause confusion. In other words, (2.9) (or (2.7)) is a point transformation while here we are interested in coordinate transformations. Here coordinate (or basis) transformations are only relations between different possible mathematical descriptions of the same state of the body.

Similarly, for a change of basis in the stress free reference configuration we require

$$\psi = \psi_{sf}(\mathbf{F}_t, \vartheta) = \psi_{sf}(\mathbf{F}_t\mathbf{Q}^t, \vartheta), \tag{2.46}$$

$$\mathbf{T} = \mathbf{f}(\mathbf{F}_t, \vartheta) = \mathbf{f}(\mathbf{F}_t\mathbf{Q}^t, \vartheta), \tag{2.47}$$

$\forall\ \mathbf{Q} \in \mathcal{O}$ and $\forall\ (\mathbf{F}_t, \vartheta) \in \mathcal{D}_{sf}$ and for a change of basis in the stressed reference configuration we require

$$\psi = \psi_o(\mathbf{H}_t, \mathbf{T}^o, \vartheta) = \psi_o(\mathbf{H}_t\mathbf{Q}^t, \mathbf{Q}\mathbf{T}^o\mathbf{Q}^t, \vartheta), \tag{2.48}$$

$$\mathbf{T} = \mathbf{h}(\mathbf{H}_t, \mathbf{T}^o, \vartheta) = \mathbf{h}(\mathbf{H}_t\mathbf{Q}^t, \mathbf{Q}\mathbf{T}^o\mathbf{Q}^t, \vartheta), \tag{2.49}$$

$\forall\ \mathbf{Q} \in \mathcal{O}$ and $\forall\ (\mathbf{H}_t, \mathbf{T}^o, \vartheta) \in \mathcal{D}_o$.

3. Material symmetry

Let us begin by examining the restriction that the material symmetry seeks to place on the mathematical description of the mechanical response of the body within the framework of continuum mechanics. Consider an observer who has chosen a coordinate system and has mathematically represented the (stressed or stress free) reference configuration of the body i.e., identify the region of Euclidean space that this body occupies and has found the spatial variation of the state variables. Now, say without the knowledge of the observer, this reference configuration of the body is deformed (or rotated). The question is will this deformation (or rotation) be recognized by the observer? Theoretically, if the observer cannot identify the deformation, then the functional form of the Helmoltz potential at each given Euclidean point should be same for this deformed and initial reference configuration. Here it is pertinent to point out that since the initial and deformed configuration are indistinguishable, the state of the different material points that occupy the Euclidean point, has to be same.

In other words, this restriction arises due to equivalence of a set of point transformations in the reference configuration, as opposed to coordinate transformations in the previous case. Thus, the set of equivalent point transformations depends on the state of the body.

Let $\mathcal{G}_{sf} \subseteq \mathcal{H}$, the unimodular group, i.e., the set of linear transformations with determinant equal to one, represent the set of all deformations of the stress free reference configuration that are indistinguishable. Then, we require

$$\psi = \psi_{sf}(\mathbf{F}_t, \vartheta) = \psi_{sf}(\mathbf{F}_t \mathbf{G}_{sf}^t, \vartheta), \tag{2.50}$$

$$\mathbf{T} = \mathbf{f}(\mathbf{F}_t, \vartheta) = \mathbf{f}(\mathbf{F}_t \mathbf{G}_{sf}^t, \vartheta), \tag{2.51}$$

$\forall\ \mathbf{G}_{sf} \in \mathcal{G}_{sf}$ and $\forall\ (\mathbf{F}_t, \vartheta) \in \mathcal{D}_{sf}$, or

$$\psi = \psi_o(\mathbf{H}_t, \mathbf{T}^o, \vartheta) = \psi_o(\mathbf{H}_t \mathbf{G}_o^t, \mathbf{T}^o, \vartheta), \tag{2.52}$$

$$\mathbf{T} = \mathbf{h}(\mathbf{H}_t, \mathbf{T}^o, \vartheta) = \mathbf{h}(\mathbf{H}_t \mathbf{G}_o^t, \mathbf{T}^o, \vartheta), \tag{2.53}$$

$\forall\ \mathbf{G}_o \in \mathcal{G}_o \subseteq \mathcal{H}$, the set of all deformations of the stressed reference configuration that are indistinguishable and $\forall\ (\mathbf{H}_t, \mathbf{T}^o, \vartheta) \in \mathcal{D}_o$ at a given Euclidean point.

It is worthwhile to make a few observations. First, the importance of the above conditions being evaluated at a given Euclidean point cannot be overemphasized, especially since the stress field, $\mathbf{T}^o$, in the reference configuration would be non-uniform, in general. Secondly, since the value of the state variables of the material point occupying this Euclidean point, in the initial and deformed reference configurations is same and the basis used to represent the stress is unaltered, the matrix components of the stress, $\mathbf{T}^o$ will not change.

The rotation of the body is mathematically different from a change of basis. Towards, this let us examine why $J_4 = \mathbf{M} \cdot \mathbf{CM}$ satisfies the requirement (2.46) and

the condition (2.50). Let

$$\mathcal{G}_{sf} = \{\mathbf{G} \in \mathcal{G}_{sf} | \mathbf{GM} = \mathbf{M} \& \mathbf{G} \in \mathcal{O}^{+}\}, \tag{2.54}$$

where $\mathbf{M}$ is a given vector, at times called fiber direction. Due to a change of basis in the stress free reference configuration

$$(\mathbf{QM}) \cdot (\mathbf{QCQ}^{t})(\mathbf{QM}) = \mathbf{M} \cdot \mathbf{CM}, \tag{2.55}$$

$\forall\ \mathbf{Q} \in \mathcal{O}$. On the other hand due to rotation of the body

$$\mathbf{M} \cdot \mathbf{GCG}^{t}\mathbf{M} = (\mathbf{G}^{t}\mathbf{M}) \cdot \mathbf{C}(\mathbf{G}^{t}\mathbf{M}) = \mathbf{M} \cdot \mathbf{CM}, \tag{2.56}$$

for all $\mathbf{G} \in \mathcal{G}_{sf}$. The second equality follows immediately from observing that if $\mathbf{G} \in \mathcal{G}_{sf}$ then $\mathbf{G}^{t} \in \mathcal{G}_{sf}$. Now say, $\mathcal{G}_{sf} = \mathcal{O}^{+}$ then $\mathbf{M} \cdot \mathbf{CM}$ does not satisfy (2.50).

Using arguments similar to those made above, one can seek the set of equivalent point transformations for the current configuration, i.e., one can deform the current configuration and seek the set of deformations that are not identifiable and let this set be denoted by $\mathcal{G}_{t}$. Now

$$\psi = \psi_{sf}(\mathbf{F}_{t}, \vartheta) = \psi_{sf}(\mathbf{G}_{t}\mathbf{F}_{t}, \vartheta), \tag{2.57}$$

$$\mathbf{T} = \mathbf{f}(\mathbf{F}_{t}, \vartheta) = \mathbf{f}(\mathbf{G}_{t}\mathbf{F}_{t}, \vartheta), \tag{2.58}$$

$\forall\ \mathbf{G}_{t} \in \mathcal{G}_{t}$ and $\forall\ (\mathbf{F}_{t}, \vartheta) \in \mathcal{D}_{sf}$, or equivalently

$$\psi = \psi_{o}(\mathbf{H}_{t}, \mathbf{T}^{o}, \vartheta) = \psi_{o}(\mathbf{G}_{t}\mathbf{H}_{t}, \mathbf{T}^{o}, \vartheta), \tag{2.59}$$

$$\mathbf{T} = \mathbf{h}(\mathbf{H}_{t}, \mathbf{T}^{o}, \vartheta) = \mathbf{h}(\mathbf{G}_{t}\mathbf{H}_{t}, \mathbf{T}^{o}, \vartheta), \tag{2.60}$$

$\forall\ \mathbf{G}_{t} \in \mathcal{G}_{t}$ and $\forall\ (\mathbf{H}_{t}, \mathbf{T}^{o}, \vartheta) \in \mathcal{D}_{o}$ at a given Euclidean point.

It is clear from the above that the material symmetry of the body depends on

the configuration it is in. Given the material symmetry group[12] of the body in a (reference) configuration Noll's rule [61] expresses the symmetry group in another configuration, in terms of the gradient of motion relating the two configurations and the symmetry group of the first (reference) configuration. Towards obtaining this rule, note that

$$\mathbf{T} = \mathbf{f}(\mathbf{F}_t, \vartheta) = \mathbf{f}(\mathbf{H}_t\mathbf{F}_o, \vartheta) = \overline{\mathbf{h}}(\mathbf{H}_t, \vartheta), \tag{2.61}$$

using (2.13). On application of (2.51) and (2.61) we obtain

$$\overline{\mathbf{h}}(\mathbf{H}_t, \vartheta) = \mathbf{f}(\mathbf{F}\mathbf{G}_{sf}, \vartheta) = \mathbf{f}(\mathbf{H}_t\mathbf{F}_o\mathbf{G}_{sf}\mathbf{F}_o^{-1}\mathbf{F}_o, \vartheta) = \overline{\mathbf{h}}(\mathbf{H}_t\mathbf{F}_o\mathbf{G}_{sf}\mathbf{F}_o^{-1}, \vartheta). \tag{2.62}$$

This shows that if $\mathbf{G}_{sf} \in \mathcal{G}_{sf}$ then $\mathbf{F}_o\mathbf{G}_{sf}\mathbf{F}_o^{-1} \in \mathcal{G}_o$. Thus

$$\mathcal{G}_o = \mathbf{F}_o\mathcal{G}_{sf}\mathbf{F}_o^{-1}. \tag{2.63}$$

The above is known as Noll's rule. It is worthwhile to note that even if $\mathcal{G}_{sf} \subseteq \mathcal{O}^+$, $\mathbf{G}_o \subseteq \mathcal{H}$. In fact, it has been shown by Winemann et. al. [26] that $\mathbf{G}_o$ contains non-orthogonal but unimodular elements when $\mathbf{F}_o = \lambda\mathbf{1} + \lambda_3\mathbf{e}\otimes\mathbf{e}$, where $\mathbf{e}$ is a unit vector, say, along whose direction the body is stretched.

Other rules, similar to the Noll's rule, obtained in Coleman and Noll [62], Hoger [63] are based on the assumption that $\mathcal{G}_o \subseteq \mathcal{O}^+ \subset \mathcal{H}$. Here we record the rule due to Hoger [63], because of its utility later. Combining (2.45) and (2.53) we obtain

$$\mathbf{h}(\mathbf{H}_t, \mathbf{T}^o, \vartheta) = \mathbf{Q}\mathbf{h}(\mathbf{Q}\mathbf{H}_t\mathbf{Q}^t, \mathbf{T}^o, \vartheta)\mathbf{Q}^t, \tag{2.64}$$

$\forall\ \mathbf{Q} \in \mathcal{G}_o^Q \subseteq \mathcal{G}_o$, where $\mathcal{G}_o^Q$ is the set of all proper orthogonal elements in $\mathcal{G}_o$. Evaluating

[12]It can be shown that the set of equivalent point transformations form a group see Ogden [60] section 4.2.3 for details

(2.64) at $\mathbf{H}_t = \mathbf{1}$ and $\vartheta = \vartheta_o$ and noting that $\mathbf{h}(\mathbf{1}, \mathbf{T}^o, \vartheta_o) = \mathbf{T}^o$, we obtain

$$\mathbf{T}^o\mathbf{Q} = \mathbf{Q}\mathbf{T}^o. \tag{2.65}$$

Thus, the above equation is only a necessary condition.

D. Representations from stress free reference configuration for isotropic bodies

This section focuses on developing representations for stress and Helmoltz potential from stress free reference configuration satisfying the above restrictions.

1. Representation for stress

Substituting (2.17a) in (2.47)

$$\mathbf{T} = \mathbf{f}(\mathbf{F}_t, \vartheta) = \mathbf{f}(\mathbf{F}_t\mathbf{Q}^t, \vartheta) = \mathbf{f}(\mathbf{V}\mathbf{R}\mathbf{Q}^t, \vartheta). \tag{2.66}$$

Since, the above holds for all $\mathbf{Q} \in \mathcal{O}$, choosing $\mathbf{Q} = \mathbf{R}$

$$\mathbf{T} = \mathbf{f}(\mathbf{V}, \vartheta) = \overline{\mathbf{f}}(\mathbf{B}, \vartheta). \tag{2.67}$$

The last equality arises because $\mathbf{B} = \mathbf{V}^2$ and square-root theorem[13] ensures the existence of an unique $\mathbf{V}$ such that $\mathbf{V} = \sqrt{\mathbf{B}}$. Substituting (2.67) in (2.43)

$$\mathbf{T} = \overline{\mathbf{f}}(\mathbf{B}, \vartheta) = \mathbf{Q}\overline{\mathbf{f}}(\mathbf{Q}\mathbf{B}\mathbf{Q}^t, \vartheta)\mathbf{Q}^t \tag{2.68}$$

$\forall\ \mathbf{Q} \in \mathcal{O}$.

Theorem 2.1: A symmetric second order tensor valued function $\overline{\mathbf{f}}$ defined over the space of symmetric second order tensors and non-negative reals, satisfies (2.68) if

[13]See Gurtin [56] section 2 for proof

and only if it has a representation

$$\mathbf{T} = \overline{\mathbf{f}}(\mathbf{B}, \vartheta) = \alpha_0 \mathbf{1} + \alpha_1 \mathbf{B} + \alpha_2 \mathbf{B}^2 \tag{2.69}$$

where α_0, α_1, α_2 are functions of principal invariants of $\mathbf{B}$ and ϑ i.e.,

$$\alpha_i = \hat{\alpha}_i(I_1, I_2, I_3, \vartheta) \tag{2.70}$$

Proof: [14] Before proving the above theorem we prove the following theorem:

Theorem 2.2: Let α be a scalar function defined over the space of symmetric positive definite second order tensors. Then $\alpha(\mathbf{QBQ}^t) = \alpha(\mathbf{B}) \; \forall \; \mathbf{Q} \in \mathcal{O}$ if and only if there exist a function $\overline{\alpha}$, defined on $\mathcal{R}^+ \times \mathcal{R}^+ \times \mathcal{R}^+$, such that $\alpha(\mathbf{B}) = \overline{\alpha}(\lambda_1, \lambda_2, \lambda_3)$, where $\overline{\alpha}(\lambda_1, \lambda_2, \lambda_3)$ is insensitive to permutations of λ_i and λ_1, λ_2, λ_3 are the eigen values of $\mathbf{B}$. Hence, $\alpha(\mathbf{B}) = \hat{\alpha}(I_1, I_2, I_3)$.

Proof: [15] Writing $\mathbf{B}$ in the spectral form

$$\mathbf{B} = \lambda_1 \mathbf{b}_1 \otimes \mathbf{b}_1 + \lambda_2 \mathbf{b}_2 \otimes \mathbf{b}_2 + \lambda_3 \mathbf{b}_3 \otimes \mathbf{b}_3, \tag{2.71}$$

where $\mathbf{b}_i$'s are the orthonormal eigen vectors of $\mathbf{B}$ and hence

$$\mathbf{QBQ}^t = \lambda_1 \mathbf{Qb}_1 \otimes \mathbf{Qb}_1 + \lambda_2 \mathbf{Qb}_2 \otimes \mathbf{Qb}_2 + \lambda_3 \mathbf{Qb}_3 \otimes \mathbf{Qb}_3. \tag{2.72}$$

Since, $\alpha(\mathbf{QBQ}^t) = \alpha(\mathbf{B}) \; \forall \; \mathbf{Q} \in \mathcal{O}$, $\alpha(\mathbf{B})$ must be independent of the orientation of the eigen directions of $\mathbf{B}$ and must depend on $\mathbf{B}$ only through its eigen values, λ_1, λ_2, λ_3.

Next, choose $\mathbf{Q}$ to be a rotation of $\pi/2$ about $\mathbf{b}_3$ so that $\mathbf{Qb}_1 = \mathbf{b}_2$, $\mathbf{Qb}_2 = -\mathbf{b}_1$

[14] Adapted from Serrin [64] and Ogden [60]. The original proof is due to Rivlin and Ericksen [65]

[15] Adapted from Ogden [60]

and $\mathbf{Q}\mathbf{b}_3 = \mathbf{b}_3$. Hence,

$$\alpha(\mathbf{B}) = \alpha(\lambda_2 \mathbf{b}_1 \otimes \mathbf{b}_1 + \lambda_1 \mathbf{b}_2 \otimes \mathbf{b}_2 + \lambda_3 \mathbf{b}_3 \otimes \mathbf{b}_3) \tag{2.73}$$

from which we deduce that $\overline{\alpha}(\lambda_1, \lambda_2, \lambda_3) = \overline{\alpha}(\lambda_2, \lambda_1, \lambda_3)$. In similar fashion it can be shown that $\overline{\alpha}$ is insensitive to other permutations of λ_i's.

Finally, recalling that the eigen values are the solutions of the characteristic equation

$$\lambda^3 - I_1\lambda^2 + I_2\lambda - I_3 = 0, \tag{2.74}$$

in principal, λ_i's can be expressed uniquely in terms of the principal invariants and hence $\alpha(\mathbf{B}) = \hat{\alpha}(I_1, I_2, I_3)$.

The converse of the theorem 2.2 is proved easily from the property of trace and determinants. Hence, we have proved theorem 2.2.

Theorem 2.3: If $\overline{\mathbf{f}}$ satisfies (2.68) then the eigen values of $\overline{\mathbf{f}}(\mathbf{B}, \vartheta)$ are functions of the principal invariants of $\mathbf{B}$ and ϑ.

Proof: Let $\gamma(\mathbf{B}, \vartheta)$ be the eigen value of $\overline{\mathbf{f}}(\mathbf{B}, \vartheta)$. Then,

$$\det[\overline{\mathbf{f}}(\mathbf{B}, \vartheta) - \gamma(\mathbf{B}, \vartheta)\mathbf{1}] = 0. \tag{2.75}$$

The corresponding eigen value of $\overline{\mathbf{f}}(\mathbf{Q}\mathbf{B}\mathbf{Q}^t, \vartheta)$ is $\gamma(\mathbf{Q}\mathbf{B}\mathbf{Q}^t, \vartheta)$ and hence

$$\det[\overline{\mathbf{f}}(\mathbf{Q}\mathbf{B}\mathbf{Q}^t, \vartheta) - \gamma(\mathbf{Q}\mathbf{B}\mathbf{Q}^t, \vartheta)\mathbf{1}] = 0. \tag{2.76}$$

This can be written as

$$\det[\mathbf{Q}\{\overline{\mathbf{f}}(\mathbf{B}, \vartheta) - \gamma(\mathbf{Q}\mathbf{B}\mathbf{Q}^t, \vartheta)\mathbf{1}\}\mathbf{Q}^t] = 0, \tag{2.77}$$

by using (2.68) and the relation $\mathbf{Q}\mathbf{Q}^t = \mathbf{1}$. Using the property of determinants the

above equation reduces to

$$\det[\overline{\mathbf{f}}(\mathbf{B},\vartheta) - \gamma(\mathbf{Q}\mathbf{B}\mathbf{Q}^t,\vartheta)\mathbf{1}] = 0, \tag{2.78}$$

which has to hold for all $\mathbf{Q} \in \mathcal{O}$. Comparing (2.75) and (2.78)

$$\gamma(\mathbf{Q}\mathbf{B}\mathbf{Q}^t,\vartheta) = \gamma(\mathbf{B},\vartheta), \tag{2.79}$$

for all $\mathbf{Q} \in \mathcal{O}$, which by theorem 2.2 implies that $\gamma(\mathbf{B},\vartheta) = \hat{\alpha}(I_1, I_2, I_3, \vartheta)$

Theorem 2.4: If $\mathbf{T} = \overline{\mathbf{f}}(\mathbf{B},\vartheta)$ satisfies (2.68) then $\overline{\mathbf{f}}(\mathbf{B},\vartheta)$ is coaxial with $\mathbf{B}$.

Proof: Consider an eigen vector $\mathbf{b}_1$ of $\mathbf{B}$ and define an orthogonal transformation $\mathbf{Q}$ by

$$\mathbf{Q}\mathbf{b}_1 = -\mathbf{b}_1, \qquad \mathbf{Q}\mathbf{b}_j = \mathbf{b}_j \qquad \text{if} \qquad \mathbf{b}_1 \cdot \mathbf{b}_j = 0, \tag{2.80}$$

i.e. $\mathbf{Q}$ is a reflection on the plane normal to $\mathbf{b}_1$. Now, $\mathbf{Q}\mathbf{B}\mathbf{Q}^t = \mathbf{B}$ and hence, by (2.68), $\mathbf{Q}\mathbf{T} = \mathbf{T}\mathbf{Q}$. We therefore have

$$\mathbf{Q}(\mathbf{T}\mathbf{b}_1) = \mathbf{T}(\mathbf{Q}\mathbf{b}_1) = -\mathbf{T}\mathbf{b}_1, \tag{2.81}$$

and we see that $\mathbf{Q}$ transforms the vector $\mathbf{T}\mathbf{b}_1$ into its opposite. Since, the only vectors transformed by the reflection $\mathbf{Q}$ into their opposites are the multiples of $\mathbf{b}_1$, it follows that $\mathbf{b}_1$ is an eigen vector of $\mathbf{T}$. Similarly, it can be shown that every eigen vector of $\mathbf{B}$ is also an eigen vector of $\mathbf{T}$. Hence, $\overline{\mathbf{f}}(\mathbf{B},\vartheta)$ is coaxial with $\mathbf{B}$.

Now we prove theorem 2.1.

Clearly, if (2.69) along with (2.70) holds then (2.68) is satisfied and hence we have to prove only the converse.

It follows from theorem 2.3 and theorem 2.4 that $\overline{\mathbf{f}}(\mathbf{B})$ is coaxial with $\mathbf{B}$ and its eigen values are functions of the principal invariants of $\mathbf{B}$ and ϑ. Let λ_1,λ_2,λ_3 and

f_1,f_2,f_3 be the eigen values of $\mathbf{B}$ and $\overline{\mathbf{f}}(\mathbf{B})$ respectively and consider the equations

$$\alpha_0 + \alpha_1\lambda_i + \alpha_2\lambda_i^2 = f_i, \qquad (i = 1, 2, 3) \tag{2.82}$$

for the three unknowns α_0, α_1, α_2. Assuming the λ_i and f_i are given and that λ_i's are distinct it follows that α_i's are determined uniquely in terms of λ_i and f_i which are themselves determined uniquely by the principal invariants of $\mathbf{B}$ and ϑ. Thus, since $\mathbf{B}$ is coaxial with $\overline{\mathbf{f}}(\mathbf{B})$ and α_i are functions of the principal invariants of $\mathbf{B}$ and ϑ; equation (2.69) follows from (2.82) provided the eigen values of $\mathbf{B}$ are distinct, of course. When the eigen values of $\mathbf{B}$ are not distinct α_2 or α_1 and α_2 could be chosen arbitrarily, depending on whether the algebraic multiplicity of the eigen values is 2 or 3 respectively. However, this choice may cause some α_i to become discontinuous even when $\overline{\mathbf{f}}(\mathbf{B})$ remains continuous, Truesdell and Noll [22] and Serrin [64] provide example of such cases.

Finally, from (2.21) we obtain

$$\mathbf{B}^2 = I_1\mathbf{B} - I_2\mathbf{1} + I_3\mathbf{B}^{-1}. \tag{2.83}$$

Then, observing that the principal invariants of the positive definite, $\mathbf{B}$, are related bijectively to the invariants J_1, J_2 and J_3, as defined in (2.20), we note that

$$\alpha_i = \hat{\alpha}_i(I_1, I_2, I_3, \vartheta) = \overline{\alpha}_i(J_1, J_2, J_3, \vartheta) \tag{2.84}$$

for $i = (0, 1, 2)$. Substituting (2.83) and (2.84) in (2.69) we obtain

$$\mathbf{T} = \alpha_0\mathbf{1} + \alpha_1\mathbf{B} + \alpha_2\mathbf{B}^{-1}. \tag{2.85}$$

Henceforth, the above equation would be considered as the most general representation for stress from stress-free reference configuration.

a. Restrictions on the constitutive representation

Note that the above representation for stress was obtained only by enforcing the restrictions due to the coordinate frame invariance. Now, we examine their status with respect to the restrictions arising due to material symmetry. The condition (2.51) requires

$$\mathbf{T} = \overline{\mathbf{f}}(\mathbf{F}_t\mathbf{F}_t^t, \vartheta) = \overline{\mathbf{f}}(\mathbf{F}_t\mathbf{G}_{sf}^t\mathbf{G}_{sf}\mathbf{F}_t^t, \vartheta), \tag{2.86}$$

$\forall\ \mathbf{G}_{sf} \in \mathcal{G}_{sf}$ and $\forall\ (\mathbf{F}_t, \vartheta) \in \mathcal{D}_{sf}$. Thus, if and only if $\mathcal{G}_{sf} \subseteq \mathcal{O}^+$ the above holds. Since, it is irrelevant whether $\mathcal{G}_{sf} \subset \mathcal{O}^+$ or $\mathcal{G}_{sf} = \mathcal{O}^+$, a stress free configuration is isotropic.

Next, we use the condition (2.58), which for the present case evaluates to requiring

$$\mathbf{T} = \overline{\mathbf{f}}(\mathbf{F}_t\mathbf{F}_t^t, \vartheta) = \overline{\mathbf{f}}(\mathbf{G}_t\mathbf{F}_t\mathbf{F}_t^t\mathbf{G}_t^t, \vartheta), \tag{2.87}$$

$\forall\ (\mathbf{F}_t, \vartheta) \in \mathcal{D}_{sf}$. From this we infer the elements in $\mathcal{G}_t$. If we assume that $\mathcal{G}_t \subseteq \mathcal{O}$ then $\mathbf{T}\mathbf{G}_t = \mathbf{G}_t\mathbf{T}$, obtained from (2.85). Thus, members of the set $\mathcal{G}_t$ has to commute with $\mathbf{T}$. It follows from theorem 3 page 157 in Halmos [57] that only those transformations that leave the characteristic spaces of $\mathbf{T}$ unchanged can be members of the set $\mathcal{G}_t$. Note the similarity of this restriction with (2.65).

Finally since, $\mathbf{T} = \mathbf{0}$ when $\mathbf{F}_t = \mathbf{1}$ and $\vartheta = \vartheta_o$

$$\overline{\alpha}_0(3, 3, 1, \vartheta_o) + \overline{\alpha}_1(3, 3, 1, \vartheta_o) + \overline{\alpha}_2(3, 3, 1, \vartheta_o) = 0. \tag{2.88}$$

2. Representation for Helmoltz potential

Substituting (2.17a) in (2.46) we obtain

$$\psi = \psi_{sf}(\mathbf{F}_t, \vartheta) = \psi_{sf}(\mathbf{F}_t\mathbf{Q}^t, \vartheta) = \psi_{sf}(\mathbf{V}\mathbf{R}\mathbf{Q}^t, \vartheta). \tag{2.89}$$

Since the above has to hold for all $\mathbf{Q} \in \mathcal{O}$, choosing $\mathbf{Q} = \mathbf{R}$

$$\psi = \psi_{sf}(\mathbf{V}, \vartheta) = \hat{\psi}_{sf}(\mathbf{B}, \vartheta). \tag{2.90}$$

Substituting the above in (2.42) we obtain

$$\psi = \hat{\psi}_{sf}(\mathbf{B}, \vartheta) = \hat{\psi}_{sf}(\mathbf{Q}\mathbf{B}\mathbf{Q}^t, \vartheta). \tag{2.91}$$

Then, it follows from theorem 2.2 that for the above to hold

$$\psi = \hat{\psi}_{sf}(\mathbf{B}, \vartheta) = \check{\psi}_{sf}(I_1, I_2, I_3, \vartheta). \tag{2.92}$$

Since the principal invariants of $\mathbf{B}$ are related bijectively to the invariants J_1, J_2 and J_3

$$\psi = \overline{\psi}_{sf}(J_1, J_2, J_3, \vartheta). \tag{2.93}$$

E. Constitutive relations for stress

In this section, some constitutive relations for stress from a stress free reference configuration popular in the literature is recorded. As already mentioned, in this thesis only unconstrained materials are studied.

1. Blatz-Ko constitutive relation

The first constitutive relation that we record was proposed by Blatz and Ko [66] to model polyurethane and foam rubber. A general form of this constitutive relation is

$$\mathbf{T} = \frac{\mu_1}{J_3}\left[\mu_m(J_3)\mathbf{1} + \mu_2\mathbf{B} - (1-\mu_2)\mathbf{B}^{-1}\right], \tag{2.94}$$

where,

$$\mu_m = J_3^{2\mu_3} - \mu_2\left[J_3^{2\mu_3} + J_3^{-2\mu_3}\right],$$

μ_1,μ_2 and μ_3 are material parameters such that $\mu_1 > 0$, $0 \leq \mu_2 \leq 1$, $\mu_3 > 0$ and in general depends on $\mathbf{X}$, in which case the body is inhomogeneous. Of special interest are the two special forms of the above relation, obtained when $\mu_2 = 1$ and $\mu_2 = 0$ used to model polyurethane and foam rubber respectively. Then, when $\mu_2 = 1$

$$\mathbf{T} = \frac{\mu_1}{J_3}\left[\mathbf{B} - J_3^{-2\mu_3}\mathbf{1}\right], \tag{2.95}$$

and when $\mu_2 = 0$

$$\mathbf{T} = \frac{\mu_1}{J_3}\left[J_3^{2\mu_3}\mathbf{1} - \mathbf{B}^{-1}\right]. \tag{2.96}$$

2. Exponential constitutive relation

Fung [67] observed that the stress stretch response of soft tissues could be exponential. Based on this observation and heuristic considerations we study a constitutive relation of the form

$$\mathbf{T} = \mu_1\mu_2 \exp(Q)\left[2\mathbf{B} + \left(J_1 - \frac{5}{J_3^2}\right)\mathbf{1}\right], \tag{2.97}$$

where $Q = \mu_2[J_1J_3 + \frac{5}{J_3} - 8]$ and μ_1, μ_2 are material parameters such that $\mu_1 > 0$ and $\mu_2 > 0$. Note that $\mathbf{T} = \mathbf{0}$ when $\mathbf{F}_t = \mathbf{1}$. We shall assume, the above constitutive relation to model soft tissues, as a first approximation. We shall at times call a material whose constitutive relation is given by (2.97) as biological material.

F. Issues relating to material symmetry

Finally, we address the issue of when the initial and the rotated reference configurations are distinguishable? In engineering mechanics, the members of the symmetry group of a solid are those rotations that does not change the mechanical response. However, we find this unsatisfactory.

Towards this, we find that the uniaxial stress versus stretch response could change

with the direction even for isotropic bodies. It is well known that for Neumann boundary value problems the solution is not unique (see for example Truesdell and Noll [22], Beatty [68]). The boundary value problems corresponding to most of the experiments performed for characterizing the body, namely uniaxial, biaxial, torsion experiments, are purely Neumann boundary value problems[16], especially when the deformation is completely specified but for some parameters in them. Thus, the assumed form of the displacement need not be the only solution, within the context of finite elasticity. Here, we construct a deformation for uniaxial extension that is admissible for a constitutive relation describing the mechanical response of a homogeneous, isotropic, body from a stress free configuration, such that the uniaxial stress (T_{xx}) versus stretch (λ_{sx}) response in x - direction is different from the uniaxial stress (T_{yy}) versus stretch (λ_{sy}) response in y - direction. Clearly, we are studying the mechanical response of a homogeneous, isotropic bodies which according to the prevailing conjecture should not show directional dependence.

Consider a deformation of the form

$$x = \lambda_1 X + \kappa_1 Y, \quad y = -\kappa_1 \frac{\lambda_2}{\lambda_1} X + \lambda_2 Y, \quad z = \lambda_3 Z. \tag{2.98}$$

where (X, Y, Z) and (x, y, z) represents the coordinates of a typical material point before and after deformation in cartesian coordinates. Here λ_1, λ_2, λ_3 and κ_1 are constants. The matrix representation of the gradient of deformation in Cartesian coordinates is

$$\mathbf{F}_t = \begin{pmatrix} \lambda_1 & \kappa_1 & 0 \\ -\frac{\lambda_2}{\lambda_1}\kappa_1 & \lambda_2 & 0 \\ 0 & 0 & \lambda_3 \end{pmatrix}, \tag{2.99}$$

[16]The boundary value problem should not be confused with the stress or displacement controlled experiment.

and that of the left Cauchy-Green stretch tensor is

$$\mathbf{B} = \begin{pmatrix} \lambda_1^2 + \kappa_1^2 & 0 & 0 \\ 0 & (\frac{\lambda_2}{\lambda_1})^2(\lambda_1^2 + \kappa_1^2) & 0 \\ 0 & 0 & \lambda_3^2 \end{pmatrix}, \tag{2.100}$$

and its inverse has a matrix representation

$$\mathbf{B}^{-1} = \begin{pmatrix} \frac{1}{\lambda_1^2+\kappa_1^2} & 0 & 0 \\ 0 & (\frac{\lambda_1}{\lambda_2})^2\frac{1}{(\lambda_1^2+\kappa_1^2)} & 0 \\ 0 & 0 & \frac{1}{\lambda_3^2} \end{pmatrix}. \tag{2.101}$$

Hence, the invariants

$$J_1 = (\lambda_1^2 + \kappa_1^2)(1 + (\frac{\lambda_2}{\lambda_1})^2) + \lambda_3^2, \tag{2.102}$$

$$J_2 = \frac{1}{\lambda_1^2 + \kappa_1^2}(1 + (\frac{\lambda_1}{\lambda_2})^2) + \frac{1}{\lambda_3^2}, \tag{2.103}$$

$$J_3 = \frac{\lambda_2\lambda_3}{\lambda_1}(\lambda_1^2 + \kappa_1^2). \tag{2.104}$$

Thus, $\lambda_3\lambda_2/\lambda_1 > 0$. In the absence of body forces, it could be trivially verified that the balance of linear momentum is satisfied for a homogeneous body.

Let us consider biaxial stretching (i.e. $T_{xx} = T_1$, $T_{yy} = T_2$ and all other matrix components of the stress are zero) of a body whose mechanical response is governed by, for example, a special form of Blatz-Ko constitutive relation (2.95) and we identify the material parameter μ_1, with the characteristic stress to non-dimensionalize stress. It is pertinent to note that Horgan [69] found this special form of the Blatz-Ko potential to be globally elliptic.

Now, the parameters λ_1, λ_2, λ_3 and κ_1 have to be evaluated from the boundary

conditions

$$T_1 = \frac{\lambda_1}{\lambda_2\lambda_3} - (\frac{\lambda_2\lambda_3}{\lambda_1}(\lambda_1^2+\kappa_1^2))^{-(2\mu_3+1)}, \tag{2.105}$$

$$T_2 = \frac{\lambda_2}{\lambda_1\lambda_3} - (\frac{\lambda_2\lambda_3}{\lambda_1}(\lambda_1^2+\kappa_1^2))^{-(2\mu_3+1)}, \tag{2.106}$$

$$T_3 = 0 = \frac{\lambda_3\lambda_1}{\lambda_2(\lambda_1^2+\kappa_1^2)} - (\frac{\lambda_2\lambda_3}{\lambda_1}(\lambda_1^2+\kappa_1^2))^{-(2\mu_3+1)}. \tag{2.107}$$

Equation (2.107) can be solved to obtain λ_3 as

$$\lambda_3 = (\frac{\lambda_1}{\lambda_2(\lambda_1^2+\kappa_1^2)})^{\frac{\mu_3}{(\mu_3+1)}} \tag{2.108}$$

Now, equations (2.105) and (2.106) have to be solved for λ_1, λ_2 and κ_1. We immediately find that there are more unknowns than available equations. So, let us assume[17]

$$\kappa_1^2 = K(\lambda_1^2+\lambda_2^2-2), \quad K = 0.5 \tag{2.109}$$

such that $\kappa_1 = 0$ when $\mathbf{F}_t = \mathbf{1}$, since the reference configuration is stress free. Substituting (2.109) in (2.105) and (2.106) we obtain two non-linear equations in λ_1 and λ_2.

First let us consider the uniaxial stretching in the x - direction. Now, $T_2 = 0$. For a given value of λ_1, we numerically solve the non-linear equation (2.106) to obtain λ_2 using bisection algorithm. The initiation of the algorithm ensures the existence of at least one solution[18]. Having obtained the value of λ_2 we use (2.105) to compute the non-dimensional stress T_1 required to maintain the given stretch ratio of λ_1. For

[17]We note that only for certain functional forms of κ_1 the equations (2.105) and (2.106) has a real valued solution and it depends on the specific form of the constitutive relation used.

[18]Since, $T_2(\lambda_2)$ is a continuous function in λ_2 and initiation of the bisection algorithm requires two initial guesses - λ_2^{g1}, λ_2^{g2} - such that $T_2(\lambda_2^{g1})T_2(\lambda_2^{g2}) < 0$, initiation of the bisection algorithm ensures the existence of a solution such that $T_2(\lambda_2) = 0$ in the interval $[\lambda_2^{g1},\lambda_2^{g2}]$

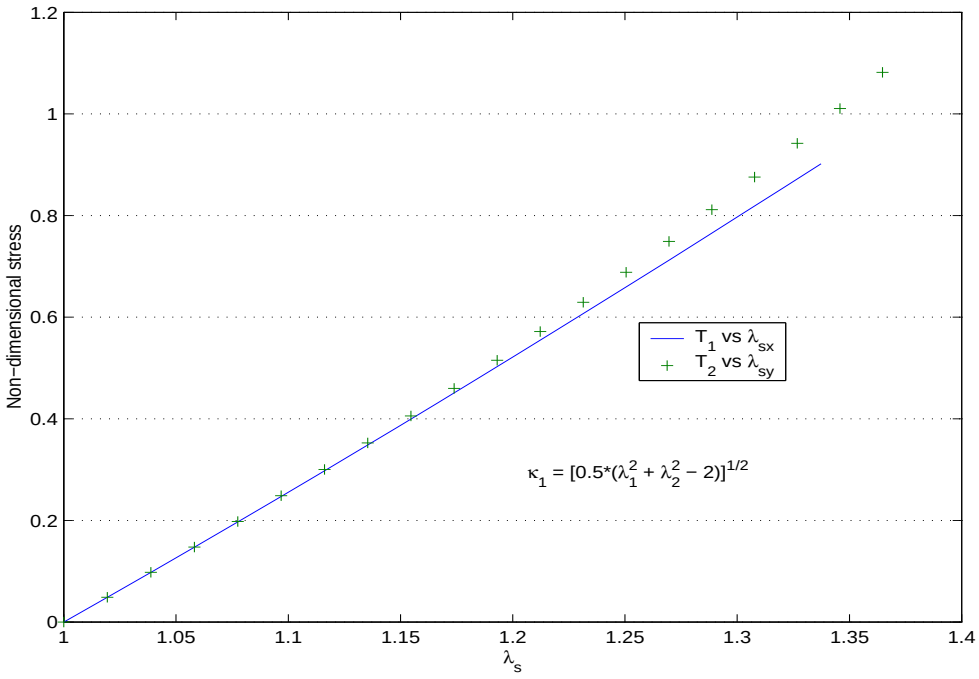

Fig. 1. Stress vs. stretch plot for uniaxial extension along x and y direction.

the assumed form of homogeneous deformation (2.98) the stretch ratio along the x-direction is computed to be, $\lambda_{sx} = \sqrt{\lambda_1^2 + (\frac{\lambda_2}{\lambda_1}\kappa_1)^2}$. Figure 1 captures this variation.

Similarly, we consider the uniaxial stretching in the y - direction. Now, $T_1 = 0$. For a given value of λ_2 we numerically solve the non-linear equation (2.105) to obtain λ_1 using bisection algorithm. Using this value of λ_1 and the assumed value of λ_2 we can determine the non-dimensional stress T_2 required to maintain a stretch ratio, λ_2, from (2.106). For this case we compute the stretch along the y - direction as, $\lambda_{sy} = \sqrt{\lambda_2^2 + \kappa_1^2}$. Figure 1 captures this variation also. It is clear from the figure that the response in the two directions are different. Equivalently, a 90^o rotation of the body about z - direction changes the stress required to engender identical stretches. Here it is pertinent to note that the non-linear equations were solved to an accuracy of 10^{-10}. Figure 2a plots the same stresses as a function of the independent variable λ_1 and

λ_2 respectively. Figure 2b plots the change in the angle between two line segments in the current and the reference configuration. If the line segments in the reference configuration are assumed to be oriented along the $\mathbf{E}_X$ and $\mathbf{E}_Y$ then the change in angle is given by

$$\theta_c - \theta_r = \cos^{-1}\left(\frac{(\lambda_1^2 - \lambda_2^2)\kappa_1}{\lambda_1\sqrt{\lambda_1^2 + (\frac{\lambda_2}{\lambda_1}\kappa_1)^2}\sqrt{\lambda_2^2 + \kappa_1^2}}\right) - 90. \tag{2.110}$$

Thus, the two candidate deformations for a given Neumann boundary value problem do not differ by just a rigid body deformation.

It is well known that transversely isotropic bodies shear when the uniaxial stretching direction doesn't coincide with the fiber direction. However, for these transversely isotropic bodies the principal direction of the stress and the left stretch tensor will be different. In contrast, for deformation (2.98) the body shears and the principal directions of the stress and the left stretch tensor are the same. It should be recognized that this requirement of the principal directions being same for isotropic bodies suggest only that $B_{11} = (\frac{\partial x}{\partial X})^2 + (\frac{\partial x}{\partial Y})^2 + (\frac{\partial x}{\partial Z})^2 = \Lambda_1^2$ and not that $(\frac{\partial x}{\partial X})^2 = \Lambda_1^2$. Of course, other components of $\mathbf{B}$ should also have suitable values. Thus, in fact the most general homogeneous deformation possible for uniaxial, biaxial or triaxial stretching of an isotropic body is

$$x = \lambda_1 X + \kappa_1 Y + \kappa_2 Z, \quad y = \kappa_3 X + \lambda_2 Y + \kappa_4 Z, \quad z = \kappa_5 X + \kappa_6 Y + \lambda_3 Z, \tag{2.111}$$

where λ_i's and κ_i's are constants that have to satisfy certain conditions.

Of course, if it is experimentally observed that the body does not or cannot shear then $\kappa_i = 0$ and the mechanical response will not exhibit directional dependence. Also, here it is not claimed that the directional dependence of the mechanical response of any body is fully captured by the deformation of the proposed form. But, the

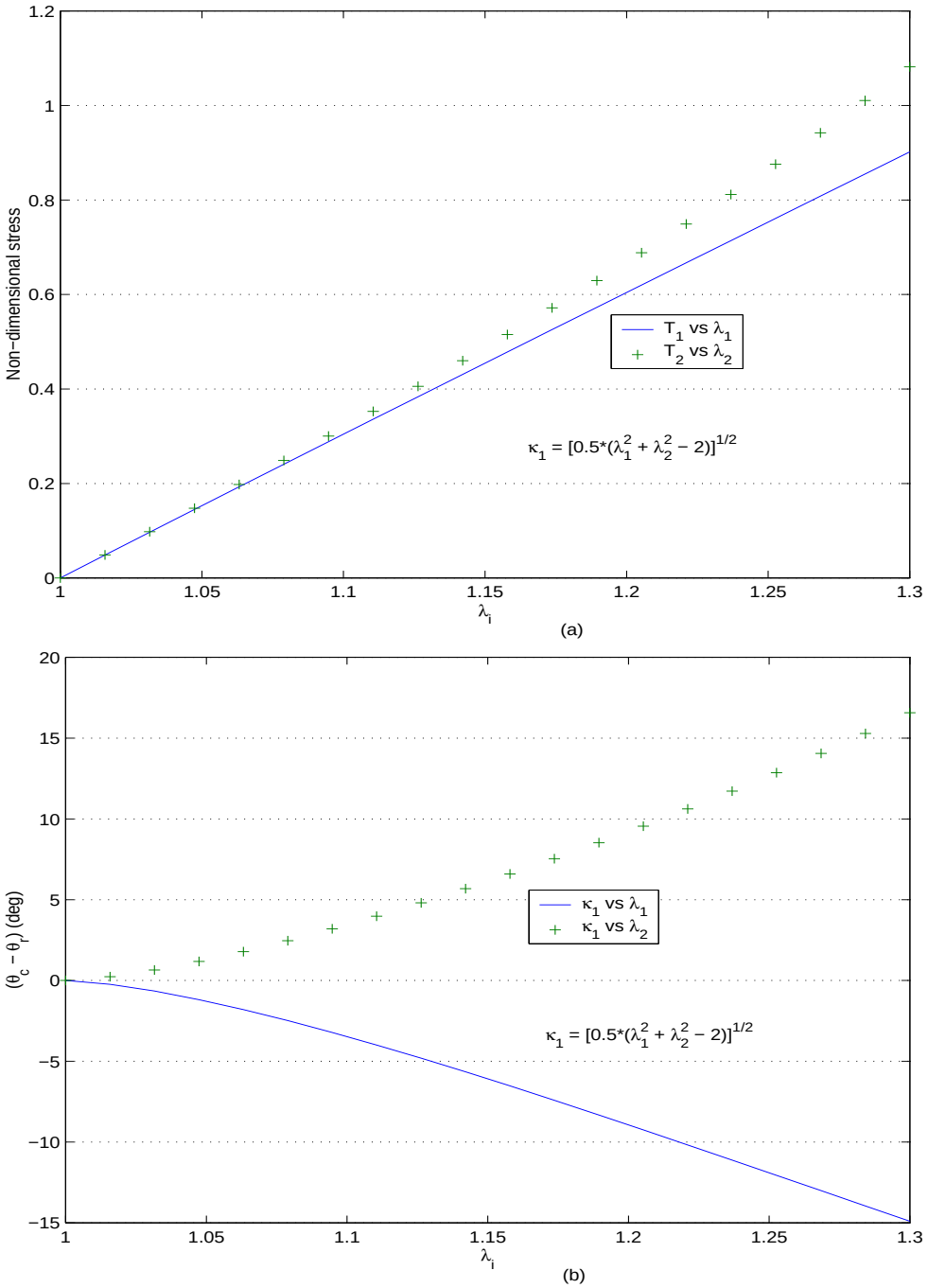

Fig. 2. (a) Stress vs. λ_i plot for uniaxial extension along x and y direction (b) $\theta_c - \theta_r$ vs. λ_i plot for uniaxial extension along x and y direction.

purpose of the above is to show that even a body that is indistinguishable to any rotation otherwise, can mechanically respond differently. Another purpose here is to provide concrete and simple example to show that purely Neumann boundary condition results in non-unique solutions. The above boundary value problem is not an exception but similar solutions are obtained for inflation, extension, twisting and shearing of annular right circular homogeneous incompressible isotropic cylinders in Saravanan [70]. Moreover, Saravanan and Rajagopal ([71],[72]) show that the mechanical response of inhomogeneous bodies from stress free reference configuration varies with the direction of loading. Consequently, we advocate caution in the use of mechanical test in determining the symmetry group of a given body, experimentally.

CHAPTER III

REPRESENTATIONS FROM STRESSED REFERENCE CONFIGURATION

As seen in the previous chapter, stress free configurations of bodies have enjoyed a very special status in the development of representations for stress in solids, for the simplification that it presumably affords. From philosophical point of view, all that one requires is some configuration to enable description of the body. Hence, it is mathematically reasonable to require the reference configuration to be stress free. However, such representations serve little purpose to an experimentalist, since such configurations, in many cases, are physically unattainable and hence the need to develop representation for stress from a configuration that is not stress free. It is this issue that we focus in this chapter. In subsequent chapters we show that mathematical analysis using this representation is no more difficult than analysis using representation from stress free reference configuration.

Certain variables, like density, internal energy, entropy, stress determine the state of the body and are called state variables. Hence, the value of these state variables[1] cannot change due to different equivalent mathematical representations of the same state. To elaborate, changes in the coordinate system or the reference configuration cannot change the value of the density or internal energy at a material point in a given state of the body. To solve problems of interest one has to choose the coordinate basis and the reference configuration, which determines the domain of the function that mathematically depicts these state variables. While the domain of these function depends on the particular choice of the coordinate basis and the reference configuration,

[1]The value of the components of a tensor of order greater than zero do depend on the coordinate basis. Then, as remarked in chapter II, two representations are different only if their orbits do not coincide.

their co-domain doesn't. Just like one requires to choose a coordinate system to algebraically represent a curve in space, the reference configuration facilitates algebraic representation of the stress. This is the concept used for obtaining a representation to capture the thermo-mechanical response from a reference configuration that is not stress free, in the following sections.

We begin by assuming that the stressed configuration which is to be used as reference is obtained through a smooth bijective mapping from a stress free configuration. Using the concept outlined above we develop a representation for stress from the stressed configuration in terms of the stress, $\mathbf{T}^o$ in the stressed configuration and the gradient of motion from this configuration $\mathbf{H}_t$. Then, it is easy to see that the same derivation holds for piecewise smooth bijective mapping between the stressed and stress free configuration. Thus, the representation obtained here could be used to study prestressed body provided the prestresses could be relieved, theoretically, by finite number of cuts.

A. Representation for stress

In this section, we obtain a representation for stress from a stressed reference configuration. As described above the sought representation for $\mathbf{h}(\mathbf{H}_t, \mathbf{T}^o, \vartheta)$, is obtained by observing that

$$\mathbf{T} = \overline{\mathbf{f}}(\mathbf{B}, \vartheta) = \overline{\mathbf{f}}(\mathbf{H}_t \mathbf{B}_o \mathbf{H}_t^t, \vartheta) = \mathbf{h}(\mathbf{H}_t, \mathbf{T}^o, \vartheta), \tag{3.1}$$

where $\overline{\mathbf{f}}(\mathbf{B}, \vartheta)$ is the representation for stress from a stress free reference configuration obtained in the previous chapter and we have made use of the equations (2.13) and (2.16) to obtain the above equation. Now, to obtain $\mathbf{h}$ we have to express $\mathbf{B}_o$ in terms of $\mathbf{T}^o$.

Towards this, from (2.21) we obtain

$$\mathbf{B}^2 = I_1\mathbf{B} - I_2\mathbf{1} + I_3\mathbf{B}^{-1}, \tag{3.2}$$

$$\mathbf{B}^{-2} = \frac{1}{I_3}[\mathbf{B} - I_1\mathbf{1} + I_2\mathbf{B}^{-1}], \tag{3.3}$$

where I_i are the principal invariants of $\mathbf{B}$. Using the above equations and the general expression for stress from stress free reference configuration, (2.85) a straightforward computation yields

$$\mathbf{T}^2 = \beta_0\mathbf{1} + \beta_1\mathbf{B} + \beta_2\mathbf{B}^{-1}, \tag{3.4}$$

where

$$\begin{aligned}
\beta_0 &= \alpha_0^2 + 2\alpha_1\alpha_2 - J_2J_3^2\alpha_1^2 - \frac{J_1}{J_3^2}\alpha_2^2,\\
\beta_1 &= 2\alpha_1\alpha_0 + \alpha_1^2J_1 + \frac{1}{J_3^2}\alpha_2^2,\\
\beta_2 &= 2\alpha_2\alpha_0 + \alpha_1^2J_3^2 + J_2\alpha_2^2.
\end{aligned}$$

Thus, $\beta_i = \overline{\beta}_i(J_1, J_2, J_3, \vartheta)$, are scalar valued functions of the invariants of $\mathbf{B}$ and temperature. Solving for $\mathbf{B}$ and $\mathbf{B}^{-1}$ in equations (2.85) and (3.4) we obtain

$$\mathbf{B} = \frac{1}{\Delta}[(\beta_0\alpha_2 - \alpha_0\beta_2)\mathbf{1} + \beta_2\mathbf{T} - \alpha_2\mathbf{T}^2], \tag{3.5}$$

$$\mathbf{B}^{-1} = \frac{1}{\Delta}[(\alpha_0\beta_1 - \beta_0\alpha_1)\mathbf{1} - \beta_1\mathbf{T} + \alpha_1\mathbf{T}^2], \tag{3.6}$$

when $\Delta = (\alpha_1\beta_2 - \alpha_2\beta_1) \neq 0$[2].

Now, as defined in chapter II, let $\boldsymbol{\chi}(\mathbf{X}, t_o)$ denote the motion field from the stress-free reference configuration to a stressed configuration which we plan to use as the reference and moreover let $\mathbf{T}^o$ denote the stress field in the stressed configuration.

[2]We later show that this condition has to be satisfied by any admissible constitutive relation provided the body is not under state of stress corresponding to hydrostatic pressure.

Then, using the above equations the left Cauchy-Green stretch tensor and its inverse at a material point in the stressed reference configuration could be written as

$$\mathbf{B}_o = \delta_0\mathbf{1} + \delta_1\mathbf{T}^o + \delta_2(\mathbf{T}^o)^2, \tag{3.7}$$

$$\mathbf{B}_o^{-1} = \kappa_0\mathbf{1} + \kappa_1\mathbf{T}^o + \kappa_2(\mathbf{T}^o)^2, \tag{3.8}$$

where

$$\delta_0 = \frac{1}{\Delta}\left[-\frac{J_1^r}{J_3^{r2}}a_2^3 + (2a_1 - J_2^r a_0)\,a_2^2 - \left(J_2^r J_3^{r2}a_1^2 + a_0^2\right)a_2 - J_3^{r2}a_1^2 a_0\right], \tag{3.9}$$

$$\delta_1 = \frac{1}{\Delta}\left[2a_2a_0 + J_3^{r2}a_1^2 + J_2^r a_2^2\right], \qquad \delta_2 = -\frac{a_2}{\Delta}, \tag{3.10}$$

$$\kappa_0 = \frac{1}{\Delta}\left[J_2^r J_3^{r2}a_1^3 + (J_1^r a_0 - 2a_2)\,a_1^2 + \left(a_0^2 + \frac{J_1^r}{J_3^{r2}}a_2^2\right)a_1 + \frac{1}{J_3^{r2}}a_0a_2^2\right], \tag{3.11}$$

$$\kappa_1 = -\frac{1}{\Delta}\left[2a_1a_0 + J_1^r a_1^2 + \frac{a_2^2}{J_3^{r2}}\right], \qquad \kappa_2 = \frac{a_1}{\Delta}, \tag{3.12}$$

$$\Delta = J_3^{r2}a_1^3 - J_1^r a_2 a_1^2 + J_2^r a_2^2 a_1 - \frac{1}{J_3^{r2}}a_2^3, \tag{3.13}$$

and $a_i = \overline{\alpha}_i(J_1^r, J_2^r, J_3^r, \vartheta)$ where J_1^r, J_2^r and J_3^r are invariants of $\mathbf{B}_o$. Now it is pertinent to observe that if $\mathbf{T}^o = \mathbf{0}$, $\vartheta = \vartheta_o$, $J_1^r = 3$, $J_2^r = 3$ and $J_3^r = 1$, then it follows from (2.88) that $a_0 + a_1 + a_2 = 0$ and hence $\delta_0 = \kappa_0 = 1$, as it should be.

Here, it is important to recognize that the parameters J_i^r, $i = \{1, 2, 3\}$, depend only on $\mathbf{T}^o$ and therefore are constants at a given material point and a stressed configuration. Hence, they are treated as parameters in the constitutive equation and are determined from the restrictions that these parameters have to satisfy, as illustrated shortly.

Next, substituting equations (3.7) and (3.8) in

$$J_1 = \mathbf{1}\cdot\mathbf{B} = tr(\mathbf{H}_t\mathbf{F}_o\mathbf{F}_o^t\mathbf{H}_t^t) = \widetilde{\mathbf{C}}\cdot\mathbf{B}_o, \tag{3.14}$$

$$J_2 = \mathbf{1}\cdot\mathbf{B}^{-1} = tr(\mathbf{H}_t^{-t}\mathbf{F}_o^{-t}\mathbf{F}_o^{-1}\mathbf{H}_t^{-1}) = \widetilde{\mathbf{C}}^{-1}\cdot\mathbf{B}_o^{-1}, \tag{3.15}$$

we obtain

$$J_1 = \widetilde{J}_{m1}(\mathcal{L}_{\widetilde{J}}) = \delta_0\widetilde{J}_1 + \delta_1\widetilde{J}_4 + \delta_2\widetilde{J}_5, \tag{3.16}$$

$$J_2 = \widetilde{J}_{m2}(\mathcal{L}_{\widetilde{J}}) = \kappa_0\widetilde{J}_2 + \kappa_1\widetilde{J}_6 + \kappa_2\widetilde{J}_7, \tag{3.17}$$

$$J_3 = \widetilde{J}_{m3}(\mathcal{L}_{\widetilde{J}}) = \widetilde{J}_3 J_3^r, \tag{3.18}$$

where, $\mathcal{L}_{\widetilde{J}} = \{\widetilde{J}_1, \widetilde{J}_2, \widetilde{J}_3, \widetilde{J}_4, \widetilde{J}_5, \widetilde{J}_6, \widetilde{J}_7\}$,

$$\widetilde{J}_1 = \widetilde{\mathbf{C}} \cdot \mathbf{1}, \qquad \widetilde{J}_2 = \widetilde{\mathbf{C}}^{-1} \cdot \mathbf{1}, \qquad \widetilde{J}_3 = det(\mathbf{H}_t) \tag{3.19}$$

$$\widetilde{J}_4 = \widetilde{\mathbf{C}} \cdot \mathbf{T}^o, \qquad \widetilde{J}_6 = \widetilde{\mathbf{C}}^{-1} \cdot \mathbf{T}^o, \tag{3.20}$$

$$\widetilde{J}_5 = \widetilde{\mathbf{C}} \cdot (\mathbf{T}^o)^2, \qquad \widetilde{J}_7 = \widetilde{\mathbf{C}}^{-1} \cdot (\mathbf{T}^o)^2. \tag{3.21}$$

Hence,

$$\begin{aligned} \mathbf{T} = \mathbf{h}(\mathbf{H}_t, \mathbf{T}^o, \vartheta) = {} & \alpha_0\mathbf{1} + \alpha_1\mathbf{H}_t\left[\delta_0\mathbf{1} + \delta_1\mathbf{T}^o + \delta_2(\mathbf{T}^o)^2\right]\mathbf{H}_t^t \\ & + \alpha_2\mathbf{H}_t^{-t}\left[\kappa_0\mathbf{1} + \kappa_1\mathbf{T}^o + \kappa_2(\mathbf{T}^o)^2\right]\mathbf{H}_t^{-1}, \end{aligned} \tag{3.22}$$

when $\Delta \neq 0$ and where $\alpha_i = \overline{\alpha}_i(\widetilde{J}_{m1}, \widetilde{J}_{m2}, \widetilde{J}_{m3}, \vartheta)$.

Finally we consider the case, when $\Delta = 0$. Then, a straightforward computation from equations (2.85) and (3.4) shows that

$$\beta_2\mathbf{T} - \alpha_2\mathbf{T}^2 = [\alpha_0\beta_2 - \alpha_2\beta_0]\mathbf{1}. \tag{3.23}$$

It then follows that for the above equation to hold all the three eigen values of $\mathbf{T}$ should be equal and is given by

$$p = \begin{cases} \frac{1}{2\alpha_2}\left[\beta_2 \pm \sqrt{\beta_2^2 - 4\alpha_2(\alpha_0\beta_2 - \alpha_2\beta_0)}\right] & \text{, when } \alpha_2 \neq 0, \\ \alpha_0 & \text{, when } \alpha_2 = 0, \end{cases} . \tag{3.24}$$

We note that since Δ is a function of the invariants of $\mathbf{B}$ it cannot be zero when all

the eigen values of $\mathbf{B}$ are distinct. Hence, the algebraic multiplicity of the eigen values of $\mathbf{B}$ must be two or three when $\Delta = 0$. In appendix-A we show that, in general, both solutions, i.e. $\mathbf{B} = \lambda\mathbf{1}$ and $\mathbf{B} = \lambda\mathbf{1} + \lambda_3\mathbf{e}\otimes\mathbf{e}$ are possible for many constitutive relations. Since, it is physically unrealistic for a body to shorten or lengthen along a single direction on application of a hydrostatic pressure, we propose to place restriction on the constitutive relations so that these solutions are not possible. (We elaborate on these restrictions shortly.)

Therefore, as before assuming that $\boldsymbol{\chi}(\mathbf{X}, t_o)$ exist, when $\Delta = 0$, $\mathbf{T}^o = p^o\mathbf{1}$ and

$$\mathbf{B}_o = \delta_3\mathbf{1}, \qquad \mathbf{B}_o^{-1} = \frac{1}{\delta_3}\mathbf{1}. \tag{3.25}$$

where

$$p^o = \begin{cases} \frac{1}{2a_2}\left[b_2 \pm \sqrt{\left(a_1^2 J_3^{r2} - a_2^2 J_2^r\right)^2 + 4a_2^3\left(2a_1 - \frac{J_1^r}{J_3^{r2}}a_2\right)}\right] & \text{, when } a_2 \neq 0, \\ a_0 & \text{, when } a_2 = 0, \end{cases} . \tag{3.26}$$

$b_2 = 2a_2a_0 + a_1^2J_3^{r2} + J_2^ra_2^2$, $J_1^r = 3\delta_3$, $J_2^r = 3/\delta_3$, $J_3^r = \delta_3^{3/2}$. Substituting (3.25) in (3.14) and (3.15)

$$\widetilde{J}_{m1} = \delta_3\widetilde{J}_1, \qquad \widetilde{J}_{m2} = \frac{1}{\delta_3}\widetilde{J}_2, \qquad \widetilde{J}_{m3} = J_3^r\widetilde{J}_3, \tag{3.27}$$

and hence

$$\mathbf{T} = \mathbf{h}(\mathbf{H}_t, \mathbf{T}^o, \vartheta) = \alpha_0\mathbf{1} + \alpha_1\delta_3\widetilde{\mathbf{B}} + \alpha_2\frac{1}{\delta_3}\widetilde{\mathbf{B}}^{-1}, \tag{3.28}$$

when $\Delta = 0$ where $\alpha_i = \overline{\alpha}_i(\widetilde{J}_{m1}, \widetilde{J}_{m2}, \widetilde{J}_{m3}, \vartheta)$ and we observe that δ_3 depends only on $\mathbf{T}^o$, which is established next.

B. Restrictions on constitutive representation

We obtain J_i^r from the requirement that $\mathbf{B}_o\mathbf{B}_o^{-1} = \mathbf{1}$ and the requirement that $\mathbf{T} = \mathbf{T}^o$ when $\mathbf{H}_t = \mathbf{1}$ and $\vartheta = \vartheta_o$.

Taking the product of equations (3.7) and (3.8) and using Cayley-Hamilton theorem we obtain

$$\mathbf{0} = \gamma_1\mathbf{1} + \gamma_2\mathbf{T}^o + \gamma_3(\mathbf{T}^o)^2 \tag{3.29}$$

where

$$\gamma_1 = \delta_0\kappa_0 + K_3[\kappa_1\delta_2 + \delta_1\kappa_2 + \delta_2\kappa_2K_1] - 1, \tag{3.30}$$

$$\gamma_2 = \delta_1\kappa_0 + \kappa_1\delta_0 + \delta_2\kappa_2K_3 - K_2[\kappa_1\delta_2 + \delta_1\kappa_2 + \delta_2\kappa_2K_1], \tag{3.31}$$

$$\gamma_3 = \delta_2\kappa_0 + \delta_1\kappa_1 + \delta_0\kappa_2 - \delta_2\kappa_2K_2 + K_1[\kappa_1\delta_2 + \delta_1\kappa_2 + \delta_2\kappa_2K_1], \tag{3.32}$$

K_i's are the principal invariants of $\mathbf{T}^o$. A sufficient condition that ensures (3.29) is:

$$\gamma_1 = 0, \qquad \gamma_2 = 0, \qquad \gamma_3 = 0. \tag{3.33}$$

We note that the above is a necessary condition when the eigen values of $\mathbf{T}^o$ are distinct.

Then, the requirement that $\mathbf{T} = \mathbf{T}^o$ when $\mathbf{H}_t = \mathbf{1}$ and $\vartheta = \vartheta_o$ could be cast as requiring

$$[c_0 + c_1\delta_0 + c_2\kappa_0]\mathbf{1} + [c_1\delta_1 + c_2\kappa_1 - 1]\mathbf{T^o} + [c_1\delta_2 + c_2\kappa_2](\mathbf{T}^o)^2 = \mathbf{0}, \tag{3.34}$$

where, $c_i = \overline{\alpha}_i(J^r_{m1}, J^r_{m2}, J^r_{m3}, \vartheta_o)$ and

$$J^r_{m1} = 3\delta_0 + tr(\mathbf{T}^o)\delta_1 + tr((\mathbf{T}^o)^2)\delta_2, \tag{3.35}$$

$$J^r_{m2} = 3\kappa_0 + tr(\mathbf{T}^o)\kappa_1 + tr((\mathbf{T}^o)^2)\kappa_2, \tag{3.36}$$

$$J^r_{m3} = J^r_3. \tag{3.37}$$

As before, a sufficient condition that ensures (3.34) is

$$c_0 + c_1\delta_0 + c_2\kappa_0 = 0, \qquad c_1\delta_1 + c_2\kappa_1 = 1, \qquad c_1\delta_2 + c_2\kappa_2 = 0. \tag{3.38}$$

The equations (3.33) and (3.38) are solved for the unknowns $J_1^r,\ J_2^r,\ J_3^r$. This is illustrated in section-E.

For the case when $\Delta = 0$

$$\overline{c}_0 + \overline{c}_1\delta_3 + \frac{\overline{c}_2}{\delta_3} = p^o, \tag{3.39}$$

where $\overline{c}_i = \overline{\alpha}_i(3\delta_3, \frac{3}{\delta_3}, \delta_3^{3/2}, \vartheta_o)$, is solved for the only unknown, δ_3.

It remains to be shown that the above system of equations has a solution. This can be shown only when $\overline{\alpha}_i$'s are specified.

Finally, when $\Delta = 0$, since the algebraic multiplicity of the eigen values of $\mathbf{T}^o$ was three, we required the algebraic multiplicity of the eigen values of $\mathbf{B}_o$ to be three as well. However, as noted in the appendix-A there exist solutions for which the algebraic multiplicity of the eigen values of $\mathbf{B}_o$ is two. Since, such solutions are physically unrealistic we require

$$\Delta = J_3^{r2}a_1^3 - J_1^r a_2 a_1^2 + J_2^r a_2^2 a_1 - \frac{1}{J_3^{r2}}a_2^3 \neq 0, \quad \text{when} \quad (J_1^r, J_2^r, J_3^r) \in (\mathcal{S} - \mathcal{P}), \tag{3.40}$$

where

$$\begin{aligned} \mathcal{S} &= \{(J_1^r, J_2^r, J_3^r) | 0 < J_1^r < \infty, 0 < J_2^r < \infty, 0 < J_3^r < \infty\} \\ \mathcal{P} &= \left\{(3\Lambda^2, \frac{3}{\Lambda^2}, \Lambda^3) | 0 < \Lambda < \infty\right\}. \end{aligned} \tag{3.41}$$

Many a times, when $a_1 \neq 0$, we find it useful to express the condition (3.40) as

$$J_3^{r2} \neq J_1^r \frac{a_2}{a_1} - J_2^r \left(\frac{a_2}{a_1}\right)^2 + \frac{1}{J_3^{r2}} \left(\frac{a_2}{a_1}\right)^3. \tag{3.42}$$

Immediately we infer that if $\frac{a_2}{a_1} < 0$, the restriction (3.40) holds. Thus, the E-inequalities (refer Truesdell and Noll [22] section 51) ensures $\Delta \neq 0$.

For the eigen value, p^o to be real we require $\beta_2^2 - 4\overline{\alpha}_2[\overline{\alpha}_0\beta_2 - \overline{\alpha}_2\beta_0] \geq 0$, i.e.,

$$\left(a_1^2(J_3^r)^2 - a_2^2 J_2^r\right)^2 + 4a_2^3\left(2a_1 - \frac{J_1^r}{(J_3^r)^2}a_2\right) \geq 0, \qquad \text{when} \qquad (J_1^r, J_2^r, J_3^r) \in \mathcal{P} \tag{3.43}$$

Factorizing (3.43), when $a_1 \neq 0$, we obtain

$$\left(\Lambda^4 - \frac{a_2}{a_1}\right)^3\left(\Lambda^4 + \frac{3a_2}{a_1}\right) \geq 0. \tag{3.44}$$

Immediately we infer that

$$-\frac{1}{3} \leq \frac{a_2}{a_1\Lambda^4} \leq 1 \tag{3.45}$$

when $(J_1^r, J_2^r, J_3^r) \in \mathcal{P}$.

a. Restrictions due to material symmetry

The above expression for stress from stressed reference configuration was obtained only enforcing coordinate frame invariance. Hence, let us now explore the restriction due to material symmetry. For the restriction (2.53) to hold we require

$$\mathbf{T}^o = \mathbf{G}_o\mathbf{T}^o\mathbf{G}_o^t. \tag{3.46}$$

In the following we shall assume that $\mathcal{G}_o \subseteq \mathcal{O}^3$, as before. Now, $\mathbf{T}^o\mathbf{G}_o = \mathbf{G}_o\mathbf{T}^o$. Thus, the representation of $\mathbf{T}^o$ should be such that it commutes with all the members of the

[3]We note that this assumption yields just a necessary condition for there exist non-orthogonal but unimodular $\mathbf{G}_o$ for which (3.46) holds. For example, when $\mathbf{T}^o = diag[T_1, T_1, T_2]$ with $T_2 \neq 0$ then a class of such $\mathbf{G}_o$ is

$$\mathbf{G}_o = \begin{pmatrix} 1 & 0 & 0 \\ 0 & \cos(\theta) & -\omega\sin(\theta) \\ 0 & \sin(\theta)/\omega & \cos(\theta) \end{pmatrix}, \tag{3.47}$$

where $\omega^2 = T_1/T_2$ and $0 \leq \theta \leq 2\pi$, a constant.

set $\mathcal{G}_o$. Unlike, the case for stress free configuration, now it matters whether $\mathcal{G}_o \subseteq \mathcal{O}$ or $\mathcal{G}_o = \mathcal{O}$ and hence a stressed configuration is anisotropic. Note that the restriction (3.46) is same as (2.65) and would be used in section G to determine the material symmetry of the prestressed body.

The requirement (2.60) when $\mathcal{G}_t \subseteq \mathcal{O}$ reduces to requiring $\mathbf{T}\mathbf{G}_t = \mathbf{G}_t\mathbf{T}$, as in the case when a stress free configuration is used as a reference.

C. Representation for Helmoltz potential from a stressed reference configuration

As discussed in the introduction, the representations are derived from the observation that the value of the Helmoltz potential at a material point in the body, at a particular state doesn't depend on the specific configuration used as reference, even though the formula used to compute them does. This reduces the problem to a simple calculus problem in composite functions. To elaborate, say we know the representation of the function, $\psi_{sf} = \hat{\psi}(J_1, J_2, J_3, \vartheta)$ per unit volume in the current configuration. However, we are interested in finding the function $\psi_o = \hat{\psi}(\mathcal{L}_{\widetilde{J}}, \vartheta)$ such that

$$\int_{V(\kappa_{sf}(\mathcal{B}))} \psi_{sf}(J_1, J_2, J_3, \vartheta) J_3 dV = \int_{V(\kappa_o(\mathcal{B}))} \psi_o(\mathcal{L}_{\widetilde{J}}, \vartheta) \widetilde{J}_3 dV, \tag{3.48}$$

where $V(\kappa_{sf}(\mathcal{B}))$ denote the volume of the configuration κ_{sf} and $V(\kappa_o(\mathcal{B}))$ the volume of the configuration κ_o. Now, by virtue of having obtained functions $\widetilde{J}_{m1}$, $\widetilde{J}_{m2}$ and $\widetilde{J}_{m3}$ such that

$$J_1 = \widetilde{J}_{m1}, \qquad J_2 = \widetilde{J}_{m2}, \qquad J_3 = \widetilde{J}_{m3}$$

(see equations (3.16) to (3.18)) equation (3.48) becomes

$$\int_{V(\kappa_o(\mathcal{B}))} [\psi_{sf}(\widetilde{J}_{m1}, \widetilde{J}_{m2}, \widetilde{J}_{m3}, \vartheta) - \psi_o(\mathcal{L}_{\widetilde{J}}, \vartheta)] \widetilde{J}_3 dV = 0. \tag{3.49}$$

For the above equation to hold for any arbitrary subparts of the body in the configuration κ_o

$$\psi_o(\mathcal{L}_{\widetilde{J}}, \vartheta) = \psi_{sf}(\widetilde{J}_{m1}, \widetilde{J}_{m2}, \widetilde{J}_{m3}, \vartheta), \tag{3.50}$$

at all material points in $\mathcal{B}$. Hence, we could write

$$\psi = \overline{\psi}(\mathbf{H}_t, \mathbf{T}^o, \vartheta) = \hat{\psi}(\widetilde{J}_{m1}, \widetilde{J}_{m2}, \widetilde{J}_{m3}, \vartheta), \tag{3.51}$$

and consider the above equation as the most general representation for Helmoltz potential satisfying coordinate frame indifference.

D. A thermodynamical framework for elastic response when the reference configuration is stressed

In this section, we establish the connection between the Helmoltz potential and the stress using the framework of thermodynamics. Towards this we compute $\frac{d\psi}{dt}$ as[4]

$$\begin{aligned}
\frac{d\psi}{dt} &= \frac{\partial\hat{\psi}}{\partial\widetilde{J}_{m1}}\frac{d\widetilde{J}_{m1}}{dt} + \frac{\partial\hat{\psi}}{\partial\widetilde{J}_{m2}}\frac{d\widetilde{J}_{m2}}{dt} + \frac{\partial\hat{\psi}}{\partial\widetilde{J}_{m3}}\frac{d\widetilde{J}_{m3}}{dt} + \frac{\partial\hat{\psi}}{\partial\vartheta}\frac{d\vartheta}{dt} \\
&= \mathbf{N}\cdot\mathbf{D} + [\mathbf{A}+\mathbf{M}]\cdot\frac{d\mathbf{T}^o}{dt} + \left[G + \frac{\partial\hat{\psi}}{\partial\vartheta}\right]\frac{d\vartheta}{dt},
\end{aligned} \tag{3.52}$$

where

$$\begin{aligned}
\mathbf{N} &= \widetilde{J}_{m3}\frac{\partial\hat{\psi}}{\partial\widetilde{J}_{m3}}\mathbf{1} + 2\frac{\partial\hat{\psi}}{\partial\widetilde{J}_{m1}}\mathbf{H}_t\left[\delta_0\mathbf{1} + \delta_1\mathbf{T}^o + \delta_2(\mathbf{T}^o)^2\right]\mathbf{H}_t^t \\
&\quad -2\frac{\partial\hat{\psi}}{\partial\widetilde{J}_{m2}}\mathbf{H}_t^{-t}\left[\kappa_0\mathbf{1} + \kappa_1\mathbf{T}^o + \kappa_2(\mathbf{T}^o)^2\right]\mathbf{H}_t^{-1},
\end{aligned} \tag{3.53}$$

$$\mathbf{A} = \frac{\partial\hat{\psi}}{\partial\widetilde{J}_{m1}}\left[\delta_1\mathbf{C} + 2\delta_2\mathbf{C}\mathbf{T}^o\right] + \frac{\partial\hat{\psi}}{\partial\widetilde{J}_{m2}}\left[\kappa_1\mathbf{C}^{-1} + 2\kappa_2\mathbf{C}^{-1}\mathbf{T}^o\right], \tag{3.54}$$

[4]Note that $\frac{d\hat{\psi}}{d\vartheta} = G + \frac{\partial\hat{\psi}}{\partial\vartheta}$

$$\begin{aligned}\mathbf{M} &= \frac{\partial\hat{\psi}}{\partial\widetilde{J}_{m1}}\left[\frac{\partial\delta_0}{\partial\mathbf{T}^o}\widetilde{J}_1+\frac{\partial\delta_1}{\partial\mathbf{T}^o}\widetilde{J}_4+\frac{\partial\delta_2}{\partial\mathbf{T}^o}\widetilde{J}_5\right]+\frac{\partial\hat{\psi}}{\partial\widetilde{J}_{m2}}\left[\frac{\partial\kappa_0}{\partial\mathbf{T}^o}\widetilde{J}_2\right.\\ &\left.+\frac{\partial\kappa_1}{\partial\mathbf{T}^o}\widetilde{J}_6+\frac{\partial\kappa_2}{\partial\mathbf{T}^o}\widetilde{J}_7\right]+\frac{\partial\hat{\psi}}{\partial\widetilde{J}_{m3}}\widetilde{J}_3\frac{\partial J_3^r}{\partial\mathbf{T}^o}, \qquad (3.55)\end{aligned}$$

$$\begin{aligned}G &= \frac{\partial\hat{\psi}}{\partial\widetilde{J}_{m1}}\left[\frac{\partial\delta_0}{\partial\vartheta}\widetilde{J}_1+\frac{\partial\delta_1}{\partial\vartheta}\widetilde{J}_4+\frac{\partial\delta_2}{\partial\vartheta}\widetilde{J}_5\right]+\frac{\partial\hat{\psi}}{\partial\widetilde{J}_{m2}}\left[\frac{\partial\kappa_0}{\partial\vartheta}\widetilde{J}_2+\frac{\partial\kappa_1}{\partial\vartheta}\widetilde{J}_6+\frac{\partial\kappa_2}{\partial\vartheta}\widetilde{J}_7\right]\\ &+\frac{\partial\hat{\psi}}{\partial\widetilde{J}_{m3}}\widetilde{J}_3\frac{\partial J_3^r}{\partial\vartheta}, \qquad (3.56)\end{aligned}$$

Substituting (3.52) in (2.41), the 2^{nd} law of thermodynamics, we obtain

$$\begin{aligned}&\frac{1}{\vartheta}\mathbf{q}\cdot grad(\vartheta)+[\mathbf{A}+\mathbf{M}]\cdot\frac{d\mathbf{T}^o}{dt}+\left[G+\frac{\partial\hat{\psi}}{\partial\vartheta}+\rho\eta\right]\frac{d\vartheta}{dt}\\ &+[\psi\mathbf{1}+\mathbf{N}-\mathbf{T}]\cdot\mathbf{D}\leq 0. \qquad (3.57)\end{aligned}$$

Hence, we require that

$$\eta = -\frac{1}{\rho}\left[G+\frac{\partial\hat{\psi}}{\partial\vartheta}\right], \qquad (3.58)$$

$$\mathbf{T} = \psi\mathbf{1}+\mathbf{N}, \qquad (3.59)$$

Therefore

$$\begin{aligned}\overline{\alpha}_0(\widetilde{J}_{m1},\widetilde{J}_{m2},\widetilde{J}_{m3},\vartheta) &= \psi+\widetilde{J}_{m3}\frac{\partial\hat{\psi}}{\partial\widetilde{J}_{m3}}, \qquad \overline{\alpha}_1(\widetilde{J}_{m1},\widetilde{J}_{m2},\widetilde{J}_{m3},\vartheta)=2\frac{\partial\hat{\psi}}{\partial\widetilde{J}_{m1}},\\ \overline{\alpha}_2(\widetilde{J}_{m1},\widetilde{J}_{m2},\widetilde{J}_{m3},\vartheta) &= -2\frac{\partial\hat{\psi}}{\partial\widetilde{J}_{m2}}, \qquad (3.60)\end{aligned}$$

Substituting (3.59), (3.58), (3.52), (3.51), (2.40) and (2.23) in (2.31), the balance of energy equation we obtain

$$[\mathbf{A}+\mathbf{M}]\cdot\frac{d\mathbf{T}^o}{dt}+\rho\vartheta\frac{d\eta}{dt}=\rho g-div(\mathbf{q}), \qquad (3.61)$$

where

$$\rho\frac{d\eta}{dt} = -\left[\left(G + \frac{\partial\psi}{\partial\vartheta}\right)\mathbf{1} + \mathbf{G}_N\right]\cdot\mathbf{D} - \frac{\partial G}{\partial\mathbf{T}^o}\cdot\frac{d\mathbf{T}^o}{dt} - \frac{\partial G}{\partial\vartheta}\frac{d\vartheta}{dt} - \frac{d}{dt}\left(\frac{\partial\psi}{\partial\vartheta}\right). \tag{3.62}$$

where, $\mathbf{G}_N = 2\mathbf{H}_t\frac{\partial G}{\partial\mathbf{C}}\mathbf{H}_t^t$.

While we could in principle obtain the evolution of density from (2.25), the stress from (3.59), the entropy from (3.58), internal energy from the constitutive prescription of Helmoltz potential, the motion from (2.27) and temperature from (3.61), there is no equation to predict the evolution of $\mathbf{T}^o$. Hence, we require additional principles like maximum rate of entropy production to govern its evolution. Here we shall assume that $\frac{d\mathbf{T}^o}{dt} = \mathbf{0}$ and call such a process elastic.

E. Illustrative example

In this section, we specialize the general constitutive representations for stress from stressed reference configurations obtained above, for two classes of constitutive relations introduced in section E of chapter II.

1. Blatz-Ko constitutive relation from a stressed reference configuration

First, we consider the constitutive relation introduced by Blatz and Ko [66] for homogeneous bodies from a stress free configuration. Here we modify this relation, relaxing the requirement that the reference configuration be stress free. Towards this, we begin by noting that for this case

$$\alpha_0 = \frac{\mu_m\mu_1}{\widetilde{J}_{m3}}, \qquad \alpha_1 = \frac{\mu_1\mu_2}{\widetilde{J}_{m3}}, \qquad \alpha_2 = \frac{\mu_1[\mu_2 - 1]}{\widetilde{J}_{m3}}, \tag{3.63}$$

where $\mu_m = \widetilde{J}_{m3}^{2\mu_3} - \mu_2[\widetilde{J}_{m3}^{2\mu_3} + \widetilde{J}_{m3}^{-2\mu_3}]$, μ_1, μ_2 and μ_3 are material parameters and depends at most on $\mathbf{P}$. Substituting the above in equations (3.9) through (3.13)

$$\begin{aligned}\delta_0 &= \frac{\mu_1^3}{\Delta}\left[-\frac{J_1^r}{J_3^{r5}}(\mu_2-1)^3 + \frac{1}{J_3^{r3}}(2\mu_2 - J_2^r\mu_m^r)(\mu_2-1)^2\right.\\ &\qquad \left. -\frac{1}{J_3^r}\left(J_2^r\mu_2^2 + \left(\frac{\mu_m^r}{J_3^r}\right)^2\right)(\mu_2-1) - \mu_2^2\frac{\mu_m^r}{J_3^r}\right], \qquad (3.64)\end{aligned}$$

$$\delta_1 = \frac{\mu_1^2}{\Delta}\left[\frac{2}{J_3^{r2}}\mu_m^r(\mu_2-1) + \mu_2^2 + \frac{J_2^r}{J_3^{r2}}(\mu_2-1)^2\right], \qquad (3.65)$$

$$\delta_2 = -\frac{\mu_1(\mu_2-1)}{J_3^r\Delta}, \qquad \kappa_2 = \frac{\mu_1\mu_2}{J_3^r\Delta}, \qquad (3.66)$$

$$\kappa_1 = -\frac{\mu_1^2}{J_3^{r2}\Delta}\left[2\mu_2\mu_m^r + J_1^r\mu_2^2 + \frac{(\mu_2-1)^2}{J_3^{r2}}\right], \qquad (3.67)$$

$$\begin{aligned}\kappa_0 &= \frac{\mu_1^3}{\Delta}\left[\frac{J_2^r}{J_3^r}\mu_2^3 + [J_1^r\mu_m^r - 2(\mu_2-1)]\frac{\mu_2^2}{J_3^{r3}} + \left(\mu_m^{r2} + \frac{J_1^r}{J_3^{r2}}(\mu_2-1)^2\right)\frac{\mu_2}{J_3^{r3}}\right.\\ &\qquad \left. +\frac{\mu_m^r}{J_3^{r5}}(\mu_2-1)^2\right], \qquad (3.68)\end{aligned}$$

$$\Delta = \mu_1^3\left[\frac{\mu_2^3}{J_3^r} - \frac{J_1^r}{J_3^{r3}}(\mu_2-1)\mu_2^2 + \frac{J_2^r}{J_3^{r3}}(\mu_2-1)^2\mu_2 - \frac{1}{J_3^{r5}}(\mu_2-1)^3\right], \qquad (3.69)$$

where $\mu_m^r = (J_3^r)^{2\mu_3} - \mu_2[(J_3^r)^{2\mu_3} + (J_3^r)^{-2\mu_3}]$ and hence

$$\begin{aligned}\mathbf{T} &= \frac{\mu_1}{\widetilde{J}_{m3}}\left\{\mu_m\mathbf{1} + \mu_2\mathbf{H}_t\left[\delta_0\mathbf{1} + \delta_1\mathbf{T}^o + \delta_2\mathbf{T}^{o2}\right]\mathbf{H}_t^t\right.\\ &\qquad \left. +(\mu_2-1)\mathbf{H}_t^{-t}\left[\kappa_0\mathbf{1} + \kappa_1\mathbf{T}^o + \kappa_2\mathbf{T}^{o2}\right]\mathbf{H}_t^{-1}\right\}, \qquad (3.70)\end{aligned}$$

obtained from (3.22) assuming $\Delta \neq 0$. In fact, it can be easily shown that $\Delta \neq 0$, when $0 \leq \mu_2 \leq 1$, the region of interest.

Next, the requirement that $\mathbf{T} = \mathbf{T}^o$ when $\mathbf{H}_t = \mathbf{1}$ and $\vartheta = \vartheta_o$, requires

$$\frac{J_1^r\mu_1\mu_2(J_3^r-1)(\mu_2-1)^3}{J_3^r\left(\mu_2^3[J_3^{r4} + (J_2^r - J_1^r)J_3^{r2}] + \mu_2^2[J_1^r - 2J_2^r]J_3^{r2} + \mu_2 J_2^r J_3^{r2} + (1-\mu_2)^3\right)} = 0. \qquad (3.71)$$

Hence, $\mu_2 = 0$ or $\mu_2 = 1$ or $J_3^r = 1$ to satisfy the above equation. The requirement

(3.33) results in a set of three nonlinear equations which has to be solved numerically. Since, here we do not study in any detail the general Blatz-Ko model no details of the same is presented.

Then, when $\mu_2 = 1$, we obtain a special form of the Blatz-Ko constitutive relation used to study the response of polyurethane. For this case

$$\alpha_0 = -\frac{\mu_1}{J_{m3}^{[2\mu_3+1]}}, \qquad \alpha_1 = \frac{\mu_1}{J_{m3}}, \qquad \alpha_2 = 0. \tag{3.72}$$

Now, we compute

$$\begin{aligned}
\delta_0 &= \frac{1}{(J_3^r)^{2\mu_3}}, \qquad \delta_1 = \frac{J_3^r}{\mu_1}, \qquad \delta_2 = 0, \\
\kappa_0 &= J_2^r - \frac{J_1^r}{(J_3^r)^{2(\mu_3+1)}} + \frac{1}{(J_3^r)^{2(2\mu_3+1)}}, \kappa_1 = \frac{1}{\mu_1}\left[\frac{2}{(J_3^r)^{(2\mu_3+1)}} - \frac{J_1^r}{J_3^r}\right], \kappa_2 = \frac{1}{\mu_1^2},
\end{aligned}$$

from the results presented in equations (3.64) to (3.69). Then, the stress is given by

$$\mathbf{T} = -\frac{\mu_1}{\widetilde{J}_{m3}^{[2\mu_3+1]}}\mathbf{1} + \frac{1}{\widetilde{J}_{m3}}\mathbf{H}_t\left[\frac{\mu_1}{(J_3^r)^{2\mu_3}}\mathbf{1} + J_3^r\mathbf{T}^o\right]\mathbf{H}_t^t. \tag{3.73}$$

In this case, the requirement that $\mathbf{T} = \mathbf{T}^o$ when $\mathbf{H}_t = \mathbf{1}$ and $\vartheta = \vartheta_o$, places no restriction. The condition (3.33) requires

$$\begin{aligned}
J_1^r &= \frac{2}{(J_3^r)^{2\mu_3}} + (J_3^r)^{4\mu_3+2} - \frac{(J_3^r)^{2(\mu_3+1)}}{\mu_1^2}\left[\frac{K_3}{\mu_1}(J_3^r)^{2\mu_3+1} + K_2\right], \\
J_2^r &= \frac{J_1^r}{(J_3^r)^{2(\mu_3+1)}} - \frac{1}{(J_3^r)^{2(2\mu_3+1)}} + \frac{1}{(J_3^r)^{2\mu_3}}\left[1 - \frac{K_3 J_3^r}{\mu_1^3}\right], \\
0 &= (J_3^r)^{-2\mu_3} + J_3^r\frac{K_1}{\mu_1} + \frac{(J_3^r)^{2(\mu_3+1)}}{\mu_1^2}\left[\frac{K_3}{\mu_1}(J_3^r)^{2\mu_3+1} + K_2\right] - (J_3^r)^{2(2\mu_3+1)}
\end{aligned} \tag{3.74}$$

First, the equation (3.74c) is solved for J_3^r using bisection algorithm and then substituted in (3.74a) and (3.74b) to obtain J_1^r and J_2^r respectively. Thus, in this case, $\mathbf{T}^o$ and material parameters μ_1 and μ_3 have to be specified.

Next, we study the case, when $\mu_2 = 0$, a special form of the Blatz-Ko relation

used to study the response of foam rubber. For this case

$$\alpha_0 = \mu_1 J_{m3}^{[2\mu_3+1]}, \qquad \alpha_1 = 0 \qquad \alpha_2 = -\frac{\mu_1}{J_{m3}}. \tag{3.75}$$

Equations (3.64) to (3.69) simplifies to

$$\begin{aligned}
\delta_0 &= J_1^r J_3^r - J_2^r (J_3^r)^{2(\mu_3+1)} + (J_3^r)^{2(2\mu_3+1)}, \delta_1 = \frac{J_2^r J_3^{r3} - 2(J_3^r)^{(2\mu_3+3)}}{\mu_1}, \delta_2 = \frac{J_3^{r4}}{\mu_1^2}, \\
\kappa_0 &= (J_3^r)^{2\mu_3}, \qquad \kappa_1 = -\frac{J_3^r}{\mu_1}, \qquad \kappa_2 = 0,
\end{aligned}$$

for this case and hence, the stress is given by

$$\mathbf{T} = \mu_1 \widetilde{J}_{m3}^{[2\mu_3-1]} \mathbf{1} - \frac{1}{\widetilde{J}_{m3}} \mathbf{H}_t^{-t} \left[\mu_1 (J_3^r)^{2\mu_3} \mathbf{1} - J_3^r \mathbf{T}^o \right] \mathbf{H}_t^{-1}. \tag{3.76}$$

As before, while the requirement that $\mathbf{T} = \mathbf{T}^o$ when $\mathbf{H}_t = \mathbf{1}$ and $\vartheta = \vartheta_o$, places no restriction, (3.33) results in

$$\begin{aligned}
J_2^r &= 3(J_3^r)^{2\mu_3} - J_3^r \frac{K_1}{\mu_1}, \\
J_1^r &= J_2^r (J_3^r)^{2\mu_3+1} - (J_3^r)^{4\mu_3+1} + (J_3^r)^{-(2\mu_3+1)} + \frac{K_3}{\mu_1^3} (J_3^r)^{-(2(\mu_3+2))}, \\
0 &= \left[\frac{K_1}{\mu_1} - (J_3^r)^{2\mu_3-1} \right] (J_3^r)^{2(\mu_3+2)} + \left[1 + \frac{K_3}{\mu_1^3} J_3^{r5} \right] (J_3^r)^{1-2\mu_3} - \frac{K_2}{\mu_1^2} J_3^{r5}.
\end{aligned} \tag{3.77}$$

First, we solve the nonlinear equation (3.77c) for J_3^r and substitute it (3.77a) and (3.77b) to obtain J_2^r and J_1^r respectively. Thus, for this case too, $\mathbf{T}^o$ and material parameters μ_1 and μ_3 have to be specified.

2. Exponential constitutive relation from a stressed reference configuration

From (2.97) we obtain

$$\alpha_0 = \mu_1 \mu_2 \exp(Q) \left[\widetilde{J}_{m1} - \frac{5}{\widetilde{J}_{m3}^2} \right], \qquad \alpha_1 = 2\mu_1 \mu_2 \exp(Q), \qquad \alpha_2 = 0, \tag{3.78}$$

where $Q = \mu_2 \left[\widetilde{J}_{m1}\widetilde{J}_{m3} + \frac{5}{\widetilde{J}_{m3}} - 8\right]$, while the material parameter μ_2 is a positive constant, the parameter μ_1 is a function of $\mathbf{P}$ but $\mu_1(\mathbf{P}) > 0$. Then, from equations (3.9) through (3.13) we compute

$$\begin{aligned}
\delta_0 &= -\frac{J_1^r}{2} + \frac{5}{2(J_3^r)^2}, \qquad \delta_1 = \frac{\exp(-Q^r)}{2\mu_1\mu_2}, \qquad \delta_2 = 0, \\
\kappa_0 &= J_2^r + \frac{J_1^r}{2(J_3^r)^2}\left[J_1^r - \frac{5}{(J_3^r)^2}\right] + \frac{1}{4(J_3^r)^2}\left[J_1^r - \frac{5}{(J_3^r)^2}\right]^2, \\
\kappa_1 &= -\frac{\exp(-Q^r)}{2(J_3^r)^2\mu_1\mu_2}\left[2J_1^r - \frac{5}{(J_3^r)^2}\right], \qquad \kappa_2 = \frac{\exp(-2Q^r)}{4\mu_1^2\mu_2^2(J_3^r)^2},
\end{aligned} \tag{3.79}$$

where $Q^r = \mu_2\left[J_1^r J_3^r + \frac{5}{J_3^r} - 8\right]$. The stress is now given by

$$\mathbf{T} = \mu_1\mu_2\exp(Q)\left\{\left(\widetilde{J}_{m1} - \frac{5}{\widetilde{J}_{m3}^2}\right)\mathbf{1} + 2\mathbf{H}_t\left[\delta_0\mathbf{1} + \delta_1\mathbf{T}^o\right]\mathbf{H}_t^t\right\}. \tag{3.80}$$

where

$$\widetilde{J}_{m1} = \delta_0\widetilde{J}_1 + \delta_1\widetilde{J}_4, \qquad \widetilde{J}_{m3} = J_3^r\widetilde{J}_3. \tag{3.81}$$

The requirement $\mathbf{T} = \mathbf{T}^o$ when $\mathbf{H}_t = \mathbf{1}$ and $\vartheta = \vartheta_o$, translates into requiring $3\delta_0 + \delta_1 tr(\mathbf{T}^o) = J_1^r$ which yields

$$J_1^r = \frac{3}{(J_3^r)^2} + \exp(-Q^r)\frac{tr(\mathbf{T}^o)}{5\mu_1\mu_2}. \tag{3.82}$$

On substituting (3.79) into (3.33), we obtain

$$\begin{aligned}
J_2^r &= \frac{2J_3^{r2}}{5 - J_1^r J_3^{r2}}\left[1 - \frac{K_3\exp(-3Q^r)}{8\mu_1^3\mu_2^3 J_3^{r2}}\right] + \frac{J_1^r}{2J_3^{r2}}\left[\frac{5}{J_3^{r2}} - J_1^r\right] - \frac{1}{4J_3^{r2}}\left[J_1^r - \frac{5}{J_3^{r2}}\right]^2, \\
0 &= 2J_1^r - \frac{5}{J_3^{r2}} + \frac{K_3 J_3^{r4}\exp(-3Q^r)}{2\mu_1^3\mu_2^3(5 - J_1^r J_3^{r2})^2} + \frac{K_2 J_3^{r2}\exp(-2Q^r)}{2\mu_1^2\mu_2^2(5 - J_1^r J_3^{r2})} - \frac{4J_3^{r6}}{(5 - J_1^r J_3^{r2})^2}, \\
0 &= K_3\frac{\exp(-3Q^r)}{8\mu_1^3\mu_2^3} + K_2\frac{\exp(-2Q^r)}{4\mu_1^2\mu_2^2}\delta_0 + K_1\frac{\exp(-Q^r)}{2\mu_1\mu_2}\delta_0^2 + \delta_0^3 - J_3^{r2},
\end{aligned} \tag{3.83}$$

The nonlinear equations (3.83b) and (3.83c) are solved simultaneously by Newton's method for J_1^r and J_3^r in the neighborhood of $(3, 1)$ respectively. Then, equation

(3.83a) is used to compute J_2^r. The so determined value of J_i^r satisfies (3.82), when verified numerically. Thus, in this case material parameters μ_1 and μ_2 needs to be specified apart from $\mathbf{T}^o$.

F. Representation for infinitesimal deformation from a stressed reference configuration

In many instances like in the study of the response of metals, finding approximate solutions to boundary value problems, stability of solutions, one is interested in small deformations from a stressed reference configuration. In this section, we develop representations for the same. Usually (see Truesdell and Noll [22], Ieşan [16]), Taylor series expansion of the stress about the stressed reference configuration, is used to obtain this representation. Here we shall linearize (3.22) to obtain the representation for infinitesimal deformation from a stressed reference configuration.

We begin with the following definitions:

$$\mathbf{K} = \mathbf{F}_t - \mathbf{1}, \quad \widetilde{\mathbf{K}} = \mathbf{H}_t - \mathbf{1}, \tag{3.84}$$

$$\mathbf{E} = \mathbf{K} + \mathbf{K}^t, \quad \widetilde{\mathbf{E}} = \widetilde{\mathbf{K}} + \widetilde{\mathbf{K}}^t, \tag{3.85}$$

$$\epsilon = tr(\mathbf{K}\mathbf{K}^t), \quad \widetilde{\epsilon} = tr(\widetilde{\mathbf{K}}\widetilde{\mathbf{K}}^t), \tag{3.86}$$

where $\mathbf{K}$ denotes gradient of displacement from a stress-free configuration and $\widetilde{\mathbf{K}}$ gradient of displacement from a non stress-free configuration.

For a given coordinate basis in the current and the reference configuration, when

$$\epsilon \ll 1, \quad \widetilde{\epsilon} \ll 1, \tag{3.87}$$

we compute

$$(B)_{ij} = \delta_{ij} + (E)_{ij} + o(\epsilon), \qquad (\widetilde{B})_{ij} = \delta_{ij} + (\widetilde{E})_{ij} + o(\widetilde{\epsilon}), \tag{3.88}$$

$$(B^{-1})_{ij} = \delta_{ij} - (E)_{ij} + o(\epsilon), \qquad (\widetilde{B}^{-1})_{ij} = \delta_{ij} - (\widetilde{E})_{ij} + o(\widetilde{\epsilon}), \tag{3.89}$$

$$J_1 = 3 + tr(\mathbf{E}) + o(\epsilon), \qquad \widetilde{J}_1 = 3 + tr(\widetilde{\mathbf{E}}) + o(\widetilde{\epsilon}), \tag{3.90}$$

$$J_2 = 3 - tr(\mathbf{E}) + o(\epsilon), \qquad \widetilde{J}_2 = 3 - tr(\widetilde{\mathbf{E}}) + o(\widetilde{\epsilon}), \tag{3.91}$$

$$J_3 = 1 + \tfrac{1}{2}tr(\mathbf{E}) + o(\epsilon), \qquad \widetilde{J}_3 = 1 + \frac{1}{2}tr(\widetilde{\mathbf{E}}) + o(\widetilde{\epsilon}), \tag{3.92}$$

where δ_{ij} denotes kronecher delta.

It then immediately follows that

$$(T)_{ij} = \alpha_0^l(tr(\mathbf{E}))\delta_{ij} + \alpha_1^l(tr(\mathbf{E}))(E)_{ij} + o(\epsilon), \tag{3.93}$$

where

$$\alpha_0^l(tr(\mathbf{E})) = \alpha_0 + \alpha_1 + \alpha_2, \tag{3.94}$$

$$\alpha_1^l(tr(\mathbf{E})) = \alpha_1 - \alpha_2, \tag{3.95}$$

when stress free reference configuration is used and J_i's are given by (3.90) - (3.92). It is worth while to note that, α_i^l's can be non-linear functions of $tr(\mathbf{E})$. Further, even though α_i^l's are function of all three invariants, they are functions of only $tr(\mathbf{E})$ because, the invariants are computed using (3.90) through (3.92). Thus, the error in the computed stress is due to the error in the estimated value of the matrix components $(B)_{ij}$ and not in the constitutive relation for $\mathbf{T}$.

When $\alpha_0^l(tr(\mathbf{E})) = tr(\mathbf{E})\lambda$ and $\alpha_1^l(tr(\mathbf{E})) = \mu$, where λ and μ are the popular lamè constants, (3.93) reduces to

$$(T)_{ij} = tr(\mathbf{E})\lambda\delta_{ij} + \mu(E)_{ij}. \tag{3.96}$$

Thus, when

$$\alpha_1 - \alpha_2 = \mu, \tag{3.97}$$

$$\alpha_0 + \alpha_1 + \alpha_2 = \lambda f(J_1, J_2, J_3), \tag{3.98}$$

where $f(J_1, J_2, J_3)$ is some function such that $f(J_1, J_2, J_3) = tr(\mathbf{E})$ when J_i's are given by equations (3.90) through (3.92), is admissible.

If we use a stressed reference configuration, the linearized representation for the Cauchy stress is given by

$$\begin{aligned}(T)_{ij} = {} & \gamma_0^l \delta_{ij} + \gamma_1^l (\widetilde{E})_{ij} + \gamma_2^l (T^o)_{ij} + \gamma_3^l (T^o)_{ia}(T^o)_{aj} + \gamma_4^l [(\widetilde{K})_{ia}(T^o)_{aj} \\ & + (T^o)_{ia}(\widetilde{K})_{ja}] + \gamma_5^l [(\widetilde{K})_{ia}(T^o)_{ab}(T^o)_{bj} + (T^o)_{ia}(T^o)_{ab}(\widetilde{K})_{jb}] \\ & + \gamma_6^l [(\widetilde{K})_{ai}(T^o)_{aj} + (T^o)_{ia}(\widetilde{K})_{aj}] + \gamma_7^l [(\widetilde{K})_{ai}(T^o)_{ab}(T^o)_{bj} \\ & + (T^o)_{ia}(T^o)_{ab}(\widetilde{K})_{bj}] + o(\widetilde{\epsilon}),\end{aligned} \tag{3.99}$$

where

$$\gamma_0^l(tr(\widetilde{\mathbf{E}}), \mathbf{T}^o) = \alpha_0 + \delta_0 \alpha_1 + \kappa_0 \alpha_2, \tag{3.100}$$

$$\gamma_1^l(tr(\widetilde{\mathbf{E}}), \mathbf{T}^o) = \delta_0 \alpha_1 - \kappa_0 \alpha_2, \tag{3.101}$$

$$\gamma_2^l(tr(\widetilde{\mathbf{E}}), \mathbf{T}^o) = \delta_1 \alpha_1 + \kappa_1 \alpha_2, \tag{3.102}$$

$$\gamma_3^l(tr(\widetilde{\mathbf{E}}), \mathbf{T}^o) = \delta_2 \alpha_1 + \kappa_2 \alpha_2, \tag{3.103}$$

$$\gamma_4^l(tr(\widetilde{\mathbf{E}}), \mathbf{T}^o) = \delta_1 \alpha_1, \qquad \gamma_5^l(tr(\widetilde{\mathbf{E}}), \mathbf{T}^o) = \delta_2 \alpha_1, \tag{3.104}$$

$$\gamma_6^l(tr(\widetilde{\mathbf{E}}), \mathbf{T}^o) = -\kappa_1 \alpha_2, \qquad \gamma_7^l(tr(\widetilde{\mathbf{E}}), \mathbf{T}^o) = -\kappa_2 \alpha_2, \tag{3.105}$$

and

$$\begin{aligned} J_{m1} &= \delta_0[3 + tr(\widetilde{\mathbf{E}})] + \delta_1[\widetilde{\mathbf{E}} \cdot \mathbf{T}^o + tr(\mathbf{T}^o)] + \delta_2[\widetilde{\mathbf{E}} \cdot (\mathbf{T}^o)^2 + tr((\mathbf{T}^o)^2)], \\ J_{m2} &= \kappa_0[3 - tr(\widetilde{\mathbf{E}})] + \kappa_1[tr(\mathbf{T}^o) - \widetilde{\mathbf{E}} \cdot \mathbf{T}^o] + \kappa_2[tr((\mathbf{T}^o)^2) - \widetilde{\mathbf{E}} \cdot (\mathbf{T}^o)^2], \\ J_{m3} &= J_3^r[1 + \frac{1}{2}tr(\widetilde{\mathbf{E}})], \end{aligned} \tag{3.106}$$

and $\widetilde{J}_i$ is given by equations (3.90) through (3.92) and we computed $\mathbf{H}_t^{-1}$ as $(H_t^{-1})_{ij}$ $= \delta_{ij} - (\widetilde{K})_{ij} + o(\widetilde{\epsilon})$. It is evident from equations (3.100) through (3.105) that the value of γ_i^l depends on the stress in the reference configuration, $\mathbf{T}^o$. Hence, even within the context of linearized representations, the incremental stress depends on the state of stress in the reference configuration, a well known result see for example, Truesdell and Noll [22], Biot [23].

Next, we assume that the magnitude of the stress in the stressed reference configuration is small, so that we could assume that the deformation from the stress-free reference configuration to stressed configuration is infinitesimal and use the popular constitutive specification for Cauchy stress, (3.96) from stress-free reference configuration. This permits analytical study of the error in the estimated stresses from the stressed configuration when this dependence on the stress in the reference configuration is not considered.

We next record the expressions required to compute δ_i's, κ_i's. Let $\mathbf{K}_o = \mathbf{F}_o - \mathbf{1}$, $\mathbf{E}_o = \mathbf{K}_o + \mathbf{K}_o^t$, then

$$x = tr(\mathbf{E}_o) = \frac{1}{3\lambda + \mu} tr(\mathbf{T}^o), \tag{3.107}$$

obtained from taking trace of (3.96) and rearranging. Noting,

$$J_1^r = 3 + x, \quad J_2^r = 3 - x, \quad (J_3^r)^2 = 1 + x. \tag{3.108}$$

we compute

$$\frac{1}{(J_3^r)^2} = 1 - x, \quad \frac{J_1^r}{(J_3^r)^2} = 3 - 2x. \tag{3.109}$$

Now, we assume

$$a_0(x) = x\lambda - \mu - 2a_2(x), \qquad a_1(x) = \mu + a_2(x). \tag{3.110}$$

where $a_2(x)$ is still an arbitrary function of x. We observe that equation (3.110) is consistent with requirements (3.97) and (3.98).

Now, we compute linear approximation of δ_i's and κ_i's by substituting the above equations in equations (3.9) through (3.13) as

$$\begin{aligned}
\Delta &= \mu^3 + x\mu^2(2a_2 + \mu), \\
\delta_0 &= \frac{1}{\Delta}\{\mu^3 + x\mu^2(2a_2 + \mu - \lambda) - \lambda x^2[a_2(\lambda + 2\mu) + \mu^2]\}, \\
\delta_1 &= \frac{1}{\Delta}\{\mu^2 + x[2a_2(\lambda + \mu) + \mu^2]\}, \\
\delta_2 &= -\frac{a_2}{\Delta}, \\
\kappa_0 &= \frac{1}{\Delta}\{\mu^3 + x\mu^2(\lambda + \mu + 2a_2) + x^2\lambda[a_2(\lambda + 2\mu) + \mu(\lambda + \mu)]\}, \\
\kappa_1 &= -\frac{1}{\Delta}\{\mu^2 + x[2a_2(\lambda + \mu) + \mu(\mu + 2\lambda)]\}, \\
\kappa_2 &= \frac{\mu + a_2}{\Delta}.
\end{aligned} \tag{3.111}$$

Here we note that to approximate $d_1x + d_2x^2$ as d_1x, when $x \ll 1$ requires a priori estimate of d_i's.

We find it helpful to define $t = tr(\widetilde{\mathbf{E}})$, $\overline{\alpha}_2(t) = \alpha_2(t + x)$ and note that $tr(\mathbf{E}) = t + x$. Now,

$$\alpha_1 = \mu + \overline{\alpha}_2(t), \qquad \alpha_2 = \overline{\alpha}_2(t), \qquad \alpha_0 = (t + x)\lambda - \mu - 2\overline{\alpha}_2(t), \tag{3.112}$$

and observe that the above equations is consistent with the requirement (3.97) and

(3.98) and assumption (3.110).

Using the above equations now we compute γ_i's given by equations (3.100) to (3.105) as

$$\gamma_0^l = t\lambda + (\frac{\lambda}{\mu})^2 \frac{x^2}{[1+x(1+2a_2/\mu)]}(\overline{\alpha}_2 - a_2), \tag{3.113}$$

$$\gamma_1^l = \mu - \frac{x\lambda}{1+x(1+2a_2/\mu)} * \left\{(1+\frac{2\overline{\alpha}_2}{\mu}) + x[(2+\frac{\lambda}{\mu})(\frac{\overline{\alpha}_2+a_2}{\mu} + \frac{2\overline{\alpha}_2 a_2}{\mu^2}) + 1]\right\}, \tag{3.114}$$

$$\gamma_2^l = 1 + \frac{2x\lambda}{[1+x(1+2a_2/\mu)]}\frac{a_2-\overline{\alpha}_2}{\mu^2}, \tag{3.115}$$

$$\gamma_3^l = \frac{1}{1+x(1+2a_2/\mu)}\frac{a_2-\overline{\alpha}_2}{\mu^2}, \tag{3.116}$$

$$\gamma_4^l = \frac{\mu+\overline{\alpha}_2}{\mu}[1 + \frac{2xa_2\lambda}{\mu^2[1+x(1+2a_2/\mu)]}], \tag{3.117}$$

$$\gamma_5^l = -\frac{(\mu+\overline{\alpha}_2)a_2}{\mu^3[1+x(1+2a_2/\mu)]}, \tag{3.118}$$

$$\gamma_6^l = \frac{\overline{\alpha}_2}{\mu}[1 + \frac{2x\lambda(a_2+\mu)}{\mu^2[1+x(1+2a_2/\mu)]}], \tag{3.119}$$

$$\gamma_7^l = -\frac{(\mu+a_2)\overline{\alpha}_2}{\mu^3[1+x(1+2a_2/\mu)]}. \tag{3.120}$$

It could be observed from the above equations that if α_2 is a function of t then all γ_i's are function of t. However, here we study only the case when α_2 is a constant. It then follows that $\overline{\alpha}_2$ is also a constant. Hence, we define

$$\overline{\alpha}_2 = \alpha_2 = a_2 = \kappa, \tag{3.121}$$

a constant that could take any value.

Straight forward computation yields

$$\frac{\lambda}{\mu} = \frac{\nu}{1-2\nu}, \tag{3.122}$$

where ν is the poisson's ratio. For this special case the linearized representation of

Cauchy stress from a stressed reference configuration is given by

$$\begin{aligned}\mathbf{T}-\mathbf{T}^o &= t\lambda\mathbf{1}+(\mu-\mu_e)\widetilde{\mathbf{E}}+\gamma_4^s[\widetilde{\mathbf{K}}\mathbf{T}^o+\mathbf{T}^o\widetilde{\mathbf{K}}^t]+\gamma_5^s[\widetilde{\mathbf{K}}(\mathbf{T}^o)^2+(\mathbf{T}^o)^2\widetilde{\mathbf{K}}^t] \\ &+ \gamma_6^s[\widetilde{\mathbf{K}}^t\mathbf{T}^o+\mathbf{T}^o\widetilde{\mathbf{K}}]+\gamma_7^s[\widetilde{\mathbf{K}}^t(\mathbf{T}^o)^2+(\mathbf{T}^o)^2\widetilde{\mathbf{K}}], \qquad (3.123)\end{aligned}$$

where

$$\mu_e = \frac{x\lambda}{1+x(1+2\kappa/\mu)}\left\{(1+\frac{2\kappa}{\mu})+x[(2+\frac{\lambda}{\mu})(\frac{2\kappa}{\mu}+\frac{2\kappa^2}{\mu^2})+1]\right\}, \qquad (3.124)$$

$$\gamma_4^s = \frac{\mu+\kappa}{\mu}[1+\frac{2x\kappa\lambda}{\mu^2[1+x(1+2\kappa/\mu)]}], \qquad (3.125)$$

$$\gamma_5^s = -\frac{(\mu+\kappa)\kappa}{\mu^3[1+x(1+2\kappa/\mu)]}, \qquad (3.126)$$

$$\gamma_6^s = \frac{\kappa}{\mu}[1+\frac{2x\lambda(\kappa+\mu)}{\mu^2[1+x(1+2\kappa/\mu)]}], \qquad (3.127)$$

$$\gamma_7^s = -\frac{(\mu+\kappa)\kappa}{\mu^3[1+x(1+2\kappa/\mu)]}. \qquad (3.128)$$

obtained by substituting equation (3.121) in equations (3.113) through (3.120).

Figure 3 plots μ_e/μ as a function of $tr(\mathbf{T}^o/\mu)$ fixing the values of κ/μ and ν. Here we have used the equations (3.107) to compute x in terms of $tr(\mathbf{T}^o)$. It immediately transpires from (3.124) that when $\kappa/\mu > \kappa_o(x,\nu)$ [5], $\mu_e > 0$ and vice versa. Further, the value of μ_e depends on the magnitude of κ/μ.

When $\mid 2x\kappa/\mu \mid \ll 1$, $\mid 2x\lambda\kappa/\mu^2 \mid \ll 1$ and $\mid 2x(\kappa/\mu+1)\lambda/\mu \mid \ll 1$ we obtain

$$\gamma_4^s = 1+\frac{\kappa}{\mu}, \quad \gamma_6^s = \frac{\kappa}{\mu}, \quad \gamma_5^s = \gamma_7^s = -\frac{\kappa}{\mu^2}(1+\frac{\kappa}{\mu}). \qquad (3.129)$$

Noting that, the value of the matrix components of $\mathbf{T}^o/\mu$ would be of the order 10^{-3}, therefore if $\kappa/\mu \ll 1000$, then we could neglect the terms like $\mathbf{K}\mathbf{T}^o$, to obtain

$$\mathbf{T}-\mathbf{T}^o = \lambda\mathbf{1}tr(\mathbf{E})+(\mu-\mu_e)\widetilde{\mathbf{E}}. \qquad (3.130)$$

[5] Analytical determination of this parameter is not required for the discussion below

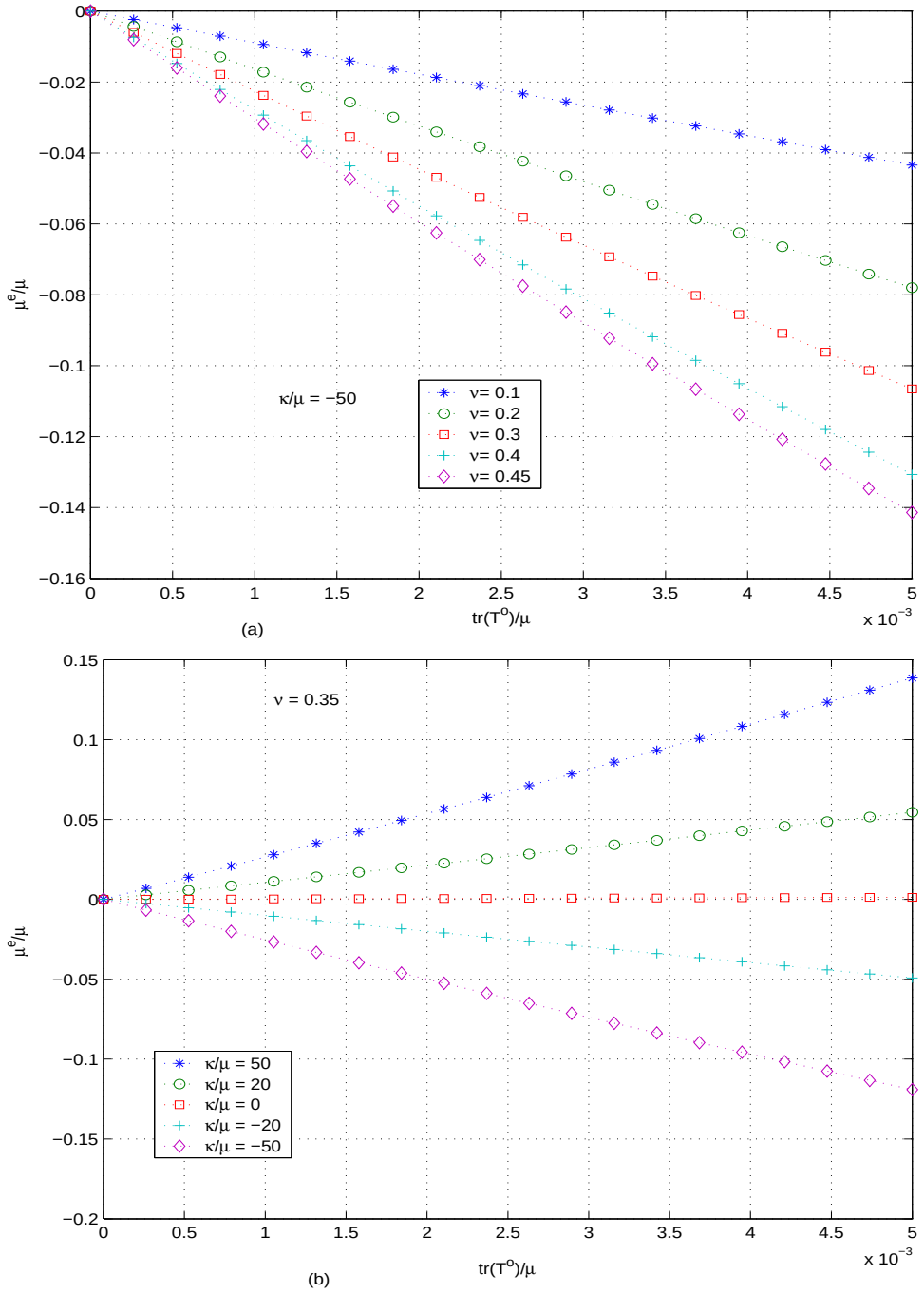

Fig. 3. μ_e/μ vs. $tr(\mathbf{T}^o)/\mu$ when (a) $\kappa/\mu = -50$ for various values of ν (b) $\nu = 0.35$ for various values of κ/μ.

G. Representation for prestresses

In this section, we concern ourself with developing representations for the prestress fields. The purpose of this section is to explore the restrictions and minimum assumptions that could help theoretically determine the prestress field. Later, these competing assumptions can be verified through specific experiments to obtain the prestress field in a given body. We also examine the possibility of representing the prestresses using Fourier series.

The prestress fields has to satisfy balance of linear momentum under static conditions, i.e.,

$$Div(\mathbf{T}^o) + \rho_o \mathbf{b} = \mathbf{0}, \tag{3.131}$$

along with the traction free boundary condition

$$(\mathbf{T}^o)^t \mathbf{n} = \mathbf{0}, \tag{3.132}$$

where, $\mathbf{n}$ is the unit normal on the surface of the body. One of the issues here is whether the body forces can be neglected. Though, it is customary to neglect the body forces, the appropriateness of this requires detailed study. Even though we neglect the body forces, we note that inclusion of them in the procedure outlined below only complicates the algebraic manipulations.

If body forces were to be considered, then it immediately follows that uniform prestress fields is not possible, since the balance of linear momentum (3.131) cannot be satisfied. When $\mathbf{b} = \mathbf{0}$, Hoger [73] showed that the prestress field cannot be uniform. Briefly, in the absence of body forces and traction on the boundary of the body, the volume average of the stresses computed using the mean stress theorem (see Gurtin [74]), is zero. Hence, the cartesian components of the stress should take both positive and negative values in the body. Thus, the prestress field has to be non-uniform.

Now, there are two approaches to specify the prestress field. One of them is to assume that all the points in the body have the same material symmetry and specify the symmetry. Then, the prestress field has to satisfy (3.46), (3.131) and (3.132). However, the requirement that the entire body have the same symmetry is restrictive. See Hoger [63] for details of this approach. Another approach, is to assume that the prestress is a function of the subset of the coordinates, (P, Q, R) and to integrate the reduced balance of linear momentum equations. The reduction made possible due to traction free boundary condition. A variant of this approach was followed by Hoger [73]. Using this approach one can obtain prestress fields such that the entire body has the same symmetry or different symmetries. These methods of prescription of the prestresses is possible because it is not necessary for the prestresses to satisfy the compatibility conditions, since prestresses arise mostly due to misfit of subparts of the body. However, there would arise some restrictions, since we require the prestresses to be relieved by finite number of cuts. We are unable to quantify these restrictions and hence assume that the prescribed prestress fields satisfies these restriction.

It is well known (see Hoger [73]) that the prestress distribution depends on the geometry of the body. Hence, we outline the procedure for obtaining the prestress distribution in three different geometries.

1. Prestress fields in rectangular slabs

First, we consider a body, $\mathcal{B}$ that is a rectangular slab, defined as

$$\mathcal{B} = \{(P, Q, R) | P_1 \leq P \leq P_2, Q_1 \leq Q \leq Q_2, R_1 \leq R \leq R_2\}, \tag{3.133}$$

where (P, Q, R) denote the coordinates of a typical point in Cartesian coordinates. Here P_i's, Q_i's and R_i's are constants and ($\mathbf{E}_p$, $\mathbf{E}_q$, $\mathbf{E}_r$) cartesian coordinate basis.

We begin by exploring the case when $\hat{\mathbf{T}}^o := \mathbf{T}^o(P)$. First, we obtain the restrictions due to traction free boundary condition (3.132). For surfaces, $Q = Q_1$ and $Q = Q_2$ to be traction free, $\mathbf{T}^o(P)\mathbf{E}_q = \mathbf{0}$. Consequently

$$(T^o(P))_{pq} = (T^o(P))_{qq} = (T^o(P))_{qr} = 0. \tag{3.134}$$

Similarly, for surfaces $R = R_1$ and $R = R_2$ to be traction free, the condition $\mathbf{T}^o(P)\mathbf{E}_r = \mathbf{0}$ requires

$$(T^o(P))_{pr} = (T^o(P))_{qr} = (T^o(P))_{rr} = 0. \tag{3.135}$$

Finally, for surfaces $P = P_1$ and $P = P_2$ to be traction free, $\mathbf{T}(P_i)\mathbf{E}_p = \mathbf{0}$ for $i = \{1, 2\}$. Hence

$$(T^o(P_i))_{pp} = (T^o(P_i))_{pq} = (T^o(P_i))_{pr} = 0, \tag{3.136}$$

for $i = \{1, 2\}$. Using (3.134) and (3.135), the balance of linear momentum (3.131) in the absence of body forces requires $(T^o(P))_{pp} = \textit{constant}$. Then, the boundary condition (3.136) implies that $(T^o(P))_{pp} = 0$. Thus, the rectangular slab cannot support prestress fields of the form $\hat{\mathbf{T}}^o := \mathbf{T}^o(P)$.

Next, we consider the case when, $\hat{\mathbf{T}}^o := \mathbf{T}^o(P, Q)$. For this case, the traction free condition (3.132) requires

$$(T^o(P, Q))_{qr} = (T^o(P, Q))_{pr} = (T^o(P, Q))_{rr} = 0, \tag{3.137}$$

$$(T^o(P_i, Q))_{pp} = (T^o(P_i, Q))_{pq} = (T^o(P, Q_i))_{qq} = (T^o(P, Q_i))_{pq} = 0, \tag{3.138}$$

for $i = \{1, 2\}$. Using (3.137), the balance of linear momentum (3.131) reduces to

$$\frac{\partial (T^o)_{pp}}{\partial P} + \frac{\partial (T^o)_{pq}}{\partial Q} = 0, \tag{3.139}$$

$$\frac{\partial (T^o)_{pq}}{\partial P} + \frac{\partial (T^o)_{qq}}{\partial Q} = 0. \tag{3.140}$$

Integrating the above equations, we obtain

$$(T^o)_{pp} = -\int_{P_1}^{P} \frac{\partial (T^o)_{pq}}{\partial Q} dP, \tag{3.141}$$

$$(T^o)_{qq} = -\int_{Q_1}^{Q} \frac{\partial (T^o)_{pq}}{\partial P} dQ. \tag{3.142}$$

Then, for the boundary condition (3.138) to hold

$$(T^o)_{pq}(P_i, Q) = (T^o)_{pq}(P, Q_i) = 0, \tag{3.143}$$

$$\int_{P_1}^{P_2} \frac{\partial (T^o)_{pq}}{\partial Q} dP = \int_{Q_1}^{Q_2} \frac{\partial (T^o)_{pq}}{\partial P} dQ = 0, \tag{3.144}$$

for $i = \{1, 2\}$. A class of function for $(T^o)_{pq}$ that satisfies the requirements (3.143) and (3.144) is

$$(T^o)_{pq} = \epsilon_1 \sin(2\pi k_p \frac{P - P_1}{P_2 - P_1}) \sin(2\pi k_q \frac{Q - Q_1}{Q_2 - Q_1}), \tag{3.145}$$

where k_p and k_q are arbitrary integers and ϵ_1 is a constant. Since, divergence is a linear operator any linear combination of these functions too is admissible, making a Fourier series representation for prestresses possible. Thus, a traction free rectangular slab doesn't ensure stress free condition.

Let us explore the above prestress field. When $(T^o)_{pq}$ is given by (3.145) the normal stress components are given by

$$(T^o)_{pp} = \epsilon_1 \frac{k_q (P_2 - P_1)}{k_p (Q_2 - Q_1)} [\cos(2\pi k_p \frac{P - P_1}{P_2 - P_1}) - 1] \cos(2\pi k_q \frac{Q - Q_1}{Q_2 - Q_1}), \tag{3.146}$$

$$(T^o)_{qq} = \epsilon_1 \frac{k_p (Q_2 - Q_1)}{k_q (P_2 - P_1)} \cos(2\pi k_p \frac{P - P_1}{P_2 - P_1}) [\cos(2\pi k_q \frac{Q - Q_1}{Q_2 - Q_1}) - 1], \tag{3.147}$$

obtained from (3.141) and (3.142) respectively. It follows that the three eigen values of $\mathbf{T}^o$ are $\{0,\ 0.5[(T^o)_{pp} + (T^o)_{qq}] \pm 0.5 \sqrt{[(T^o)_{pp} + (T^o)_{qq}]^2 + 4(T^o)_{pq}^2}\}$. Noting that the matrix components of the stress $(T^o)_{pp}$, $(T^o)_{qq}$, $(T^o)_{pq}$ cannot be identically zero at a material point, we immediately conclude that the three eigen values of $\mathbf{T}^o$ are distinct.

It then, immediately follows from the work of Coleman and Noll [62] and (3.46) that the appropriate symmetry group, (which is a subset of the proper orthogonal group,) for this case is monoclinic. Thus, this procedure permits prestress fields such that the entire body has a particular symmetry.

Following on similar lines if $\hat{\mathbf{T}}^o := \mathbf{T}^o(P,Q,R)$ then we obtain

$$\begin{aligned}
(T^o)_{pp} &= -\int_{P_1}^{P}(\frac{\partial(T^o)_{pq}}{\partial Q}+\frac{\partial(T^o)_{pr}}{\partial R})dP,\\
(T^o)_{qq} &= -\int_{Q_1}^{Q}(\frac{\partial(T^o)_{pq}}{\partial P}+\frac{\partial(T^o)_{qr}}{\partial R})dQ,\\
(T^o)_{rr} &= -\int_{R_1}^{R}(\frac{\partial(T^o)_{pr}}{\partial P}+\frac{\partial(T^o)_{qr}}{\partial Q})dR,
\end{aligned}$$

from integrating the balance of linear momentum (3.131). Further, to ensure traction free conditions (3.132) the functions $(T^o)_{pq}$,$(T^o)_{pr}$ and $(T^o)_{qr}$ should be such that

$$\begin{aligned}
\int_{P_1}^{P_2}(\frac{\partial(T^o)_{pq}}{\partial Q}+\frac{\partial(T^o)_{pr}}{\partial R})dP &= 0,\\
\int_{Q_1}^{Q_2}(\frac{\partial(T^o)_{pq}}{\partial P}+\frac{\partial(T^o)_{qr}}{\partial R})dQ &= 0,\\
\int_{R_1}^{R_2}(\frac{\partial(T^o)_{pr}}{\partial P}+\frac{\partial(T^o)_{qr}}{\partial Q})dR &= 0,
\end{aligned}$$

$$\begin{aligned}
(T^o(P_i,Q,R))_{pq} = (T^o(P,Q_i,R))_{pq} &= 0,\\
(T^o(P_i,Q,R))_{pr} = (T^o(P,Q,R_i))_{pr} &= 0,\\
(T^o(P,Q_i,R))_{qr} = (T^o(P,Q,R_i))_{qr} &= 0,
\end{aligned}$$

for $i = (1, 2)$. A class of functions that satisfy the above requirements is

$$\begin{aligned}
(T^o)_{pq} &= \epsilon_1 \sin(2\pi k_p^1 \frac{P - P_1}{P_2 - P_1}) \sin(2\pi k_q^1 \frac{Q - Q_1}{Q_2 - Q_1}) \sin(2\pi k_r^1 \frac{R - R_1}{R_2 - R_1}), \\
(T^o)_{pr} &= \epsilon_2 \sin(2\pi k_p^2 \frac{P - P_1}{P_2 - P_1}) \sin(2\pi k_q^2 \frac{Q - Q_1}{Q_2 - Q_1}) \sin(2\pi k_r^2 \frac{R - R_1}{R_2 - R_1}), \\
(T^o)_{qr} &= \epsilon_3 \sin(2\pi k_p^3 \frac{P - P_1}{P_2 - P_1}) \sin(2\pi k_q^3 \frac{Q - Q_1}{Q_2 - Q_1}) \sin(2\pi k_r^3 \frac{R - R_1}{R_2 - R_1}),
\end{aligned}$$

as above k_j^i are arbitrary integers and ϵ_i's are constant.

2. Prestress fields in right circular annular cylinders

Next, we consider a body, $\mathcal{B}$ that is the annular region between the two coaxial right circular cylinders:

$$\mathcal{B} = \{(R, \Theta, Z) | R_i \leq R \leq R_o, 0 \leq \Theta \leq 2\pi, Z_b \leq Z \leq Z_e\}. \tag{3.148}$$

where (R, Θ, Z) are coordinates of a typical point in cylindrical polar coordinates and R_i, R_o, Z_b and Z_e are constants.

We begin by examining prestress fields of the form $\hat{\mathbf{T}}^o := \mathbf{T}^o(R)$. Following arguments similar to that described above, if surfaces defined by $R = R_i$, $R = R_o$, $Z = Z_b$, $Z = Z_e$ are traction free, then

$$(T^o(R))_{ZZ} = (T^o(R))_{RZ} = (T^o(R))_{Z\Theta} = 0, \tag{3.149}$$

$$(T^o(R_i))_{RR} = (T^o(R_o))_{RR} = (T^o(R_i))_{R\Theta} = (T^o(R_o))_{R\Theta} = 0. \tag{3.150}$$

Using (3.149), the balance of linear momentum (3.131) reduces to

$$\frac{d(T^o)_{RR}}{dR} + \frac{((T^o)_{RR} - (T^o)_{\Theta\Theta})}{R} = 0, \tag{3.151}$$

$$\frac{d(T^o)_{R\Theta}}{dR} + \frac{2(T^o)_{R\Theta}}{R} = 0. \tag{3.152}$$

These equations can easily be integrated to obtain

$$(T^o)_{R\Theta} = \frac{k}{R^2}, \tag{3.153}$$

$$(T^o)_{RR} = \frac{1}{R}\int_{R_i}^{R}(T^o)_{\Theta\Theta}dR, \tag{3.154}$$

where k is a constant. Then, the boundary condition (3.150) requires that

$$(T^o)_{R\Theta} = 0, \tag{3.155}$$

$$\int_{R_i}^{R_o}(T^o)_{\Theta\Theta}dR = 0. \tag{3.156}$$

Thus, any variation of $(T^o)_{\Theta\Theta}$ with zero mean suffices. For example,

$$\begin{aligned}
(T^o)_{\Theta\Theta} &= \begin{cases} \epsilon_1[1-2*\sum_{n=0}^{k-1}(-1)^n H(\overline{R}-\frac{n}{k})], & k \text{ is even}, \\ \epsilon_1[1-\frac{2k}{(k+1)}\sum_{n=0}^{k-1}(-1)^n H(\overline{R}-\frac{n}{k})], & k \text{ is odd}, \end{cases} \quad \text{PWC Variation} \\
(T^o)_{\Theta\Theta} &= \epsilon_1(1-2\overline{R}), \qquad \text{Linear Variation} \\
(T^o)_{\Theta\Theta} &= \epsilon_1 \sin(2k\pi\overline{R}), \qquad \text{Sinusoidal Variation} \\
(T^o)_{\Theta\Theta} &= \epsilon_1 \cos(2k\pi\overline{R}), \qquad \text{Cosine Variation}
\end{aligned} \tag{3.157}$$

where $\overline{R} = \frac{R-R_i}{R_o-R_i}$, $R_p = \frac{R_i}{(R_o-R_i)}$, ϵ_1 is a constant and k is an integer. Then, we compute T_{RR} from (3.154) as

$$(T^o)_{RR} = \begin{cases} \epsilon_1[\frac{1}{2k}((-1)^m(2m+1)-1)-(-1)^m\overline{R}]\frac{1}{(\overline{R}+R_p)}, & k \text{ is even}, \\ \epsilon_1\{\overline{R}-\frac{k}{(k+1)}[(1+(-1)^m)\overline{R} & \\ \quad -\frac{1}{2k}((-1)^m(2m+1)-1)]\}\frac{1}{(\overline{R}+R_p)}, & k \text{ is odd}, \end{cases} ,$$

for PWC variation, where $m = \text{floor}(k * \overline{R})$[6].

$$
\begin{aligned}
(T^o)_{RR} &= \epsilon_1(1-\overline{R})\overline{R}\frac{1}{(\overline{R}+R_p)}, \qquad \text{Linear Variation} \\
(T^o)_{RR} &= \frac{\epsilon_1}{2k\pi}[1-\cos(2k\pi\overline{R})]\frac{1}{(\overline{R}+R_p)}, \qquad \text{Sinusoidal Variation} \\
(T^o)_{RR} &= \frac{\epsilon_1}{2k\pi}\sin(2k\pi\overline{R})\frac{1}{(\overline{R}+R_p)}, \qquad \text{Cosine Variation}
\end{aligned}
$$

Finally, we shall examine issues regarding material symmetry. The three eigen values for this state of stress are 0, $(T^o)_{RR}$, $(T^o)_{\Theta\Theta}$. The condition (3.156) implies that there exist at least one material point in the body where $(T^o)_{\Theta\Theta} = 0$ and at this location $(T^o)_{RR}$ cannot be zero. Thus, there exist regions in the body where the three eigen values of $\mathbf{T}^o$ are independent and regions where only two eigen values of $\mathbf{T}^o$ are independent. It then follows from (3.46) and the representations given in Coleman and Noll [62] that regions that have three independent eigen values of $\mathbf{T}^o$ have rhombic symmetry while regions that have two independent eigen values of $\mathbf{T}^o$ are transversely isotropic. Thus, stress field of the form $\hat{\mathbf{T}}^o = \mathbf{T}^o(R)$ result in different regions of the body possessing different symmetries.

Next, we consider prestresses of the form $\hat{\mathbf{T}}^o := \mathbf{T}^o(R, Z)$. Since, the reference configuration is free of traction on the boundary

$$
\begin{aligned}
T^o_{RR}(R_i, Z) = T^o_{RR}(R_o, Z) = T^o_{R\Theta}(R_i, Z) = T^o_{R\Theta}(R_o, Z) &= 0, \\
T^o_{RZ}(R_i, Z) = T^o_{RZ}(R_o, Z) = T^o_{RZ}(R, Z_b) = T^o_{RZ}(R, Z_e) &= 0, \\
T^o_{ZZ}(R, Z_b) = T^o_{ZZ}(R, Z_e) = T^o_{Z\Theta}(R, Z_b) = T^o_{Z\Theta}(R, Z_e) &= 0, \qquad (3.158)
\end{aligned}
$$

Apart from satisfying these conditions, the stress field $\mathbf{T}^o$ has to satisfy the balance

[6] 'floor(x)' rounds x to the nearest integer towards $-\infty$.

of linear momentum

$$\begin{aligned}
\frac{\partial T^o_{RR}}{\partial R} + \frac{\partial T^o_{RZ}}{\partial Z} + \frac{T^o_{RR} - T^o_{\Theta\Theta}}{R} &= 0, \\
\frac{\partial T^o_{R\Theta}}{\partial R} + \frac{\partial T^o_{\Theta Z}}{\partial Z} + \frac{2T^o_{R\Theta}}{R} &= 0, \\
\frac{\partial T^o_{RZ}}{\partial R} + \frac{\partial T^o_{ZZ}}{\partial Z} + \frac{T^o_{RZ}}{R} &= 0,
\end{aligned} \tag{3.159}$$

in the absence of body forces. Integrating the above equations we obtain

$$\begin{aligned}
T^o_{RR} &= \frac{1}{R}\int_{R_i}^{R}\left[T^o_{\Theta\Theta} - R\frac{\partial T^o_{RZ}}{\partial Z}\right]dR, \\
T^o_{\Theta Z} &= -\frac{1}{R^2}\int_{Z_b}^{Z}\frac{\partial (T^o_{R\Theta}R^2)}{\partial R}dZ, \\
T^o_{ZZ} &= -\frac{1}{R}\int_{Z_b}^{Z}\frac{\partial (RT^o_{RZ})}{\partial R}dZ.
\end{aligned} \tag{3.160}$$

The boundary conditions (3.158) now require

$$\begin{aligned}
0 &= \frac{1}{R_o}\int_{R_i}^{R_o}\left[T_{\Theta\Theta} - R\frac{\partial T_{RZ}}{\partial Z}\right]dR, \\
0 &= -\frac{1}{R^2}\int_{Z_b}^{Z_e}\frac{\partial (T_{R\Theta}R^2)}{\partial R}dZ, \\
0 &= -\frac{1}{R}\int_{Z_b}^{Z_e}\frac{\partial (RT_{RZ})}{\partial R}dZ,
\end{aligned}$$

Thus, we specify $T^o_{\Theta\Theta}$, T^o_{RZ} and $T^o_{R\Theta}$ such that the above conditions and (3.158)b are met and use equations (3.160) to obtain T^o_{RR}, $T^o_{\Theta Z}$ and T^o_{ZZ}. A set of specification meeting these requirements are

$$\begin{aligned}
T^o_{RZ} &= \epsilon_1 \sin(2\pi K_1 \overline{R})\sin(2\pi L_1 \overline{Z}), \\
T^o_{R\Theta} &= \epsilon_2 \sin(2\pi K_2 \overline{R})\sin(2\pi L_2 \overline{Z}), \\
T^o_{\Theta\Theta} &= \epsilon_3 \sin(2\pi K_3 \overline{R})\sin(2\pi L_3 \overline{Z}) - \epsilon_1 \frac{L_1(R_o - R_i)}{K_1(Z_e - Z_b)}\cos(2\pi L_1 \overline{Z}),
\end{aligned} \tag{3.161}$$

where $\overline{R} = (R - R_i)/(R_o - R_i)$ and $\overline{Z} = (Z - Z_b)/(Z_e - Z_b)$ and K_1, K_2, K_3, L_1, L_2

and L_3 are integers and ϵ_1, ϵ_2 and ϵ_3 are constants. Substituting these in (3.160) we obtain

$$\begin{aligned}
T^o_{RR} &= \frac{\epsilon_3}{2\pi K_3}\frac{R_o-R_i}{R}\left[1-\cos(2\pi K_3\overline{R})\right]\sin(2\pi L_3\overline{Z}) \\
&\quad -\epsilon_1\frac{L_1(R_o-R_i)}{K_1(Z_e-Z_b)}\left\{1-\cos(2\pi K_1\overline{R})-\frac{R_o-R_i}{2\pi K_1 R}\sin(2\pi K_1\overline{R})\right\}\cos(2\pi L_1\overline{Z}), \\
T^o_{\Theta Z} &= -\epsilon_2\frac{Z_e-Z_b}{2\pi L_2}\left[1-\cos(2\pi L_2\overline{Z})\right]\left[\frac{2}{R}\sin(2\pi K_2\overline{R})+\frac{2\pi K_2}{R_o-R_i}\cos(2\pi K_2\overline{R})\right], \\
T^o_{ZZ} &= -\epsilon_1\frac{Z_e-Z_b}{2\pi L_1}\left[1-\cos(2\pi L_1\overline{Z})\right]\left[\frac{1}{R}\sin(2\pi K_1\overline{R})+\frac{2\pi K_1}{R_o-R_i}\cos(2\pi K_1\overline{R})\right].
\end{aligned} \tag{3.162}$$

Thus, for this case too the components of the prestress field that are specified can be represented as a fourier series.

3. Prestress fields in spherical shells

Finally, we consider a body, $\mathcal{B}$ that is the region between the two concentric spheres:

$$\mathcal{B} = \{(R,\Theta,\Phi)|R_i \le R \le R_o, 0 \le \Theta \le 2\pi, 0 \le \Phi \le \pi\}. \tag{3.163}$$

where (R,Θ,Φ) are coordinates of a typical point in spherical coordinates and R_i, R_o are constants.

We examine if the prestress fields of the form $\hat{\mathbf{T}}^o := \mathbf{T}^o(R)$ are possible. Following arguments similar to that proposed above, if surfaces defined by $R = R_i$, $R = R_o$, are traction free, then

$$\begin{aligned}
(T^o(R_i))_{RR} = (T^o(R_o))_{RR} = (T^o(R_i))_{R\Theta} = (T^o(R_o))_{R\Theta} &= 0, \\
(T^o(R_i))_{R\Phi} = (T^o(R_o))_{R\Phi} &= 0.
\end{aligned} \tag{3.164}$$

Now, the balance of linear momentum (3.131) reduces to

$$\frac{d(T^o)_{RR}}{dR} + \frac{1}{R}[2(T^o)_{RR} - (T^o)_{\Theta\Theta} - (T^o)_{\Phi\Phi} + (T^o)_{R\Theta}\cot(\Phi)] = 0, \quad (3.165)$$

$$\frac{d(T^o)_{R\Theta}}{dR} + \frac{1}{R}[3(T^o)_{R\Theta} + ((T^o)_{\Theta\Theta} - (T^o)_{\Phi\Phi})\cot(\Theta)] = 0, \quad (3.166)$$

$$\frac{d(T^o)_{R\Phi}}{dR} + \frac{1}{R}[3(T^o)_{R\Phi} + 2(T^o)_{\Theta\Phi}\cot(\Theta)] = 0. \quad (3.167)$$

Since, $\hat{\mathbf{T}}^o := \mathbf{T}^o(R)$ it is required that

$$(T^o)_{R\Theta} = 0, \qquad (T^o)_{\Theta\Phi} = 0, \qquad (T^o)_{\Theta\Theta} = (T^o)_{\Phi\Phi}, \quad (3.168)$$

so that the balance of linear momentum (3.165) through (3.167) could be satisfied. Substituting (3.168) in equations (3.165) through (3.167) and integrating we obtain

$$(T^o)_{RR} = \frac{2}{R^2}\int_{R_i}^{R} R(T^o)_{\Theta\Theta}dR, \qquad (T^o)_{R\Phi} = t^i_{R\Phi}\frac{R_i^3}{R^3}, \quad (3.169)$$

where $t^i_{R\Phi} = (T^o)_{R\Phi}(R_i)$. It follows from (3.164b) that $t^i_{R\Phi} = 0$ and hence $(T^o)_{R\Phi} = 0$. Also, it follows from (3.164a) that

$$\int_{R_i}^{R_o} R(T^o)_{\Theta\Theta}dR = 0. \quad (3.170)$$

Thus, on prescribing $(T^o)_{\Theta\Theta}$ satisfying (3.170) the entire prestress field is determined. For example

$$(T^o)_{\Theta\Theta} = (T^o)_{\Phi\Phi} = \epsilon_1\cos(2k\pi\overline{R}), \qquad \text{cosine variation}, \quad (3.171)$$

$$(T^o)_{\Theta\Theta} = (T^o)_{\Phi\Phi} = \epsilon_1\left[R - \frac{2(R_o^2 + R_i^2 + R_oR_i)}{3(R_o + R_i)}\right], \quad \text{Linear Variation} \quad (3.172)$$

satisfies the above requirement and hence from (3.169a)

$$(T^o)_{RR} = \epsilon_1\left[\frac{R_o - R_i}{k\pi R}\sin(2k\pi\overline{R}) + \frac{1}{2}\left(\frac{R_o - R_i}{k\pi R}\right)^2\left(\cos(2k\pi\overline{R}) - 1\right)\right], \text{cosine variation},$$

$$(T^o)_{RR} = \epsilon_1\frac{2}{3}\left[R - \frac{R_i^3}{R^2} - \left(1 - \frac{R_i^2}{R^2}\right)\frac{R_o^2 + R_i^2 + R_oR_i}{R_o + R_i}\right], \quad \text{Linear Variation}$$

We again observe that since divergence is a linear operator, a linear combination of the solution (3.171) of the form

$$(T^o)_{\Theta\Theta} = \sum_{i=1}^{n} \epsilon_i \cos(2k_i \pi \overline{R}), \tag{3.173}$$

is also admissible. Thus, prestresses can be represented using Fourier series.

Finally, we end this section with an examination of the material symmetry of a prestressed spherical shell when the prestresses vary only along the radial direction. For this case the principal stresses are $(T^o)_{RR}$, $(T^o)_{\Theta\Theta}$, $(T^o)_{\Phi\Phi}$. From (3.168), $(T^o)_{\Theta\Theta}$ $= (T^o)_{\Phi\Phi}$. Since, in this case at most only two of the three principal stresses are independent, it follows from (3.46) and the representations given in Coleman and Noll [62] that the spherical shell with radially varying prestresses is predominantly transversely isotropic but in regions where $(T^o)_{\Theta\Theta} = (T^o)_{RR}$, it is isotropic.

CHAPTER IV

FORMULATION AND SOLUTION OF BOUNDARY VALUE PROBLEMS

In this chapter, we develop techniques to solve the governing equations that arise from the study of compressible, prestressed and inhomogeneous bodies. Towards this, we first generalize, (2.27) the balance of linear momentum, to the case for which $\mathbf{T}$ is only piecewise continuous. Then, we shall record a general form of the governing equation arising from the study of the static deformation of compressible, prestressed, inhomogeneous bodies and present a possible scheme for solving the governing equation. Then, we simplify the governing equation by assuming specific forms of deformation and representations for stress, recorded in the previous chapter. This serves as examples, illustrating the working and efficacy of the developed scheme. Since, from now on we consider only isothermal response of the body, we shall not specify explicitly the dependence of the constitutive relations on the temperature.

A. Formulation of the boundary value problem

Many a times, the prestresses, $\mathbf{T}^o$ and/or material moduli[1] are only piecewise continuous over the body resulting in the stress, $\mathbf{T}$ to be only piecewise continuous in κ_t. To facilitate the study of these bodies, (2.27) has to be generalized. Towards this, let material points in $\mathcal{B}_s \subseteq \mathcal{B}$, be bijectively mapped to a regular region of the Euclidean space (see Kellogg [58]) in which $\mathbf{T}^o$ and material moduli are differentiable functions. The balance of linear momentum requires

$$\int_{\partial\kappa_t^s} \mathbf{T}\mathbf{n}da + \int_{\kappa_t^s} \rho\mathbf{b}dv = \int_{\kappa_t^s} \rho\frac{d^2\widetilde{\boldsymbol{\chi}}}{dt^2}dv, \tag{4.1}$$

[1]For example the shear modulus.

where κ_t^s is the region occupied by the material points $\mathcal{B}_s$ in the current configuration and $\partial\kappa_t^s$ its boundary, $\mathbf{n}$ is the outward unit normal field to $\partial\kappa_t^s$. Using arguments as outlined in chapter II from (4.1) we obtain

$$div(\mathbf{T}) + \rho\mathbf{b} = \rho\frac{d^2\widetilde{\boldsymbol{\chi}}}{dt^2}, \quad \forall \quad \mathbf{x} \in \kappa_t^s. \tag{4.2}$$

Equivalently (4.1) could be expressed as

$$\int_{\partial\kappa_o^s} \mathbf{T}\mathbf{H}_t^{-t}\mathbf{N}\widetilde{J}_3 dA + \int_{\kappa_o^s} \rho_o\mathbf{b}dV = \int_{\kappa_o^s} \rho_o\frac{d^2\widetilde{\boldsymbol{\chi}}}{dt^2}dV, \tag{4.3}$$

where, κ_o^s is the region occupied by the material points $\mathcal{B}_s$ in the reference configuration and $\partial\kappa_o^s$ its boundary, $\mathbf{N}$ is the outward unit normal field to $\partial\kappa_o^s$, $\rho_o = \rho\widetilde{J}_3$ is the density in the stressed reference configuration. Using standard arguments we obtain

$$\widetilde{Div}(\widetilde{\mathbf{S}}) + \rho_o\mathbf{b} = \mathbf{0}, \quad \forall \quad \mathbf{P} \in \kappa_o^s, \tag{4.4}$$

where we have assumed that $\frac{d^2\widetilde{\boldsymbol{\chi}}}{dt^2} = \mathbf{0}$, since this is the case studied here. We note that while (4.3) has to hold even when κ_o is not a regular region, (4.4) holds only when κ_o is a regular region. In particular, κ_o has to be a bounded closed region and hence (4.4) need not hold for unbounded domains. Thus, none of the techniques or results herein hold for unbounded domains.

For definitiveness we begin by assuming $\partial\kappa_o^s \cap \partial\kappa_o = \emptyset$. Newton's law of action and reaction requires

$$[\mathbf{T}(\mathbf{x}^-) - \mathbf{T}(\mathbf{x}^+)]\mathbf{n}(\mathbf{x}) = \mathbf{0}, \quad \forall \quad \mathbf{x} \in \partial\kappa_t^s, \tag{4.5}$$

where $\mathbf{T}(\mathbf{x}^-)$ is the cauchy stress at $\mathbf{x}$ determined by approaching it through points contained in κ_t^s and $\mathbf{T}(\mathbf{x}^+)$ is the cauchy stress at $\mathbf{x}$ determined by approaching it through points contained in $\kappa_t - \kappa_t^s$. This allows the components of $\mathbf{T}$ to be

discontinuous at $\mathbf{x}$. However, if $\mathbf{T}$ were to be computed using (3.22) then

$$\widetilde{\boldsymbol{\chi}}(\mathbf{P}^-) = \widetilde{\boldsymbol{\chi}}(\mathbf{P}^+) \quad \forall \quad \mathbf{P} \in \partial\kappa_o^s. \tag{4.6}$$

Since $\widetilde{\boldsymbol{\chi}}$ is a bijective mapping, the material points that occupied the surface $\partial\kappa_o^s$ would occupy the surface $\partial\kappa_t^s$ and hence one can specify fields as a function of $\mathbf{x}$ or equivalently as a function of $\mathbf{P}$. Though from a physical standpoint the state variables, like stress, can only be function of $\mathbf{x}$, the bijective mapping, $\widetilde{\boldsymbol{\chi}}$ allows us to mathematically view them as functions of $\mathbf{P}$ for some benefits that this affords.

Now, on the part of the interface, $\partial\kappa_o^s$, that is the boundary of the body, $\mathbf{T}(\mathbf{x}^+)\mathbf{n}$ and $\widetilde{\boldsymbol{\chi}}(\mathbf{P}^+)$ are specified, instead of being computed from equation (4.5) and (4.6) respectively. And hence, the boundary conditions ought to be

$$\begin{aligned} \widetilde{\boldsymbol{\chi}}(\mathbf{P}^-) &= \mathbf{x}_b, \quad \forall \quad \mathbf{P} \in \partial\kappa_o, \\ \mathbf{T}(\widetilde{\boldsymbol{\chi}}(\mathbf{P}^-))\mathbf{n}(\widetilde{\boldsymbol{\chi}}(\mathbf{P}^-)) &= \mathbf{t}_{\mathbf{n}}^b, \quad \forall \quad \mathbf{P} \in \partial\kappa_o. \end{aligned} \tag{4.7}$$

When the deformation is inhomogeneous and/or the body is inhomogeneous the traction is many a times non-uniform. Consequently, rarely can one prescribe (4.7)b in such detail, as required. In experiments or in structural analysis, the quantity that is often estimated or computed is the integrated traction

$$\mathbf{L}_j = \int_{\partial\mathcal{P}_j} \widetilde{J}_3 \mathbf{T}\mathbf{H}_t^{-t}\mathbf{N} \quad dA, \tag{4.8}$$

where, $\mathbf{N}$ is the normal to the boundary of the body in the reference configuration and $\partial\mathcal{P}_j \subseteq \partial\kappa_o$ is a regular surface (see Kellogg [58]) such that $\cup_{j=1}^n \partial\mathcal{P}_j = \partial\kappa_o$. The other global quantity that is of interest is the integrated moment

$$\mathbf{M}_j = \int_{\partial\mathcal{P}_j} \widetilde{J}_3 \mathbf{x} \wedge \mathbf{T}\mathbf{H}_t^{-t}\mathbf{N} \quad dA - \mathbf{r}_o \wedge \mathbf{L}_{\partial\mathcal{P}}. \tag{4.9}$$

Here we have computed the moment about an arbitrary point, identified by its position vector $\mathbf{r}_o$ represented using the coordinate system in the current configuration.

The integrated traction and moment has and can be defined only in the current configuration. However, to facilitate the mathematical computation of the integrated traction or momentum when the coordinates of the material point in the reference configuration are used as independent variables, advantage is taken of the bijective mapping $\widetilde{\boldsymbol{\chi}}(\mathbf{P})$ to obtain the above expressions. Further, equations (4.8) and (4.9) only approximate the requirement (4.7b).

Thus, we have to solve (4.4) subject to the boundary condition (4.7). However, many a times it may not be possible to prescribe boundary condition (4.7b) in such detail. In these cases we solve (4.4) subject to boundary conditions (4.7a), (4.8) and (4.9).

The requirement (4.7) differs from the classical requirement in that both the traction and the deformation have to be specified for the entire boundary of the body. Next, we shall show that mathematically all that is required is the coordinates of some material point in the current configuration and the value of the gradient of the deformation for the same material point, i.e., value of $\widetilde{\boldsymbol{\chi}}$ and $\mathbf{H}_t$ at a material point, given the constitutive relations and the form of the deformation (see for example (4.30)). Thus, if the constitutive relation (including any of the material parameters) and form of the deformation is known or from a purely mathematical standpoint it may suffice to prescribe either the deformation or the traction on the boundary or both the traction and deformation on part of the boundary. In practice, an experimentalist doesn't know the constitutive relation (assuming that the form of the deformation has been inferred from the experiment) and a structural analyst doesn't know the form of the deformation (assuming that the constitutive prescriptions have been made) hence requiring both the traction and the deformation to be specified for

the entire boundary. On the other hand for stimulations, like in the present study, where assumptions are made regarding both the required constitutive relations and form of the deformation, it suffices to prescribe boundary conditions just sufficient to infer the unknown components of $\widetilde{\boldsymbol{\chi}}$ and $\mathbf{H}_t$ at a material point. Then, the traction and/or the deformation on the rest of the boundary, for which they were not specified, is studied and compared for various choices of the constitutive relations and/or forms of the deformation.

B. General solution to the boundary value problem

Substituting (3.22) in (4.4) and grouping we obtain[2]

$$\begin{aligned} a^1_{ijk}(x_{a,b}, x_c, P_d)\frac{\partial^2 x_i}{\partial P_j \partial P_k} &= a^1(x_{a,b}, x_c, P_d), \\ a^2_{ijk}(x_{a,b}, x_c, P_d)\frac{\partial^2 x_i}{\partial P_j \partial P_k} &= a^2(x_{a,b}, x_c, P_d), \\ a^3_{ijk}(x_{a,b}, x_c, P_d)\frac{\partial^2 x_i}{\partial P_j \partial P_k} &= a^3(x_{a,b}, x_c, P_d), \end{aligned} \tag{4.10}$$

$\forall\ \mathbf{P} \in \kappa^s_o$ and where, $i, j, k \in \{1, 2, 3\}$, $j \leq k$[3] and sum over repeated index, $x_{a,b} = \frac{\partial x_a}{\partial P_b}$, x_c the coordinates of a typical material point in the current configuration, P_d the coordinates of a typical material point in the reference configuration. Now, in principal we can solve the above equations for $\frac{\partial^2 x_i}{\partial P_j \partial P_k}$ and obtain

$$\frac{\partial^2 x_i}{\partial P_j \partial P_k} = g_{ijk}(x_{a,b}, x_c, P_d). \tag{4.11}$$

[2]Here a^d_{ijk}'s depends on many other variables, but we highlight only those that are relevant for this study.

[3]Here we assume differentiability of $\frac{\partial^2 x_i}{\partial P_j \partial P_k}$.

It follows from elementary theorems in linear algebra that, there exist many g_{ijk}'s for a given a^d_{ijk}. However, only a subset of them would satisfy the requirements

$$\begin{aligned}
&\frac{Dg_{i11}}{DP_2} = \frac{Dg_{i12}}{DP_1}, \quad \frac{Dg_{i22}}{DP_1} = \frac{Dg_{i12}}{DP_2}, \quad \frac{Dg_{i33}}{DP_1} = \frac{Dg_{i13}}{DP_3} \\
&\frac{Dg_{i11}}{DP_3} = \frac{Dg_{i13}}{DP_1}, \quad \frac{Dg_{i22}}{DP_3} = \frac{Dg_{i23}}{DP_2}, \quad \frac{Dg_{i33}}{DP_2} = \frac{Dg_{i23}}{DP_3},
\end{aligned} \tag{4.12}$$

so that the higher order partial derivatives of x_i are differentiable. Further, partial derivatives of any order of g_{ijk} with respect to P_d should exist. Note that here to compute $\frac{D(\cdot)}{DP_1}$ only P_2 and P_3 are held constant. Hence

$$\frac{Dg_{ijk}}{DP_d} = \frac{\partial g_{ijk}}{\partial P_d} + \frac{\partial g_{ijk}}{\partial x_c} x_{c,d} + \frac{\partial g_{ijk}}{\partial x_{a,b}} g_{abd}, \tag{4.13}$$

sum over repeated index.

We can never obtain the functions g_{ijk} without an assumption on the form of $\widetilde{\boldsymbol{\chi}}$, because equations (4.10)a through (4.10)c, linear in g_{ijk}'s has infinity of possible solutions. Hence, we assume the deformation to be of certain form, as in semi-inverse methods, so that the equations (4.10)a through (4.10)c yield an unique solution for the unknown g_{ijk}. Then, we ensure that the assumed form of the deformation is consistent with the specified boundary condition and the requirement (4.12). This would become clearer as we elaborate further.

For illustration, now let us assume $\kappa^s_o = \kappa_o$. Let (P^g_1, P^g_2, P^g_3), denote the coordinates of a point on the boundary. From the boundary condition (4.7a) we know (x^g_1, x^g_2, x^g_3). Then, the traction boundary condition (4.7b)[4] is used to obtain $x^g_{a,b}$. Since, we have to find the nine unknowns $x^g_{a,b}$ by solving three, probably non-linear, equations obtained from the traction boundary condition, it is quite probable that

[4]Equivalently when (4.7b) has to be approximated by (4.8) and (4.9) then all the components of $x^g_{a,b}$ has to be assumed.

we might need to assume the value of some. The assumed value should result in the boundary condition at all the remaining material points being satisfied. This too would become more evident as we proceed.

Now, we can compute $\mathbf{x}^1$ at $\mathbf{P}^1$ whose coordinates are $(P_1^g + h_1, P_2^g + h_2, P_3^g + h_3)$ from

$$x_c^1(P_1^g + h_1, P_2^g + h_2, P_3^g + h_3) = x_c^g(P_1^g, P_2^g, P_3^g) + \sum_{n=1}^{m} \frac{1}{n!} \left[h_1 \frac{D}{DP_1} + h_2 \frac{D}{DP_2} + h_3 \frac{D}{DP_3} \right]^n (x_c)|_{(P_1,P_2,P_3)=(P_1^g,P_2^g,P_3^g)} + e_m \quad (4.14)$$

where

$$e_m = \frac{1}{(m+1)!} \left[h_1 \frac{D}{DP_1} + h_2 \frac{D}{DP_2} + h_3 \frac{D}{DP_3} \right]^{m+1} (x_c)|_{(P_1,P_2,P_3)=(P_1^g+f_1h_1,P_2^g+f_2h_2,P_3^g+f_3h_3)}, \quad (4.15)$$

with $0 < f_i < 1$. Similarly, we compute $\frac{Dx_c}{DP_d}$ from

$$\frac{Dx_c}{DP_d}|_{(P_1,P_2,P_3)=(P_1^g+h_1,P_2^g+h_2,P_3^g+h_3)} = \sum_{n=1}^{m} \frac{1}{(n-1)!} \left[h_1 \frac{D}{DP_1} + h_2 \frac{D}{DP_2} + h_3 \frac{D}{DP_3} \right]^{n-1} \frac{Dx_c}{DP_d}|_{(P_1,P_2,P_3)=(P_1^g,P_2^g,P_3^g)} + e_m^d \quad (4.16)$$

where

$$e_m^d = \frac{1}{m!} \left[h_1 \frac{D}{DP_1} + h_2 \frac{D}{DP_2} + h_3 \frac{D}{DP_3} \right]^{m} \frac{Dx_c}{DP_d}|_{(P_1,P_2,P_3)=(P_1^g+f_1^*h_1,P_2^g+f_2^*h_2,P_3^g+f_3^*h_3)}, \quad (4.17)$$

with $0 < f_i^* < 1$. Since, we know the function g_{ijk} $(= \frac{D^2x_i}{DP_jDP_k})$ we can compute the higher order partial derivatives, with care being exercised for these partial derivatives only the appropriate P_i's are to be held constant.

For the above series to converge we require

$$\lim_{m\to\infty} e_m \to 0. \quad (4.18)$$

This in turn requires $\frac{D^n x_i}{D^{m_1}P_1 D^{m_2}P_2 D^{m_3}P_3}$ to exist $\forall\ \mathbf{P} \in \kappa_o^s$, where $m_3 = n - (m_1 + m_2)$ and $\frac{D^n x_i}{D^{m_1}P_1 D^{m_2}P_2 D^{m_3}P_3}\big|_{\mathbf{P}=\mathbf{P}_b^-}$ to exist and be bounded $\forall\ \mathbf{P}_b \in \partial\kappa_o^s$ for any given integer value of n, m_1 and m_2, such that $m_1 + m_2 \leq n$. Here $\frac{D^n x_i}{D^{m_1}P_1 D^{m_2}P_2 D^{m_3}P_3}\big|_{\mathbf{P}=\mathbf{P}_b^-}$ denotes the partial derivative computed at $\mathbf{P}_b$ by approaching $\mathbf{P}_b$ from points within κ_o^s. Thus, the partial derivative need not exist at $\mathbf{P}_b$. This translates into requiring $g_{ijk} \in C^\infty(\omega)$ where $\omega = \{(P_i, x_i, x_{a,b}) | P_i^1 \leq P_i \leq P_i^2, x_i^1 \leq x_i \leq x_i^2, x_{ab}^{min} \leq x_{a,b} \leq x_{ab}^{max}\}$, is a 15 dimensional space.

We define[5]

$$\begin{aligned}\epsilon(d_1, d_2, \ldots, d_{12}) &= \int_{\partial\kappa_o} \|\widetilde{\boldsymbol{\chi}}((\mathbf{P}^f)^-) - \mathbf{x}_b\|^2 dA \\ &\quad + \int_{\partial\kappa_o} \|\mathbf{T}(\widetilde{\boldsymbol{\chi}}((\mathbf{P}^f)^-))\mathbf{n}(\widetilde{\boldsymbol{\chi}}((\mathbf{P}^f)^-)) - \mathbf{t}_{\mathbf{n}}^b\|^2 dA, \quad (4.19)\end{aligned}$$

where d_1 through d_9 represent the nine unknowns, $x_{a,b}^g$ and d_{10} through d_{12} represent the three unknowns x_c^g, $\widetilde{\boldsymbol{\chi}}((\mathbf{P}^f)^-)$ and $\mathbf{T}(\widetilde{\boldsymbol{\chi}}((\mathbf{P}^f)^-))\mathbf{n}(\widetilde{\boldsymbol{\chi}}((\mathbf{P}^f)^-))$ is the value of $\widetilde{\boldsymbol{\chi}}$ and traction at $\mathbf{P}^f$ when approached from points in κ_o, for the assumed values of d_i. While the value of some of the d_i^s's would be known a priori, the value of the others would have to be obtained such that $\epsilon(d_1^s, d_2^s, \ldots, d_{12}^s) = 0$. We find it easier and efficient to devise numerical schemes for specific instances instead of a general scheme to obtain the unknown d_i^s. Many such schemes take advantage of the observation

[5]Modified as

$$\begin{aligned}\epsilon(d_1, d_2, \ldots, d_{12}) &= \int_{\partial\kappa_o} \|\widetilde{\boldsymbol{\chi}}((\mathbf{P}^f)^-) - \mathbf{x}_b\|^2 dA \\ &\quad + \sum_{i=1}^{n} \| \int_{\partial\mathcal{P}_i} \widetilde{J}_3 \mathbf{T}((\mathbf{P}^f)^-)\mathbf{H}_t^{-t}\mathbf{N} dA - \mathbf{L}_i\|^2 \\ &\quad + \sum_{i=1}^{n} \| \int_{\partial\mathcal{P}_i} \widetilde{J}_3 \mathbf{x} \wedge \mathbf{T}((\mathbf{P}^f)^-)\mathbf{H}_t^{-t}\mathbf{N} dA - \mathbf{M}_i\|^2,\end{aligned}$$

when the boundary condition (4.7)b is approximated by (4.8) and (4.9) and $\mathbf{L}_i$ is integrated traction and $\mathbf{M}_i$ is integrated moment.

that $\epsilon = 0$ is the minimum.

If we could not find d_i^s's such that $\epsilon = 0$, then the assumed form of the deformation or the constitutive relation or both is not appropriate for the prescribed boundary condition. In particular, for a given constitutive relation this does not mean that there exist no solution for the boundary value problem. We could only conclude that the solution for the boundary value problem does not exist in the assumed form for the deformation. If the form of the deformation and constitutive relation is known to be appropriate then the prescribed boundary conditions is not consistent. In some cases, as in inflation of a spherical shell or annular right circular cylinder, for a given form of deformation and constitutive relation the magnitude of the boundary traction cannot exceed a particular value (see Beatty [68] Chung et. al. [75]).

Extension of the above scheme when $\kappa_o^s \subset \kappa_o$ though straightforward is tedious, in that we would have functions of the form (4.19) for each of the interfaces apart from the boundary of the body. Next, we illustrate how this can be handled in a simple problem.

1. Solution to a special case

For many forms of the deformation studied here, the balance of linear momentum, (4.10) reduces to an equation of the form

$$\frac{d^2r}{dR^2} = f(R, r, d), \tag{4.20}$$

with the requirement

$$r(R_o) = r_o, \qquad h(R_o, r(R_o), d(R_o)) = (T_{rr})_o, \tag{4.21}$$

where, $d = \frac{dr}{dR}$ and $R_i \leq R \leq R_o$. We shall first solve (4.21b) to obtain $d(R_o) = d^o$. Now the solution to (4.20) is given by Taylor's series

$$\begin{aligned} r(R) &= r_o + \frac{(R-R_o)}{1!}d^o + \frac{(R-R_o)^2}{2!}f(R_o, r_o, d^o) + \frac{(R-R_o)^3}{3!}\frac{d^3r}{dR^3}\mid_{R=R_o} \\ &\quad + \cdots + \frac{(R-R_o)^m}{m!}\frac{d^mr}{dR^m}\mid_{R=R_o} + e_m, \end{aligned} \tag{4.22}$$

where[6]

$$\begin{aligned} \frac{d^3r}{dR^3} &:= f_1(R,r,d) = \frac{\partial f}{dR} + d\frac{\partial f}{\partial r} + f\frac{\partial f}{\partial d}, \\ \frac{d^4r}{dR^4} &:= f_2(R,r,d) = \frac{\partial^2 f}{\partial R^2} + 2\left[d\frac{\partial^2 f}{\partial r \partial R} + f\frac{\partial^2 f}{\partial R \partial d} + fd\frac{\partial^2 f}{\partial r \partial d}\right] \\ &\quad + d^2\frac{\partial^2 f}{\partial r^2} + f^2\frac{\partial^2 f}{\partial d^2} + f\left[\frac{\partial f}{\partial d}\right]^2 + d\frac{\partial f}{\partial r}\frac{\partial f}{\partial d} + \frac{\partial f}{\partial d}\frac{\partial f}{\partial R} + f\frac{\partial f}{\partial r}, \\ \frac{d^{m+3}r}{dR^{m+3}} &:= f_{m+1}(R,r,d) = \frac{\partial f_m}{\partial R} + d\frac{\partial f_m}{\partial r} + f\frac{\partial f_n}{\partial d}, \\ e_m &= \frac{(R-R_o)^{m+1}}{(m+1)!}\frac{d^{m+1}r}{dR^{m+1}}\mid_{R=\xi}, \end{aligned} \tag{4.23}$$

$R_i < \xi < R_o$. For the above series to converge we require

$$\lim_{m\to\infty} e_m \to 0. \tag{4.24}$$

If $\frac{d^nr}{dR^n}$ is differentiable in the interval $R_i < R < R_o$ then (4.24) holds. Thus, if $f(R,r,d)$ $\in C^\infty(\omega)$ where $\omega = \{(R,r,d)|R_i \leq R \leq R_o, r_i \leq r \leq r_o, d^{min} \leq d \leq d^{max}\}$[7] then we can find $r(R)$ and/or derivatives of any order. Thus, the governing equation (4.20) with its requirement, (4.21) has a unique solution if

- The equation (4.21b) has an unique solution for the unknown d^o

[6]We follow the standard notation that $\frac{d(\cdot)}{dR}$ denotes the total derivative with respect to R and $\frac{\partial(\cdot)}{\partial R}$ denotes the partial derivative with respect to R.

[7]For cases in which we cannot obtain a priori sharper estimates for r_i, d^{min} and d^{max}, $\omega = \{(R,r,d)|R_i \leq R \leq R_o, 0 < r \leq r_o, 0 < d < \infty\}$.

- $f(R, r, d) \in C^{\infty}(\omega)$.

While the above scheme is implementable in *matlab* or *maple* it is still computationally costly. Hence, for the stimulations here we resort to numerical computation. For this we convert the second order ODE, (4.20) to a system of two first order ODEs by a simple change of variables

$$u = r, \qquad v = r_{,R}. \tag{4.25}$$

Then, the differential equations relating these functions are

$$u_{,R} = v, \qquad v_{,R} = f(R, u, v), \tag{4.26}$$

with the condition

$$u(R_o) = r_o, \qquad v(R_o) = d^o. \tag{4.27}$$

This system of first order ODE's is integrated using ODE45 in *matlab*.

a. Solution scheme for piecewise constant variation

In this case, the material functions and $\mathbf{T}^o$ is piecewise continuous and hence the governing equation (4.20) has to be solved in each sub-domain in which the parameter varies continuously. At the interface, conditions (4.5) and (4.6) has to be satisfied. Here, in other words, we require that there be no de-bonding at the interface.

Now, if R_1, R_2, ..., R_n denote the locations[8] where the material parameter is discontinuous then we begin by solving the governing equation (4.20) with the boundary conditions (4.21) over the domain $R_1 < R \leq R_o$ (instead of over the domain $R_i \leq R \leq R_o$). Now the value of $r(R_1^+) = r_1^+$ and $\frac{dr}{dR}|_{R=R_1^+} = d_1^+$ is known. Then, the

[8] $R = R_j$, a constant, denotes a surface across which the material parameter is discontinuous and $R_1 > R_2 > R_n$.

value of $\frac{dr}{dR}|_{R=R_1^-} = d_1^-$ is obtained by solving[9]

$$y_1(R_1^-, r_1^-, d_1^-) = y_1(R_1^+, r_1^+, d_1^+), \tag{4.28}$$

where the only unknown is d_1^-, since $r_1^- = r_1^+$. Now, we solve the governing equation (4.20) for the condition $r(R_1^-) = r_1^-$ and $\frac{dr}{dR}|_{R=R_1^-} = d_1^-$ over the domain $R_2 < R < R_1$. This process is continued till the other boundary of the body (i.e. $R = R_i$) is reached. Thus, now the governing equation (4.20) with its requirement (4.21) has an unique solution if

- The equation (4.21b) has an unique solution for the unknown d^o
- The equation $y_j(R_j^-, r_j^-, d_j^-) = y_j(R_j^+, r_j^+, d_j^+)$, has an unique solution for the unknown d_j^- for each j
- $f(R, r, d) \in C^\infty(\omega_j)$ where $\omega_j = \{(R, r, d)|R_j < R < R_{j+1}, r_j < r < r_{j+1}, d_j^{min} < d < d_j^{max}\}$[10] for each j

As before, here the governing equations for each subpart of the body is solved numerically.

C. Illustrative examples

In this section, we formulate different classes of boundary value problems along the lines outlined above. While the solution procedure for these class of deformations is independent of the specific constitutive relation, except that it has to satisfy certain restrictions, the actual solution depends on the specific form of the same. Given the

[9]For the assumed form of deformation and hence the stress, the requirement (4.5) reduces to a scalar equation

[10]As before, if sharper estimates for r_i, d_j^{min} and d_j^{max} are not available $\omega_j = \{(R, r, d)|R_j < R < R_{j+1}, 0 < r < r_{j+1}, 0 < d < \infty\}$

work of Ericksen [76] that only homogeneous deformation is possible in all homogeneous compressible bodies, this is at the least surprising.

1. Inflation of a spherical shell

In this subsection we focus on a body, $\mathcal{B}$ that is the annular region between two concentric spheres

$$\mathcal{B} = \{(R, \Theta, \Phi) | R_i \leq R \leq R_o, 0 \leq \Theta \leq 2\pi, 0 \leq \Phi \leq \pi\}. \tag{4.29}$$

and seek a semi-inverse solution of the form

$$r = f(R), \qquad \theta = \Theta, \qquad \phi = \Phi, \tag{4.30}$$

for the deformation in spherical polar coordinates with (R, Θ, Φ) denoting the coordinates of a typical material point in the reference configuration and (r, θ, ϕ) denoting the coordinates of a typical material point in the current configuration. This deformation carries the region between two concentric spheres into a region between two other concentric spheres.

For the assumed deformation, (4.30) the matrix components of deformation gradient and left Cauchy-Green stretch tensor in spherical coordinates are given by

$$\mathbf{H}_t = \begin{pmatrix} r_{,R} & 0 & 0 \\ 0 & \frac{r}{R} & 0 \\ 0 & 0 & \frac{r}{R} \end{pmatrix}, \qquad \widetilde{\mathbf{B}} = \begin{pmatrix} r_{,R}^2 & 0 & 0 \\ 0 & \left(\frac{r}{R}\right)^2 & 0 \\ 0 & 0 & \left(\frac{r}{R}\right)^2 \end{pmatrix}, \tag{4.31}$$

where, $(\cdot)_{,R} = \frac{d(\cdot)}{dR}$, a frequently adopted notation to denote differentiation.

Then, the invariants can be written as

$$\widetilde{J_1} = r_{,R}^2 + 2\left(\frac{r}{R}\right)^2, \qquad \widetilde{J_2} = r_{,R}^{-2} + 2\left(\frac{R}{r}\right)^2, \qquad \widetilde{J_3} = r_{,R}\left(\frac{r}{R}\right)^2, \tag{4.32}$$

For the assumed deformation, (4.30) all other g_{ijk} except g_{111} (i.e., $r_{,RR}$) is zero. Hence, the requirements (4.12) can be met if and only if $\alpha_i = \overline{\alpha}_i(\mathbf{H}_t, \mathbf{T}^o(R), R)$. The prestress fields satisfying this requirement were obtained in section (G.3) of chapter III. The matrix components of this prestresses is

$$\mathbf{T}^o = \begin{pmatrix} T^o_{RR}(R) & 0 & 0 \\ 0 & T^o_{\Theta\Theta}(R) & 0 \\ 0 & 0 & T^o_{\Phi\Phi}(R) \end{pmatrix}, \tag{4.33}$$

in spherical coordinate basis with $T^o_{\Theta\Theta}(R) = T^o_{\Phi\Phi}(R)$. It then follows from equations (3.20) and (3.21) that

$$\begin{aligned} \widetilde{J}_4 &= r^2_{,R} T^o_{RR} + 2T^o_{\Theta\Theta}\left(\frac{r}{R}\right)^2, \qquad \widetilde{J}_5 = r^2_{,R}(T^o_{RR})^2 + 2(T^o_{\Theta\Theta})^2\left(\frac{r}{R}\right)^2, \\ \widetilde{J}_6 &= r^{-2}_{,R} T^o_{RR} + 2T^o_{\Theta\Theta}\left(\frac{R}{r}\right)^2, \qquad \widetilde{J}_7 = r^{-2}_{,R}(T^o_{RR})^2 + 2(T^o_{\Theta\Theta})^2\left(\frac{R}{r}\right)^2, \end{aligned} \tag{4.34}$$

Now, equations (3.16) through (3.18) yields

$$\widetilde{J}_{m1} = r^2_{,R} m_1 + 2\left(\frac{r}{R}\right)^2 m_2, \qquad \widetilde{J}_{m2} = r^{-2}_{,R} m_3 + 2\left(\frac{R}{r}\right)^2 m_4, \qquad \widetilde{J}_{m3} = J^r_3 r_{,R}\left(\frac{r}{R}\right)^2, \tag{4.35}$$

where

$$\begin{aligned} m_1 &= \delta_0 + \delta_1 T^o_{RR} + \delta_2 T^{o2}_{RR}, \qquad m_2 = \delta_0 + \delta_1 T^o_{\Theta\Theta} + \delta_2 T^{o2}_{\Theta\Theta}, \\ m_3 &= \kappa_0 + \kappa_1 T^o_{RR} + \kappa_2 T^{o2}_{RR}, \quad m_4 = \kappa_0 + \kappa_1 T^o_{\Theta\Theta} + \kappa_2 T^{o2}_{\Theta\Theta}. \end{aligned} \tag{4.36}$$

The components of stress in spherical coordinate basis for the special boundary value

problem being studied is

$$\left\{\begin{array}{c} T_{rr} \\ T_{\theta\theta} \\ T_{\phi\phi} \\ T_{r\theta} \\ T_{r\phi} \\ T_{\theta\phi} \end{array}\right\} = \left\{\begin{array}{c} \alpha_0 + \alpha_1 m_1 r_{,R}^2 + \alpha_2 m_3 r_{,R}^{-2} \\ \alpha_0 + \alpha_1 m_2 (\frac{r}{R})^2 + \alpha_2 m_4 (\frac{R}{r})^2 \\ \alpha_0 + \alpha_1 m_2 (\frac{r}{R})^2 + \alpha_2 m_4 (\frac{R}{r})^2 \\ 0 \\ 0 \\ 0 \end{array}\right\}. \tag{4.37}$$

The balance of linear momentum, (4.2) in the absence of body forces and static loading, for the present case, reduces to

$$\frac{dT_{rr}}{dr} + \frac{2}{r}[T_{rr} - T_{\theta\theta}] = 0. \tag{4.38}$$

Recognizing that this equation would reduce to the form

$$f_1 r_{,RR} + f_2 = 0, \tag{4.39}$$

we seek to find f_1 and f_2. Towards this we compute

$$\widetilde{J}_{m1,R} = 2r_{,R} r_{,RR} m_1 + g_1, \tag{4.40}$$

$$\widetilde{J}_{m2,R} = -\frac{2}{r_{,R}^3} r_{,RR} m_3 + g_2, \tag{4.41}$$

$$\widetilde{J}_{m3,R} = J_3^r r_{,RR} \left(\frac{r}{R}\right)^2 + g_3, \tag{4.42}$$

where

$$\begin{aligned} g_1 &= 4\frac{r}{R^2}\left[r_{,R} - \frac{r}{R}\right] m_2 + r_{,R}^2 m_{1,R} + 2\left(\frac{r}{R}\right)^2 m_{2,R}, \\ g_2 &= 4\frac{R}{r^2}\left[1 - \frac{R}{r} r_{,R}\right] m_4 + r_{,R}^{-2} m_{3,R} + 2\left(\frac{R}{r}\right)^2 m_{4,R}, \\ g_3 &= 2J_3^r \frac{r}{R}\left(\frac{r_{,R}}{R} - \frac{r}{R^2}\right) r_{,R} + J_{3,R}^r r_{,R} \left(\frac{r}{R}\right)^2, \end{aligned}$$

$$
\begin{aligned}
m_{1,R} &= \delta_{0,R} + \delta_{1,R} T^o_{RR} + \delta_1 T^o_{RR,R} + \delta_{2,R} T^{o2}_{RR} + 2\delta_2 T^o_{RR} T^o_{RR,R}, \\
m_{2,R} &= \delta_{0,R} + \delta_{1,R} T^o_{\Theta\Theta} + \delta_1 T^o_{\Theta\Theta,R} + \delta_{2,R} T^{o2}_{\Theta\Theta} + 2\delta_2 T^o_{\Theta\Theta} T^o_{\Theta\Theta,R}, \\
m_{3,R} &= \kappa_{0,R} + \kappa_{1,R} T^o_{RR} + \kappa_1 T^o_{RR,R} + \kappa_{2,R} T^{o2}_{RR} + 2\kappa_2 T^o_{RR} T^o_{RR,R}, \\
m_{4,R} &= \kappa_{0,R} + \kappa_{1,R} T^o_{\Theta\Theta} + \kappa_1 T^o_{\Theta\Theta,R} + \kappa_{2,R} T^{o2}_{\Theta\Theta} + 2\kappa_2 T^o_{\Theta\Theta} T^o_{\Theta\Theta,R},
\end{aligned}
$$

Noting

$$
\begin{aligned}
\frac{dT_{rr}}{dR} &= \frac{\partial \alpha_0}{\partial R} + \frac{\partial \alpha_0}{\partial \widetilde{J}_{m1}} \widetilde{J}_{m1,R} + \frac{\partial \alpha_0}{\partial \widetilde{J}_{m2}} \widetilde{J}_{m2,R} + \frac{\partial \alpha_0}{\partial \widetilde{J}_{m3}} \widetilde{J}_{m3,R} \\
&\quad + \left[\frac{\partial \alpha_1}{\partial R} + \frac{\partial \alpha_1}{\partial \widetilde{J}_{m1}} \widetilde{J}_{m1,R} + \frac{\partial \alpha_1}{\partial \widetilde{J}_{m2}} \widetilde{J}_{m2,R} + \frac{\partial \alpha_1}{\partial \widetilde{J}_{m3}} \widetilde{J}_{m3,R} \right] m_1 r^2_{,R} \\
&\quad + \left[\frac{\partial \alpha_2}{\partial R} + \frac{\partial \alpha_2}{\partial \widetilde{J}_{m1}} \widetilde{J}_{m1,R} + \frac{\partial \alpha_2}{\partial \widetilde{J}_{m2}} \widetilde{J}_{m2,R} + \frac{\partial \alpha_2}{\partial \widetilde{J}_{m3}} \widetilde{J}_{m3,R} \right] \frac{m_3}{r^2_{,R}} \\
&\quad + \alpha_1 r^2_{,R} m_{1,R} + \frac{\alpha_2}{r^2_{,R}} m_{3,R} + 2[\alpha_1 m_1 r_{,R} - \frac{\alpha_2}{r^3_{,R}} m_3] r_{,RR}. \qquad (4.43)
\end{aligned}
$$

We find

$$
\begin{aligned}
f_1 &= \left[\frac{\partial \alpha_0}{\partial \widetilde{J}_{m1}} + \frac{\partial \alpha_1}{\partial \widetilde{J}_{m1}} m_1 r^2_{,R} + \frac{\partial \alpha_2}{\partial \widetilde{J}_{m1}} \frac{m_3}{r^2_{,R}} \right] 2 r_{,R} m_1 \\
&\quad - \left[\frac{\partial \alpha_0}{\partial \widetilde{J}_{m2}} + \frac{\partial \alpha_1}{\partial \widetilde{J}_{m2}} m_1 r^2_{,R} + \frac{\partial \alpha_2}{\partial \widetilde{J}_{m2}} \frac{m_3}{r^2_{,R}} \right] \frac{2}{r^3_{,R}} m_3 \\
&\quad + \left[\frac{\partial \alpha_0}{\partial \widetilde{J}_{m3}} + \frac{\partial \alpha_1}{\partial \widetilde{J}_{m3}} m_1 r^2_{,R} + \frac{\partial \alpha_2}{\partial \widetilde{J}_{m3}} \frac{m_3}{r^2_{,R}} \right] J^r_3 \left(\frac{r}{R} \right)^2 + 2[\alpha_1 m_1 r_{,R} - \frac{\alpha_2}{r^3_{,R}} m_3],
\end{aligned}
$$

$$
\begin{aligned}
f_2 &= \left[\frac{\partial \alpha_0}{\partial R} + \frac{\partial \alpha_1}{\partial R} m_1 r^2_{,R} + \frac{\partial \alpha_2}{\partial R} \frac{m_3}{r^2_{,R}} \right] + \left[\frac{\partial \alpha_0}{\partial \widetilde{J}_{m1}} + \frac{\partial \alpha_1}{\partial \widetilde{J}_{m1}} m_1 r^2_{,R} + \frac{\partial \alpha_2}{\partial \widetilde{J}_{m1}} \frac{m_3}{r^2_{,R}} \right] g_1 \\
&\quad + \left[\frac{\partial \alpha_0}{\partial \widetilde{J}_{m2}} + \frac{\partial \alpha_1}{\partial \widetilde{J}_{m2}} m_1 r^2_{,R} + \frac{\partial \alpha_2}{\partial \widetilde{J}_{m2}} \frac{m_3}{r^2_{,R}} \right] g_2 \\
&\quad + \left[\frac{\partial \alpha_0}{\partial \widetilde{J}_{m3}} + \frac{\partial \alpha_1}{\partial \widetilde{J}_{m3}} m_1 r^2_{,R} + \frac{\partial \alpha_2}{\partial \widetilde{J}_{m3}} \frac{m_3}{r^2_{,R}} \right] g_3 + \alpha_1 r^2_{,R} m_{1,R} + \frac{\alpha_2}{r^2_{,R}} m_{3,R} \\
&\quad + 2 \frac{r_{,R}}{r} \left\{ \alpha_1 \left[m_1 r^2_{,R} - m_2 \left(\frac{r}{R} \right)^2 \right] + \alpha_2 \left[\frac{m_3}{r^2_{,R}} - m_4 \left(\frac{R}{r} \right)^2 \right] \right\}. \qquad (4.44)
\end{aligned}
$$

We envisage solving (4.39) for the mixed boundary condition[11]

$$r(R_o) = r_o, \qquad T_{rr}(r_o) = 0, \tag{4.45}$$

by the method outlined in the last section. For the Taylor series to converge we require $f_2/f_1 \in C^\infty(\omega)$ where $\omega = \{(R, r, d)|R_i \leq R \leq R_o, 0 < r \leq r_o, 0 < d < \infty\}$, where $d = r_{,R}$ as before. We find that if $\alpha_i \in C^\infty(\omega_a)$ where $\omega_a = \{(\widetilde{J}_{m1}, \widetilde{J}_{m2}, \widetilde{J}_{m3}, R)|0 < \widetilde{J}_{m1} < \infty, 0 < \widetilde{J}_{m2} < \infty, 0 < \widetilde{J}_{m3} < \infty, R_i \leq R \leq R_o\}$ and if $f_1 \neq 0$ when $(R, r, d) \in \omega$, then $f_2/f_1 \in C^\infty(\omega)$. Of course, if α_i is only piecewise continuous then $f_2/f_1 \in C^\infty(\omega_j^s)$ where $\omega_j^s = \{(R, r, d)|R_j \leq R \leq R_{j+1}, 0 < r \leq r_o, 0 < d < \infty\}$, for $j = \{i, 1, 2, \ldots, n, o\}$, sub-domains in which $\alpha_i \in C^\infty(\omega_a^j)$ where $\omega_a^j = \{(\widetilde{J}_{m1}, \widetilde{J}_{m2}, \widetilde{J}_{m3}, R)|0 < \widetilde{J}_{m1} < \infty, 0 < \widetilde{J}_{m2} < \infty, 0 < \widetilde{J}_{m3} < \infty, R_j \leq R \leq R_{j+1}\}$. For this case, in addition to the above, there should exist a real valued solution to the interface condition, (4.28) for the deformation (4.30) to be realizable in a given body.

a. Blatz-Ko constitutive relation

Next, we study the inflation of a sphere made up of Blatz-Ko material. The Blatz-Ko constitutive relation from a stressed reference configuration was obtained in chapter III section-E. Here we focus on a special form of the Blatz-Ko constitutive relation

[11]Here we take a mathematical viewpoint and present only boundary conditions that are essential to solve the governing equation. We shall assume that on the rest of the boundary the computed traction and deformation is realized. In fact, here we compare the boundary traction and deformation realized at the inner surface of the sphere, resulting from various constitutive prescriptions of prestress fields as indicated in section A.

(3.73), originally introduced to study polyurethane. For this constitutive relation

$$\begin{aligned} f_1 &= \mu_1 \left[m_1 \left(\frac{R}{r}\right)^2 + J_3^r \left(\frac{r}{R}\right)^2 \frac{2\mu_3+1}{\widetilde{J}_{m3}^{2(\mu_3+1)}} \right], \\ f_2 &= \mu_{1,R} \left[\frac{m_1 r_{,R}^2}{\widetilde{J}_{m3}} - \frac{1}{\widetilde{J}_{m3}^{2\mu_3+1}} \right] + \mu_1 \left[\frac{2\mu_3+1}{\widetilde{J}_{m3}^{2(\mu_3+1)}} - \frac{m_1 r_{,R}^2}{\widetilde{J}_{m3}^2} \right] g_3 \\ &\quad + \left\{ r_{,R}^2 m_{1,R} + 2\frac{r_{,R}}{r} \left[m_1 r_{,R}^2 - m_2 \left(\frac{r}{R}\right)^2 \right] \right\} \frac{\mu_1}{\widetilde{J}_{m3}} \end{aligned} \tag{4.46}$$

where now,

$$\begin{aligned} m_1 &= \frac{1}{(J_3^r)^{2\mu_3}} + \frac{J_3^r}{\mu_1} T_{RR}^o, \qquad m_2 = \frac{1}{(J_3^r)^{2\mu_3}} + \frac{J_3^r}{\mu_1} T_{\Theta\Theta}^o, \\ m_{1,R} &= \left[\frac{T_{RR}^o}{\mu_1} - \frac{2\mu_3}{(J_3^r)^{2\mu_3+1}} \right] J_{3,R}^r + \frac{J_3^r}{\mu_1} T_{RR,R}^o - J_3^r T_{RR}^o \frac{\mu_{1,R}}{\mu_1^2}, \quad J_{3,R}^r = \frac{l_1}{l_2}, \end{aligned}$$

$$\begin{aligned} l_1 &= J_3^r \left[\frac{K_{1,R}}{\mu_1} - \frac{K_1}{\mu_1^2}\mu_{1,R} \right] + (J_3^r)^{2\mu_3+1} \left[\left(\frac{K_{3,R}}{\mu_1^3} - \frac{3K_3}{\mu_1^4}\mu_{1,R} \right) (J_3^r)^{2(\mu_3+1)} \right. \\ &\quad \left. + \left(\frac{K_{2,R}}{\mu_1^2} - \frac{2K_2}{\mu_1^3}\mu_{1,R} \right) J_3^r \right], \\ l_2 &= 2(2\mu_3+1)(J_3^r)^{4\mu_3+1} - (2\mu_3+1)(J_3^r)^{2\mu_3} \left[\frac{K_3}{\mu_1^3}(J_3^r)^{2(\mu_3+1)} + J_3^r \frac{K_2}{\mu_1^2} \right] \\ &\quad -(J_3^r)^{2\mu_3+1} \left[2\frac{K_3}{\mu_1^3}(\mu_3+1)(J_3^r)^{2\mu_3+1} + \frac{K_2}{\mu_1^2} \right] + 2\mu_3 (J_3^r)^{-(2\mu_3+1)} - \frac{K_1}{\mu_1}, \\ K_1 &= T_{RR}^o + 2T_{\Theta\Theta}^o, \qquad K_2 = T_{\Theta\Theta}^{o2} + 2T_{RR}^o T_{\Theta\Theta}^o, \qquad K_3 = T_{RR}^o T_{\Theta\Theta}^{o2}, \\ K_{1,R} &= T_{RR,R}^o + 2T_{\Theta\Theta,R}^o, \qquad K_{2,R} = 2T_{\Theta\Theta}^o T_{\Theta\Theta,R}^o + 2[T_{RR,R}^o T_{\Theta\Theta}^o + T_{RR}^o T_{\Theta\Theta,R}^o], \\ K_{3,R} &= T_{RR,R}^o T_{\Theta\Theta}^{o2} + 2T_{RR}^o T_{\Theta\Theta}^o T_{\Theta\Theta,R}^o \end{aligned} \tag{4.47}$$

and we have assumed that μ_3 is a constant. Solving the boundary condition (4.45b) for d^o we obtain

$$d^o = \left(\frac{R_o}{r_o} \right)^{\frac{2\mu_3}{\mu_3+1}}. \tag{4.48}$$

It can be immediately seen that if $\mu_1 \in C^\infty(\omega_R)$ and $T_{\Theta\Theta}^o \in C^\infty(\omega_R)$, where $\omega_R = \{R | R_i \le R \le R_o\}$ then $f_2/f_1 \in C^\infty(\omega)$, provided $f_1 \neq 0$ which in turn requires $\frac{T_{RR}^o}{\mu_1}$

$\neq T_{cr}$, a value which can be determined only numerically. Thus, the constitutive prescription of $T^o_{\Theta\Theta}$[12] should ensure that $f_1 \neq 0$ so that $f_2/f_1 \in C^\infty(\omega)$.

If the variation of μ_1 and/or $\mathbf{T}^o$ is only piecewise continuous, then at the interface (surface defined by $R = \textit{constant}$ across which μ_1 and/or $\mathbf{T}^o$ is discontinuous) we require $T_{rr}(r_j^-) = T_{rr}(r_j^+)$ which translates to finding $(d_j^-)_* > 0$ such that

$$y((d_j^-)_*) = 0, \tag{4.49}$$

where

$$\begin{aligned} y(d_j^-) &= \mu_1(R_j^-)\left\{ d_j^- \frac{m_1(R_j^-)}{J_3^r(R_j^-)}\left(\frac{R_j^-}{r_j^-}\right)^2 - \left[\frac{1}{d_j^- J_3^r(R_j^-)}\left(\frac{R_j^-}{r_j^-}\right)^2\right]^{2\mu_3+1}\right\} \\ &\quad -\mu_1(R_j^+)\left\{ d_j^+ \frac{m_1(R_j^+)}{J_3^r(R_j^+)}\left(\frac{R_j^+}{r_j^+}\right)^2 - \left[\frac{1}{d_j^+ J_3^r(R_j^+)}\left(\frac{R_j^+}{r_j^+}\right)^2\right]^{2\mu_3+1}\right\} \end{aligned} \tag{4.50}$$

In general, it is not possible to solve (4.49) analytically and hence we seek numerical solution using the bisection algorithm. Since, (4.50) is a continuous function in d_j^- and since when $\mu_3 > -0.5$,

$$\lim_{d_j^- \to 0} y(d_j^-) \to -\infty, \qquad \text{and} \lim_{d_j^- \to \infty} y(d_j^-) \to \infty, \tag{4.51}$$

there exist $(d_j^-)_* \in (0, \infty)$ such that $y((d_j^-)_*) = 0$. Further, since (4.50) is monotonic in d_j^- for $d_j^- > 0$, $m_1(R_j^-) > 0$ and $\mu_3 > -0.5$, (4.49) has an unique real valued solution, $(d_j^-)_*$. Thus, the constitutive prescriptions of μ_3 and $T^o_{\Theta\Theta}$ should ensure $m_1 > 0$ and $\mu_3 > -0.5$ so that $f_1 \neq 0$ and hence $f_2/f_1 \in C^\infty(\omega_j^s)$ and (4.49) has an unique solution. Therefore, there exist an unique deformation of the form (4.30) for the class of Blatz Ko constitutive relation studied here when $R_i > 0$, for the assumed variations of μ_1 and $T^o_{\Theta\Theta}$.

[12] T^o_{RR} is derived from $T^o_{\Theta\Theta}$ see section (G.3) of chapter III for details

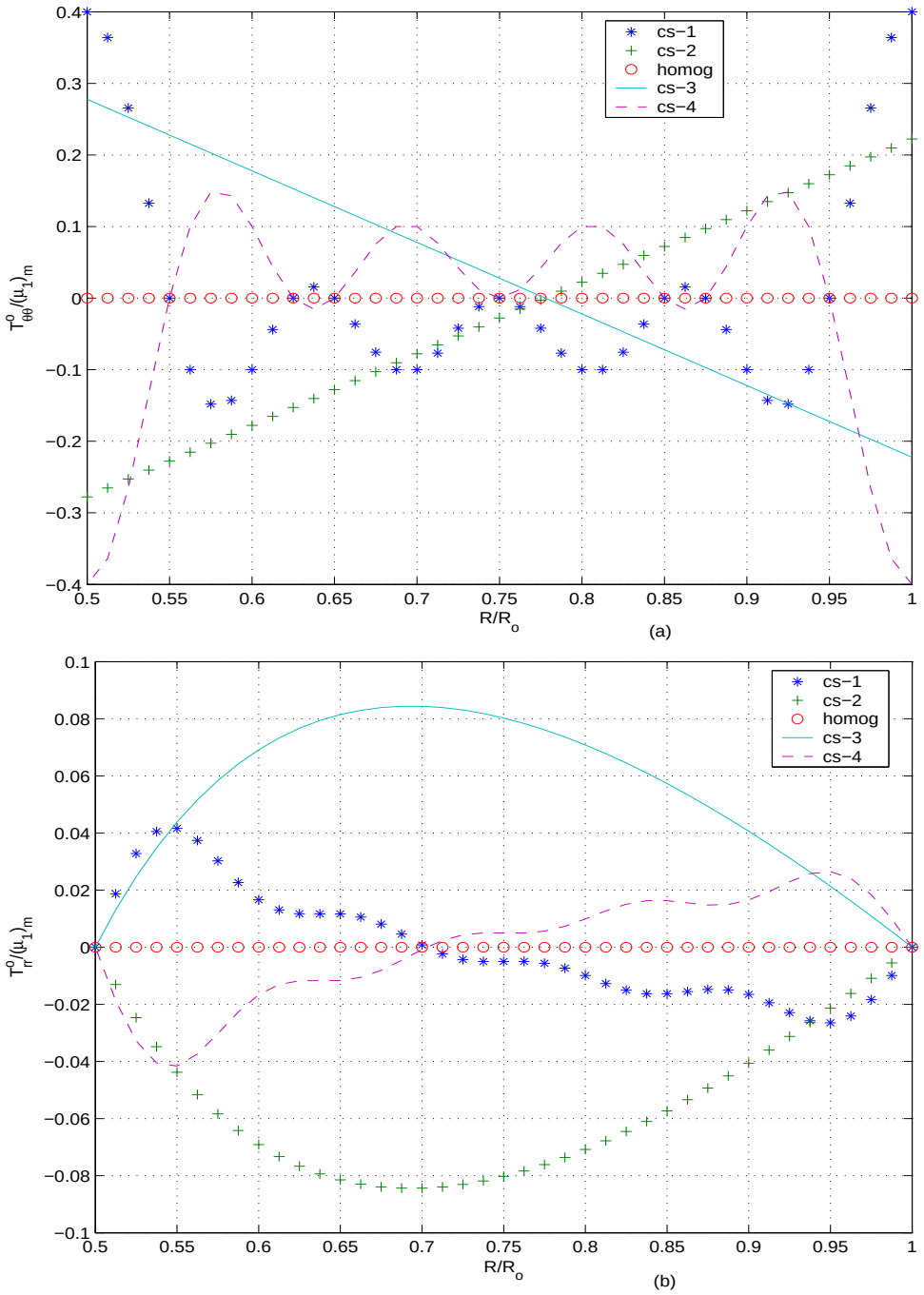

Fig. 4. Plot of prestresses (a) $T^o_{\Theta\Theta}/(\mu_1)_m$ (b) $T^o_{RR}/(\mu_1)_m$ vs. R/R_o in a spherical shell with $R_o = 1$ and $R_i = 0.5$.

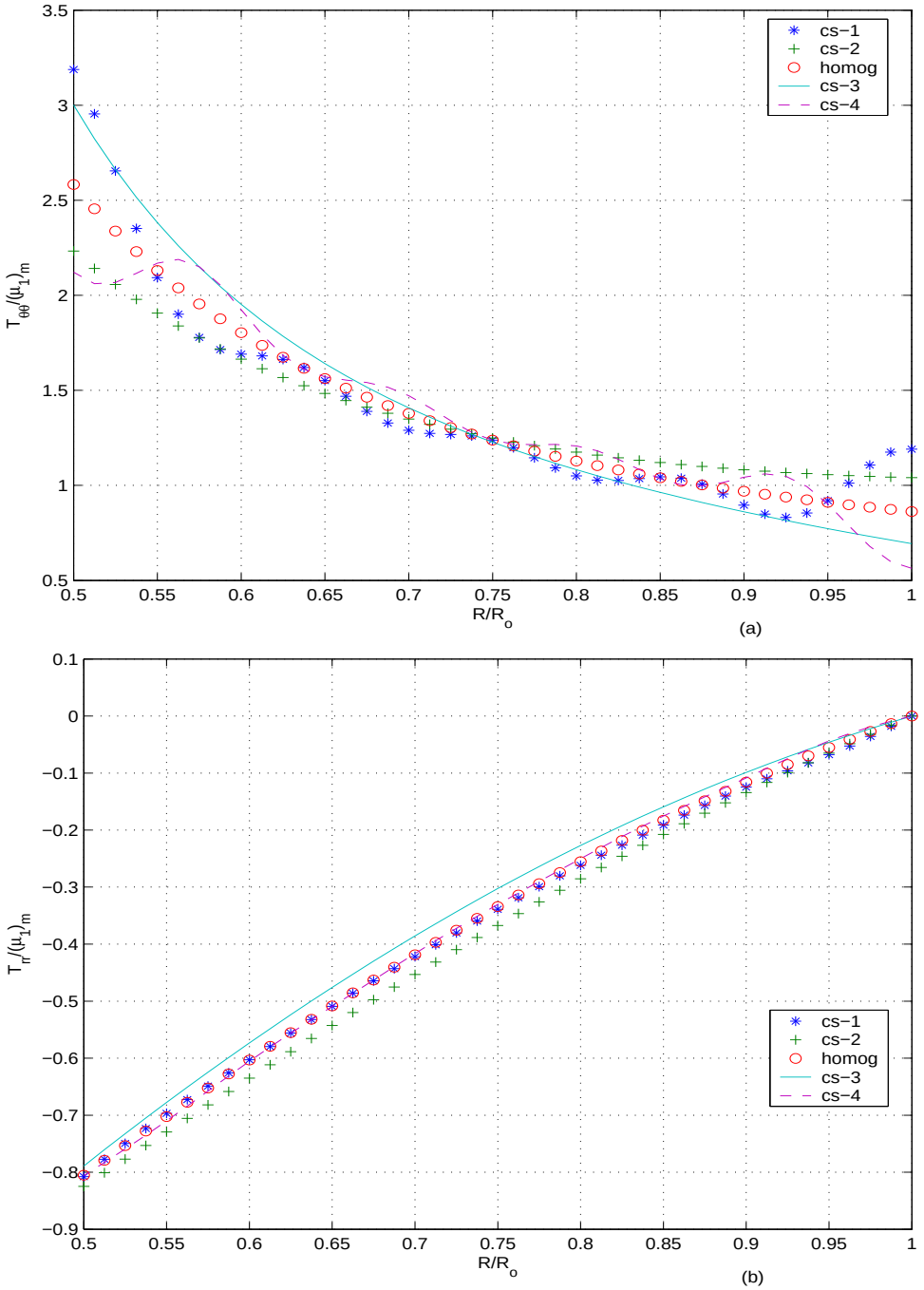

Fig. 5. Plot of stresses (a) $T^o_{\theta\theta}/(\mu_1)_m$ (b) $T^o_{rr}/(\mu_1)_m$ in a spherical shell with $R_o = 1$ and $R_i = 0.5$ made of Blatz Ko material for various prestress distributions shown in figure 4 when $r_o = 1.2R_o$, $\mu_3 = 6.25$ and $\mu_1 = 1$.

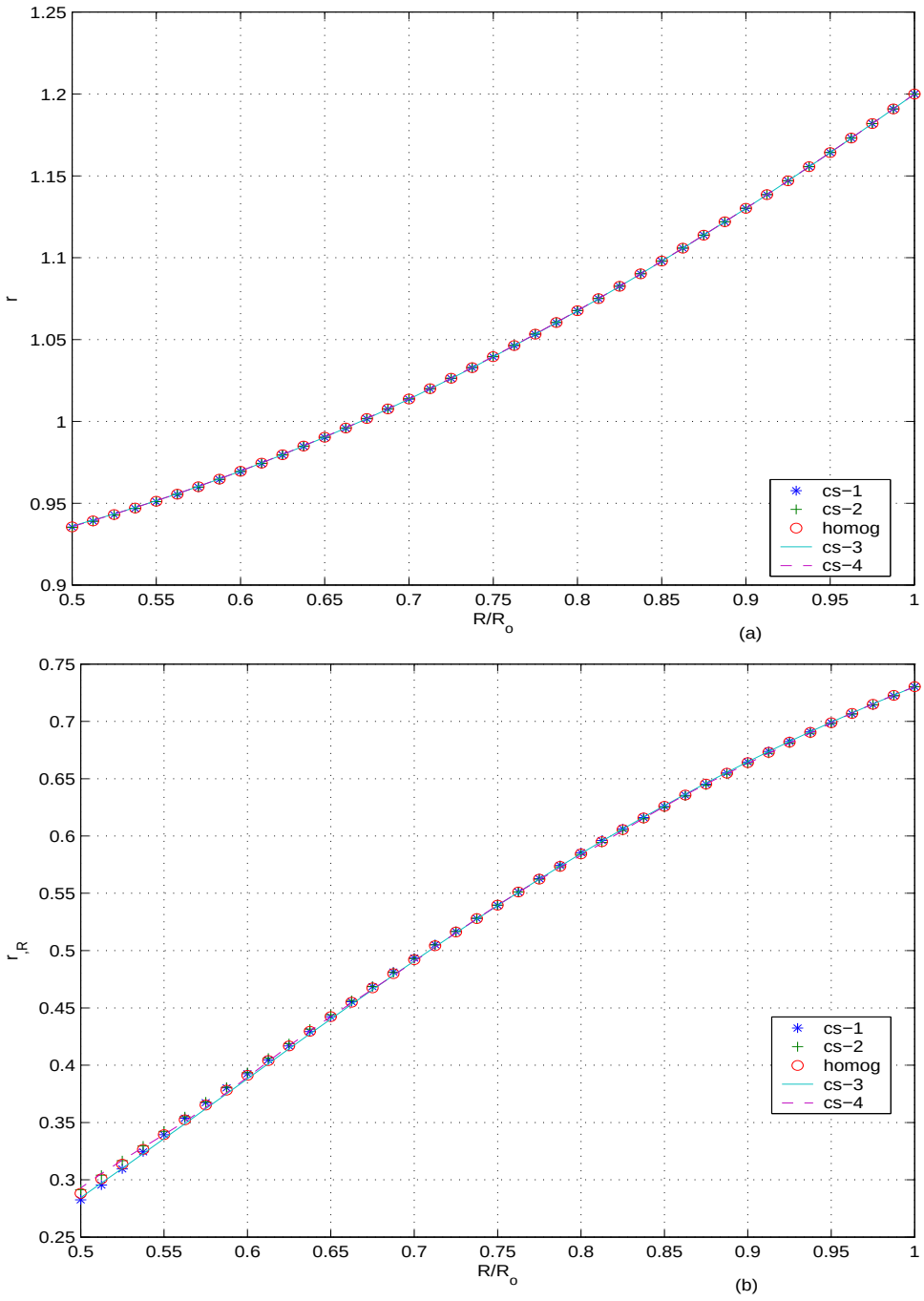

Fig. 6. Plot of (a) r (b) $r_{,R}$ vs. R/R_o in a spherical shell with $R_o = 1$ and $R_i = 0.5$ made of Blatz Ko material for various prestress distributions shown in figure 4 when $r_o = 1.2R_o$, $\mu_3 = 6.25$ and $\mu_1 = 1$.

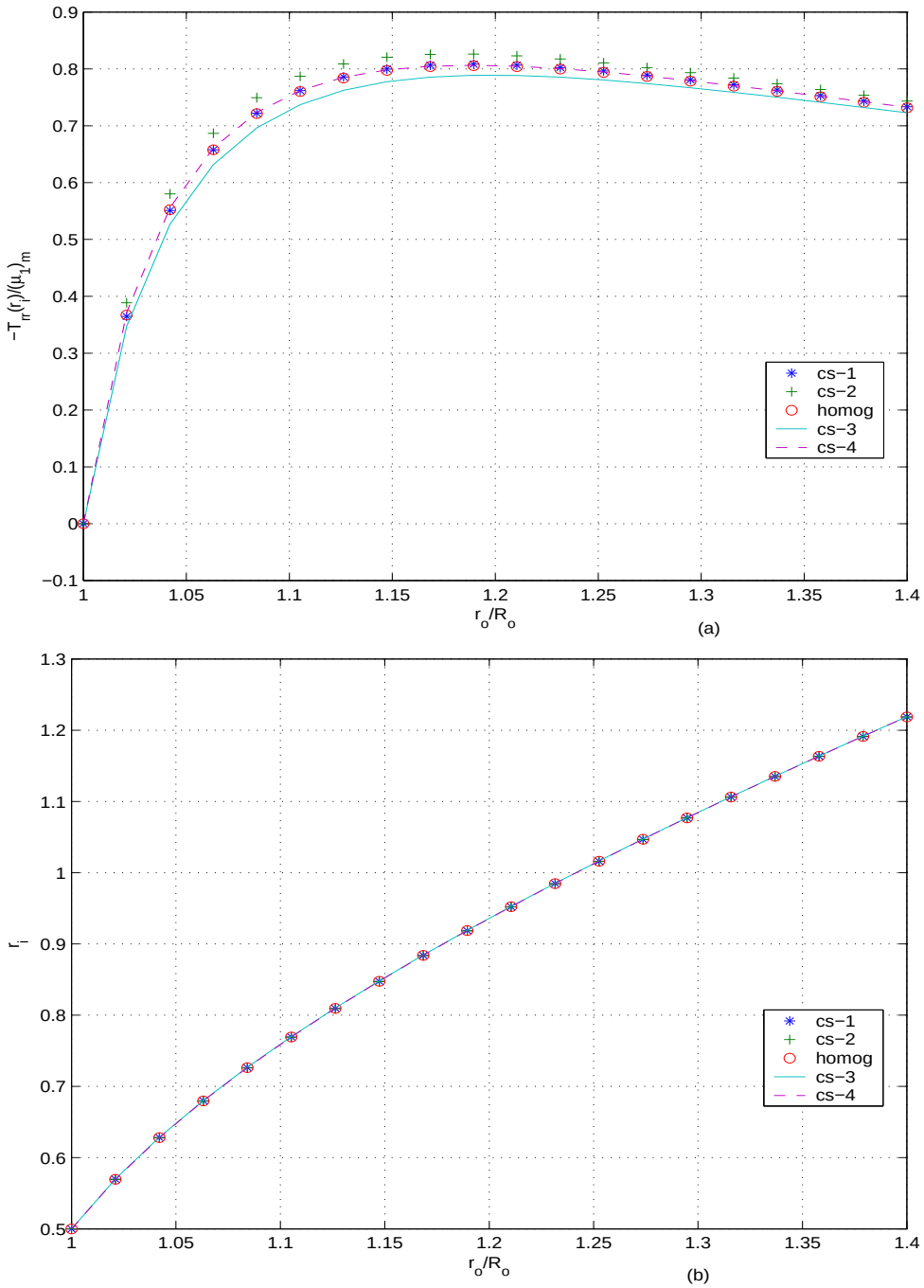

Fig. 7. Plot of (a) $-T_{rr}(r_i)/(\mu_1)_m$ (b) r_i vs. r_o/R_o of a spherical shell with $R_o = 1$ and $R_i = 0.5$ made of Blatz Ko material for various prestress distributions shown in figure 4 when $\mu_3 = 6.25$ and $\mu_1 = 1$.

Figure 4 plots the prestress distributions studied here. 'cs-1' corresponds to the case

$$T^o_{\Theta\Theta} = \epsilon_1 \left[\cos(2\pi\overline{R}) + \cos(4\pi\overline{R}) + \cos(6\pi\overline{R}) + \cos(8\pi\overline{R})\right], \tag{4.52}$$

with $\epsilon_1 = 0.1$ which is the cosine variation recorded in section (G.3) of chapter III. 'cs-2' and 'cs-3' corresponds to the linear variation with $\epsilon_1 = 1$ and $\epsilon_1 = -1$ respectively. For 'cs-4' too, $T^o_{\Theta\Theta}$ is given by (4.52) but now $\epsilon_1 = -0.1$.

Figure 5 plots the stresses and figure 6 plots $r(R)$ and $r_{,R}$ when the spherical shell with $R_o = 1$ and $R_i = 0.5$ is inflated so that $r_o = 1.2R_o$. Here it is assumed that μ_1 is constant over the body, hence $(\mu_1)_m = \mu_1$. It transpires from figure 5a that the stresses in prestressed body can vary by as much as 1.3 times that in the stress free body.

Figure 7 plots $T_{rr}(r_i)$ and r_i vs. r_o for the same cases considered above. It transpires that the radial component of the normal stress required at the inner surface to engender a given inflation differs insignificantly (less than 3 percent) in the prestressed body as opposed to the stress free body, for the cases considered.

b. Exponential constitutive relation

Next, we consider the inflation of a sphere made up of a material whose constitutive relation for stress is given by (3.80). For this constitutive relation

$$\begin{aligned} f_1 &= 2m_1 r_{,R}\left[\alpha_{01} + \alpha_{11}\right] + J^r_3 \left(\frac{r}{R}\right)^2 \left[\alpha_{03} + \alpha_{13}\right] + 4m_1 r_{,R} \\ f_2 &= \frac{\mu_{1,R}}{\mu_1}\left[\widetilde{J}_{m1} - \frac{5}{\widetilde{J}^2_{m3}} + 2m_1 r^2_{,R}\right] + \left[\alpha_{01} + \alpha_{11}\right] g_1 + \left[\alpha_{03} + \alpha_{13}\right] g_3 \\ &\qquad + 2r^2_{,R} m_{1,R} + \frac{4r_{,R}}{r}\left[m_1 r^2_{,R} - m_2 \left(\frac{r}{R}\right)^2\right], \end{aligned}$$

where,

$$\begin{aligned}
\alpha_{01} &= 1+\mu_2\widetilde{J}_{m3}\left[\widetilde{J}_{m1}-\frac{5}{\widetilde{J}^2_{m3}}\right], \qquad \alpha_{03}=\frac{10}{\widetilde{J}^3_{m3}}+\mu_2\left[\widetilde{J}_{m1}-\frac{5}{\widetilde{J}^2_{m3}}\right]^2,\\
\alpha_{11} &= 2\mu_2\widetilde{J}_{m3}m_1 r^2_{,R}, \qquad \alpha_{13}=2\mu_2\left[\widetilde{J}_{m1}-\frac{5}{\widetilde{J}^2_{m3}}\right]m_1 r^2_{,R},
\end{aligned}$$

$$\begin{aligned}
m_1 &= \delta_0+\delta_1 T^o_{RR}, \qquad m_2=\delta_0+\delta_1 T^o_{\Theta\Theta}\\
\delta_0 &= -\frac{J^r_1}{2}+\frac{5}{2(J^r_3)^2}, \qquad \delta_1=\frac{\exp(-Q^r)}{2\mu_1\mu_2},\\
m_{1,R} &= \delta_{0,R}+\delta_{1,R}T^o_{RR}+\delta_1 T^o_{RR,R}, \qquad m_{2,R}=\delta_{0,R}+\delta_{1,R}T^o_{\Theta\Theta}+\delta_1 T^o_{\Theta\Theta,R},
\end{aligned}$$

$$\delta_{0,R}=-\frac{J^r_{1,R}}{2}-\frac{5}{(J^r_3)^3}J^r_{3,R}, \qquad \delta_{1,R}=-\frac{\exp(-Q^r)}{2\mu_1\mu_2}\left[\frac{\mu_{1,R}}{\mu_1}+Q^r_{,R}\right]$$

$$Q^r=\mu_2\left[J^r_1J^r_3+\frac{5}{J^r_3}-8\right], \qquad Q^r_{,R}=\mu_2\left[J^r_{1,R}J^r_3+\left(J^r_1-\frac{5}{(J^r_3)^2}\right)J^r_{3,R}\right],$$

$$J^r_{1,R}=\frac{n_3l_2-n_2l_3}{n_2l_1-n_1l_2}, \qquad J^r_{3,R}=\frac{n_1l_3-n_3l_1}{n_2l_1-n_1l_2},$$

$$\begin{aligned}
l_1 &= 2+\left[\frac{K_3\exp(-Q^r)J^{r2}_3}{\mu^3_1\mu^3_2(5-J^r_1J^{r2}_3)}+\frac{K_2}{2\mu^2_1\mu^2_2}\right]\frac{\exp(-2Q^r)J^{r4}_3}{(5-J^r_1J^{r2}_3)^2}-\frac{8J^{r8}_3}{(5-J^r_1J^{r2}_3)^3}\\
&\quad -\left[\frac{3K_3J^{r2}_3\exp(-Q^r)}{2\mu_1\mu_2(5-J^r_1J^{r2}_3)}+K_2\right]\frac{\exp(-2Q^r)J^{r3}_3}{\mu^2_1\mu_2(5-J^r_1J^{r2}_3)},\\
l_2 &= \frac{10}{J^{r3}_3}-\frac{8J^{r5}_3}{(5-J^r_1J^{r2}_3)^2}\left[3+\frac{2J^r_1J^{r2}_3}{5-J^r_1J^{r2}_3}\right]\\
&\quad +\frac{K_3J^{r3}_3\exp(-3Q^r)}{2\mu^3_1\mu^3_2(5-J^r_1J^{r2}_3)^2}\left[4+\frac{4J^r_1J^{r2}_3}{5-J^r_1J^{r2}_3}-3\left(J^r_1-\frac{5}{J^{r2}_3}\right)\mu_2J^r_3\right]\\
&\quad +\frac{K_2J^r_3\exp(-2Q^r)}{\mu^2_1\mu^2_2(5-J^r_1J^{r2}_3)}\left[1+\frac{J^r_1J^{r2}_3}{5-J^r_1J^{r2}_3}-\left(J^r_1-\frac{5}{J^{r2}_3}\right)\mu_2J^r_3\right],\\
l_3 &= \frac{J^{r4}_3\exp(-3Q^r)}{2\mu^3_1\mu^3_2(5-J^r_1J^{r2}_3)^2}\left[K_{3,R}-\frac{3K_3}{\mu_1}\mu_{1,R}\right]+\frac{J^{r2}_3\exp(-2Q^r)}{2\mu^2_1\mu^2_2(5-J^r_1J^{r2}_3)}\left[K_{2,R}-\frac{2K_2}{\mu_1}\mu_{1,R}\right],
\end{aligned}$$

$$\begin{aligned}
n_1 &= -\left[\frac{3K_3\exp(-3Q^r)}{8\mu^3_1\mu^3_2}+\frac{2K_2\exp(-2Q^r)}{4\mu^2_1\mu^2_2}\delta_0+\frac{K_1\exp(-Q^r)}{2\mu_1\mu_2}\delta^2_0\right]\mu_2J^r_3\\
&\quad -\left[\frac{K_2\exp(-2Q^r)}{4\mu^2_1\mu^2_2}+\frac{K_1\exp(-Q^r)}{\mu_1\mu_2}\delta_0+3\delta^2_0\right]\frac{1}{2},
\end{aligned}$$

$$
\begin{aligned}
n_2 &= -\left[\frac{3K_3\exp(-3Q^r)}{8\mu_1^3\mu_2^3}+\frac{2K_2\exp(-2Q^r)}{4\mu_1^2\mu_2^2}\delta_0+\frac{K_1\exp(-Q^r)}{2\mu_1\mu_2}\delta_0^2\right]\mu_2\left(J_1^r-\frac{5}{J_3^{r2}}\right)\\
&\quad -\left[\frac{K_2\exp(-2Q^r)}{4\mu_1^2\mu_2^2}+\frac{K_1\exp(-Q^r)}{\mu_1\mu_2}\delta_0+3\delta_0^2\right]\frac{5}{J_3^{r3}}-2J_3^r,\\
n_3 &= \frac{\exp(-3Q^r)}{8\mu_1^3\mu_2^3}\left[K_{3,R}-\frac{3K_3}{\mu_1}\mu_{1,R}\right]+\frac{\exp(-2Q^r)}{4\mu_1^2\mu_2^2}\left[K_{2,R}-\frac{2K_2}{\mu_1}\mu_{1,R}\right]\delta_0\\
&\quad +\frac{\exp(-Q^r)}{2\mu_1\mu_2}\left[K_{1,R}-\frac{K_1}{\mu_1}\mu_{1,R}\right]\delta_0^2,\\
K_1 &= T^o_{RR}+2T^o_{\Theta\Theta}, \qquad K_2=T^{o2}_{\Theta\Theta}+2T^o_{RR}T^o_{\Theta\Theta}, \qquad K_3=T^o_{RR}T^{o2}_{\Theta\Theta},\\
K_{1,R} &= T^o_{RR,R}+2T^o_{\Theta\Theta,R}, \qquad K_{2,R}=2T^o_{\Theta\Theta}T^o_{\Theta\Theta,R}+2[T^o_{RR,R}T^o_{\Theta\Theta}+T^o_{RR}T^o_{\Theta\Theta,R}],\\
K_{3,R} &= T^o_{RR,R}T^{o2}_{\Theta\Theta}+2T^o_{RR}T^o_{\Theta\Theta}T^o_{\Theta\Theta,R},
\end{aligned}
$$

The boundary condition (4.45b) requires to find $d^o > 0$ such that $y(d^o) = 0$, where

$$y(d) = 3m_1^o d^4 + 2m_2^o\left(\frac{r_o}{R_o}\right)^2 d^2 - \frac{5}{(J_3^{ro})^2}\left(\frac{R_o}{r_o}\right)^4, \tag{4.53}$$

$m_1^o = m_1(R_o)$, $m_2^o = m_2(R_o)$ and $J_3^{ro} = J_3^r(R_o)$. Solving (4.53) we obtain

$$(d^o)^2 = -\frac{1}{3}m_2^o\left(\frac{r}{R}\right)^2+\frac{1}{3}\sqrt{(m_2^o)^2\left(\frac{r}{R}\right)^4+\frac{15m_1^o}{(J_3^{ro})^2}\left(\frac{R}{r}\right)^4}. \tag{4.54}$$

For a real solution, d^o, to exist we require $m_1^o > 0$, which has to be ensured by constitutive prescriptions of $T^o_{\Theta\Theta}$, μ_1 and μ_2.

As before, if $\mu_1 \in C^\infty(\omega_R)$ and $T^o_{\Theta\Theta} \in C^\infty(\omega_R)$, where $\omega_R = \{R | R_i \le R \le R_o\}$ then $f_2/f_1 \in C^\infty(\omega)$, provided $f_1 \neq 0$. Thus, the constitutive prescription of $T^o_{\Theta\Theta}$, μ_1 and μ_2 should ensure that $f_1 \neq 0$ so that $f_2/f_1 \in C^\infty(\omega)$.

Here it is assumed that μ_1 is constant over the body and the prestress fields are as shown in figure 8. The various prestress field studied here correspond to those discussed above for the Blatz-Ko material but know, $\epsilon_1 = 0.05$ for 'cs-1' and $\epsilon_1 = -0.05$ for 'cs-4' and the value of ϵ_1 for other cases are same as before. Figure 9 plots the stresses, T_{rr} and $T_{\theta\theta}$ and figure 10 plots $r(R)$ and $r_{,R}$ when the spherical shell

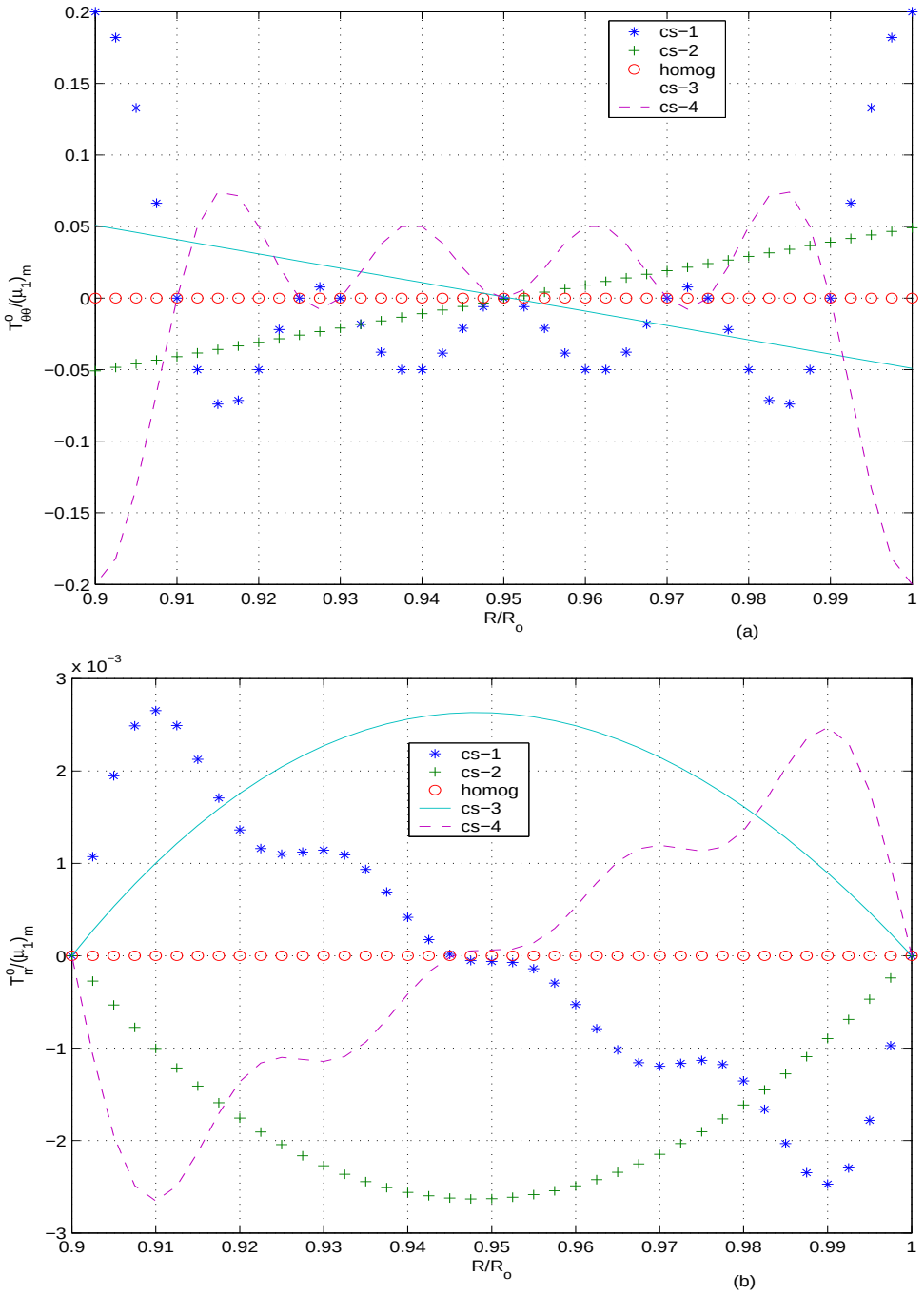

Fig. 8. Plot of prestresses (a) $T^o_{\Theta\Theta}/(\mu_1)_m$ (b) $T^o_{RR}/(\mu_1)_m$ vs. R/R_o in a spherical shell with $R_o = 1$ and $R_i = 0.5$.

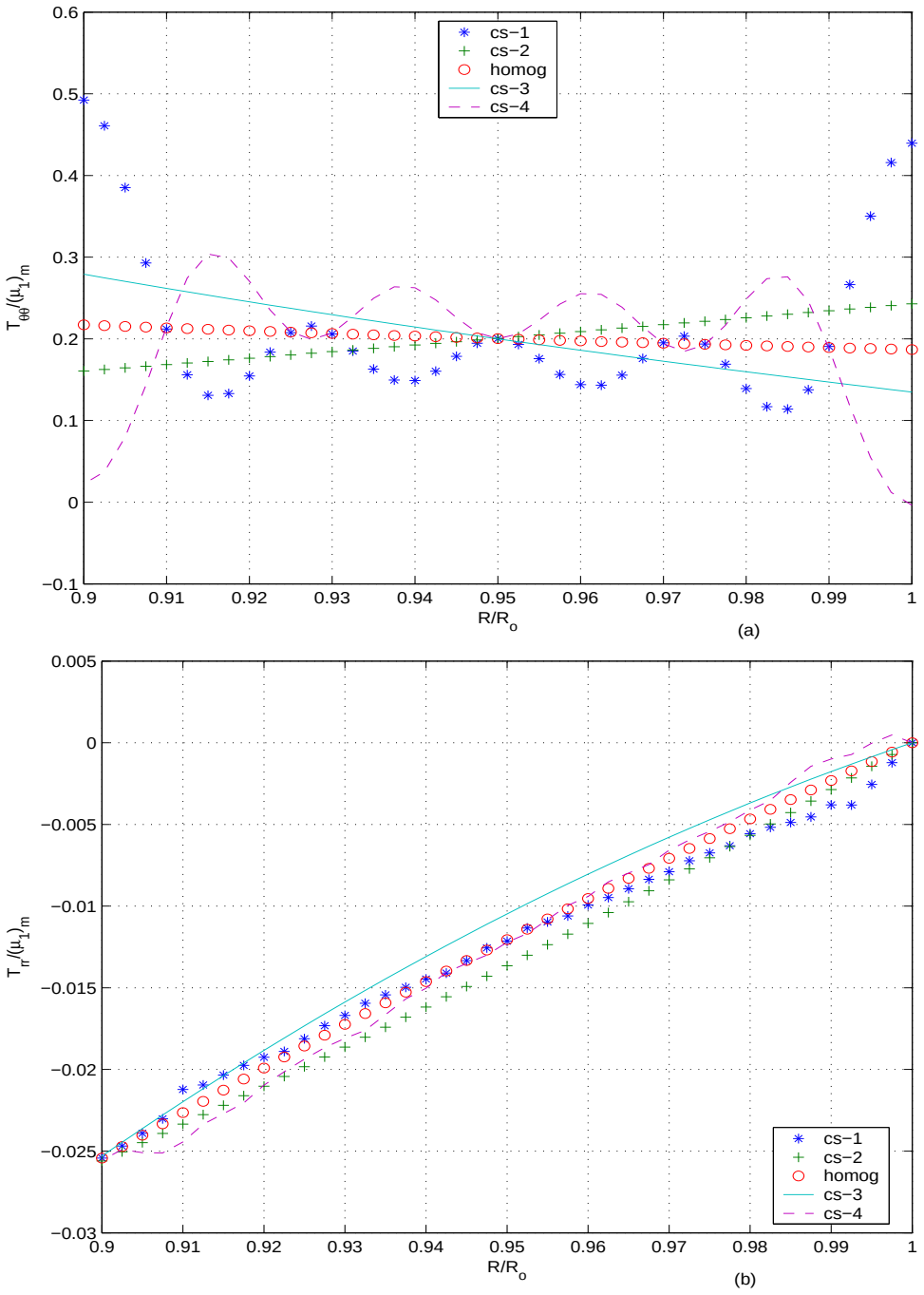

Fig. 9. Plot of stresses (a) $T_{\theta\theta}/(\mu_1)_m$ (b) $T_{rr}/(\mu_1)_m$ in a spherical shell with $R_o = 1$ and $R_i = 0.9$ made of biological material for various prestress distributions shown in figure 8 when $r_o = 1.2R_o$, $\mu_2 = 0.1$ and $\mu_1 = 1$.

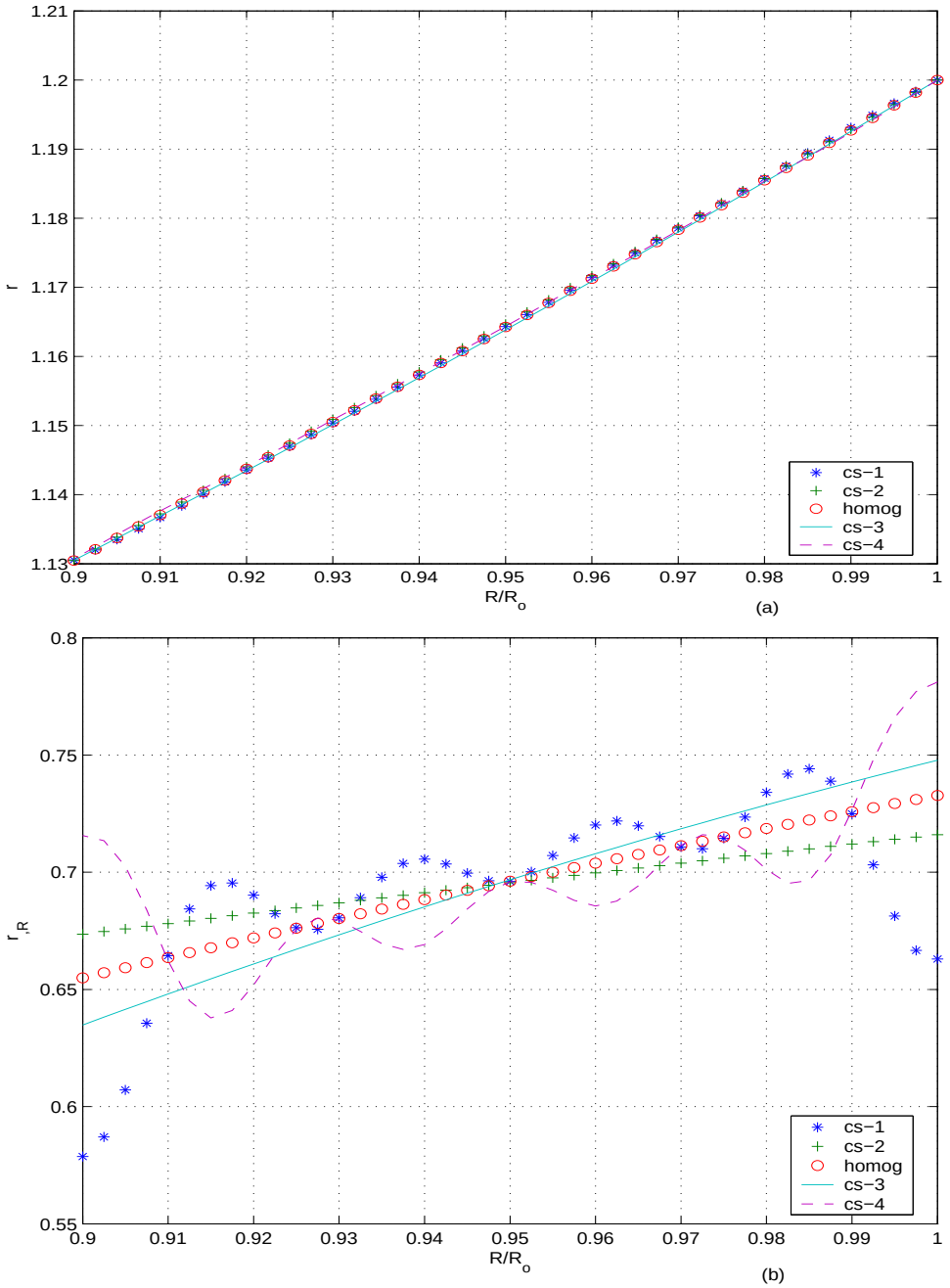

Fig. 10. Plot of (a) r (b) $r_{,R}$ vs. R/R_o in a spherical shell with $R_o = 1$ and $R_i = 0.9$ made of biological material for various prestress distributions shown in figure 8 when $r_o = 1.2R_o$, $\mu_2 = 0.1$ and $\mu_1 = 1$.

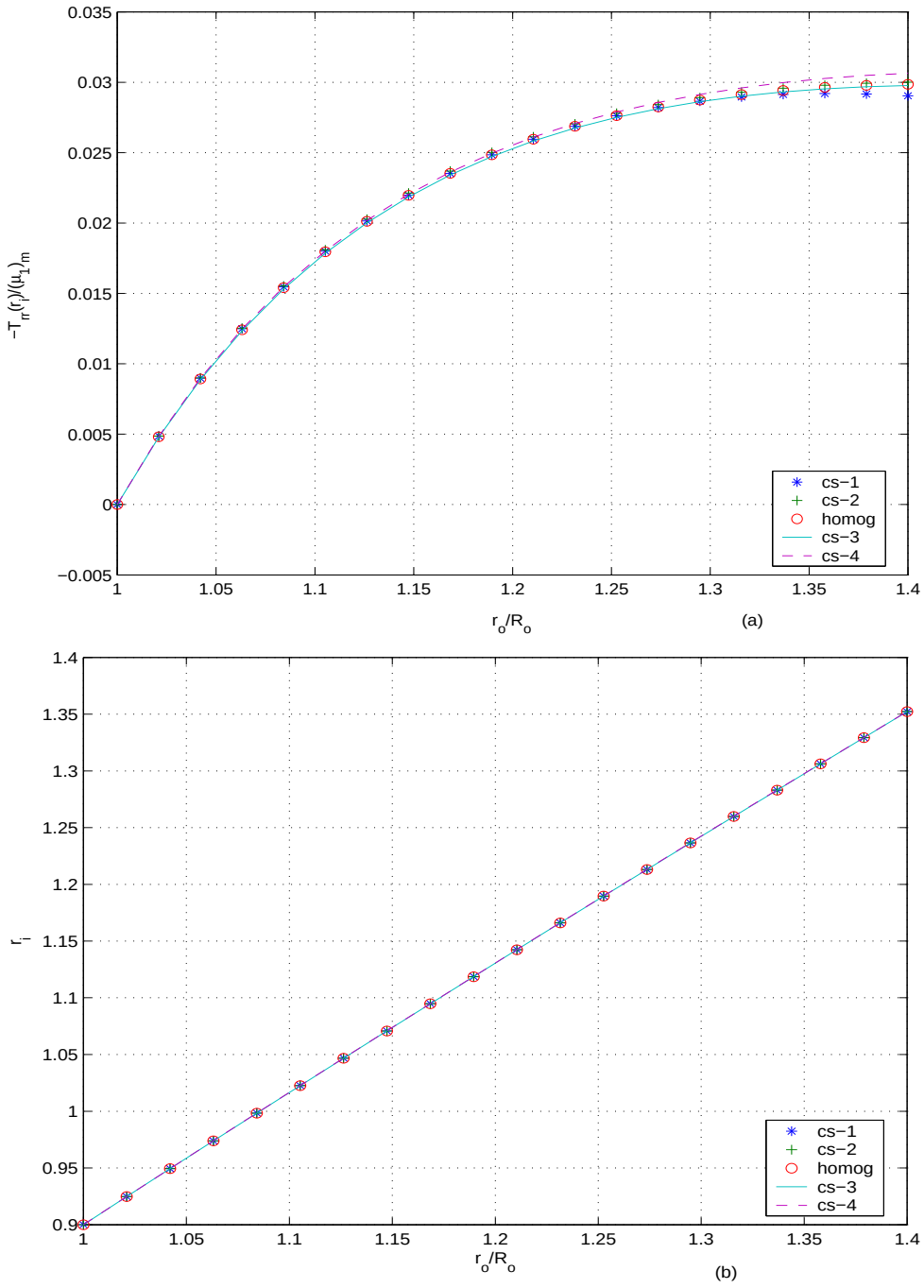

Fig. 11. Plot of (a) $-T_{rr}(r_i)/(\mu_1)_m$ (b) r_i vs. r_o/R_o of a spherical shell with $R_o = 1$ and $R_i = 0.9$ made of biological material for various prestress distributions shown in figure 8 when $r_o = 1.2R_o$, $\mu_2 = 0.1$ and $\mu_1 = 1$.

with $R_o = 1$ and $R_i = 0.9$ is inflated so that $r_o = 1.2R_o$. From figure 9a we infer that the stresses in prestressed body can be as much as 10 times less than that in the stress free body, in some cases and can be as much as 2.5 times more in other cases.

Figure 11 plots $T_{rr}(r_i)$ and r_i vs. r_o for the same cases considered above. It transpires that the radial component of the normal stress required at the inner surface to engender a given inflation does not differ significantly in the prestressed body from that in the stress free body.

2. Extension and shearing of rectangular blocks

In this subsection we focus on a body, $\mathcal{B}$ that is a rectangular region defined as

$$\mathcal{B} = \{(P, Q, R) | P_1 \leq P \leq P_2, Q_1 \leq Q \leq Q_2, R_1 \leq R \leq R_2\}, \tag{4.55}$$

where P_1, P_2, Q_1, Q_2, R_1 and R_2 are constants and seek semi-inverse solution of the form

$$x = \lambda_1 P + \kappa_1 Q + f(R), \quad y = \kappa_2 P + \lambda_2 Q + g(R), \quad z = \kappa_3 P + \kappa_4 Q + h(R), \tag{4.56}$$

for the deformation in cartesian coordinates with (P, Q, R) denoting the coordinates of a typical point in the reference configuration and (x, y, z) denoting the coordinates of a typical point in the current configuration. In (4.56), λ_i's and κ_i's are constant. While the functions $f(R)$ and $g(R)$ represent non-uniform shear along the $x - z$ and $y - z$ planes and the constants κ_i's represent uniform shear in their respective planes. Similarly, the constants λ_1 and λ_2 represent uniform extension (or shortening) along $\mathbf{e}_x$ and $\mathbf{e}_y$, $h(R)$ represents non-uniform extension (or shortening) along $\mathbf{e}_z$.

In the cartesian coordinate basis the matrix components of gradient of deforma-

tion is

$$\mathbf{H}_t = \begin{pmatrix} \lambda_1 & \kappa_1 & f_{,R} \\ \kappa_2 & \lambda_2 & g_{,R} \\ \kappa_3 & \kappa_4 & h_{,R} \end{pmatrix}, \tag{4.57}$$

where, as before $(\cdot)_{,R} = \frac{d(\cdot)}{dR}$.

For the assumed form of the deformation (4.56), it immediately follows that except, g_{i33} ($i = \{1, 2, 3\}$), all other g_{ijk} are zero. Then, if g_{i33} were to satisfy the requirement (4.12), then g_{i33} should be a function of only R. This is satisfied iff the stress in the reference configuration and the material parameters depend only on R, i.e., $\alpha_i := \overline{\alpha}_i(\mathbf{H}_t, \mathbf{T}^o(R), R)$. From the results in section G in chapter III, it follows that if the reference configuration is traction free then it is stress free. In other words, if a traction free reference configuration is used, deformation of the form (4.56) is possible only if all the material points in the body are stress free and the material parameters are at most a function of R. Thus, if a body can sustain deformation of the form (4.56) it yields information regarding its inhomogeneity and prestress distribution even if the exact representation of functions $f(R)$, $g(R)$, $h(R)$ remain unknown.

A straight forward computation shows that the balance of linear momentum (4.4) reduces to

$$\begin{aligned} a^1_{133} f_{,RR} + a^1_{233} g_{,RR} + a^1_{333} h_{,RR} &= a^1, \\ a^2_{133} f_{,RR} + a^2_{233} g_{,RR} + a^2_{333} h_{,RR} &= a^2, \\ a^3_{133} f_{,RR} + a^3_{233} g_{,RR} + a^3_{333} h_{,RR} &= a^3, \end{aligned} \tag{4.58}$$

when the deformation is of the form (4.56). Here a^d_{ijk}'s are functions of R, $f_{,R}$, $g_{,R}$, $h_{,R}$. It is possible that for certain other forms of constitutive relation this linear system of equations results in infinity of solutions. For these constitutive relations

one (or two) of the three functions can be prescribed, provided it is consistent with the boundary condition, yet to be specified. If required, by using standard techniques in linear algebra, we can obtain the restrictions on the constitutive relation so that the linear system of equations (4.58) has an unique solution.

It could also be seen that if the body is homogeneous and the reference configuration is stress free, then $a^d = 0$ ($d = \{1, 2, 3\}$) if $\mathbf{b} = \mathbf{0}$. Hence, for a homogeneous body with a stress free reference configuration and a constitutive relation such that the linear system of equations (4.58) results in an unique solution, the only possible deformation of the form (4.56) is homogeneous deformation, i.e. the only $f(R)$, $g(R)$, $h(R) \in C^\infty([R_1, R_2])$ is $f(R) = \kappa_5 R$, $g(R) = \kappa_6 R$, $h(R) = \lambda_3 R$ where κ_5, κ_6 and λ_3 are constants.

The deformation field over the entire body could be computed on specifying, { $\lambda_1,\ \lambda_2,\ \kappa_1,\ \kappa_2,\ \kappa_3,\ \kappa_4,\ f(R_1),\ g(R_1),\ h(R_1),\ f_{,R}(R_1),\ g_{,R}(R_1),\ h_{,R}(R_1)$ } using the technique outlined in section B. Now, one can adopt one of the two stand points. We can specify all the 12 constants and study the traction that has to be applied and the corresponding realizable boundary deformation of the rectangular block. If such a stand point were to be adopted then deformation of the form (4.56) is realizable for any constitutive relation of the form $\alpha_i := \overline{\alpha}_i(\mathbf{H}_t, \mathbf{T}^o(R), R)$ which yields a solution to the governing equation (4.58) and $\alpha_i \in C^\infty(\omega_a)$.

The actual boundary condition that would be prescribed are the integrated traction

$$\mathbf{L}_1 = \int_{R_1}^{R_2} \int_{Q_1}^{Q_2} J_3 \mathbf{T} \mathbf{H}_t^{-t} \mathbf{E}_1 dQdR \tag{4.59}$$

$$\mathbf{L}_2 = \int_{R_1}^{R_2} \int_{P_1}^{P_2} J_3 \mathbf{T} \mathbf{H}_t^{-t} \mathbf{E}_2 dPdR \tag{4.60}$$

$$\mathbf{L}_3 = \int_{P_1}^{P_2} \int_{Q_1}^{Q_2} J_3 \mathbf{T} \mathbf{H}_t^{-t} \mathbf{E}_3 dQdP, \tag{4.61}$$

the moments

$$\mathbf{M}_1 = \int_{R_1}^{R_2}\int_{Q_1}^{Q_2} J_3\mathbf{x}\wedge\mathbf{T}\mathbf{H}_t^{-t}\mathbf{E}_1 dQdR \tag{4.62}$$

$$\mathbf{M}_2 = \int_{R_1}^{R_2}\int_{P_1}^{P_2} J_3\mathbf{x}\wedge\mathbf{T}\mathbf{H}_t^{-t}\mathbf{E}_2 dPdR \tag{4.63}$$

$$\mathbf{M}_3 = \int_{P_1}^{P_2}\int_{Q_1}^{Q_2} J_3\mathbf{x}\wedge\mathbf{T}\mathbf{H}_t^{-t}\mathbf{E}_3 dQdP, \tag{4.64}$$

and the deformation of the boundary which yields the deformation components $\{\ \lambda_1,\ \lambda_2,\ \kappa_1,\ \kappa_2,\ \kappa_3,\ \kappa_4,\ f(R_1),\ g(R_1),\ h(R_1)\ \}$. Note that since, $\mathbf{L}_3$ and $\mathbf{M}_3$ are function of R, $\mathbf{L}_3^1$ and $\mathbf{M}_3^1$, the integrated traction and moment at R_1 and $\mathbf{L}_3^2$ and $\mathbf{M}_3^2$, the integrated traction and moment at R_2 have to be specified. However, since the integrated traction and moment should also satisfy global equilibrium conditions, $\mathbf{L}_3^1 = \mathbf{L}_3^2$, $\mathbf{M}_3^1 = \mathbf{M}_3^2$. In the above, $\mathbf{E}_i$ denotes the cartesian coordinate basis vectors in the reference configuration. Thus, the prescribed boundary conditions results in 15 equations with 12 unknowns. Hence, the boundary conditions should be consistent among themselves.

It might happen that these boundary conditions are not met, even when they are known to be consistent. Then, it only means that the solution to the boundary value problem sought is not of the assumed form. Also, there might exist other solutions to the boundary value problem for which the deformation is not of the assumed form (4.56).

a. Biaxial extension and shearing of inhomogeneous rectangular blocks

In this subsection, we present another form of deformation that certain classes of inhomogeneous rectangular blocks could exhibit. Using the same coordinate system

and body as defined before, now we study the deformation of the form

$$x = \lambda_1 P + f(Q,R), \quad y = \kappa_1 P + \lambda_2 Q + \kappa_2 R, \quad z = \kappa_3 P + \kappa_4 Q + \lambda_3 R, \tag{4.65}$$

where, λ_i's and κ_i's are constants. For the assumed form of the deformation (4.65) $g_{2jk} = g_{3jk} = 0$ and $g_{111} = 0$. Now, if g_{122}, g_{123} and g_{133} were to satisfy the requirement (4.12) then

$$\frac{\partial g_{122}}{\partial P} = \frac{\partial g_{133}}{\partial P} = 0, \tag{4.66}$$

$$\frac{\partial g_{122}}{\partial R} = \frac{\partial g_{123}}{\partial Q}, \quad \frac{\partial g_{133}}{\partial Q} = \frac{\partial g_{123}}{\partial R}. \tag{4.67}$$

Requiring the stress in the reference configuration and the material parameters to depend only on Q and R, i.e., $\alpha_i = \overline{\alpha}_i(\mathbf{H}_t, \mathbf{T}^o(Q,R), Q, R)$ ensures (4.66). Now, the balance of linear momentum (4.4) reduces to

$$\begin{aligned} a^1_{122} f_{,QQ} + a^1_{123} f_{,QR} + a^1_{133} f_{,RR} &= a^1, \\ a^2_{122} f_{,QQ} + a^2_{123} f_{,QR} + a^2_{133} f_{,RR} &= a^2, \\ a^3_{122} f_{,QQ} + a^3_{123} f_{,QR} + a^3_{133} f_{,RR} &= a^3, \end{aligned} \tag{4.68}$$

using the same notation adopted before. Now, a^d_{ijk}'s depend on Q, R, $f_{,Q}$, $f_{,R}$. Equation (4.68) could be solved to obtain g_{122}, g_{123} and g_{133}. Then, we could deduce the restriction that the constitutive relation has to satisfy so that equation (4.67) holds. This is delegated to a future work. However, we note that if the body is homogeneous and $\mathbf{T}^o = \mathbf{0}$ so that $\alpha_i = \overline{\alpha}_i(\mathbf{H}_t)$ and the system of equations (4.68) has an unique solution then $f(Q,R) = \kappa_5 Q + \kappa_6 R$.

Now, if the 10 parameters $\{\lambda_1,\ \lambda_2,\ \lambda_3,\ \kappa_1,\ \kappa_2,\ \kappa_3,\ \kappa_4,\ f(Q_1,R_1),\ f_{,Q}(Q_1,R_1),\ f_{,R}(Q_1,R_1)\}$ are specified then the deformation over the entire body could be determined using the technique outlined in section (B). Instead one could specify the

boundary conditions which as before are the integrated traction and moment given in equations (4.59) through (4.64) and the deformation of the boundary. From the deformation of the boundary we could determine the deformation components $\{\lambda_1,$ $\lambda_2,$ $\lambda_3,$ $\kappa_1,$ $\kappa_2,$ $\kappa_3,$ $\kappa_4,$ $f(Q_1, R_1),$ $f(Q_2, R_2)$ $\}$. Now, $\mathbf{L}_2$ and $\mathbf{M}_2$ is a function of Q and $\mathbf{L}_3$ and $\mathbf{M}_3$ is a function of R. Therefore, now $\mathbf{L}_2^1$ and $\mathbf{M}_2^1$ the integrated traction and moment at Q_1 and $\mathbf{L}_2^2$ and $\mathbf{M}_2^2$ the traction and moment at Q_2 would be specified. Similarly, now $\mathbf{L}_3^1$ and $\mathbf{M}_3^1$ the traction and moment at R_1 and $\mathbf{L}_3^2$ and $\mathbf{M}_3^2$ the traction and moment at R_2 would be specified.

One can similarly study deformations

$$
\begin{aligned}
&x = f(P,Q) + \kappa_1 R, \quad y = \kappa_2 P + \lambda_2 Q + \kappa_3 R, \quad z = \kappa_4 P + \kappa_5 Q + \lambda_3 R,\\
&x = f(P,R) + \kappa_1 Q, \quad y = \kappa_2 P + \lambda_2 Q + \kappa_3 R, \quad z = \kappa_4 P + \kappa_5 Q + \lambda_3 R,\\
&x = \lambda_1 P + \kappa_1 Q + \kappa_2 R, \quad y = f(P,Q) + \kappa_3 R, \quad z = \kappa_4 P + \kappa_5 Q + \lambda_3 R,\\
&x = \lambda_1 P + \kappa_1 Q + \kappa_2 R, \quad y = f(P,R) + \lambda_2 Q, \quad z = \kappa_3 P + \kappa_4 Q + \lambda_3 R,\\
&x = \lambda_1 P + \kappa_1 Q + \kappa_2 R, \quad y = f(Q,R) + \kappa_3 P, \quad z = \kappa_4 P + \kappa_5 Q + \lambda_3 R,\\
&x = \lambda_1 P + \kappa_1 Q + \kappa_2 R, \quad y = \kappa_3 P + \lambda_2 Q + \kappa_4 R, \quad z = f(P,Q) + \lambda_3 R,\\
&x = \lambda_1 P + \kappa_1 Q + \kappa_2 R, \quad y = \kappa_3 P + \lambda_2 Q + \kappa_4 R, \quad z = f(P,R) + \kappa_5 Q,\\
&x = \lambda_1 P + \kappa_1 Q + \kappa_2 R, \quad y = \kappa_3 P + \lambda_2 Q + \kappa_4 R, \quad z = f(Q,R) + \kappa_5 P,
\end{aligned}
$$

3. Inflation, extension, twisting and shearing of annular right circular cylinder

Here we use cylindrical polar coordinate system in both the reference and current configuration. Let (R, Θ, Z) and (r, θ, z) denote the coordinates of a typical material point before and after deformation. Let the body in the reference configuration occupy the region enclosed between two coaxial right circular cylinders defined by

$$\mathcal{B} = \{(R, \Theta, Z) | R_i \leq R \leq R_o, 0 \leq \Theta \leq 2\pi, Z_b \leq Z \leq Z_e\}. \tag{4.69}$$

We study the deformation of the form

$$r = r(R), \quad \theta = \phi(R) + \beta\Theta + \Omega Z, \quad z = w(R) + \kappa\Theta + \lambda Z, \tag{4.70}$$

where Ω, κ, λ are constants. The function $r(R)$ describes the inflation or deflation of the annular region, $\phi(R)$ denotes the circumferential shear of the annular region while $w(R)$ denotes the transverse shear. The constant Ω denotes the angle of twist per unit length, κ the azimuthal shear, λ the axial extension and β is related to the angular displacements undergone by radial filaments.

For the assumed form of the deformation all other g_{ijk}'s except g_{i11} is zero. Now, if g_{i11} were to satisfy the requirements (4.12), then g_{i11} can depend only on R. Iff the stress in the reference configuration and the material parameters depend on R alone, i.e., $\alpha_i = \overline{\alpha}_i(\mathbf{H}_t, \mathbf{T}^o(R), R)$, this requirement would be met.

When the deformation is given by (4.70), the balance of linear momentum (4.4) reduces to

$$\begin{aligned} a^1_{111} r_{,RR} + a^1_{211}\phi_{,RR} + a^1_{311} w_{,RR} &= a^1, \\ a^2_{111} r_{,RR} + a^2_{211}\phi_{,RR} + a^2_{311} w_{,RR} &= a^2, \\ a^3_{111} r_{,RR} + a^3_{211}\phi_{,RR} + a^3_{311} w_{,RR} &= a^3. \end{aligned} \tag{4.71}$$

Here a^d_{i11} depends on R, r, $r_{,R}$, $\phi_{,R}$, $w_{,R}$.

Thus, if the 10 parameters $\{$ Ω, κ, λ, β, $r(R_i)$, $\phi(R_i)$, $w(R_i)$, $r_{,R}(R_i)$, $\phi_{,R}(R_i)$, $w_{,R}(R_i)\}$ are known then the deformation field over the entire body can be computed using the technique outlined in section (B).

Now, the boundary traction that would be specified are the axial load,

$$L = 2\pi \int_{r_i}^{r_o} T_{zz} r dr, \tag{4.72}$$

pressure, $P_i = -T_{rr}(r_i)$, $P_o = -T_{rr}(r_o)$, longitudinal shear stress $T_{rz}(r_i)$, $T_{rz}(r_o)$ circumferential shear stress $T_{r\theta}(r_i)$, $T_{r\theta}(r_o)$ and the torque,

$$T = 2\pi \int_{r_i}^{r_o} T_{z\theta} r^2 dr, \tag{4.73}$$

Then, from the prescribed boundary deformation we obtain the deformation components $\{\ \Omega,\ \kappa,\ \lambda,\ \beta,\ r(R_i),\ \phi(R_i),\ w(R_i)\ \}$. Thus, there are 15 equations to determine 10 unknowns.

We study a subclass of the above deformation, namely, inflation, extension and twisting of right circular annular cylinders in some detail in the next chapter.

4. Circumferentially varying deformation

Next, we study the feasibility of the deformation of the form

$$r = \Lambda_r R, \qquad \theta = \phi(R, Z) + \Theta, \qquad z = \lambda_z Z. \tag{4.74}$$

in right circular annular cylinders defined in (4.69). In this subsection we shall begin by assuming that the reference configuration is stress free and homogeneous. Now, the matrix components of the gradient of deformation represented using cylindrical polar coordinate basis is

$$\mathbf{F}_t = \begin{pmatrix} \Lambda_r & 0 & 0 \\ \Lambda_r R\phi_{,R} & \Lambda_r & \Lambda_r R\phi_{,Z} \\ 0 & 0 & \lambda_z \end{pmatrix} \tag{4.75}$$

It then immediately follows that

$$\mathbf{F}_t^{-1} = \begin{pmatrix} \frac{1}{\Lambda_r} & 0 & 0 \\ -\frac{R\phi_{,R}}{\Lambda_r} & \frac{1}{\Lambda_r} & -\frac{R\phi_{,Z}}{\lambda_z} \\ 0 & 0 & \frac{1}{\lambda_z} \end{pmatrix},$$

$$\mathbf{C} = \begin{pmatrix} \Lambda_r^2 + (\Lambda_r R\phi_{,R})^2 & \Lambda_r^2 R\phi_{,R} & \Lambda_r^2 R^2 \phi_{,R}\phi_{,Z} \\ \Lambda_r^2 R\phi_{,R} & \Lambda_r^2 & \Lambda_r^2 R\phi_{,Z} \\ \Lambda_r^2 R^2 \phi_{,R}\phi_{,Z} & \Lambda_r^2 R\phi_{,Z} & (\Lambda_r R\phi_{,Z})^2 + \lambda_z^2 \end{pmatrix}, \tag{4.76}$$

$$\mathbf{C}^{-1} = \begin{pmatrix} \frac{1}{\Lambda_r^2} & -\frac{R\phi_{,R}}{\Lambda_r^2} & 0 \\ -\frac{R\phi_{,R}}{\Lambda_r^2} & \frac{1}{\Lambda_r^2} + R^2\left[\left(\frac{\phi_{,R}}{\Lambda_r}\right)^2 + \left(\frac{\phi_{,Z}}{\lambda_z}\right)^2\right] & -\phi_{,Z}\frac{R}{\lambda_z^2} \\ 0 & -\phi_{,Z}\frac{R}{\lambda_z^2} & \frac{1}{\lambda_z^2} \end{pmatrix}, \tag{4.77}$$

$$\mathbf{B} = \begin{pmatrix} \Lambda_r^2 & \Lambda_r^2 R\phi_{,R} & 0 \\ \Lambda_r^2 R\phi_{,R} & \Lambda_r^2\left\{1 + R^2\left[\phi_{,R}^2 + \phi_{,Z}^2\right]\right\} & R\lambda_z\Lambda_r\phi_{,Z} \\ 0 & R\lambda_z\Lambda_r\phi_{,Z} & \lambda_z^2 \end{pmatrix}, \tag{4.78}$$

$$\mathbf{B}^{-1} = \begin{pmatrix} \frac{1}{\Lambda_r^2}\left[1 + (R\phi_{,R})^2\right] & -\frac{R\phi_{,R}}{\Lambda_r^2} & \frac{R^2}{\lambda_z\Lambda_R}\phi_{,R}\phi_{,Z} \\ -\frac{R\phi_{,R}}{\Lambda_r^2} & \frac{1}{\Lambda_r^2} & -\frac{R}{\lambda_z\Lambda_r}\phi_{,Z} \\ \frac{R^2}{\lambda_z\Lambda_r}\phi_{,R}\phi_{,Z} & -\frac{R}{\lambda_z\Lambda_r}\phi_{,Z} & \frac{1+(R\phi_{,Z})^2}{\lambda_z^2} \end{pmatrix}. \tag{4.79}$$

$$\mathbf{N} = \begin{pmatrix} \left[1 + (R\phi_{,R})^2\right]\frac{1}{\Lambda_r^3} & -\left(\frac{R\phi_{,R}}{\Lambda_r}\right)^3 - 2\frac{R\phi_{,R}}{\Lambda_r^3} - R^3\frac{\phi_{,R}}{\Lambda_r}\left(\frac{\phi_{,Z}}{\lambda_z}\right)^2 & \left(\frac{R}{\lambda_z}\right)^2\frac{\phi_{,R}}{\Lambda_r}\phi_{,Z} \\ -\frac{R}{\Lambda_r^3}\phi_{,R} & \frac{1}{\Lambda_r^3}\left[(R\phi_{,R})^2 + 1\right] + \left(\frac{R}{\lambda_z}\phi_{,Z}\right)^2\frac{1}{\Lambda_r} & -\frac{R}{\Lambda_r}\frac{\phi_{,Z}}{\lambda_z^2} \\ \left(\frac{R}{\Lambda_r}\right)^2\phi_{,R}\frac{\phi_{,Z}}{\lambda_z} & -\frac{R}{\lambda_z}\phi_{,Z}\left[\left(\frac{R\phi_{,R}}{\Lambda_r}\right)^2 + \frac{1}{\Lambda_r^2} + (\frac{R\phi_{,Z}}{\lambda_z})^2 + \frac{1}{\lambda_z^2}\right] & \left[(R\phi_{,Z})^2 + 1\right]\frac{1}{\lambda_z^3} \end{pmatrix} \tag{4.80}$$

where $\mathbf{N} = \mathbf{F}_t^{-t}\mathbf{F}_t^{-1}\mathbf{F}_t^{-t}$

The invariants are

$$\begin{aligned} J_1 &= 2\Lambda_r^2 + \lambda_z^2 + (\Lambda_r R)^2 \left[\phi_{,R}^2 + \phi_{,Z}^2\right], \\ J_2 &= \frac{1}{\Lambda_r^2}\left[2 + (R\phi_{,R})^2\right] + \frac{1}{\lambda_z^2}\left[1 + (R\phi_{,Z})^2\right], \\ J_3 &= \lambda_z \Lambda_r^2. \end{aligned} \tag{4.81}$$

It follows from (2.85) that a general representation for stress when the reference configuration is stress free is

$$\mathbf{S} = J_3 \mathbf{T}\mathbf{F}_t^{-t} = \gamma_0 \mathbf{F}_t^{-t} + \gamma_1 \mathbf{F}_t + \gamma_2 \mathbf{F}_t^{-t}\mathbf{F}_t^{-1}\mathbf{F}_t^{-t}, \tag{4.82}$$

where here $\gamma_i = J_3 \overline{\alpha}_i(J_1, J_2, J_3)$.

Then we record,

$$\begin{aligned} J_{1,R} &= \Lambda_r^2 \left\{2R\left[\phi_{,R}^2 + \phi_{,Z}^2\right] + 2R^2\left[\phi_{,R}\phi_{,RR} + \phi_{,Z}\phi_{,ZR}\right]\right\}, \\ J_{1,Z} &= 2\left(\Lambda_r R\right)^2\left[\phi_{,R}\phi_{,ZR} + \phi_{,Z}\phi_{,ZZ}\right], \\ J_{2,R} &= 2R\left[\left(\frac{\phi_{,R}}{\Lambda_r}\right)^2 + \left(\frac{\phi_{,Z}}{\lambda_z}\right)^2\right] + 2R^2\left[\frac{1}{\Lambda_r^2}\phi_{,R}\phi_{,RR} + \frac{1}{\lambda_z^2}\phi_{,Z}\phi_{,ZR}\right], \\ J_{2,Z} &= 2R^2\left[\frac{1}{\Lambda_r^2}\phi_{,R}\phi_{,ZR} + \frac{1}{\lambda_z^2}\phi_{,Z}\phi_{,ZZ}\right], \\ J_{1,\Theta} &= J_{2,\Theta} = J_{3,R} = J_{3,\Theta} = J_{3,Z} = 0. \end{aligned} \tag{4.83}$$

For the assumed deformation (4.74), the balance of linear momentum reduces to

$$\begin{aligned} \frac{\partial S_{rR}}{\partial R} + \frac{\partial S_{rZ}}{\partial Z} + \frac{S_{rR} - S_{\theta\Theta}}{R} - S_{\theta R}\frac{\partial \theta}{\partial R} - S_{\theta Z}\frac{\partial \theta}{\partial Z} &= 0, \\ \frac{\partial S_{\theta R}}{\partial R} + \frac{\partial S_{\theta Z}}{\partial Z} + \frac{S_{\theta R} + S_{r\Theta}}{R} + S_{rR}\frac{\partial \theta}{\partial R} + S_{rZ}\frac{\partial \theta}{\partial Z} &= 0, \\ \frac{\partial S_{zR}}{\partial R} + \frac{\partial S_{zZ}}{\partial Z} + \frac{S_{zR}}{R} &= 0, \end{aligned} \tag{4.84}$$

and evaluates to

$$\begin{aligned}
&[\gamma_{0,1}J_{1,R}+\gamma_{0,2}J_{2,R}]\frac{1}{\Lambda_r}+[\gamma_{1,1}J_{1,R}+\gamma_{1,2}J_{2,R}]\Lambda_r+\\
&[\gamma_{2,1}J_{1,R}+\gamma_{2,2}J_{2,R}]\left[1+(R\phi_{,R})^2\right]\frac{1}{\Lambda_r^3}+[\gamma_{2,1}J_{1,Z}+\gamma_{2,2}J_{2,Z}]\left(\frac{R}{\lambda_z}\right)^2\frac{\phi_{,R}\phi_{,Z}}{\Lambda_r}\\
&+2\gamma_2\left[R\phi_{,R}^2+R^2\phi_{,R}\phi_{,RR}\right]\frac{1}{\Lambda_r^3}+\gamma_2\left(\frac{R}{\lambda_z}\right)^2[\phi_{,RZ}\phi_{,Z}+\phi_{,R}\phi_{,ZZ}]\frac{1}{\Lambda_r}\\
&-\gamma_1\Lambda_r R\left(\phi_{,R}^2+\phi_{,Z}^2\right)+\gamma_2\frac{R}{\Lambda_r}\left(\frac{\phi_{,R}}{\Lambda_r}\right)^2=0,
\end{aligned}$$

$$\begin{aligned}
&\left[\left(\gamma_{1,1}\Lambda_r-\frac{\gamma_{2,1}}{\Lambda_r^3}\right)J_{1,R}+\left(\gamma_{1,2}\Lambda_r-\frac{\gamma_{2,2}}{\Lambda_r^3}\right)J_{2,R}\right]R\phi_{,R}\\
&+\left[\gamma_1\Lambda_r-\frac{\gamma_2}{\Lambda_r^3}\right][\phi_{,R}+R\phi_{,RR}]+\Lambda_r R\phi_{,Z}\left[\gamma_{1,1}J_{1,Z}+\gamma_{1,2}J_{2,Z}\right]\\
&-[\gamma_{2,1}J_{1,Z}+\gamma_{2,2}J_{2,Z}]\frac{R}{\Lambda_r}\frac{\phi_{,Z}}{\lambda_z^2}+\gamma_1\Lambda_r R\phi_{,ZZ}-\gamma_2\frac{R}{\Lambda_r}\frac{\phi_{,ZZ}}{\lambda_z^2}\\
&+2\phi_{,R}\left[\gamma_1\Lambda_r-\frac{\gamma_2}{\Lambda_r^3}\right]=0,
\end{aligned}$$

$$\begin{aligned}
&[\gamma_{2,1}J_{1,R}+\gamma_{2,2}J_{2,R}]\left(\frac{R}{\Lambda_r}\right)^2\phi_{,R}\frac{\phi_{,Z}}{\lambda_z}\\
&+\frac{\gamma_2}{\Lambda_r^2\lambda_z}\left[2R\phi_{,R}\phi_{,Z}+R^2\left(\phi_{,RR}\phi_{,Z}+\phi_{,R}\phi_{,ZR}\right)\right]\\
&+\frac{1}{\lambda_z}\left[\gamma_{0,1}J_{1,Z}+\gamma_{0,2}J_{2,Z}\right]+\lambda_z\left[\gamma_{1,1}J_{1,Z}+\gamma_{1,2}J_{2,Z}\right]\\
&+[\gamma_{2,1}J_{1,Z}+\gamma_{2,2}J_{2,Z}]\frac{1}{\lambda_z^3}\left[1+(R\phi_{,Z})^2\right]\\
&+\gamma_2\frac{2}{\lambda_z^3}R^2\phi_{,Z}\phi_{,ZZ}+\frac{\gamma_2}{\lambda_z\Lambda_r^2}R\phi_{,R}\phi_{,Z}=0,
\end{aligned}$$

where $\gamma_{i,j}=\frac{\partial\gamma_i}{\partial J_j}$.

The above equations can be cast in the form

$$\begin{aligned} u_1\phi_{,RR} + v_1\phi_{,ZR} + w_1\phi_{,ZZ} + s_1 &= 0, \\ u_2\phi_{,RR} + v_2\phi_{,ZR} + w_2\phi_{,ZZ} + s_2 &= 0, \\ u_3\phi_{,RR} + v_3\phi_{,ZR} + w_3\phi_{,ZZ} + s_3 &= 0, \end{aligned} \tag{4.85}$$

where

$$\begin{aligned} u_1 &= \left\{ \left[\gamma_{0,1}\Lambda_r + \gamma_{1,1}\Lambda_r^3 + \frac{\gamma_{0,2}}{\Lambda_r^3} + \frac{\gamma_{1,2}}{\Lambda_r} \right] + \left[\frac{\gamma_{2,1}}{\Lambda_r} + \frac{\gamma_{2,2}}{\Lambda_r^5} \right] \left[1 + (R\phi_{,R})^2 \right] + \frac{\gamma_2}{\Lambda_r^3} \right\} 2R^2\phi_{,R}, \\ v_1 &= \left\{ \left[\gamma_{0,1}\Lambda_r + \frac{\gamma_{0,2}}{\Lambda_r\lambda_z^2} + \gamma_{1,1}\Lambda_r^3 + \frac{\Lambda_r}{\lambda_z^2}\gamma_{1,2} \right] + \left[\frac{\gamma_{2,1}}{\Lambda_r} + \frac{1}{\Lambda_r^3\lambda_z^2}\gamma_{2,2} \right] \left[1 + (R\phi_{,R})^2 \right] \right. \\ &\quad \left. + \left[\gamma_{2,1}\Lambda_r + \frac{\gamma_{2,2}}{\Lambda_r^3} \right] \left(\frac{R}{\lambda_z}\phi_{,R} \right)^2 + \frac{\gamma_2}{2\Lambda_r\lambda_z^2} \right\} 2R^2\phi_{,Z}, \\ w_1 &= \left[\gamma_{2,1}\Lambda_r + \frac{\gamma_{2,2}}{\Lambda_R\lambda_z^2} \right] 2\frac{R^4}{\lambda_z^2}\phi_{,Z}^2\phi_{,R} + \gamma_2 \left(\frac{R}{\lambda_z} \right)^2 \frac{\phi_{,R}}{\Lambda_r}, \\ s_1 &= \left[\gamma_{0,1}\Lambda_r + \gamma_{1,1}\Lambda_r^3 \right] 2R \left[\phi_{,R}^2 + \phi_{,Z}^2 \right] + \left[\frac{\gamma_{0,2}}{\Lambda_r} + \gamma_{1,2}\Lambda_r \right] 2R \left[\left(\frac{\phi_{,R}}{\Lambda_r} \right)^2 + \left(\frac{\phi_{,Z}}{\lambda_z} \right)^2 \right] \\ &\quad + \left\{ \frac{\gamma_{2,1}}{\Lambda_r} \left(\phi_{,R}^2 + \phi_{,Z}^2 \right) + \frac{\gamma_{2,2}}{\Lambda_r^3} \left[\left(\frac{\phi_{,R}}{\Lambda_r} \right)^2 + \left(\frac{\phi_{,Z}}{\lambda_z} \right)^2 \right] \right\} 2R \left[1 + (R\phi_{,R})^2 \right] \\ &\quad + 2\frac{\gamma_2}{\Lambda_r^3} R\phi_{,R}^2 - \gamma_1\Lambda_r R \left(\phi_{,R}^2 + \phi_{,Z}^2 \right) + \gamma_2 \frac{R}{\Lambda_r} \left(\frac{\phi_{,R}}{\Lambda_r} \right)^2. \end{aligned}$$

$$\begin{aligned} u_2 &= \left[\gamma_{1,1}\Lambda_r^3 + \frac{\gamma_{1,2}}{\Lambda_r} - \frac{\gamma_{2,1}}{\Lambda_r} - \frac{\gamma_{2,2}}{\Lambda_r^5} \right] 2R^3\phi_{,R}^2 + R \left[\gamma_1\Lambda_r - \frac{\gamma_2}{\Lambda_r^3} \right], \\ v_2 &= 2R^3\phi_{,R}\phi_{,Z} \left\{ 2\gamma_{1,1}\Lambda_r^3 + \left(\frac{1}{\Lambda_r} + \frac{\Lambda_r}{\lambda_z^2} \right) \gamma_{1,2} - \left(\frac{\Lambda_r}{\lambda_z^2} + \frac{1}{\Lambda_r} \right) \gamma_{2,1} + \frac{2\gamma_{2,2}}{\Lambda_r^3\lambda_z^2} \right\} \\ w_2 &= 2R^3\phi_{,Z}^2 \left\{ \left[\gamma_{1,1}\Lambda_r^3 + \Lambda_r\frac{\gamma_{1,2}}{\lambda_z^2} \right] - \left[\gamma_{2,1}\Lambda_r + \frac{\gamma_{2,2}}{\Lambda_r\lambda_z^2} \right] \frac{1}{\lambda_z^2} \right\} + \gamma_1\Lambda_r R - \gamma_2\frac{R}{\Lambda_r\lambda_z^2}, \\ s_2 &= 2R^2\phi_{,R} \left\{ \left[\gamma_{1,1}\Lambda_r^3 - \frac{\gamma_{2,1}}{\Lambda_r} \right] \left[\phi_{,R}^2 + \phi_{,Z}^2 \right] + \left[\gamma_{1,2}\Lambda_r - \frac{\gamma_{2,2}}{\Lambda_r^3} \right] \left[\left(\frac{\phi_{,R}}{\Lambda_r} \right)^2 + \left(\frac{\phi_{,Z}}{\lambda_z} \right)^2 \right] \right\} \\ &\quad + 3\phi_{,R} \left[\gamma_1\Lambda_r - \frac{\gamma_2}{\Lambda_r^3} \right]. \end{aligned}$$

$$
\begin{aligned}
u_3 &= \left[\gamma_{2,1}+\frac{\gamma_{2,2}}{\Lambda_r^4}\right]2\frac{R^4}{\lambda_z}\phi_{,R}^2\phi_{,Z}+\frac{\gamma_2}{\lambda_z}\left(\frac{R}{\Lambda_r}\right)^2\phi_{,Z},\\
v_3 &= \left\{\left[\gamma_{2,1}+\frac{\gamma_{2,2}}{\lambda_z^2\Lambda_r^2}\right]\frac{R^2}{\lambda_z}\phi_{,Z}^2+\frac{\gamma_2}{2\lambda_z\Lambda_r^2}+\frac{1}{\lambda_z}\left[\gamma_{0,1}\Lambda_r^2+\frac{\gamma_{0,2}}{\Lambda_r^2}\right]+\lambda_z\left[\gamma_{1,1}\Lambda_r^2+\frac{\gamma_{1,2}}{\Lambda_r^2}\right]\right.\\
&\qquad \left.+\frac{1}{\lambda_z^3}\left[\gamma_{2,1}\Lambda_r^2+\frac{\gamma_{2,2}}{\Lambda_r^2}\right]\left[1+(R\phi_{,R})^2\right]\right\}2R^2\phi_{,R},\\
w_3 &= \left\{\frac{1}{\lambda_z}\left[\gamma_{0,1}\Lambda_r^2+\frac{\gamma_{0,2}}{\lambda_z^2}\right]+\left[\lambda_z\Lambda_r^2\gamma_{1,1}+\frac{\gamma_{1,2}}{\lambda_z}\right]+\frac{1}{\lambda_z^3}\left[\Lambda_r^2\gamma_{2,1}+\frac{\gamma_{2,2}}{\lambda_z^2}\right]\left[1+(R\phi_{,R})^2\right]\right.\\
&\qquad \left.+\quad\frac{\gamma_2}{\lambda_z^3}\right\}2R^2\phi_{,Z},\\
s_3 &= \left\{\gamma_{2,1}\Lambda_r^2\left[\phi_{,R}^2+\phi_{,Z}^2\right]+\gamma_{2,2}\left[\left(\frac{\phi_{,R}}{\Lambda_r}\right)^2+\left(\frac{\phi_{,Z}}{\lambda_z}\right)^2\right]\right\}2\frac{R^3}{\Lambda_r^2}\phi_{,R}\frac{\phi_{,Z}}{\lambda_z}+3\frac{\gamma_2}{\lambda_z}\frac{R}{\Lambda_r^2}\phi_{,R}\phi_{,Z}.
\end{aligned}
$$

Clearly, if the system of equations (4.85) are independent then we could solve the linear system of equations and obtain $\phi_{,RR}$, $\phi_{,RZ}$ and $\phi_{,ZZ}$. Then, if ϕ satisfies (4.12), we can obtain a Taylor series solution as indicated above. However, there exist constitutive relations for which (4.12) does not hold. To illustrate this, we specialize to the exponential constitutive relation (2.97), introduced in chapter II. From which we obtain

$$
\mathbf{S}=\mu_1\mu_2\exp(Q)\left[2\mathbf{F}_t+\left(J_1-\frac{5}{J_3^2}\right)\mathbf{F}_t^{-t}\right], \tag{4.86}
$$

where $Q=\mu_2[J_1J_3+\frac{5}{J_3}-8]$.

Now

$$
\begin{aligned}
u_1 &= 2[\gamma_{01}\Lambda_r+2\mu_2J_3^2\Lambda_r^3]R^2\phi_{,R},\\
v_1 &= 2[\gamma_{01}\Lambda_r+2\mu_2J_3^2\Lambda_r^3]R^2\phi_{,Z},\\
w_1 &= 0,\\
s_1 &= 2R\Lambda_r\left[\phi_{,R}^2+\phi_{,Z}^2\right]\left[\mu_2(J_1J_3^2-5)+2\mu_2J_3^2\Lambda_r^2\right],
\end{aligned}
$$

$$
\begin{aligned}
u_2 &= 4\mu_2 J_3^2 \Lambda_r^3 R^3 \phi_{,R}^2 + 2J_3 R \Lambda_r, \\
v_2 &= 8\mu_2 J_3^2 \Lambda_r^3 R^3 \phi_{,R} \phi_{,Z}, \\
w_2 &= 4\mu_2 J_3^2 \Lambda_r^3 R^3 \phi_{,Z}^2 + 2J_3 R \Lambda_r, \\
s_2 &= 4\mu_2 J_3^2 \Lambda_r^3 R^2 \phi_{,R} + 6J_3 \Lambda_r \phi_{,R},
\end{aligned}
$$

$$
\begin{aligned}
u_3 &= 0, \\
v_3 &= 2\left[\frac{\Lambda_r^2}{\lambda_z}\gamma_{01} + 2\mu_2 J_3^3\right] R^2 \phi_{,R}, \\
w_3 &= 2\left[\frac{\Lambda_r^2}{\lambda_z}\gamma_{01} + 2\mu_2 J_3^3\right] R^2 \phi_{,Z}, \\
s_3 &= 0,
\end{aligned} \tag{4.87}
$$

where $\gamma_{01} = J_3 + \mu_2(J_1 J_3^2 - 5)$. Solving the linear system of equations we obtain

$$
\begin{aligned}
\phi_{,ZZ} &= \frac{\phi_{,R}^2}{2J_3 \Lambda_r R[\phi_{,R}^2 + \phi_{,Z}^2]}\left[s_1 \frac{u_2}{u_1} - s_2\right], \\
\phi_{,ZR} &= -\frac{\phi_{,Z}}{\phi_{,R}}\phi_{,ZZ}, \\
\phi_{,RR} &= \frac{\phi_{,Z}^2}{\phi_{,R}^2}\phi_{,ZZ} - \frac{s_1}{u_1}.
\end{aligned} \tag{4.88}
$$

Straight forward but tedious calculation shows that the requirement (4.12) is not satisfied and hence the deformation (4.74) is not possible for the constitutive relation (4.86).

Also, there are many occasions when the linear system of equations (4.85) would not be independent. One such occasion is when α_i's are dependent only on J_3 and $\alpha_2 = 0$. Blatz-Ko constitutive relation (2.94) is one such relation. Next, we study this in detail. Assuming that the reference configuration is stress free and homogeneous and $\mu_2 = 1$, the Blatz-Ko constitutive relation can be written as

$$
\mathbf{S} = \mu_1 \left[-\mu_m \mathbf{F}^{-t} + \mathbf{F}_t\right] \tag{4.89}
$$

where, $\mu_m = J_3^{-2\mu_3}$ and μ_1 and μ_3 are constants. We compute

$$\mathbf{S} = \mu_1 \begin{pmatrix} \Lambda_r - \frac{\mu_m}{\Lambda_r} & \frac{\mu_m}{\Lambda_r} R\phi_{,R} & 0 \\ \Lambda_r R\phi_{,R} & \Lambda_r - \frac{\mu_m}{\Lambda_r} & \Lambda_r R\phi_{,Z} \\ 0 & \mu_m \phi_{,Z} \frac{R}{\lambda_z} & \lambda_z - \frac{\mu_m}{\lambda_z} \end{pmatrix}, \tag{4.90}$$

with $\mu_m = (\Lambda_r^2 \lambda)^{-2\mu_3}$. On substituting (4.90) in (4.84) only (4.84)a and (4.84b) results in a non-trivial equation

$$\phi_{,R}^2 + \phi_{,Z}^2 = 0, \qquad \phi_{,RR} + \phi_{,ZZ} + \frac{\phi_{,R}}{R}\left[2 + \frac{\mu_m}{\Lambda_r^2}\right] = 0. \tag{4.91}$$

The only solution to the above equations is $\phi = constant$, a trivial solution which is the superposition of rigid body rotation along the axis of the annular cylinder over uniaxial extension along the axis of the annular cylinder.

Understanding that the only deformation of the form (4.74) possible in a homogeneous Blatz-Ko body[13] is homogeneous deformation, we examine the scenario in prestressed body. We find that the deformation, (4.74) is possible in a prestressed body only when the prestresses satisfy certain conditions, arising from the requirement that the body in the current configuration be in equilibrium.

It follows from (4.12) that since, the deformation varies only with respect to R and Z, the stresses in the reference configuration too vary only with respect to R and Z. Prestresses that vary only with respect to R and Z were obtained in section (G.2) of chapter III.

[13]By Blatz-Ko body we mean a body made up of Blatz Ko material.

For this case, we compute

$$\begin{aligned}
\widetilde{J}_{m1} &= \Lambda_r^2\left[1+(R\phi_{,R})^2\right]m_1+\Lambda_r^2 m_2+\left[\lambda_z^2+(R\Lambda_r\phi_{,Z})^2\right]m_3+2\Lambda_r^2 R\phi_{,R}m_4 \\
&\quad +2\Lambda_r^2R^2\phi_{,R}\phi_{,Z}m_5+2\Lambda_r^2R\phi_{,Z}m_6, \\
\widetilde{J}_{m2} &= \frac{n_1}{\Lambda_r^2}+\left[\frac{1}{\Lambda_r^2}+R^2\left(\frac{\phi_{,R}^2}{\Lambda_r^2}+\frac{\phi_{,Z}^2}{\lambda_z^2}\right)\right]n_2+\frac{n_3}{\lambda_z^2}-2\frac{n_4}{\Lambda_r^2}R\phi_{,R}-2R\frac{\phi_{,Z}}{\lambda_z^2}n_6, \\
\widetilde{J}_{m3} &= J_3^r\lambda_z\Lambda_r^2,
\end{aligned} \tag{4.92}$$

where

$$\begin{aligned}
m_1 &= \delta_0+\delta_1T^o_{RR}+\delta_2\left[T^{o2}_{RR}+T^{o2}_{R\Theta}+T^{o2}_{RZ}\right], \\
m_2 &= \delta_0+\delta_1T^o_{\Theta\Theta}+\delta_2\left[T^{o2}_{R\Theta}+T^{o2}_{\Theta\Theta}+T^{o2}_{\Theta Z}\right], \\
m_3 &= \delta_0+\delta_1T^o_{ZZ}+\delta_2\left[T^{o2}_{RZ}+T^{o2}_{\Theta Z}+T^{o2}_{ZZ}\right], \\
m_4 &= \delta_1T^o_{R\Theta}+\delta_2\left[T^o_{RR}T^o_{R\Theta}+T^o_{R\Theta}T^o_{\Theta\Theta}+T^o_{RZ}T^o_{\Theta Z}\right], \\
m_5 &= \delta_1T^o_{RZ}+\delta_2\left[T^o_{RR}T^o_{RZ}+T^o_{R\Theta}T^o_{\Theta Z}+T^o_{RZ}T^o_{ZZ}\right], \\
m_6 &= \delta_1T^o_{\Theta Z}+\delta_2\left[T^o_{R\Theta}T^o_{RZ}+T^o_{\Theta\Theta}T^o_{\Theta Z}+T^o_{\Theta Z}T^o_{ZZ}\right],
\end{aligned}$$

$$\begin{aligned}
n_1 &= \kappa_0+\kappa_1T^o_{RR}+\kappa_2\left[T^{o2}_{RR}+T^{o2}_{R\Theta}+T^{o2}_{RZ}\right], \\
n_2 &= \kappa_0+\kappa_1T^o_{\Theta\Theta}+\kappa_2\left[T^{o2}_{R\Theta}+T^{o2}_{\Theta\Theta}+T^{o2}_{\Theta Z}\right], \\
n_3 &= \kappa_0+\kappa_1T^o_{ZZ}+\kappa_2\left[T^{o2}_{RZ}+T^{o2}_{\Theta Z}+T^{o2}_{ZZ}\right], \\
n_4 &= \kappa_1T^o_{R\Theta}+\kappa_2\left[T^o_{RR}T^o_{R\Theta}+T^o_{R\Theta}T^o_{\Theta\Theta}+T^o_{RZ}T^o_{\Theta Z}\right], \\
n_5 &= \kappa_1T^o_{RZ}+\kappa_2\left[T^o_{RR}T^o_{RZ}+T^o_{R\Theta}T^o_{\Theta Z}+T^o_{RZ}T^o_{ZZ}\right], \\
n_6 &= \kappa_1T^o_{\Theta Z}+\kappa_2\left[T^o_{R\Theta}T^o_{RZ}+T^o_{\Theta\Theta}T^o_{\Theta Z}+T^o_{\Theta Z}T^o_{ZZ}\right],
\end{aligned}$$

We illustrate the procedure using the Blatz-Ko constitutive relation which is

$$\widetilde{\mathbf{S}}=-\frac{\mu_1\widetilde{J}_3}{\widetilde{J}_{m3}^{[2\mu_3+1]}}\mathbf{H}_t^{-t}+\mathbf{H}_t\left[\frac{\mu_1}{(J_3^r)^{(2\mu_3+1)}}\mathbf{1}+\mathbf{T}^o\right], \tag{4.93}$$

which evaluates to

$$\left\{\begin{array}{c} S_{rR} \\ S_{r\Theta} \\ S_{rZ} \\ S_{\theta R} \\ S_{\theta\Theta} \\ S_{\theta Z} \\ S_{zR} \\ S_{z\Theta} \\ S_{zZ} \end{array}\right\} = \left\{\begin{array}{c} -\frac{\mu_1 J_3}{J_{m3}^{[2\mu_3+1]}}\frac{1}{\Lambda_r} + \Lambda_r\left[\gamma_0 + T^o_{rr}\right] \\ \frac{\mu_1 J_3}{J_{m3}^{[2\mu_3+1]}} R\phi_{,R} + \Lambda_r T^o_{R\Theta} \\ \Lambda_r T^o_{RZ} \\ \Lambda_r\left\{T^o_{R\Theta} + R\left[\phi_{,R}(\gamma_0 + T^o_{RR}) + \phi_{,Z}T^o_{RZ}\right]\right\} \\ -\frac{J_3}{J_{m3}^{[2\mu_3+1]}}\frac{\mu_1}{\Lambda_r} + \Lambda_r\left\{\gamma_0 + T^o_{\Theta\Theta} + R\left[\phi_{,R}T^o_{R\Theta} + \phi_{,Z}T^o_{\Theta Z}\right]\right\} \\ \Lambda_r\left\{T^o_{\Theta Z} + R\left[\phi_{,R}T^o_{RZ} + \phi_{,Z}(\gamma_0 + T^o_{ZZ})\right]\right\} \\ \lambda_z T^o_{RZ} \\ \frac{\mu_1 J_3}{J_{m3}^{[2\mu_3+1]}}\frac{R}{\lambda_z}\phi_{,Z} + \lambda_z T^o_{\Theta Z} \\ -\frac{\mu_1 J_3}{\lambda_z J_{m3}^{[2\mu_3+1]}} + (\gamma_0 + T^o_{ZZ})\lambda_z \end{array}\right\} \tag{4.94}$$

where, $\gamma_0 = \frac{\mu_1}{(J_3^r)^{(2\mu_3+1)}}$.

Now, consider (4.84)c. This evaluates to

$$0 \;=\; \lambda_z\frac{\partial T^o_{RZ}}{\partial R} + \frac{\mu_1 J_3^2(2\mu_3+1)J^r_{3,Z}}{\lambda_z J_{m3}^{(2\mu_3+2)}} - \frac{\mu_1(2\mu_3+1)J^r_{3,Z}}{(J_3^r)^{2\mu_3+2}}\lambda_z + \frac{\partial T^o_{ZZ}}{\partial Z}\lambda_z + \frac{\lambda_z T^o_{RZ}}{R}. \tag{4.95}$$

Clearly, this is a restriction on the constitutively prescribed $\mathbf{T}^o$ rather than on the deformation, $\phi(R, Z)$. Thus, in general, deformation of the form (4.74) is not possible in a prestressed annular right circular cylinders made up of Blatz-Ko material.

Thus, the above examples illustrate how the scheme outlined in section (B) could be used to find if deformations of certain forms are possible in a given body. We just observe that the analogue of the remaining three families of the universal solution to incompressible bodies can also be studied in the above framework for compressible, prestressed and inhomogeneous bodies. Also, numerous other classes of deformation becomes amenable to solution and analysis in the above framework.

CHAPTER V

INFLATION, EXTENSION AND TWISTING OF ANNULAR AND SOLID RIGHT CIRCULAR PRESTRESSED AND INHOMOGENEOUS CYLINDERS

Study of the inflation, extension and twisting of annular and solid right circular cylinders is of significant practical interest. From industrial perspective, shafts and tubes which are the components of various structural systems have this geometry. Many a times uniaxial extension and torsion tests are conducted on solid cylindrical specimens to identify or verify material parameters or functions in the constitutive relations. First approximation of biological bodies like blood vessels, tendons belongs to this class. Further since, in the next chapter we are going to concern ourself with the response of the circumflex artery subjected to inflation and axial extension, studying this class of deformation in some detail is essential.

In this chapter, we confine ourselves to a body, $\mathcal{B}$ that is the annular region between two concentric right circular cylinders

$$\mathcal{B} = \{(R, \Theta, Z) | R_i \leq R \leq R_o, 0 \leq \Theta \leq 2\pi, Z_b \leq Z \leq Z_e\}. \tag{5.1}$$

We seek semi-inverse solution of the form

$$r = r(R), \qquad \theta = \Theta + \Omega Z, \qquad z = \lambda Z, \tag{5.2}$$

for the deformation in cylindrical polar coordinates with (R, Θ, Z) denoting the coordinates of a typical material point in the reference configuration and (r, θ, z) denoting the coordinates of a typical material point in the current configuration. In equation (5.2) Ω and λ are constant. $r(R)$ denotes inflation or deflation of the annular region, Ω the angle of twist per unit length of the body and λ the axial extension of the body.

The matrix components of the gradient of deformation represented using cylin-

drical polar basis is

$$\mathbf{H}_t = \begin{pmatrix} r_{,R} & 0 & 0 \\ 0 & \frac{r}{R} & r\Omega \\ 0 & 0 & \lambda \end{pmatrix} \tag{5.3}$$

It then immediately follows that

$$\mathbf{H}_t^{-1} = \begin{pmatrix} \frac{1}{r_{,R}} & 0 & 0 \\ 0 & \frac{R}{r} & -\frac{R\Omega}{\lambda} \\ 0 & 0 & \frac{1}{\lambda} \end{pmatrix}. \tag{5.4}$$

The right Cauchy Green stretch tensor and its inverse in cylindrical polar coordinate basis is given by

$$\widetilde{\mathbf{C}} = \begin{pmatrix} r_{,R}^2 & 0 & 0 \\ 0 & (\frac{r}{R})^2 & \frac{r^2}{R}\Omega \\ 0 & \frac{r^2}{R}\Omega & (r\Omega)^2 + \lambda^2 \end{pmatrix}, \quad \widetilde{\mathbf{C}}^{-1} = \begin{pmatrix} (\frac{1}{r_{,R}})^2 & 0 & 0 \\ 0 & (\frac{\Omega}{\lambda}R)^2 + (\frac{R}{r})^2 & -\frac{R\Omega}{\lambda^2} \\ 0 & -\frac{R\Omega}{\lambda^2} & (\frac{1}{\lambda})^2 \end{pmatrix}.$$

Hence, the invariants could be written as

$$\widetilde{J}_1 = r_{,R}^2 + (\frac{r}{R})^2 + (r\Omega)^2 + \lambda^2, \tag{5.5}$$

$$\widetilde{J}_2 = (\frac{1}{r_{,R}})^2 + (\frac{R}{r})^2 + \frac{(R\Omega)^2 + 1}{\lambda^2}, \tag{5.6}$$

$$\widetilde{J}_3 = \lambda \frac{r}{R} r_{,R}. \tag{5.7}$$

It follows from the arguments in section (C.3) in the last chapter that the prestresses can vary only along the radial direction. Then, from section (G.2) in chapter III, the matrix components of $\mathbf{T}^o$ in cylindrical coordinate basis is

$$\mathbf{T}^o = \begin{pmatrix} T^o_{RR}(R) & 0 & 0 \\ 0 & T^o_{\Theta\Theta}(R) & 0 \\ 0 & 0 & 0 \end{pmatrix}. \tag{5.8}$$

It then follows from equations (3.20) and (3.21) that

$$\widetilde{J}_4 = r_{,R}^2 T_{RR}^o + (\frac{r}{R})^2 T_{\Theta\Theta}^o, \tag{5.9}$$

$$\widetilde{J}_5 = r_{,R}^2 T_{RR}^{o2} + (\frac{r}{R})^2 T_{\Theta\Theta}^{o2}, \tag{5.10}$$

$$\widetilde{J}_6 = \frac{T_{RR}^o}{r_{,R}^2} + \left[(\frac{R}{r})^2 + (\frac{R\Omega}{\lambda})^2\right] T_{\Theta\Theta}^o, \tag{5.11}$$

$$\widetilde{J}_7 = (\frac{T_{RR}^o}{r_{,R}})^2 + \left[(\frac{R}{r})^2 + (\frac{R\Omega}{\lambda})^2\right] T_{\Theta\Theta}^{o2}. \tag{5.12}$$

Now, equations (3.16) through (3.18) yields

$$\widetilde{J}_{m1} = r_{,R}^2 m_1 + (\frac{r}{R})^2 m_2 + [(r\Omega)^2 + \lambda^2]\delta_0, \tag{5.13}$$

$$\widetilde{J}_{m2} = \frac{1}{r_{,R}^2} m_3 + \left[(\frac{R}{r})^2 + (\frac{R\Omega}{\lambda})^2\right] m_4 + \frac{\kappa_0}{\lambda^2}, \tag{5.14}$$

$$\widetilde{J}_{m3} = J_3^r \widetilde{J}_3, \tag{5.15}$$

where,

$$\begin{aligned} m_1 &= \left[\delta_0 + \delta_1 T_{RR}^o + \delta_2 T_{RR}^{o2}\right], \qquad m_2 = \left[\delta_0 + \delta_1 T_{\Theta\Theta}^o + \delta_2 T_{\Theta\Theta}^{o2}\right], \\ m_3 &= \left[\kappa_0 + \kappa_1 T_{RR}^o + \kappa_2 T_{RR}^{o2}\right], \quad m_4 = \left[\kappa_0 + \kappa_1 T_{\Theta\Theta}^o + \kappa_2 T_{\Theta\Theta}^{o2}\right]. \end{aligned} \tag{5.16}$$

The components of stress in cylindrical polar basis for the special boundary value problem being studied is

$$\begin{Bmatrix} T_{rr} \\ T_{\theta\theta} \\ T_{zz} \\ T_{r\theta} \\ T_{rz} \\ T_{\theta z} \end{Bmatrix} = \begin{Bmatrix} \alpha_0 + \alpha_1 m_1 r_{,R}^2 + \alpha_2 m_3 \frac{1}{r_{,R}^2} \\ \alpha_0 + \alpha_1 \left[m_2(\frac{r}{R})^2 + \delta_0(r\Omega)^2\right] + \alpha_2 m_4 (\frac{R}{r})^2 \\ \alpha_0 + \alpha_1 \delta_0 \lambda^2 + \alpha_2 \left[\frac{\kappa_0}{\lambda^2} + m_4(\frac{R\Omega}{\lambda})^2\right] \\ 0 \\ 0 \\ \alpha_1 \delta_0 r\Omega\lambda - \alpha_2 m_4 \frac{R^2}{r}\frac{\Omega}{\lambda} \end{Bmatrix}. \tag{5.17}$$

The balance of linear momentum, (4.2) in the absence of body forces and static

loading reduces to

$$\frac{dT_{rr}}{dR} + \frac{r_{,R}}{r}\left[T_{rr} - T_{\theta\theta}\right] = 0, \tag{5.18}$$

on recognizing that the non-zero components of the stress, $\mathbf{T}$ depends only on R. Recognizing that this equation would reduce to the form

$$f_1 r_{,RR} + f_2 = 0, \tag{5.19}$$

we seek to find f_1 and f_2. Towards this we compute

$$\begin{aligned}
\widetilde{J}_{m1,R} &= 2r_{,R}m_1 r_{,RR} + h_1 + g_1, && (5.20)\\
\widetilde{J}_{m2,R} &= -\frac{2m_3}{r_{,R}^3} r_{,RR} + h_2 + g_2, && (5.21)\\
\widetilde{J}_{m3,R} &= J^r_{3,R}\widetilde{J}_3 + J^r_3 \widetilde{J}_{3,R}, && (5.22)
\end{aligned}$$

where

$$\begin{aligned}
\widetilde{J}_{3,R} &= \frac{\lambda}{R}\left[r_{,R}^2 + r r_{,RR} - \frac{r}{R} r_{,R}\right]\\
h_1 &= m_{1,R} r_{,R}^2 + (\frac{r}{R})^2 m_{2,R} + \left[\lambda^2 + (r\Omega)^2\right]\delta_{0,R}\\
h_2 &= \frac{\kappa_{0,R}}{\lambda^2} + \frac{m_{3,R}}{r_{,R}^2} + m_{4,R}\left[(\frac{R}{r})^2 + (\frac{R\Omega}{\lambda})^2\right],
\end{aligned}$$

$$\begin{aligned}
m_{1,R} &= \delta_{0,R} + \delta_{1,R}T^o_{RR} + \delta_1 T^o_{RR,R} + \delta_{2,R}T^{o2}_{RR} + 2\delta_2 T^o_{RR}T^o_{RR,R},\\
m_{2,R} &= \delta_{0,R} + \delta_{1,R}T^o_{\Theta\Theta} + \delta_1 T^o_{\Theta\Theta,R} + \delta_{2,R}T^{o2}_{\Theta\Theta} + 2\delta_2 T^o_{\Theta\Theta}T^o_{\Theta\Theta,R},\\
m_{3,R} &= \kappa_{0,R} + \kappa_{1,R}T^o_{RR} + \kappa_1 T^o_{RR,R} + \kappa_{2,R}T^{o2}_{RR} + 2\kappa_2 T^o_{RR}T^o_{RR,R},\\
m_{4,R} &= \kappa_{0,R} + \kappa_{1,R}T^o_{\Theta\Theta} + \kappa_1 T^o_{\Theta\Theta,R} + \kappa_{2,R}T^{o2}_{\Theta\Theta} + 2\kappa_2 T^o_{\Theta\Theta}T^o_{\Theta\Theta,R}, && (5.23)
\end{aligned}$$

$$\begin{aligned}
g_1 &= 2\frac{r}{R}\left[\frac{r_{,R}}{R} - \frac{r}{R^2}\right] m_2 + 2\delta_0 r r_{,R}\Omega^2, && (5.24)\\
g_2 &= 2m_4\left[\frac{R}{r}\left(\frac{1}{r} - \frac{R r_{,R}}{r^2}\right) + R(\frac{\Omega}{\lambda})^2\right], && (5.25)
\end{aligned}$$

Noting

$$\begin{aligned}\frac{dT_{rr}}{dR} &= \frac{\partial\alpha_0}{\partial R}+\frac{\partial\alpha_0}{\partial\widetilde{J}_{m1}}\widetilde{J}_{m1,R}+\frac{\partial\alpha_0}{\partial\widetilde{J}_{m2}}\widetilde{J}_{m2,R}+\frac{\partial\alpha_0}{\partial\widetilde{J}_{m3}}\widetilde{J}_{m3,R}\\ &+\left[\frac{\partial\alpha_1}{\partial R}+\frac{\partial\alpha_1}{\partial\widetilde{J}_{m1}}\widetilde{J}_{m1,R}+\frac{\partial\alpha_1}{\partial\widetilde{J}_{m2}}\widetilde{J}_{m2,R}+\frac{\partial\alpha_1}{\partial\widetilde{J}_{m3}}\widetilde{J}_{m3,R}\right]m_1r_{,R}^2\\ &+\left[\frac{\partial\alpha_2}{\partial R}+\frac{\partial\alpha_2}{\partial\widetilde{J}_{m1}}\widetilde{J}_{m1,R}+\frac{\partial\alpha_2}{\partial\widetilde{J}_{m2}}\widetilde{J}_{m2,R}+\frac{\partial\alpha_2}{\partial\widetilde{J}_{m3}}\widetilde{J}_{m3,R}\right]\frac{m_3}{r_{,R}^2}\\ &+\alpha_1r_{,R}^2m_{1,R}+\frac{\alpha_2}{r_{,R}^2}m_{3,R}+2[\alpha_1m_1r_{,R}-\frac{\alpha_2}{r_{,R}^3}m_3]r_{,RR}. \end{aligned}\tag{5.26}$$

We find

$$\begin{aligned}f_1 &= 2\frac{\partial\alpha_1}{\partial\widetilde{J}_{m1}}m_1^2r_{,R}^3+\frac{\partial\alpha_1}{\partial\widetilde{J}_{m3}}\widetilde{J}_{m3}m_1r_{,R}+2\left[\alpha_1+\frac{\partial\alpha_0}{\partial\widetilde{J}_{m1}}\right]m_1r_{,R}+\frac{\partial\alpha_0}{\partial\widetilde{J}_{m3}}\frac{\widetilde{J}_{m3}}{r_{,R}}\\ &+\frac{\partial\alpha_2}{\partial\widetilde{J}_{m3}}\widetilde{J}_{m3}m_3\frac{1}{r_{,R}^3}-m_3\left[\alpha_2+\frac{\partial\alpha_0}{\partial\widetilde{J}_{m2}}\right]\frac{2}{r_{,R}^3}-\frac{\partial\alpha_2}{\partial\widetilde{J}_{m2}}m_3^2\frac{2}{r_{,R}^5},\\ &+\left[\frac{\partial\alpha_2}{\partial\widetilde{J}_{m1}}-\frac{\partial\alpha_1}{\partial\widetilde{J}_{m2}}\right]\frac{2m_1m_3}{r_{,R}}\end{aligned}\tag{5.27}$$

$$\begin{aligned}f_2 &= \left[\frac{\partial\alpha_0}{\partial\widetilde{J}_{m1}}+\frac{\partial\alpha_1}{\partial\widetilde{J}_{m1}}m_1r_{,R}^2+\frac{\partial\alpha_2}{\partial\widetilde{J}_{m1}}\frac{m_3}{r_{,R}^2}\right][g_1+h_1]\\ &+\left[\frac{\partial\alpha_0}{\partial\widetilde{J}_{m2}}+\frac{\partial\alpha_1}{\partial\widetilde{J}_{m2}}m_1r_{,R}^2+\frac{\partial\alpha_2}{\partial\widetilde{J}_{m2}}\frac{m_3}{r_{,R}^2}\right][g_2+h_2]\\ &+\left[\frac{\partial\alpha_0}{\partial\widetilde{J}_{m3}}+\frac{\partial\alpha_1}{\partial\widetilde{J}_{m3}}m_1r_{,R}^2+\frac{\partial\alpha_2}{\partial\widetilde{J}_{m3}}\frac{m_3}{r_{,R}^2}\right]\left[J_{3,R}^r\widetilde{J}_3+J_3^rr_{,R}(r_{,R}-\frac{r}{R})\frac{\lambda}{R}\right]\\ &+\left[\frac{\partial\alpha_0}{\partial R}+\frac{\partial\alpha_1}{\partial R}m_1r_{,R}^2+\frac{\partial\alpha_2}{\partial R}\frac{m_3}{r_{,R}^2}\right]\\ &+r_{,R}\alpha_1\left[r_{,R}\left(m_{1,R}+r_{,R}\frac{m_1}{r}\right)-m_2\frac{r}{R^2}-r\Omega^2\delta_0\right]\\ &+\alpha_2\left[\frac{1}{r_{,R}^2}\left(m_{3,R}+r_{,R}\frac{m_3}{r}\right)-\frac{R^2}{r^3}r_{,R}m_4\right].\end{aligned}\tag{5.28}$$

Here we have used the fact that m_i's would depend only on R.

If we were to seek the solution to the governing equation as a Taylor's series, for the series to converge we require $r_{,RR}$ and its higher derivatives to be bounded

on $R_i \leq R \leq R_o$. By inspection, we find that $r_{,RR}$ and its higher derivatives would be bounded at all points except at $R = 0$ and at points where $f_1 = 0$ assuming that α_i's are smooth bounded functions of $\widetilde{J}_{mi}$ and R i.e., $\alpha_i \in C^\infty(\omega_a)$ where $\omega_a = \{(\widetilde{J}_{m1}, \widetilde{J}_{m2}, \widetilde{J}_{m3}, R) | 0 < \widetilde{J}_{m1} < \infty, 0 < \widetilde{J}_{m2} < \infty, 0 < \widetilde{J}_{m3} < \infty, R_i \leq R \leq R_o\}$.

Therefore, we begin by investigating whether f_1 and f_2 is bounded at $R = 0$. Towards this, let $\hat{r}_{,R} = r_{,R}|_{R=0} \neq 0$. Now, for $r_{,RR}$ to be bounded at $R = 0$, $r(0) = 0$, the terms $r_{,R}^2 m_1/r - m_2 r/R^2$, $m_3/(r r_{,R}) - R^2 r_{,R} m_4/r^3$, $(r_{,R} - r/R)/R$, $(r - R r_{,R})/r^2$ and r/R must be bounded. For this we require $m_1(0) = m_2(0)$ and $m_3(0) = m_4(0)$ or $m_1(0) = m_2(0) = m_3(0) = m_4(0) = 0$. For the higher order derivatives of $r(R)$ to be bounded we further require $\frac{d^n m_1}{dR^n}|_{R=0} = \frac{d^n m_2}{dR^n}|_{R=0}$ and $\frac{d^n m_3}{dR^n}|_{R=0} = \frac{d^n m_4}{dR^n}|_{R=0}$ or $\frac{d^n m_1}{dR^n}|_{R=0} = \frac{d^n m_2}{dR^n}|_{R=0} = \frac{d^n m_3}{dR^n}|_{R=0} = \frac{d^n m_4}{dR^n}|_{R=0} = 0$ for any arbitrary integer, n. If this were so, it follows from Taylor series representation for functions, $m_1(R)$, $m_2(R)$, $m_3(R)$, $m_4(R)$ that $m_1(R) = m_2(R) = n_1(R)$ and $m_3(R) = m_4(R) = n_2(R)$.

Then, since

$$\begin{aligned}
\lim_{R\to 0} \frac{r}{R} &= \hat{r}_{,R}, \\
\lim_{R\to 0} \frac{(r_{,R} R - r)}{R^2} &= \frac{\hat{r}_{,RR}}{2}, \qquad \lim_{R\to 0} \frac{(r - R r_{,R})}{r^2} = -\frac{\hat{r}_{,RR}}{2\hat{r}_{,R}^2}, \\
\lim_{R\to 0} \frac{r_{,R}^2}{r} - \frac{r}{R^2} &= \hat{r}_{,RR}, \qquad \lim_{R\to 0} \frac{1}{r r_{,R}} - \frac{R^2 r_{,R}}{r^3} = -\frac{\hat{r}_{,RR}}{\hat{r}_{,R}^3},
\end{aligned}$$

where the superposed hat denotes that these are the values at $R = 0$, the terms get bounded.

Assuming that the requirement $m_1(R) = m_2(R) = n_1(R)$ and $m_3(R) = m_4(R) = n_2(R)$ is met in some body[1], we next examine if we could get any additional restriction for $r_{,RRR}$ to be bounded at $R = 0$, $r = 0$, $r_{,R}|_{R=0} = \hat{r}_{,R}$. Towards this consider the

[1]It holds in bodies for which $\delta_1 = -\delta_2 tr(\mathbf{T}^o)$.

derivative of the term $r_{,R}(r_{,R} - r/R)/R$ in the expression for $\widetilde{J}_{3,R}$ which is

$$r_{,RR}\frac{2r_{,R}R - r}{R^2} + 2r_{,R}\frac{r - Rr_{,R}}{R^3}. \tag{5.29}$$

For the term to be bounded at $R = 0$, $r = 0$, $r_{,R}|_{R=0} = \hat{r}_{,R}$, we require $r_{,RR}|_{R=0} = 0$. Hence, $\hat{f}_2 = f_2(0, 0, \hat{r}_{,R}) = 0$. Such restrictions arise for higher order derivatives too. Therefore, we cannot be assured that the solution is a converging series since we cannot show that all the higher order derivatives are bounded in the interval $0 \leq R \leq R_o$. On the other hand it should be noted that the solution could still be a converging series in special class of bodies in which these problematic terms do not arise.

The above problem does not arise in annular cylinders. However, if one believes that the solution to a boundary value problem depend continuously on its parameters, in particular R_i, then the deformation (5.2) would not be possible in annular cylinders as well unless the above restrictions are met. But there are many shear deformations that are realizable in annular cylinders that are not possible in solid right circular cylinders.

Thus, we have shown that when $\overline{\alpha}_i$ are smooth bounded functions of $\widetilde{J}_{mi}$ and R i.e., $\alpha_i \in C^\infty(\omega_a)$ then the deformation of the form (5.2) is possible in bodies that have a geometry of an annular right circular cylinder, provided suitable traction is applied at the boundary. In cases where α_i is only piecewise continuous, the deformation (5.2) is still possible provided there exist a real valued positive solution, $(d_j^-)_*$ for the interface condition, $T_{rr}(R_j^-, r_j^-, d_j^-) = T_{rr}(R_j^+, r_j^+, d_j^+)$ at each interface.

Before specializing to specific constitutive relations, we record the boundary conditions. The boundary conditions that should be prescribed are $T_{rr}(r_i)$, $T_{rr}(r_o)$, the radial component of the normal stress at the inner and outer surfaces, the axial load, L, defined in (4.72), the torque, T, defined in (4.73), the deformed inner and outer

radius, r_i and r_o, the ratio of the deformed length to original length, λ and twist per unit length, Ω. As discussed in the last chapter, we shall specify only a subset of the above conditions, sufficient enough to solve the governing equation and study the variation of the rest with respect to the specified boundary conditions. Thus, say, we might specify that $T_{rr}(r_o) = 0$, $\lambda = 1$, $\Omega = 0$ and $r_o = c$, then study the traction - $T_{rr}(r_i)$, L, T - required to realize a given value of r_o but for various values of c. Here we note that the integration for the axial load and torque were performed using Trapezoidal rule. This first order method is believed to yield accurate enough results because adaptive meshing is used while solving the ODE.

A. Blatz-Ko constitutive relation

Now, we record the simplified governing equations for the constitutive relations discussed in chapter III. First, we study the Blatz-Ko constitutive relation used to model polyurethane, recorded in (3.73). For this

$$f_1 = \mu_1 r_{,R} \frac{m_1}{\widetilde{J}_{m3}} + \frac{\mu_1(2\mu_3+1)}{r_{,R}\widetilde{J}_{m3}^{(2\mu_3+1)}}, \tag{5.30}$$

$$\begin{aligned} f_2 = {} & \mu_1 \frac{r_{,R}}{\widetilde{J}_{m3}} \left[r_{,R} \left(m_{1,R} + r_{,R} \frac{m_1}{r} \right) - m_2 \frac{r}{R^2} - \frac{r\Omega^2}{(J_3^r)^{2\mu_3}} \right] + \frac{\mu_{1,R}}{\widetilde{J}_{m3}} \left[m_1 r_{,R}^2 - \frac{1}{\widetilde{J}_{m3}^{2\mu_3}} \right] \\ & + \left[\frac{\mu_1(2\mu_3+1)}{\widetilde{J}_{m3}^{2(\mu_3+1)}} - r_{,R}^2 \mu_1 \frac{m_1}{\widetilde{J}_{m3}^2} \right] \left[J_{3,R}^r \widetilde{J}_3 + \lambda r_{,R} \left(r_{,R} - \frac{r}{R} \right) \frac{J_3^r}{R} \right], \end{aligned} \tag{5.31}$$

where,

$$\begin{aligned} m_1 &= \frac{1}{(J_3^r)^{2\mu_3}} + J_3^r \frac{T_{RR}^o}{\mu_1}, \quad m_2 = \frac{1}{(J_3^r)^{2\mu_3}} + J_3^r \frac{T_{\Theta\Theta}^o}{\mu_1}, \quad \widetilde{J}_{m3} = J_3^r \widetilde{J}_3, \\ m_{1,R} &= J_{3,R}^r \frac{T_{RR}^o}{\mu_1} + J_3^r \frac{T_{RR,R}^o}{\mu_1} - 2\mu_3 \frac{J_{3,R}^r}{(J_3^r)^{2\mu_3+1}} - J_3^r T_{RR}^o \frac{\mu_{1,R}}{\mu_1^2}, \\ m_{2,R} &= J_{3,R}^r \frac{T_{\Theta\Theta}^o}{\mu_1} + J_3^r \frac{T_{\Theta\Theta,R}^o}{\mu_1} - 2\mu_3 \frac{J_{3,R}^r}{(J_3^r)^{2\mu_3+1}} - J_3^r T_{\Theta\Theta}^o \frac{\mu_{1,R}}{\mu_1^2}, \quad J_{3,R}^r = \frac{l_1}{l_2}, \end{aligned}$$

$$
\begin{aligned}
l_1 &= J_3^r\left[\frac{K_{1,R}}{\mu_1}-\frac{K_1}{\mu_1^2}\mu_{1,R}\right]+(J_3^r)^{2\mu_3+1}\left[\left(\frac{K_{3,R}}{\mu_1^3}-\frac{3K_3}{\mu_1^4}\mu_{1,R}\right)(J_3^r)^{2(\mu_3+1)}\right.\\
&\qquad\left.+\left(\frac{K_{2,R}}{\mu_1^2}-\frac{2K_2}{\mu_1^3}\mu_{1,R}\right)J_3^r\right],\\
l_2 &= 2(2\mu_3+1)(J_3^r)^{4\mu_3+1}-(2\mu_3+1)(J_3^r)^{2\mu_3}\left[\frac{K_3}{\mu_1^3}(J_3^r)^{2(\mu_3+1)}+J_3^r\frac{K_2}{\mu_1^2}\right]\\
&\qquad-(J_3^r)^{2\mu_3+1}\left[2\frac{K_3}{\mu_1^3}(\mu_3+1)(J_3^r)^{2\mu_3+1}+\frac{K_2}{\mu_1^2}\right]+2\mu_3(J_3^r)^{-(2\mu_3+1)}-\frac{K_1}{\mu_1},\\
K_1 &= T^o_{RR}+T^o_{\Theta\Theta}, \qquad K_2=T^o_{RR}T^o_{\Theta\Theta}, \qquad K_3=0,\\
K_{1,R} &= T^o_{RR,R}+T^o_{\Theta\Theta,R}, \qquad K_{2,R}=T^o_{RR,R}T^o_{\Theta\Theta}+T^o_{RR}T^o_{\Theta\Theta,R}, \qquad K_{3,R}=0, \quad (5.32)
\end{aligned}
$$

Thus, in prestressed bodies $m_1(R)\neq m_2(R)$ and $\hat{f}_2\neq 0$. Hence, deformation (5.2) is not possible in prestressed solid right circular cylinders made up of Blatz-Ko material.

The requirement $f_1\neq 0$ yields

$$
(J_3^r)^{(2\mu_3+1)}\frac{T^o_{RR}}{\mu_1}\neq -1-\frac{2\mu_3+1}{\widetilde{J}_3^{2\mu_3}}\frac{1}{r_{,R}^2}. \tag{5.33}
$$

Hence, the value of constants in constitutive prescriptions for $T^o_{\Theta\Theta}$ [2] are such that $(J_3^r)^{(2\mu_3+1)}T^o_{RR}(R)/\mu_1>-1$ assuming $\mu_3>-0.5$. Thus, if $\mu_1\in C^\infty(\omega_R)$ and $T^o_{\Theta\Theta}\in C^\infty(\omega_R)$, where $\omega_R=\{R|R_i\leq R\leq R_o\}$ then $f_2/f_1\in C^\infty(\omega)$.

Thus, the governing equation

$$
f_1 r_{,RR}+f_2=0, \tag{5.34}
$$

is solved for the mixed boundary condition

$$
r(R_o)=r_o, \qquad T_{rr}(r_o)=0, \tag{5.35}
$$

for a specified value of Ω and λ and $R_i\leq R\leq R_o$. Solving (5.35b) for $r_{,R}(R_o)=d^o$

[2] T^o_{RR} is derived from the constitutively prescribed $T^o_{\Theta\Theta}$ see section (G.2) of chapter III for details

we obtain

$$d^o = \left(\frac{R_o}{r_o\lambda}\right)^{\frac{\mu_3}{1+\mu_3}}. \tag{5.36}$$

Hence, there exist an unique deformation of the form (5.2) for the special form of Blatz Ko constitutive relation studied here when $R_i > 0$ and $\mu_1 \in C^\infty(\omega_R)$ and $T^o_{\Theta\Theta}$ $\in C^\infty(\omega_R)$ and $(J^r_3)^{(2\mu_3+1)}T^o_{RR}(R)/\mu_1 > -1$.

If the variation of μ_1 and/or $T^o_{\Theta\Theta}$ is only piecewise continuous, then at the interface (surface defined by $R = \textit{constant}$ across which μ_1 and/or $\mathbf{T}^o$ is discontinuous) we require $T_{rr}(r^-_j) = T_{rr}(r^+_j)$ which translates to finding $(d^-_j)_* > 0$ such that

$$y((d^-_j)_*) = 0, \tag{5.37}$$

where

$$\begin{aligned} y(d^-_j) \;\; = \;\; & \mu_1(R^-_j)\left\{d^-_j\frac{m_1(R^-_j)}{\lambda J^r_3(R^-_j)}\frac{R^-_j}{r^-_j} - \left[\frac{1}{d^-_j\lambda J^r_3(R^-_j)}\frac{R^-_j}{r^-_j}\right]^{2\mu_3+1}\right\} \\ & -\mu_1(R^+_j)\left\{d^+_j\frac{m_1(R^+_j)}{\lambda J^r_3(R^+_j)}\frac{R^+_j}{r^+_j} - \left[\frac{1}{d^+_j\lambda J^r_3(R^+_j)}\frac{R^+_j}{r^+_j}\right]^{2\mu_3+1}\right\}. \end{aligned} \tag{5.38}$$

In general, it is not possible to solve (5.37) analytically and hence we seek numerical solution using the bisection algorithm. Since, (5.38) is a continuous function in d^-_j and since when $\mu_3 > -0.5$,

$$\lim_{d^-_j\to 0} y(d^-_j) \to -\infty, \qquad \text{and} \lim_{d^-_j\to\infty} y(d^-_j) \to \infty, \tag{5.39}$$

there exist $(d^-_j)_* \in (0,\infty)$ such that $y((d^-_j)_*) = 0$. Further, since (5.38) is monotonic in d^-_j for $d^-_j > 0$, $m_1(R^-_j) > 0$ and $\mu_3 > -0.5$, (5.37) has an unique real valued solution, $(d^-_j)_*$.

As before, if the constitutive prescription of $T^o_{\Theta\Theta}$ ensures that $f_1 \neq 0$ and $\mu_3 > -0.5$, then $f_2/f_1 \in C^\infty(\omega^s_j)$. Hence, there exist an unique deformation of the form

(5.2) for the class of Blatz Ko constitutive relation studied here when $R_i > 0$ and for the radial variations of μ_1, $T^o_{\Theta\Theta}$ assumed here.

1. Case-1: Pure inflation

We begin by studying the response of the annular cylinder subjected to inflation at constant length by applying a radial component of the normal stress at the inner surface and axial component of the normal stresses at the extremities of the cylinder. We shall also require that the outer surface of the cylinder be free of boundary traction. Thus, for this case we specify, $\lambda = 1$, $\Omega = 0$, $T_{rr}(r_o) = 0$ and r_o. Hence, the governing equation (5.34) can be solved and we could obtain r_i, $T_{rr}(r_i)$ and the axial load L. Figures 12 and 13 plot these quantities as a function of r_o. The prestresses corresponding to various cases, studied here, are plotted in figure 14. 'cs-1' corresponds to the case

$$T^o_{\Theta\Theta} = \epsilon_1 \left[\cos(2\pi\overline{R}) + \cos(4\pi\overline{R}) + \cos(6\pi\overline{R}) + \cos(8\pi\overline{R})\right], \tag{5.40}$$

with $\epsilon_1 = 0.2$ which is a linear combination of the cosine variation recorded in section (G.2) of chapter III. 'cs-2' and 'cs-3' corresponds to the linear variation (see section (G.2) of chapter III) with $\epsilon_1 = 1$ and $\epsilon_1 = -1$ respectively. For 'cs-4' too, $T^o_{\Theta\Theta}$ is given by (5.40) but now $\epsilon_1 = -0.2$.

Figures 15 and 16 plot the transmural variation of the stresses and figure 17 plots $r(R)$ and $r_{,R}$ when $r_o = 1.2R_o$. In all these cases we assume that μ_1 is a constant and hence $(\mu_1)_m = \mu_1$.

It transpires from figure 12 that the radial component of the normal stress required to engender a given inflation is nearly the same, in a prestressed body and the stress free body. It could also be inferred from the figure that the magnitude of the deviation depends both on the magnitude of the prestresses and whether the circum-

ferential prestresses is radially increasing or decreasing. It could be seen from figure 16 that at a given location the stresses in the current configuration of a prestressed body could vary by as much as 2 times from that in a stress free body. Also in certain regions, even the sense, i.e. tensile or compressive, of these stresses is different, when compared between the prestressed and stress free body. It is worthwhile, to note that such large deviations are observed in a component of stress along which direction there were no prestresses.

2. Case-2: Uniaxial extension

Next, we study uniaxial extension of a prestressed annular cylinder made up of Blatz-Ko material. Thus, in this case we apply only axial component of the normal stresses at the extremities of the annular cylinder and study the deformation of the body. Hence, for this case, we specify $\Omega = 0$, $T_{rr}(r_i) = 0$, $T_{rr}(r_o) = 0$ and λ. Now, the value of r_o is not specified but has to be found such that the radial component of the normal stress at the inner surface of the cylinder, $T_{rr}(r_i)$ must be zero. Therefore, we begin by solving the IVP problem

$$r_{,RR} = f(r, R, r_{,R}) = -f_2/f_1, \qquad r(R_o) = r_o^g, \qquad T_{rr}(r_o) = 0, \tag{5.41}$$

for some particular value of r_o^g. We then find the error associated with this solution; that is we evaluate the boundary condition at $R = R_i$, namely $T_{rr}(r_i)$ using the computed $r(R_i)$ and $r_{,R}(R_i)$. Unless it happens that the boundary condition, $T_{rr}(R_i, r(R_i), r_{,R}(R_i)) = 0$ is satisfied, we take a different value for r_o^g and solve the resulting IVP. Thus, we define $\epsilon(r_o^g) = T_{rr}(R_i, r(R_i), r_{,R}(R_i))$ and seek r_o such that $\epsilon(r_o) = 0$. We use bisection algorithm to find this root.

As before having specified Ω, $T_{rr}(r_i)$, $T_{rr}(r_o)$ and λ, we study the only other non-trivial boundary traction, the axial load L and the boundary deformations r_i

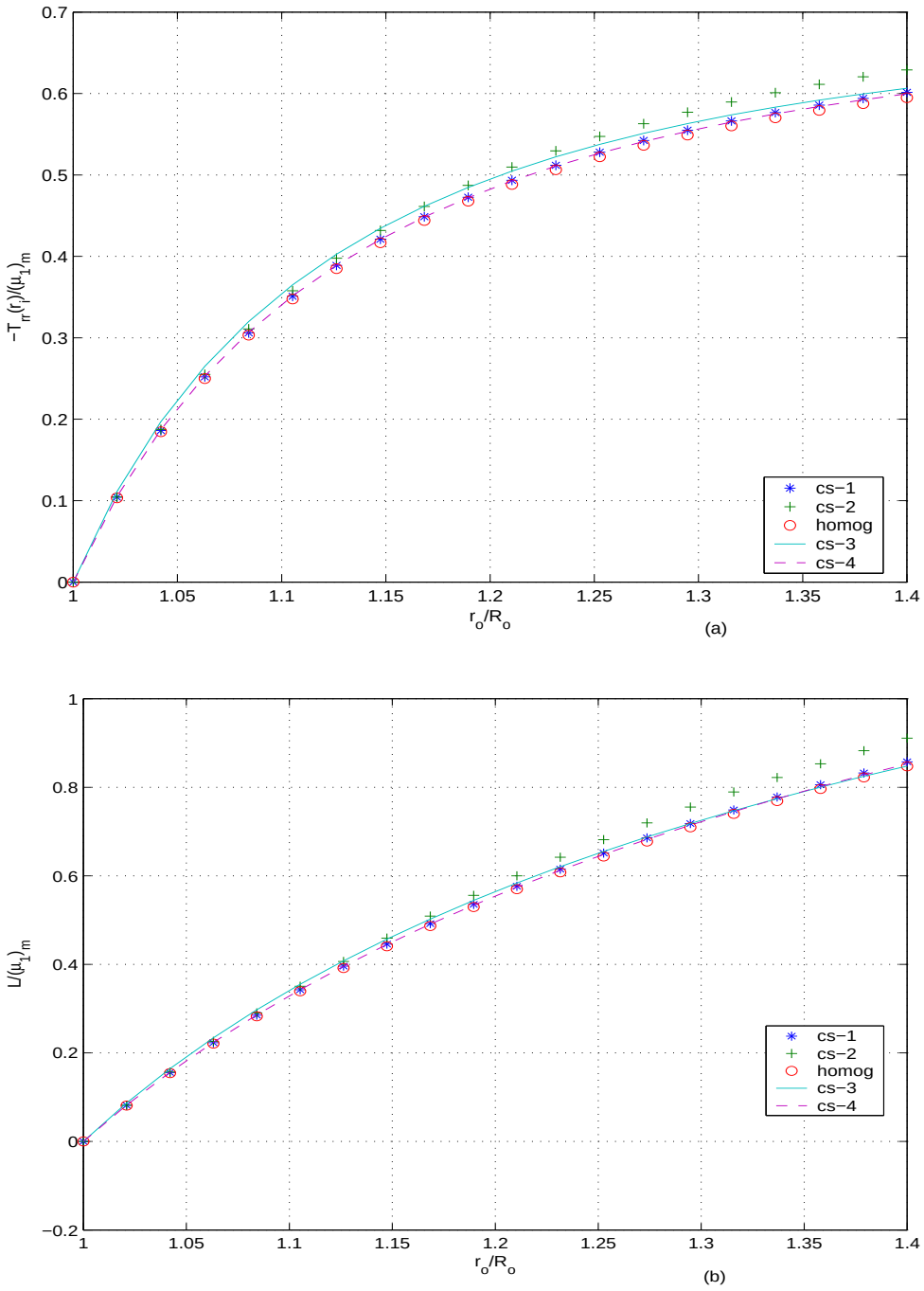

Fig. 12. Plot of (a) $-T_{rr}(r_i)/(\mu_1)_m$ (b) $L/(\mu_1)_m$ vs. r_o/R_o of an annular right circular cylinder with $R_o = 1$ and $R_i = 0.5$ made of Blatz Ko material for various prestress distributions shown in figure 14 when $\mu_3 = 6.25$ and $\mu_1 = 1$.

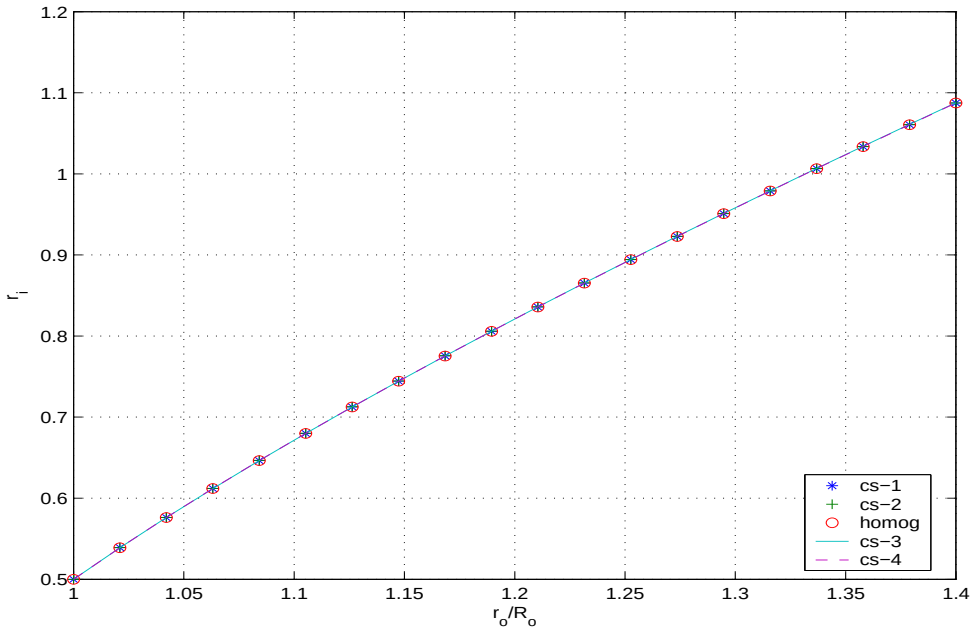

Fig. 13. Plot of r_i vs. r_o/R_o of an annular right circular cylinder with $R_o = 1$ and $R_i = 0.5$ made of Blatz Ko material for various prestress distributions shown in figure 14 when $\mu_3 = 6.25$ and $\mu_1 = 1$.

and r_o required to realize a given value of λ. Figures 18 and 19 plot the axial load L and boundary deformations respectively for various values of λ. The prestress fields studied here are same as that in the last sub-section. While figures 20 and 21 plot the transmural variation of the stresses, figure 22 plots $r(R)$ and $r_{,R}(R)$ when $\lambda = 1.2$. In all these cases we assume that μ_1 is constant.

From figure 18 we see that the axial load required to engender a given stretch, λ is greater for prestressed bodies in comparison to stress free bodies for all the cases of prestresses considered here. However, r_i and r_o are same for both the stress free body and the prestress bodies considered here as indicated by figure 19. Moreover, $r(R)$ and $r_{,R}(R)$ is also same for both the stress free body and the prestressed bodies

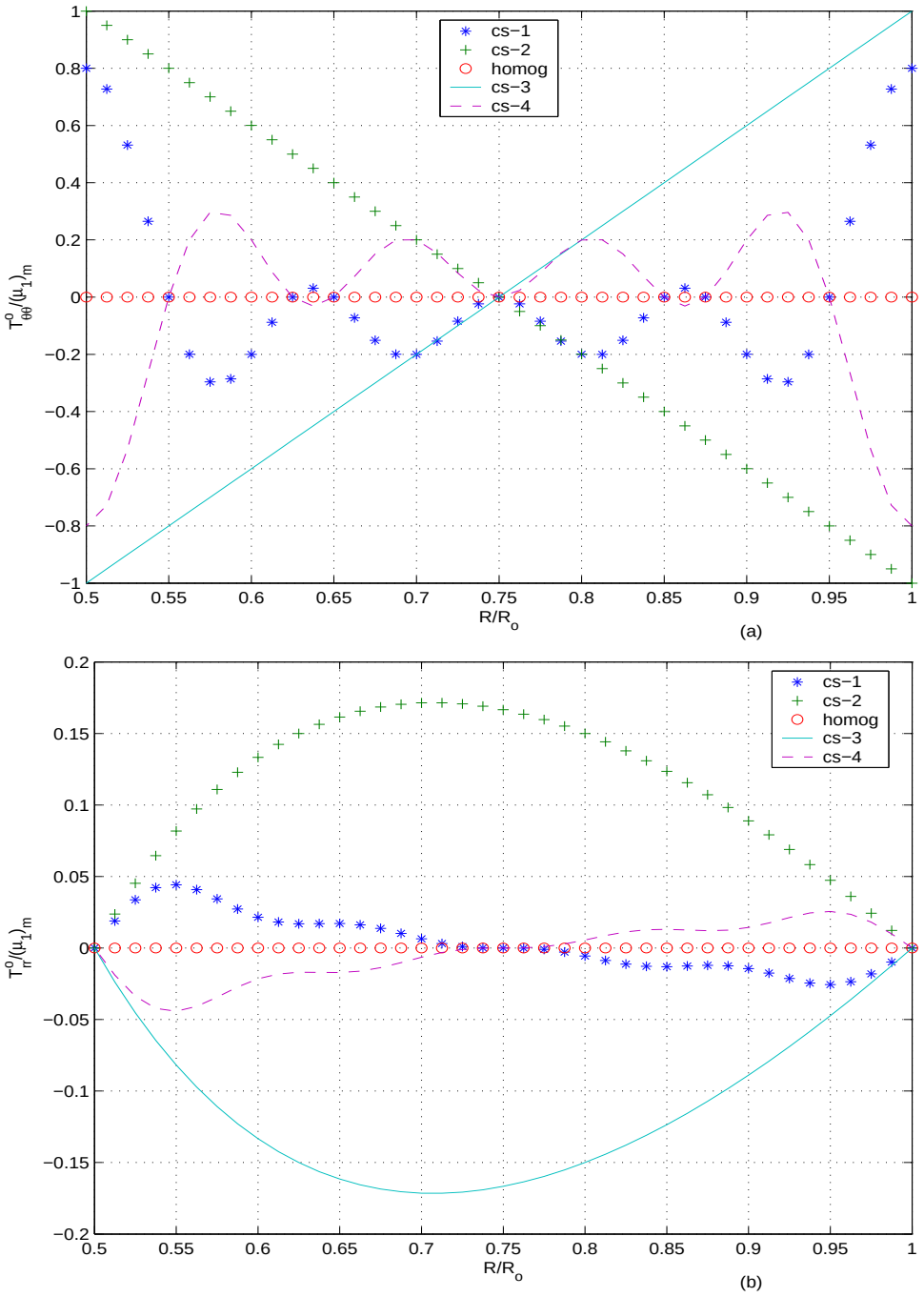

Fig. 14. Plot of prestresses (a) $T^o_{\Theta\Theta}/(\mu_1)_m$ (b) $T^o_{RR}/(\mu_1)_m$ vs. R/R_o in an annular right circular cylinder with $R_o = 1$ and $R_i = 0.5$.

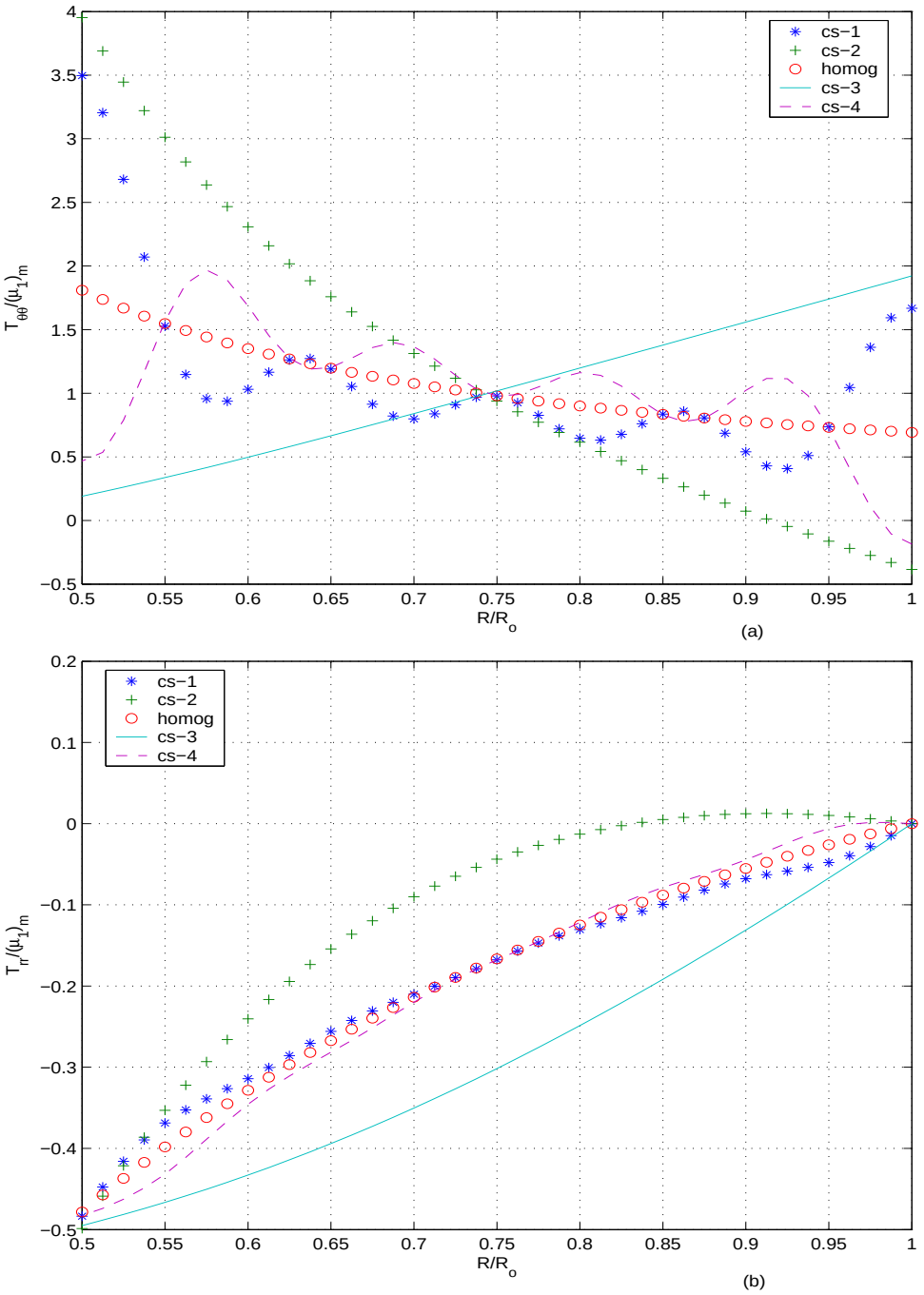

Fig. 15. Plot of stresses (a) $T_{\theta\theta}/(\mu_1)_m$ (b) $T_{rr}/(\mu_1)_m$ vs. R/R_o in an annular right circular cylinder with $R_o = 1$ and $R_i = 0.5$ made of Blatz Ko material subjected to inflation with $r_o = 1.2R_o$, for various prestress distributions shown in figure 14 when $\mu_3 = 6.25$ and $\mu_1 = 1$.

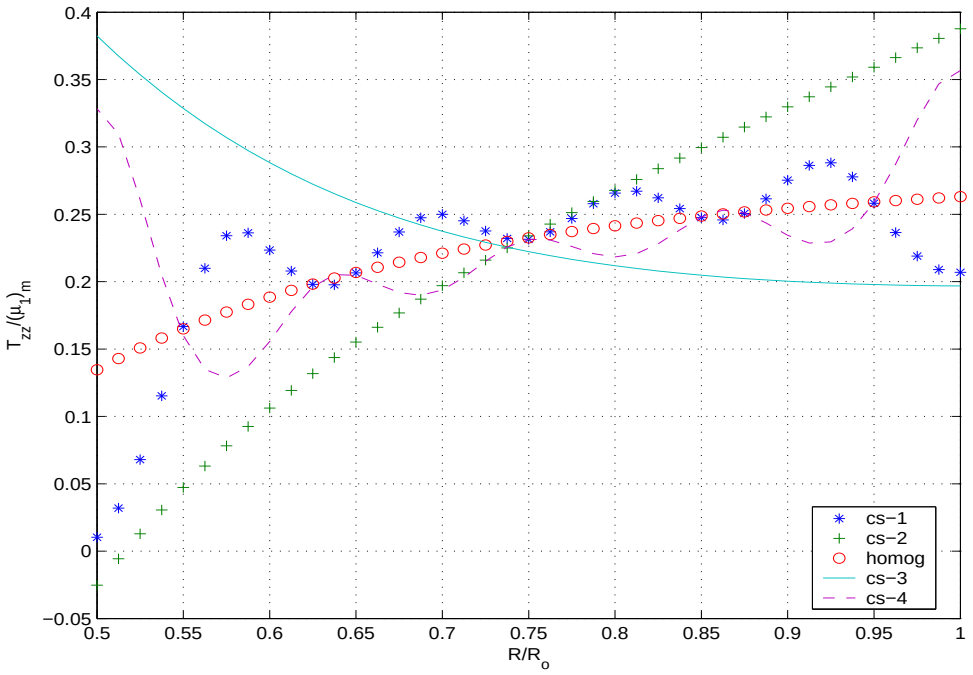

Fig. 16. Plot of stresses $T_{zz}/(\mu_1)_m$ vs. R/R_o in an annular right circular cylinder with $R_o = 1$ and $R_i = 0.5$ made of Blatz Ko material subjected to inflation with $r_o = 1.2R_o$, for various prestress distributions shown in figure 14 when $\mu_3 = 6.25$ and $\mu_1 = 1$.

considered here as inferred from figure 22. In fact, for this case the deformation of both the prestressed body and the stress free body is homogeneous. Thus, the stress distributions T_{rr} and $T_{\theta\theta}$ are same as that of the prestresses as seen by comparing figures 20 and 14. Here it is pertinent to observe that the Blatz Ko constitutive relation is one of the few that admit homogeneous solution for the class of boundary value problem being studied. Finally, we note that the axial stress, T_{zz} is not uniform in prestressed body because J_3^r is not uniform.

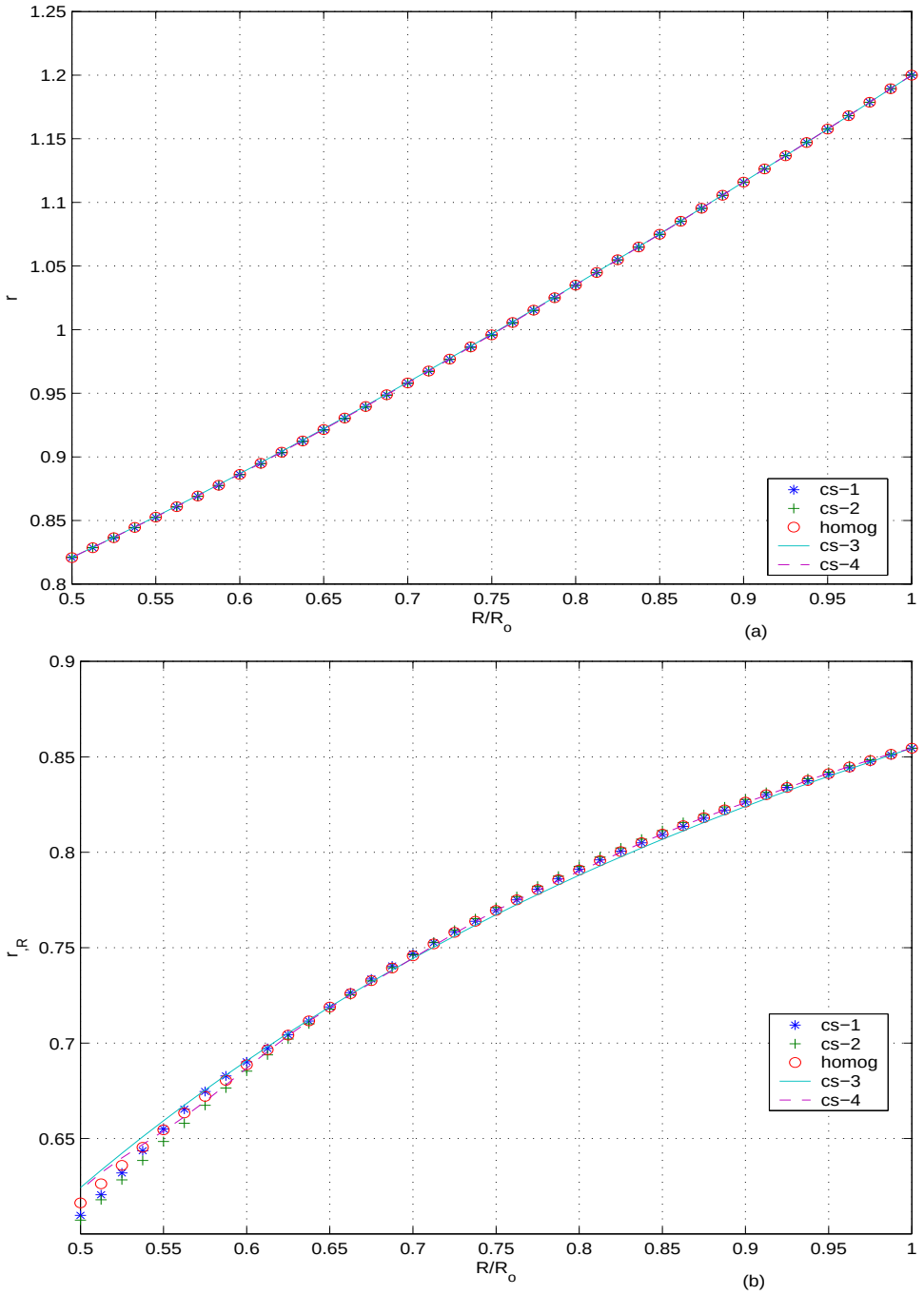

Fig. 17. Plot of (a) r (b) $r_{,R}$ vs. R/R_o in an annular right circular cylinder with $R_o = 1$ and $R_i = 0.5$ made of Blatz Ko material subjected to inflation with $r_o = 1.2R_o$, for various prestress distributions shown in figure 14 when $\mu_3 = 6.25$ and $\mu_1 = 1$.

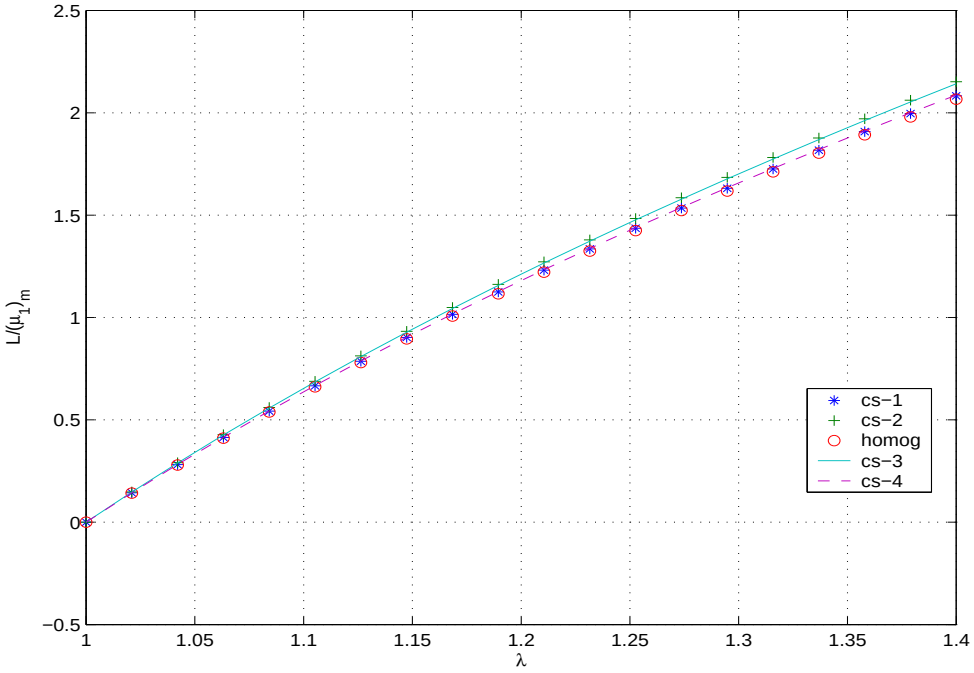

Fig. 18. Plot of $L/(\mu_1)_m$ vs. λ for an annular right circular cylinder with $R_o = 1$ and $R_i = 0.5$ made of Blatz Ko material for various prestress distributions shown in figure 14 when $\mu_3 = 6.25$ and $\mu_1 = 1$.

3. Case-3: Pure twist

Finally, we study the twisting of an annular right circular cylinder made up of Blatz-Ko material held at a constant length. In this case too, both the inner and outer surfaces are traction free and we apply axial component of the normal stresses and shear stress, $T_{\theta z}$ at the extremities of the annular cylinder. Thus, for this case we specify, $\lambda = 1$, $T_{rr}(r_i) = 0$, $T_{rr}(r_o) = 0$ and Ω. As described in detail in the previous case, we guess the value, r_o^g, solve the IVP, obtain $r(R_i)$ and $r_{,R}(R_i)$ and then verify if $T_{rr}(R_i, r(R_i), r_{,R}(R_i)) = 0$, if not we update the guessed value r_o^g, using bisection algorithm, until the boundary condition is met.

As before having specified λ, $T_{rr}(r_i)$, $T_{rr}(r_o)$ and Ω, we study the other boundary

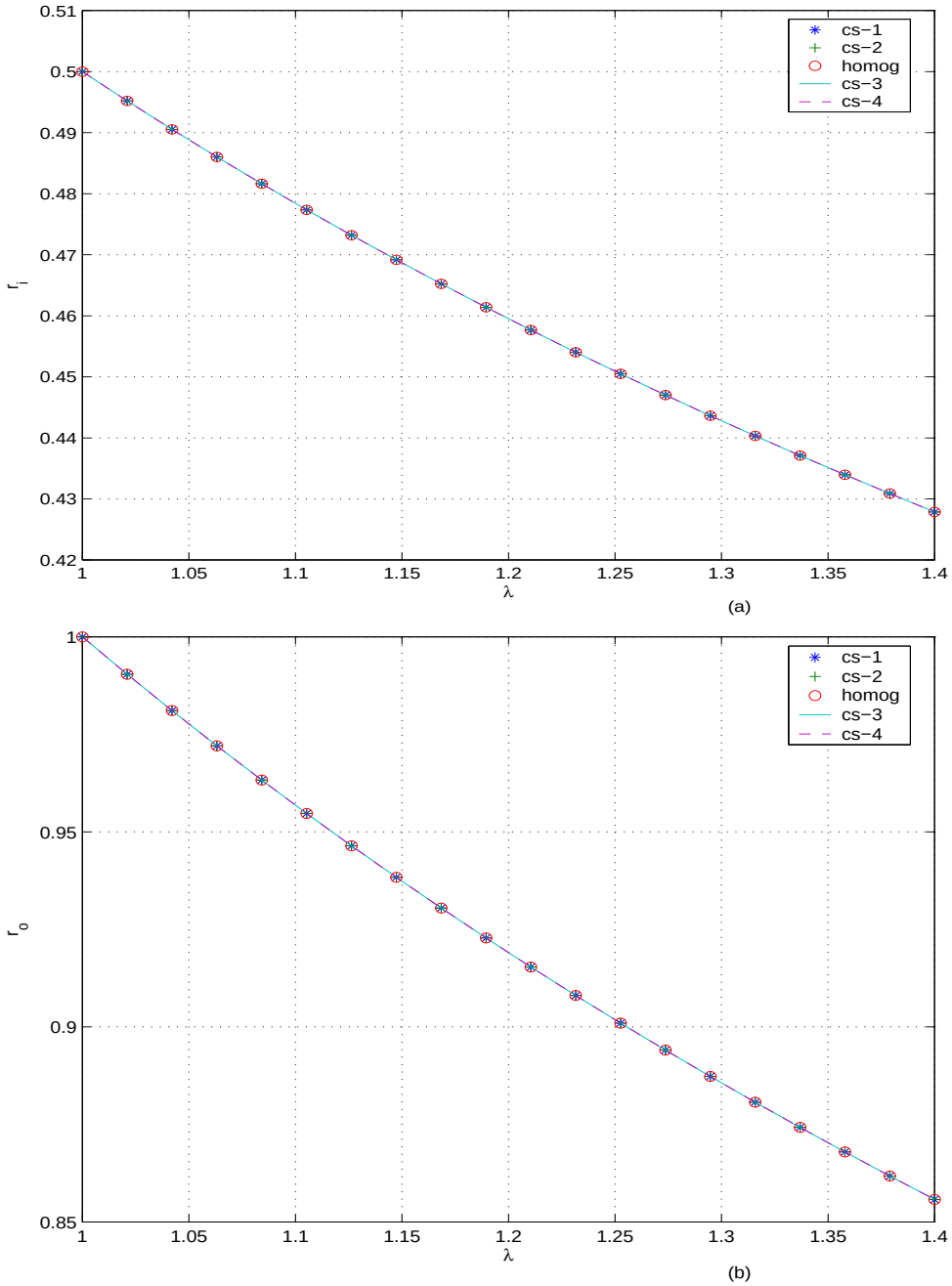

Fig. 19. Plot of (a) r_i (b) r_o vs. λ of an annular right circular cylinder with $R_o = 1$ and $R_i = 0.5$ made of Blatz Ko material for various prestress distributions shown in figure 14 when $\mu_3 = 6.25$ and $\mu_1 = 1$.

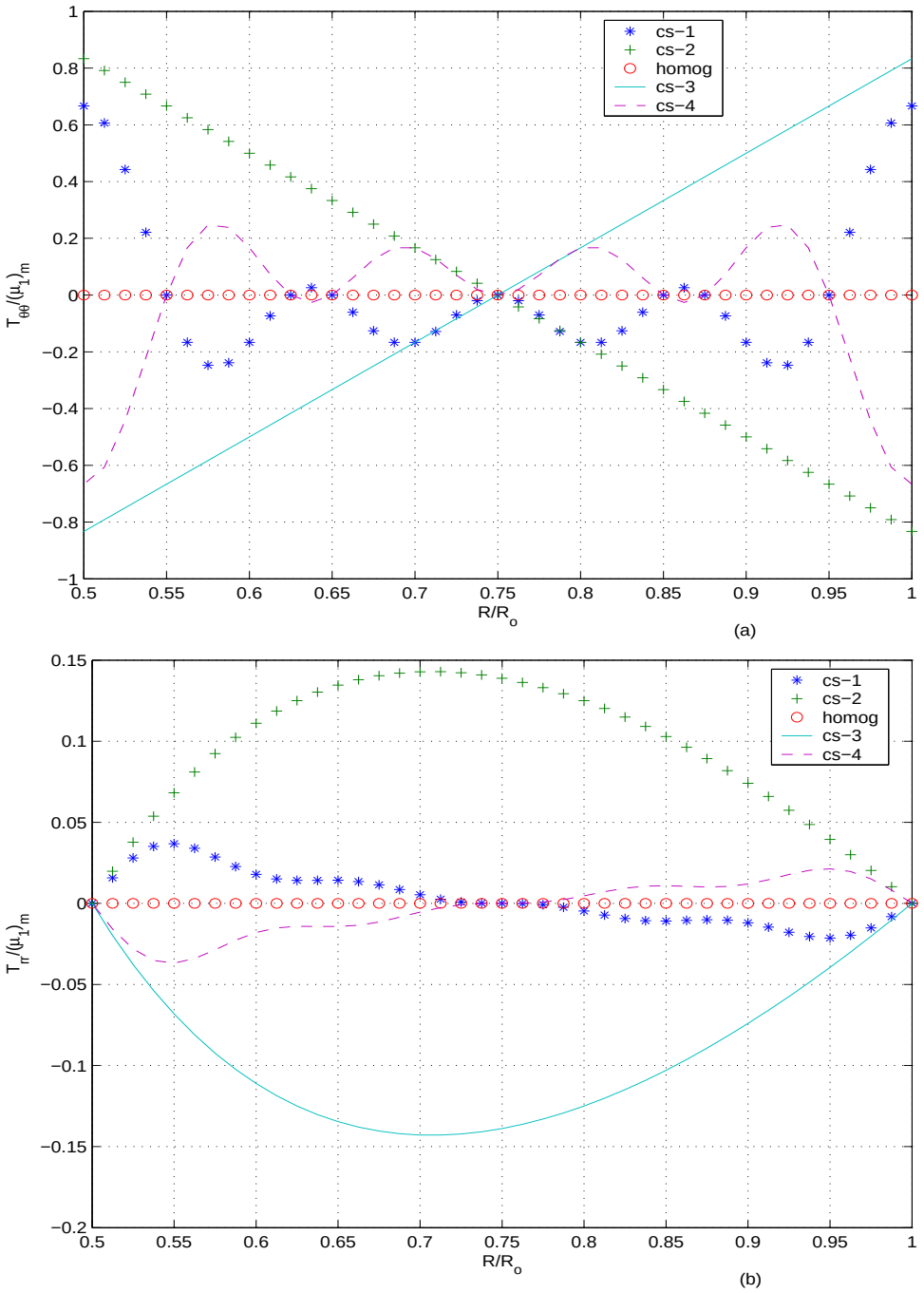

Fig. 20. Plot of stresses (a) $T_{\theta\theta}/(\mu_1)_m$ (b) $T_{rr}/(\mu_1)_m$ vs. R/R_o in an annular right circular cylinder with $R_o = 1$ and $R_i = 0.5$ made of Blatz Ko material subjected to uniaxial extension with $\lambda = 1.2$ for various prestress distributions shown in figure 14 when $\mu_3 = 6.25$ and $\mu_1 = 1$.

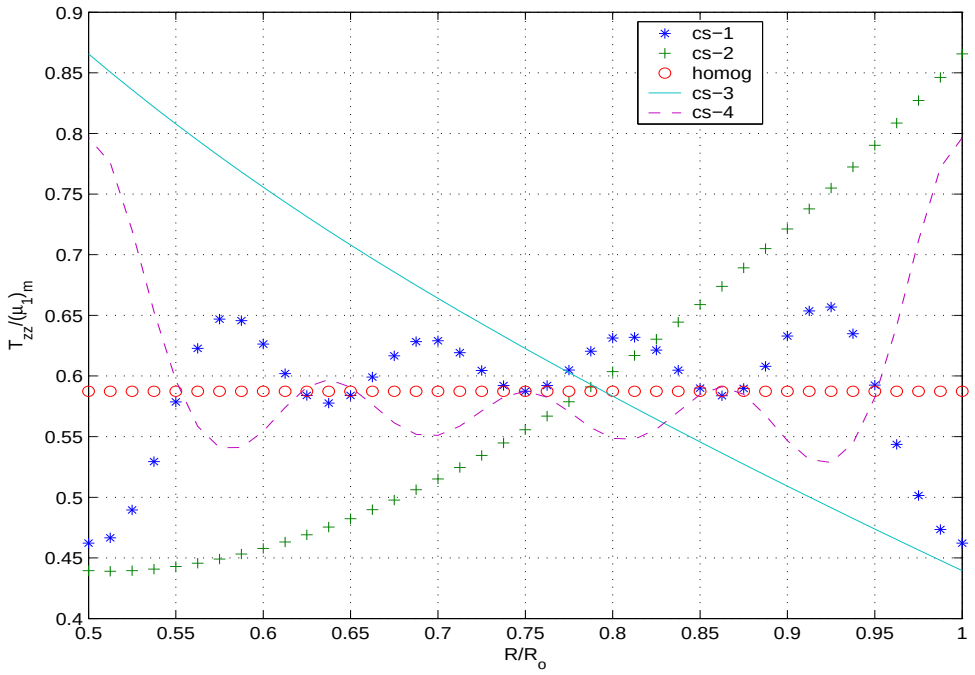

Fig. 21. Plot of stresses $T_{zz}/(\mu_1)_m$ vs. R/R_o in an annular right circular cylinder with $R_o = 1$ and $R_i = 0.5$ made of Blatz Ko material subjected to uniaxial extension with $\lambda = 1.2$ for various prestress distributions shown in figure 14 when $\mu_3 = 6.25$ and $\mu_1 = 1$.

traction, namely the axial load, L and the torque, T required along with the boundary deformation r_i and r_o to realize a given value of Ω. Figures 23 and 24 plot the axial load, the torque and the boundary deformations for various values of twist per unit length, Ω. Figures 25 and 26 plot the radial variation of the non-zero components of the stress field when $\Omega = 0.2$. Figure 27 plots $r(R)$ and $r_{,R}(R)$ for the same value of Ω. As always, in this section we assume, μ_1 to be a constant.

We infer from figure 23 that for the cases of prestresses studied, the magnitude of the torque and axial load required to realize a given value of Ω is nearly the same (within 7 percent) in the prestressed body and the stress free body. However, the amount of deviation of the axial load and torque from the stress free body, depends

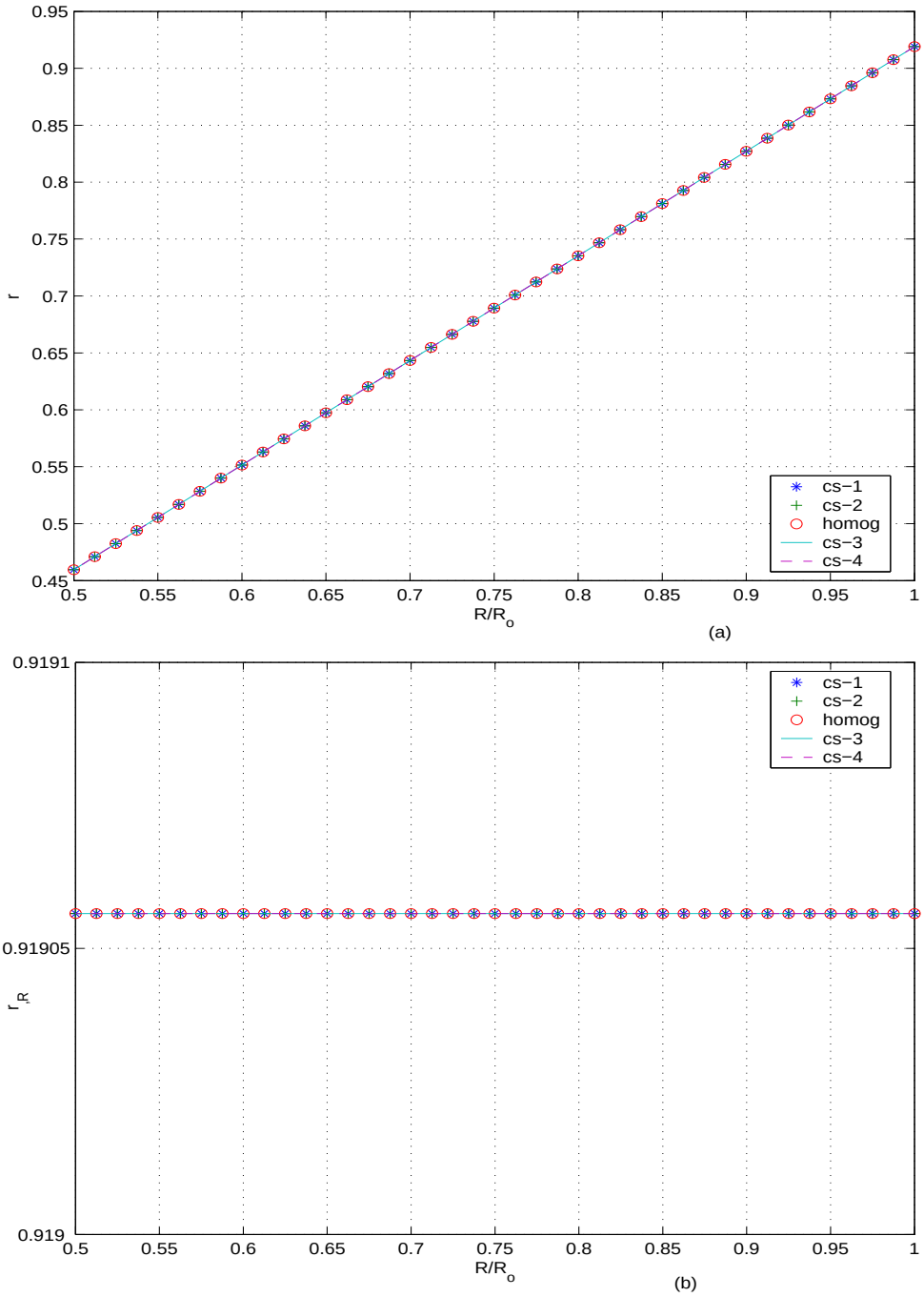

Fig. 22. Plot of (a) r (b) $r_{,R}$ vs. R/R_o in an annular right circular cylinder with $R_o = 1$ and $R_i = 0.5$ made of Blatz Ko material subjected to uniaxial extension with $\lambda = 1.2$ for various prestress distributions shown in figure 14 when $\mu_3 = 6.25$ and $\mu_1 = 1$.

on the magnitude of Ω and the nature of the radial variation of the circumferential prestresses, i.e., whether they are increasing or decreasing radially. It is interesting to observe that the axial load and the torque of the prestressed body that varies the maximum from the stress free body in the case of pure twist is same as in the above cases. We gather from figure 24 that the boundary deformation r_i and r_o in the case of prestressed body shows an insignificant (< 2 percent) deviation from the stress free body. Their magnitude of deviation depends on the magnitude of Ω and the nature of the radial variation of the circumferential prestresses. However, their sense of deviation, that is greater or lesser than the stress free body, depends only on the nature of the radial variation of the circumferential prestress.

It transpires from figures 25 and 26 that the radial variation of the stresses is significantly different in the case of prestressed body when compared with the stress free body. Even the T_{zz} and $T_{\theta z}$ component of the stresses, whose corresponding prestress values are zero, the deviation is significant; the stresses developed in the prestressed body could be as much as 1.5 times that developed in the stress free body.

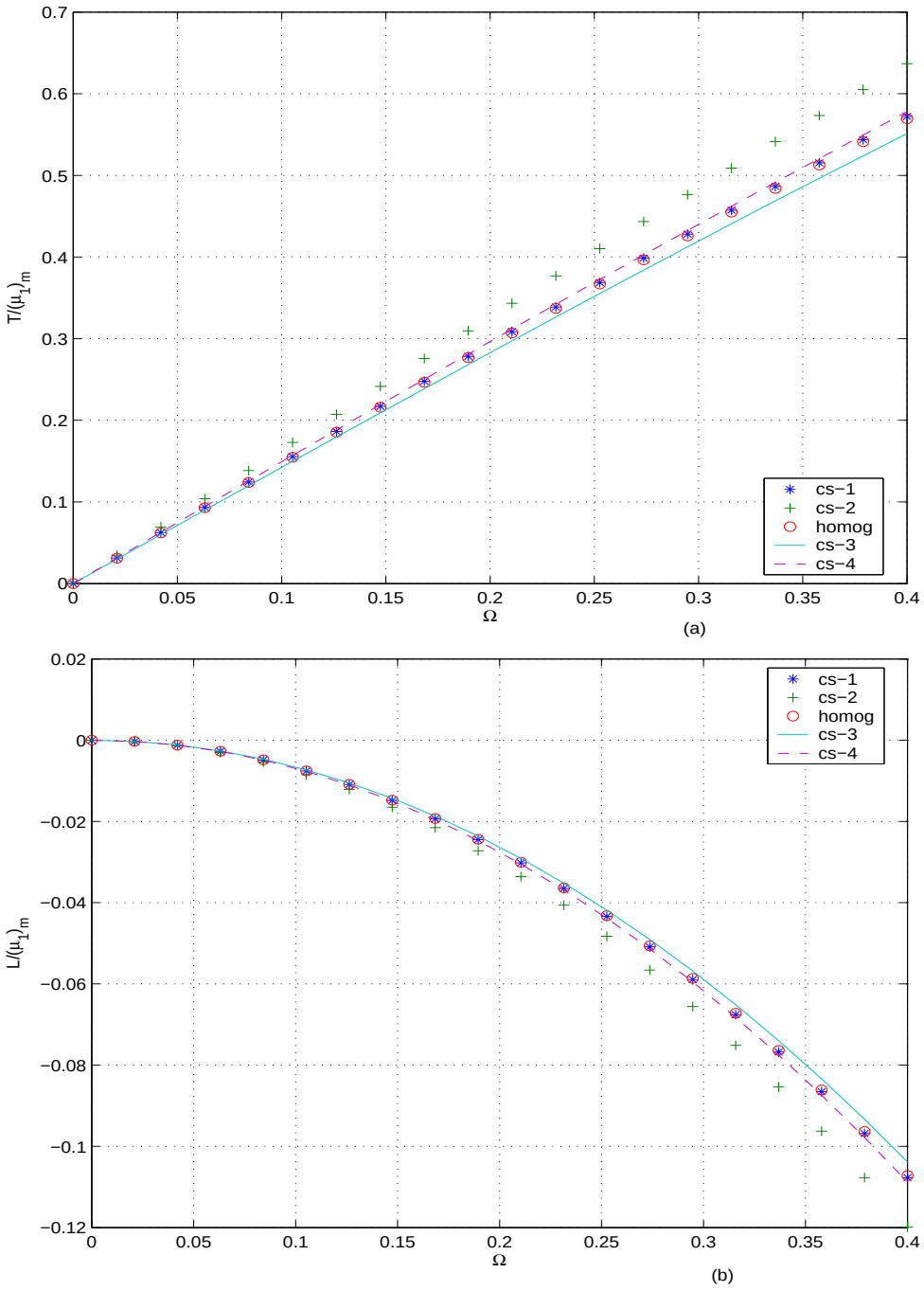

Fig. 23. Plot of (a) $T/(\mu_1)_m$ (b) $L/(\mu_1)_m$ vs. Ω for an annular right circular cylinder with $R_o = 1$ and $R_i = 0.5$ made of Blatz Ko material for various prestress distributions shown in figure 14 when $\mu_3 = 6.25$ and $\mu_1 = 1$.

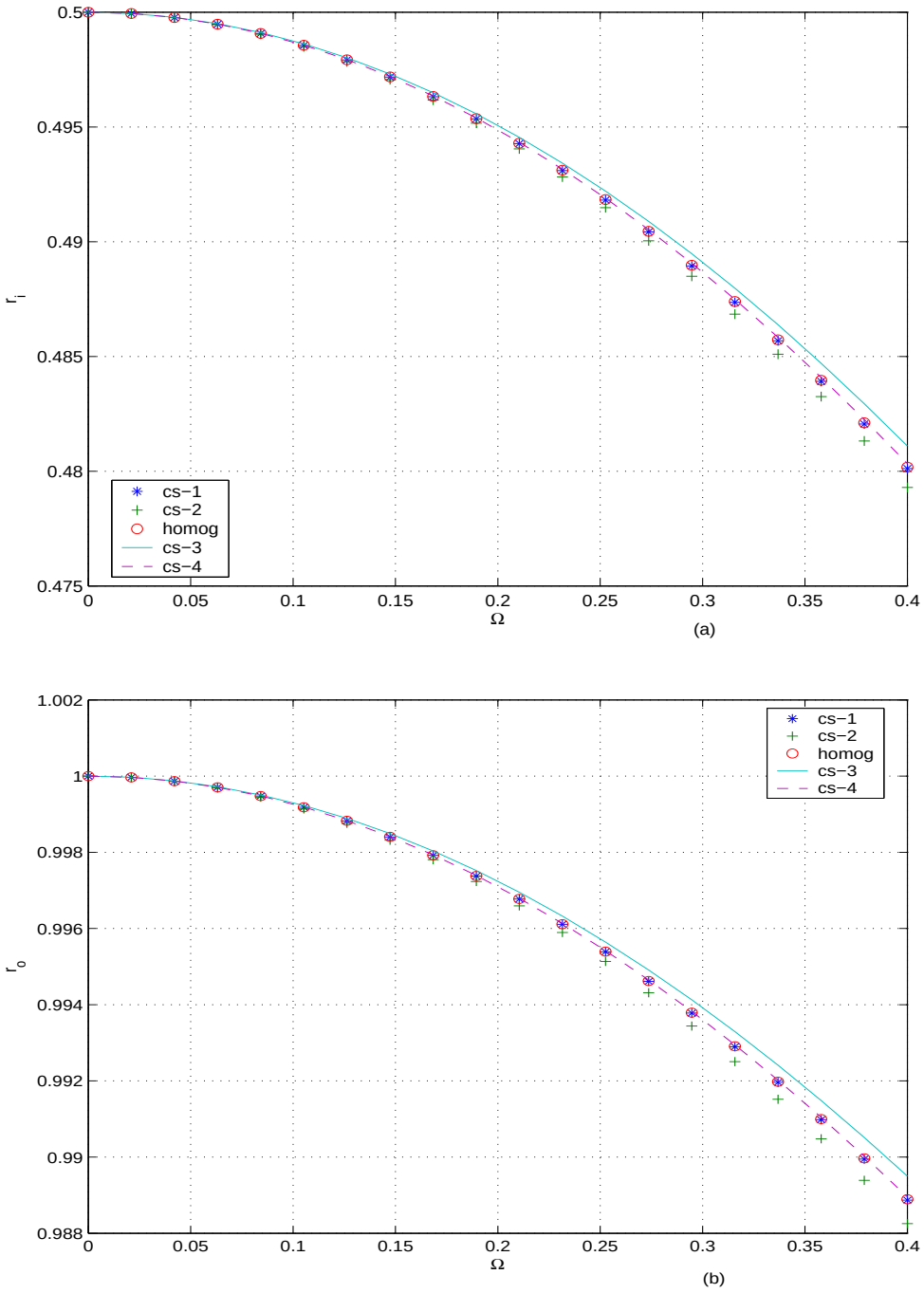

Fig. 24. Plot of (a) r_i (b) r_o vs. Ω of an annular right circular cylinder with $R_o = 1$ and $R_i = 0.5$ made of Blatz Ko material for various prestress distributions shown in figure 14 when $\mu_3 = 6.25$ and $\mu_1 = 1$.

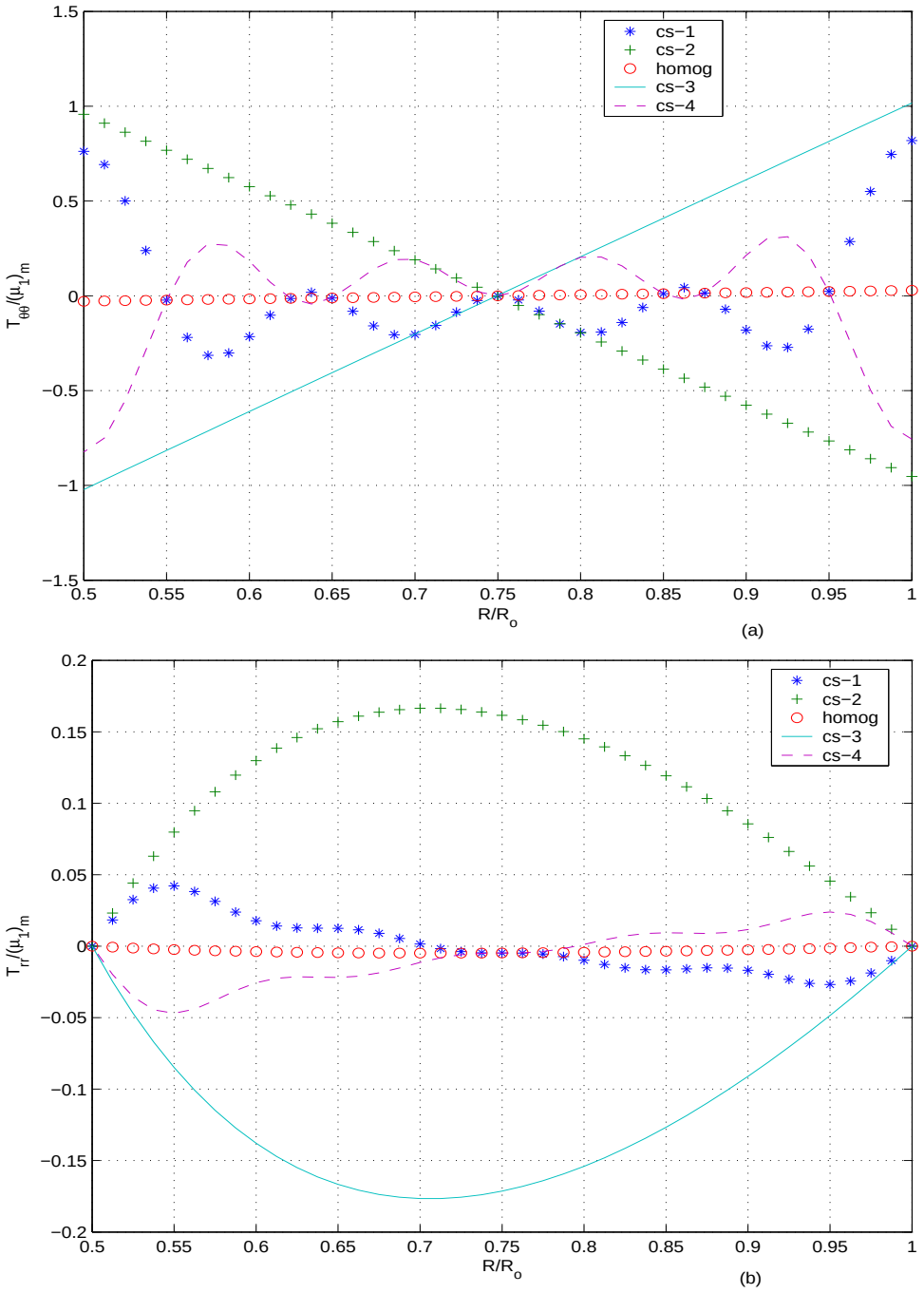

Fig. 25. Plot of stresses (a) $T_{\theta\theta}/(\mu_1)_m$ (b) $T_{rr}/(\mu_1)_m$ vs. R/R_o in an annular right circular cylinder with $R_o = 1$ and $R_i = 0.5$ made of Blatz Ko material subjected to twisting with $\Omega = 0.2$ for various prestress distributions shown in figure 14 when $\mu_3 = 6.25$ and $\mu_1 = 1$.

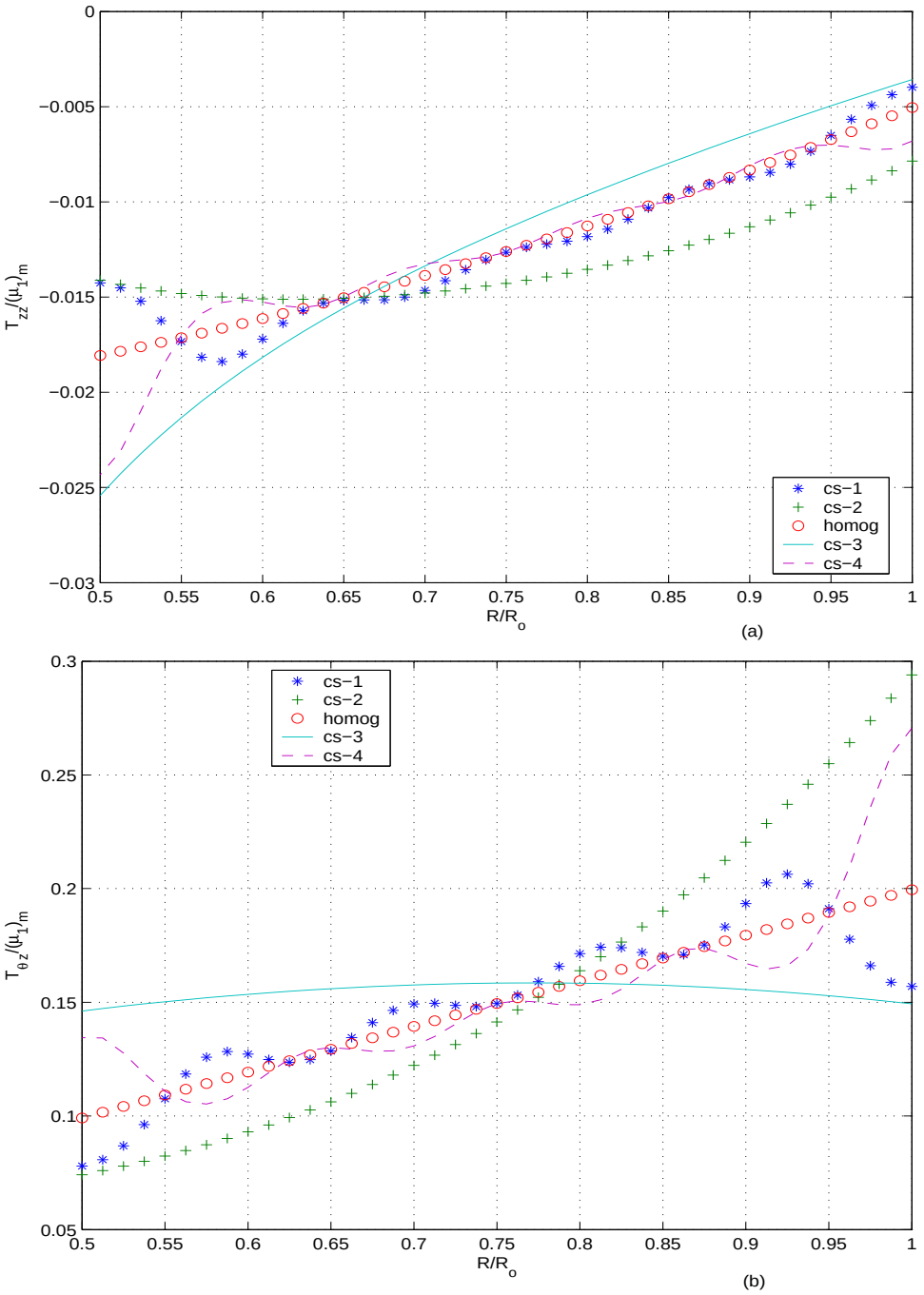

Fig. 26. Plot of stresses (a) $T_{zz}/(\mu_1)_m$ (b) $T_{\theta z}/(\mu_1)_m$ vs. R/R_o in an annular right circular cylinder with $R_o = 1$ and $R_i = 0.5$ made of Blatz Ko material subjected to twisting with $\Omega = 0.2$ for various prestress distributions shown in figure 14 when $\mu_3 = 6.25$ and $\mu_1 = 1$.

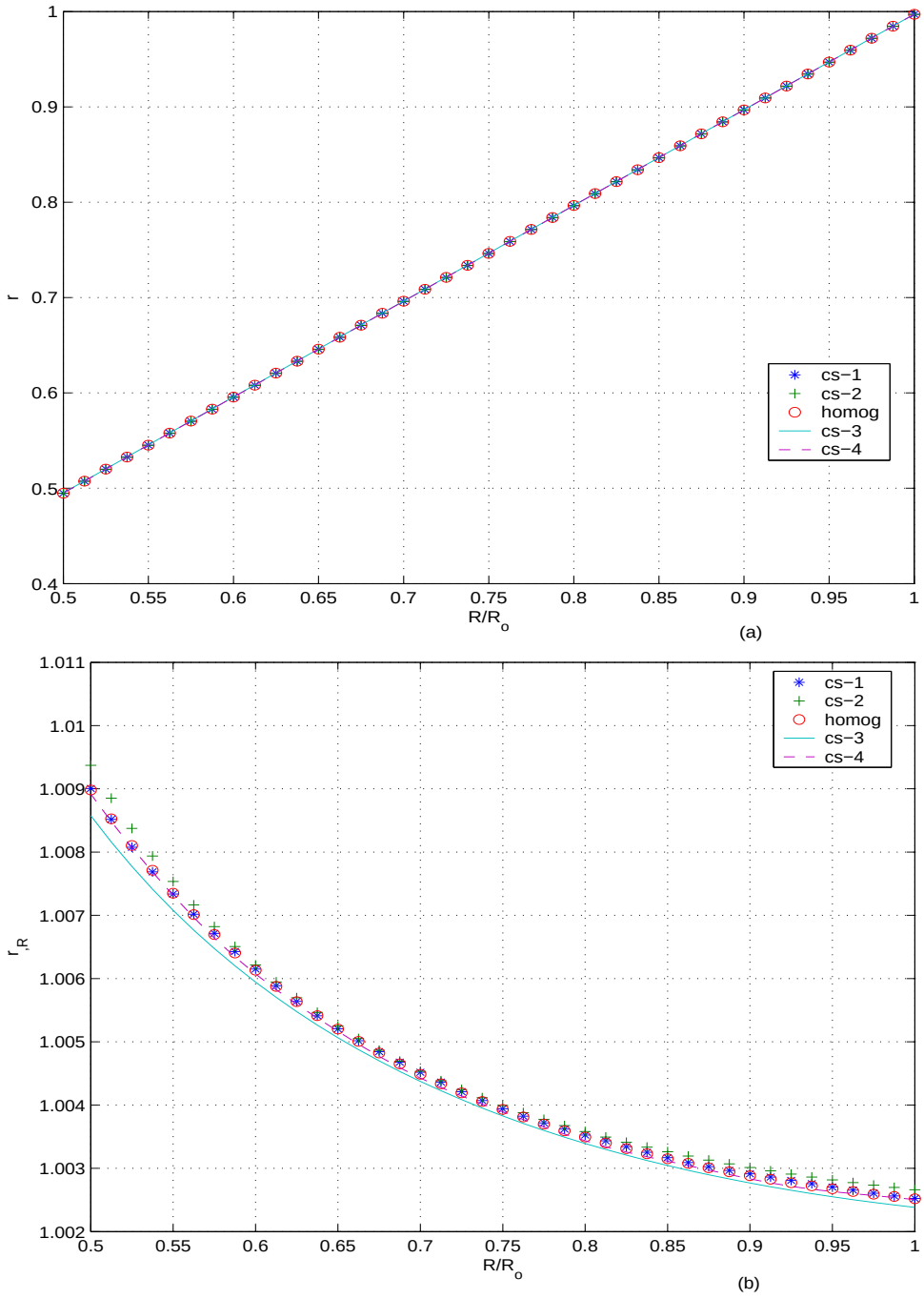

Fig. 27. Plot of (a) r (b) $r_{,R}$ vs. R/R_o in an annular right circular cylinder with $R_o = 1$ and $R_i = 0.5$ made of Blatz Ko material subjected to twisting with $\Omega = 0.2$ for various prestress distributions shown in figure 14 when $\mu_3 = 6.25$ and $\mu_1 = 1$.

B. Exponential constitutive relation

When the constitutive relation for stress is given by (3.80), the equations (5.27) and (5.28) evaluates to

$$
\begin{aligned}
f_1 &= 2\alpha_{11} m_1^2 r_{,R}^3 + \alpha_{13}\widetilde{J}_{m3} m_1 r_{,R} + 2(2+\alpha_{01}) m_1 r_{,R} + \alpha_{03}\frac{\widetilde{J}_{m3}}{r_{,R}}, \\
f_2 &= \left[\alpha_{01} + \alpha_{11} m_1 r_{,R}^2\right]\left[g_1 + h_1\right] + \left[\alpha_{03} + \alpha_{13} m_1 r_{,R}^2\right]\left[J^r_{3,R}\widetilde{J}_3 + J^r_3 r_{,R}\left(r_{,R} - \frac{r}{R}\right)\frac{\lambda}{R}\right] \\
&\quad + \frac{\mu_{1,R}}{\mu_1}\left[\widetilde{J}_{m1} - \frac{5}{\widetilde{J}^2_{m3}} + 2m_1 r_{,R}^2\right] + 2r_{,R}\left[r_{,R}\left(m_{1,R} + r_{,R}\frac{m_1}{r}\right) - m_2\frac{r}{R^2} - r\Omega^2\delta_0\right],
\end{aligned}
$$

where

$$
\begin{aligned}
\alpha_{01} &= 1 + \mu_2\left(\widetilde{J}_{m1}\widetilde{J}_{m3} - \frac{5}{\widetilde{J}_{m3}}\right), \qquad \alpha_{11} = 2\mu_2\widetilde{J}_{m3}, \\
\alpha_{03} &= \frac{10}{\widetilde{J}^3_{m3}} + \mu_2\left[\widetilde{J}_{m1} - \frac{5}{\widetilde{J}^2_{m3}}\right]^2, \qquad \alpha_{13} = 2\mu_2\left[\widetilde{J}_{m1} - \frac{5}{\widetilde{J}^2_{m3}}\right], \\
m_1 &= \delta_0 + \delta_1 T^o_{RR}, \qquad m_2 = \delta_0 + \delta_1 T^o_{\Theta\Theta}, \\
\delta_0 &= -\frac{J^r_1}{2} + \frac{5}{2(J^r_3)^2}, \qquad \delta_1 = \frac{\exp(-Q^r)}{2\mu_1\mu_2}, \\
m_{1,R} &= \delta_{0,R} + \delta_{1,R}T^o_{RR} + \delta_1 T^o_{RR,R}, \qquad m_{2,R} = \delta_{0,R} + \delta_{1,R}T^o_{\Theta\Theta} + \delta_1 T^o_{\Theta\Theta,R}, \\
\delta_{0,R} &= -\frac{J^r_{1,R}}{2} - \frac{5}{(J^r_3)^3}J^r_{3,R}, \qquad \delta_{1,R} = -\frac{\exp(-Q^r)}{2\mu_1\mu_2}\left[\frac{\mu_{1,R}}{\mu_1} + Q^r_{,R}\right] \\
Q^r &= \mu_2\left[J^r_1 J^r_3 + \frac{5}{J^r_3} - 8\right], \qquad Q^r_{,R} = \mu_2\left[J^r_{1,R}J^r_3 + \left(J^r_1 - \frac{5}{(J^r_3)^2}\right)J^r_{3,R}\right], \\
J^r_{1,R} &= \frac{n_3 l_2 - n_2 l_3}{n_2 l_1 - n_1 l_2}, \qquad J^r_{3,R} = \frac{n_1 l_3 - n_3 l_1}{n_2 l_1 - n_1 l_2},
\end{aligned}
$$

$$
\begin{aligned}
l_1 &= 2+\left[\frac{K_3\exp(-Q^r)J_3^{r2}}{\mu_1^3\mu_2^3(5-J_1^rJ_3^{r2})}+\frac{K_2}{2\mu_1^2\mu_2^2}\right]\frac{\exp(-2Q^r)J_3^{r4}}{(5-J_1^rJ_3^{r2})^2}-\frac{8J_3^{r8}}{(5-J_1^rJ_3^{r2})^3}\\
&\quad-\left[\frac{3K_3J_3^{r2}\exp(-Q^r)}{2\mu_1\mu_2(5-J_1^rJ_3^{r2})}+K_2\right]\frac{\exp(-2Q^r)J_3^{r3}}{\mu_1^2\mu_2(5-J_1^rJ_3^{r2})},\\
l_2 &= \frac{10}{J_3^{r3}}-\frac{8J_3^{r5}}{(5-J_1^rJ_3^{r2})^2}\left[3+\frac{2J_1^rJ_3^{r2}}{5-J_1^rJ_3^{r2}}\right]\\
&\quad+\frac{K_3J_3^{r3}\exp(-3Q^r)}{2\mu_1^3\mu_2^3(5-J_1^rJ_3^{r2})^2}\left[4+\frac{4J_1^rJ_3^{r2}}{5-J_1^rJ_3^{r2}}-3\left(J_1^r-\frac{5}{J_3^{r2}}\right)\mu_2J_3^r\right]\\
&\quad+\frac{K_2J_3^r\exp(-2Q^r)}{\mu_1^2\mu_2^2(5-J_1^rJ_3^{r2})}\left[1+\frac{J_1^rJ_3^{r2}}{5-J_1^rJ_3^{r2}}-\left(J_1^r-\frac{5}{J_3^{r2}}\right)\mu_2J_3^r\right],\\
l_3 &= \frac{J_3^{r4}\exp(-3Q^r)}{2\mu_1^3\mu_2^3(5-J_1^rJ_3^{r2})^2}\left[K_{3,R}-\frac{3K_3}{\mu_1}\mu_{1,R}\right]+\frac{J_3^{r2}\exp(-2Q^r)}{2\mu_1^2\mu_2^2(5-J_1^rJ_3^{r2})}\left[K_{2,R}-\frac{2K_2}{\mu_1}\mu_{1,R}\right],
\end{aligned}
$$

$$
\begin{aligned}
n_1 &= -\left[\frac{3K_3\exp(-3Q^r)}{8\mu_1^3\mu_2^3}+\frac{2K_2\exp(-2Q^r)}{4\mu_1^2\mu_2^2}\delta_0+\frac{K_1\exp(-Q^r)}{2\mu_1\mu_2}\delta_0^2\right]\mu_2J_3^r\\
&\quad-\left[\frac{K_2\exp(-2Q^r)}{4\mu_1^2\mu_2^2}+\frac{K_1\exp(-Q^r)}{\mu_1\mu_2}\delta_0+3\delta_0^2\right]\frac{1}{2},
\end{aligned}
$$

$$
\begin{aligned}
n_2 &= -\left[\frac{3K_3\exp(-3Q^r)}{8\mu_1^3\mu_2^3}+\frac{2K_2\exp(-2Q^r)}{4\mu_1^2\mu_2^2}\delta_0+\frac{K_1\exp(-Q^r)}{2\mu_1\mu_2}\delta_0^2\right]\mu_2\left(J_1^r-\frac{5}{J_3^{r2}}\right)\\
&\quad-\left[\frac{K_2\exp(-2Q^r)}{4\mu_1^2\mu_2^2}+\frac{K_1\exp(-Q^r)}{\mu_1\mu_2}\delta_0+3\delta_0^2\right]\frac{5}{J_3^{r3}}-2J_3^r,\\
n_3 &= \frac{\exp(-3Q^r)}{8\mu_1^3\mu_2^3}\left[K_{3,R}-\frac{3K_3}{\mu_1}\mu_{1,R}\right]+\frac{\exp(-2Q^r)}{4\mu_1^2\mu_2^2}\left[K_{2,R}-\frac{2K_2}{\mu_1}\mu_{1,R}\right]\delta_0\\
&\quad+\frac{\exp(-Q^r)}{2\mu_1\mu_2}\left[K_{1,R}-\frac{K_1}{\mu_1}\mu_{1,R}\right]\delta_0^2,\\
K_1 &= T^o_{RR}+T^o_{\Theta\Theta}, \qquad K_2=T^o_{RR}T^o_{\Theta\Theta}, \qquad K_3=0,\\
K_{1,R} &= T^o_{RR,R}+T^o_{\Theta\Theta,R}, \qquad K_{2,R}=T^o_{RR,R}T^o_{\Theta\Theta}+T^o_{RR}T^o_{\Theta\Theta,R}, \qquad K_{3,R}=0,
\end{aligned}
$$

In prestressed solid cylinders $m_1 \neq m_2$ and $\hat{f}_2 = f_2(0,0,\hat{r}_{,R}) \neq 0$. Hence, this deformation is not possible in residually stressed solid right circular cylinders made up of a material whose relationship between stress and gradient of deformation is given by (3.80).

For $f_1 \neq 0$, we require

$$\frac{T^o_{RR}}{\mu_1} \neq -1 - \frac{\exp(Q^r)}{\mu_2 r^2_{,R}}. \tag{5.42}$$

Therefore, we assign values to constants in the constitutive prescription of $T^o_{\Theta\Theta}$[3] such that $T^o_{RR}/\mu_1 > -1$ assuming $\mu_2 > 0$. Thus, if $\mu_1 \in C^\infty(\omega_R)$ and $T^o_{\Theta\Theta} \in C^\infty(\omega_R)$, where $\omega_R = \{R | R_i \leq R \leq R_o\}$ then $f_2/f_1 \in C^\infty(\omega)$.

Thus, as before the governing equation, (5.34) is solved for the mixed boundary condition (5.35) for a specified value of Ω and λ and $R_i \leq R \leq R_o$. The boundary condition (5.35b) requires to find d^o such that $y(d^o) = 0$, where

$$y(d) = 3m^o_1 d^4 + L_1 d^2 - \frac{5}{(\lambda J^{ro}_3)^2}\left(\frac{R_o}{r_o}\right)^2, \tag{5.43}$$

$$L_1 = m^o_2 \left(\frac{r_o}{R_o}\right)^2 + \delta^o_0 \left[(r_o\Omega)^2 + \lambda^2\right],$$

$m^o_1 = m_1(R_o)$, $m^o_2 = m_2(R_o)$, $J^{ro}_3 = J^r_3(R_o)$ and $\delta^o_0 = \delta_0(R_o)$. Solving the above equation we obtain the unique real solution

$$(d^o)^2 = -\frac{L_1}{6m^o_1} + \frac{1}{6m^o_1}\sqrt{L^2_1 + 60\frac{m^o_1}{(\lambda J^{ro}_3)^2}\left(\frac{R_o}{r_o}\right)^2}, \tag{5.44}$$

assuming $L_1 > 0$ and $\delta^o_0 > 0$. The constitutive prescription of $T^o_{\Theta\Theta}$, studied here, ensures $L_1 > 0$ and $\delta^o_0 > 0$.

Next we consider the case when μ_1 and/or $T^o_{\Theta\Theta}$ is only piecewise continuous, then at the interface we require $T_{rr}(r^-_j) = T_{rr}(r^+_j)$ which translates to finding $(d^-_j)_* > 0$ such that

$$y((d^-_j)_*) = 0, \tag{5.45}$$

[3] T^o_{RR} is derived from the constitutively prescribed $T^o_{\Theta\Theta}$ see section (G.2) of chapter III for details

where now

$$y(d_j^-) = \mu_1(R_j^-)\mu_2\exp(Q^-)\left\{3(d_j^-)^2m_1^- + O_1^- - \frac{5}{(d_i^-\lambda J_3^{r-})^2}\left(\frac{R_j^-}{r_j^-}\right)^2\right\} - \mu_1(R_j^+)\mu_2\exp(Q^+)\left\{3(d_j^+)^2m_1^+ + O_1^+ - \frac{5}{(d_i^+\lambda J_3^{r+})^2}\left(\frac{R_j^+}{r_j^+}\right)^2\right\} \quad (5.46)$$

$Q^- = \mu_2(J_{m1}^-J_{m3}^- + 5/J_{m3}^- - 8)$, $Q^+ = \mu_2(J_{m1}^+J_{m3}^+ + 5/J_{m3}^+ - 8)$, $J_{m1}^- = m_1^-(d_j^-)^2 + O_1^-$, $J_{m3}^- = J_3^{r-}(d_j^-)\frac{r_j^-}{R_j^-}\lambda$, $J_{m1}^+ = m_1^+(d_j^+)^2 + O_1^+$, $J_{m3}^+ = J_3^{r+}(d_j^+)\frac{r_j^+}{R_j^+}\lambda$, $O_1^- = m_2^-\left(\frac{r_j^-}{R_j^-}\right)^2 + \delta_0^-\left[(r_j^-\Omega)^2 + \lambda^2\right]$, $O_1^+ = m_2^+\left(\frac{r_j^+}{R_j^+}\right)^2 + \delta_0^+\left[(r_j^+\Omega)^2 + \lambda^2\right]$, $m_1^- = m_1(R_j^-)$, $m_1^+ = m_1(R_j^+)$, $J_3^{r-} = J_3^r(R_j^-)$, $J_3^{r+} = J_3^r(R_j^+)$, $\delta_0^- = \delta_0(R_j^-)$ and $\delta_0^+ = \delta_0(R_j^+)$. In general, it is not possible to solve (5.45) analytically and hence we seek numerical solution using the bisection algorithm. Since, (5.46) is a continuous function in d_j^- and since

$$\lim_{d_j^-\to 0} y(d_j^-) \to -\infty, \qquad \text{and } \lim_{d_j^-\to\infty} y(d_j^-) \to \infty, \quad (5.47)$$

there exist $(d_j^-)_* \in (0,\infty)$ such that $y((d_j^-)_*) = 0$. Further, (5.46) is not monotonic, in general. Hence, there could exist more than one solution. However, numerical investigation reveals that the solution is unique for the cases studied here.

Therefore, there exist a deformation of the form (5.2) for the exponential constitutive relation when $R_i > 0$, for the forms of μ_1 and $T_{\Theta\Theta}^o$ studied here.

1. Case-1: Pure inflation

We begin by studying the response of the annular cylinder subjected to inflation at constant length by applying a radial component of the normal stress at the inner surface and axial component of the normal stresses at the extremities of the cylinder. We shall also require that the outer surface of the cylinder be free of boundary traction. Thus, for this case we specify, $\lambda = 1$, $\Omega = 0$, $T_{rr}(r_o) = 0$, r_o and study the

variation of r_i, $T_{rr}(r_i)$ and the axial load L for various prestress fields recorded in section (G.2) of chapter III. However, we present the results of only some of the cases studied. Figure 28 plots the prestresses corresponding to various cases, whose results are recorded here. All the cases studied here correspond to the PWC variation with varying values of ϵ_1 but with the same value for k, i.e., 2. Thus, for 'cs-1' $\epsilon_1 = 0.1$, 'cs-2' $\epsilon_1 = 0.4$, 'cs-3' $\epsilon_1 = -0.4$, 'cs-4' $\epsilon_1 = -0.1$ and 'stsf' $\epsilon_1 = 0$; is a mnemonic for stress free body[4]. These cases are studied here for their relevance in understanding the mechanics of blood vessels. 'cs-1' and 'cs-2' corresponds to the case in which the inner layer is in circumferential compression while the outer is in circumferential tension corresponding to ones expectation [5] of the prestress fields in blood vessels. In keeping with our aim to understand the mechanics of the blood vessels, we assume the annular right circular cylinder to be made up of two layers with the value of material moduli, μ_1 in the innermost layer being approximately half that in the outer layer, motivated from the data in von Maltzahn [49]. Figure 29 plots the radial variation of the material parameter $\mu_1/(\mu_1)_m$ where $(\mu_1)_m \approx 5$ MPa.

While figure 30 plots $-T_{rr}(r_i)$ and L as a function of r_o for various prestress fields, figure 31 plots r_i vs. r_o. Figures 32 and 33 plot the transmural variation of the stresses and figure 34 plots $r(R)$ and $r_{,R}$ when $r_o = 1.2R_o$.

We infer from figure 30 that while the radial component of the normal stress required to engender a given r_o for the prestressed bodies studied here varies by as much as 55% from that of stress free body, the axial load required to maintain its length varies by as much as 35%. We also find that the deviation depends not only on the magnitude of the prestresses but also on whether the circumferential prestress is radially increasing or decreasing. This constitutive relation also predicts that the

[4]By a stress free body we mean a body with a stress free configuration as reference.

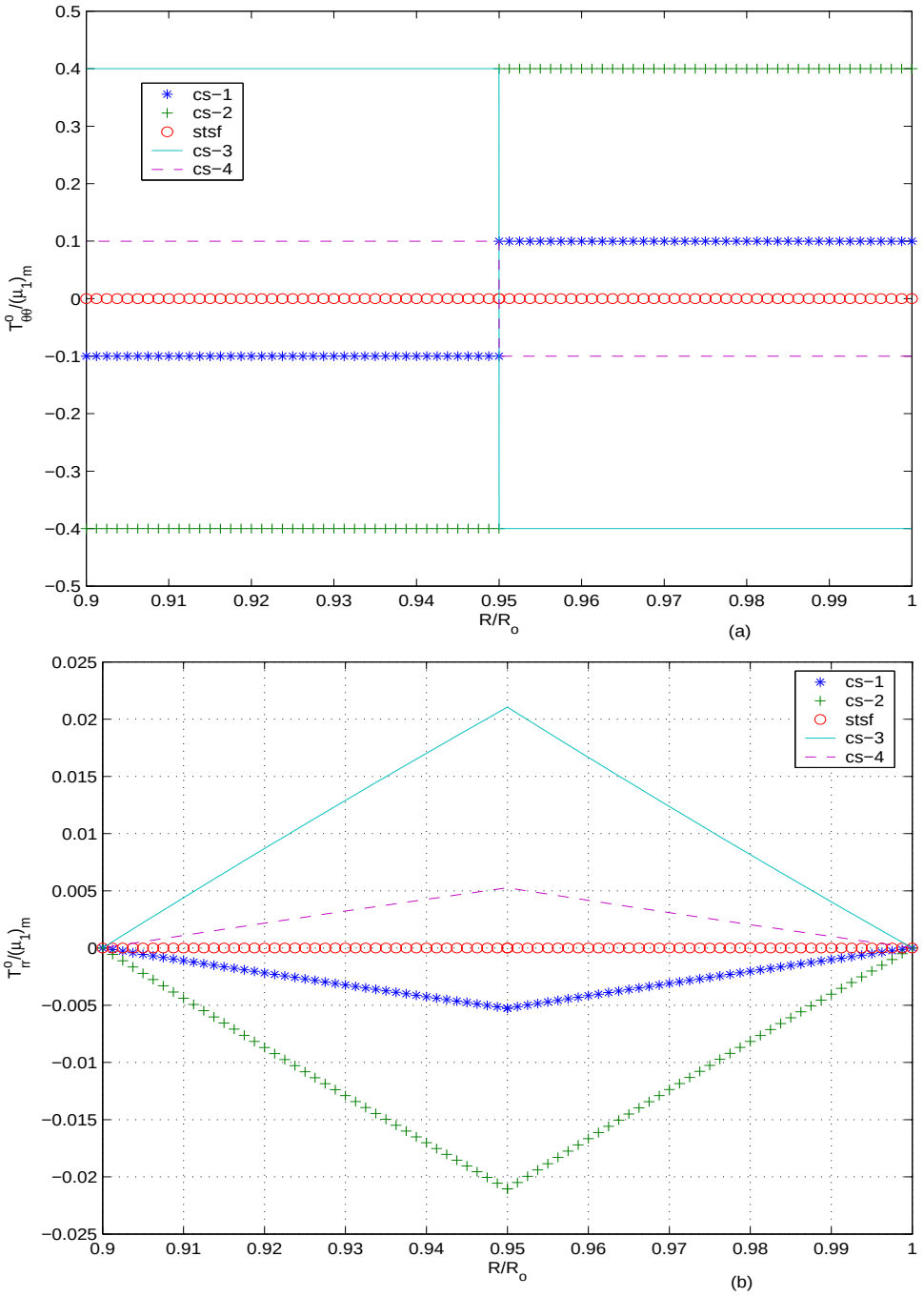

Fig. 28. Plot of prestresses (a) $T^o_{\Theta\Theta}/(\mu_1)_m$ (b) $T^o_{RR}/(\mu_1)_m$ vs. R/R_o in an annular right circular cylinder with $R_o = 1$ and $R_i = 0.9$.

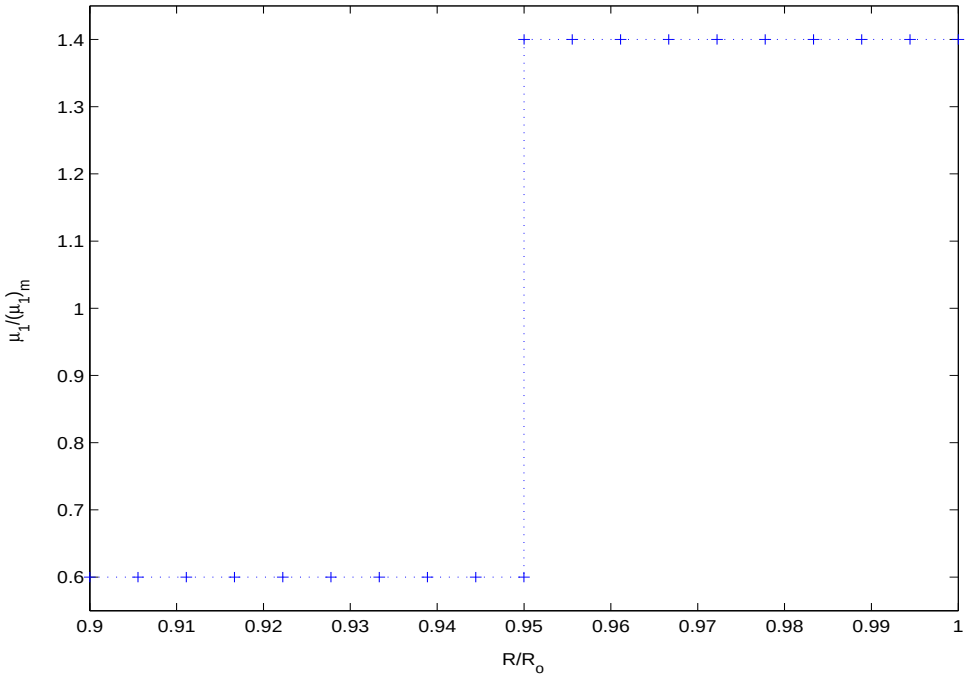

Fig. 29. Plot of μ_1 vs. R/R_o in an annular right circular cylinder with $R_o = 1$ and $R_i = 0.9$.

axial load required to maintain a constant length for increasing values of r_o, increases; irrespective of the length at which it is maintained a constant. Hence, the present constitutive relation could not satisfactorily describe the response of the blood vessels.

2. Case-2: Uniaxial extension

Next, we study the uniaxial extension of prestressed annular cylinder made up of biological material. For this case, we specify $\Omega = 0$, $T_{rr}(r_i) = T_{rr}(r_o) = 0$, and λ and compare the computed values of axial load, L and boundary deformations r_i and r_o for various prestress fields and λ. Now, we have to determine that value of r_o which results in $T_{rr}(r_i) = 0$. This is accomplished using techniques described in some detail in section (A.2) of this chapter. While figure 35 plots the axial load as a function of

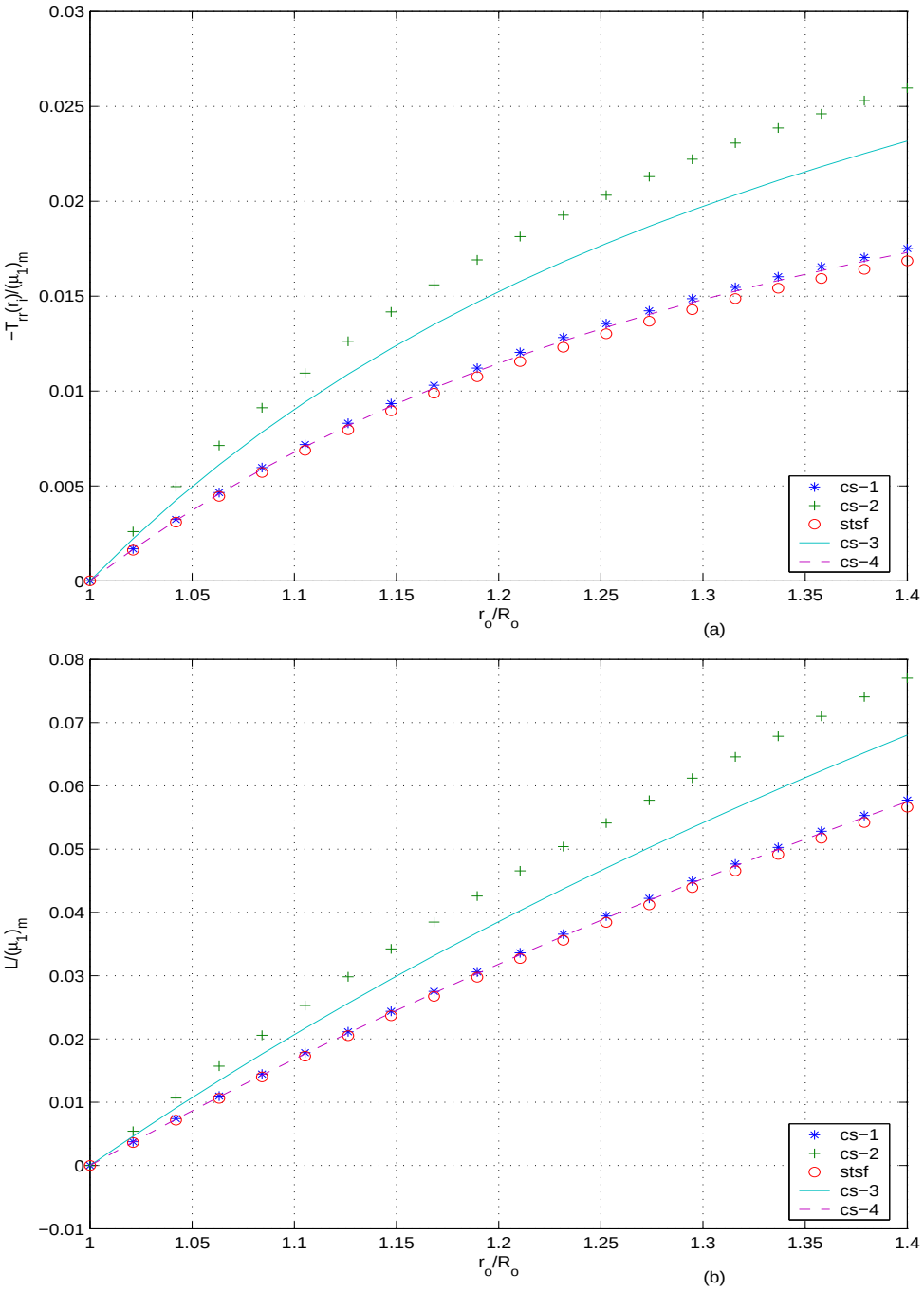

Fig. 30. Plot of (a) $-T_{rr}(r_i)/(\mu_1)_m$ (b) $L/(\mu_1)_m$ vs. r_o/R_o of an annular right circular cylinder with $R_o = 1$ and $R_i = 0.9$ made of biological material for various prestress distributions shown in figure 28 when μ_1 is as shown in figure 29 and $\mu_2 = 0.1$.

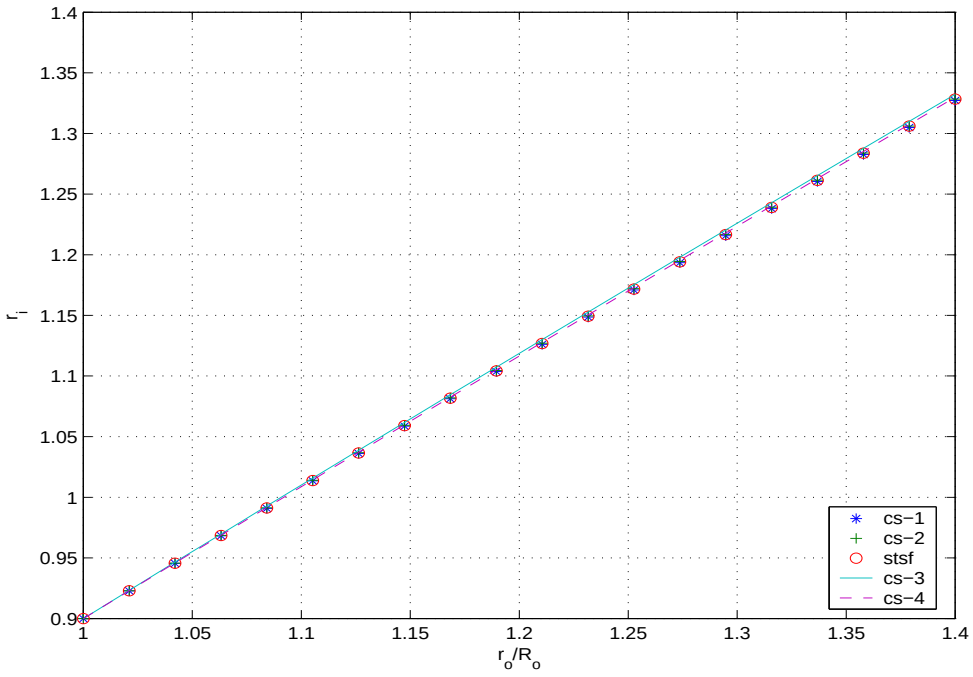

Fig. 31. Plot of r_i vs. r_o/R_o of an annular right circular cylinder with $R_o = 1$ and $R_i = 0.9$ made of biological material for various prestress distributions shown in figure 28 when μ_1 is as shown in figure 29 and $\mu_2 = 0.1$.

stretch ratio, figure 36 plots r_i and r_o as a function of λ. From figure 35 we find that the axial load required to engender a given stretch varies (by about 8%) with both the magnitude of the prestresses and the value of λ. We infer from figure 37 that axial stretching reduces the magnitude of the circumferential and radial stresses in the prestressed body by about 10%. It can be seen from figure 38 that the prestresses can accentuate or inaccentuate the differences in the material moduli between the two layers, depending on whether the circumferential prestresses are radially increasing or decreasing. Unlike in the case of Blatz-Ko bodies, the deformation is not homogeneous as seen from figure 39. Hence, for this constitutive relation the value of r_i and r_o too varies marginally (about 1%), as seen in figure 36.

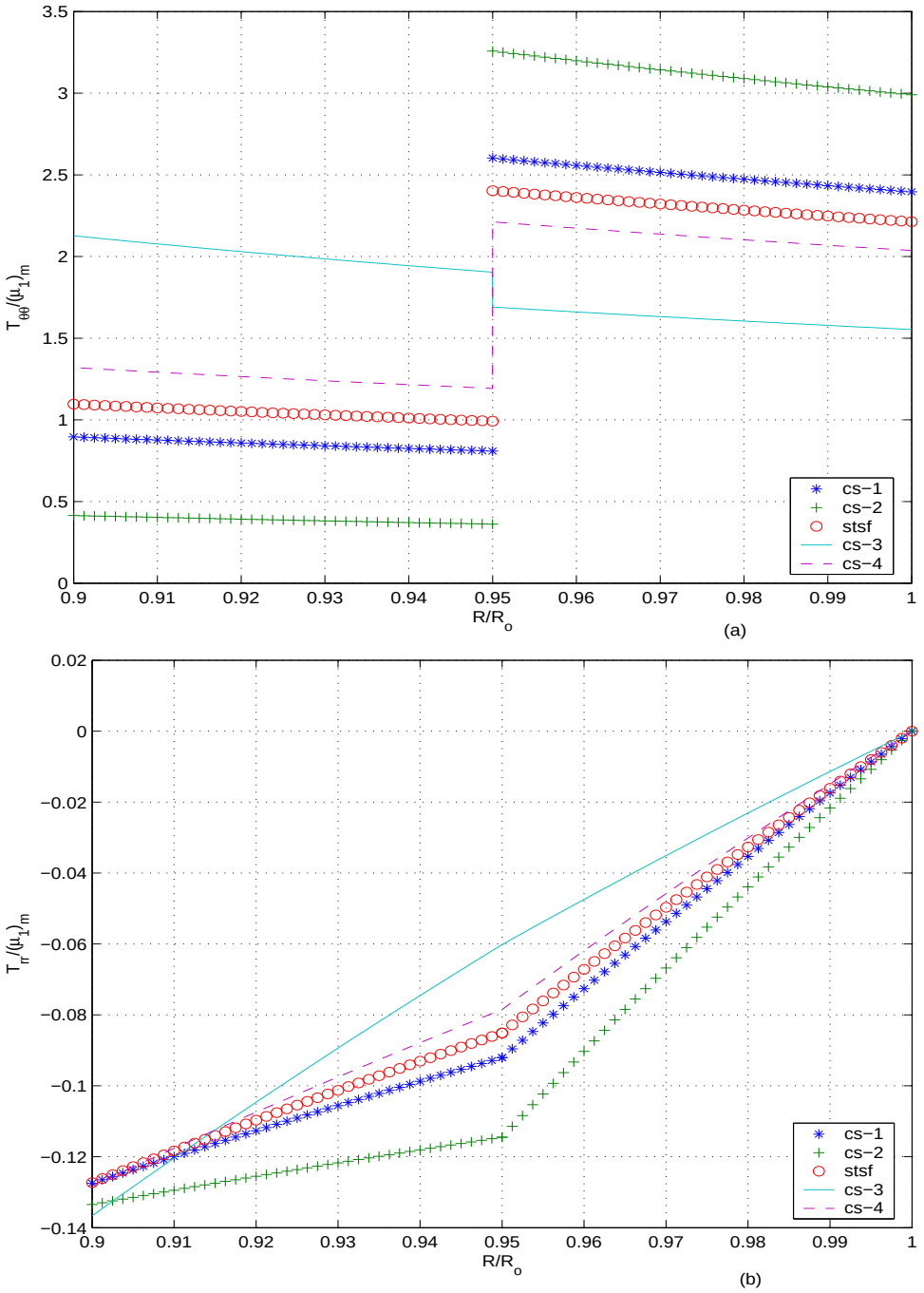

Fig. 32. Plot of stresses (a) $T_{\theta\theta}/(\mu_1)_m$ (b) $T_{rr}/(\mu_1)_m$ vs. R/R_o in an annular right circular cylinder with $R_o = 1$ and $R_i = 0.9$ made of biological material subjected to inflation with $r_o = 1.2R_o$, for various prestress distributions shown in figure 28 when μ_1 is as shown in figure 29 and $\mu_2 = 0.1$.

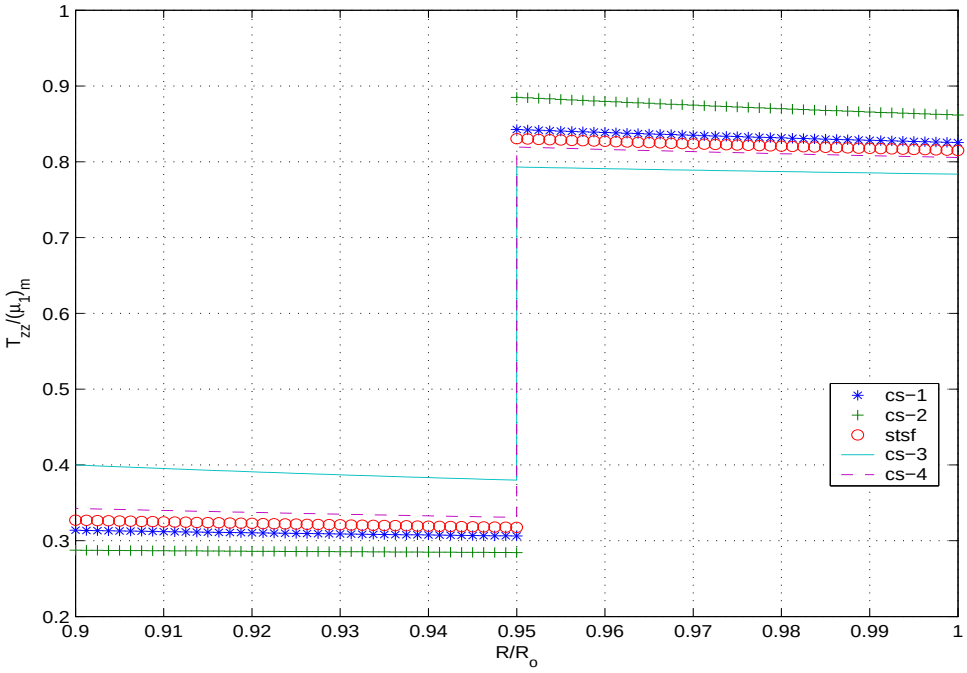

Fig. 33. Plot of stresses $T_{zz}/(\mu_1)_m$ vs. R/R_o in an annular right circular cylinder with $R_o = 1$ and $R_i = 0.9$ made of biological material subjected to inflation with $r_o = 1.2R_o$, for various prestress distributions shown in figure 28 when μ_1 is as shown in figure 29 and $\mu_2 = 0.1$.

3. Case-3: Pure twist

Finally, we study the twisting of an annular right circular cylinder made up of biological material held at a constant length. In this case too, both the inner and outer surfaces are traction free and we apply axial component of the normal stresses and shear stress, $T_{\theta z}$ at the extremities of the annular cylinder. Thus, for this case we specify, $\lambda = 1$, $T_{rr}(r_i) = 0$, $T_{rr}(r_o) = 0$ and Ω. As described in detail in section (A.2) of this chapter, we guess the value, r_o^g, solve the IVP, obtain $r(R_i)$ and $r_{,R}(R_i)$ and then verify if $T_{rr}(R_i, r(R_i), r_{,R}(R_i)) = 0$, if not we update the guessed value r_o^g until the boundary condition is met.

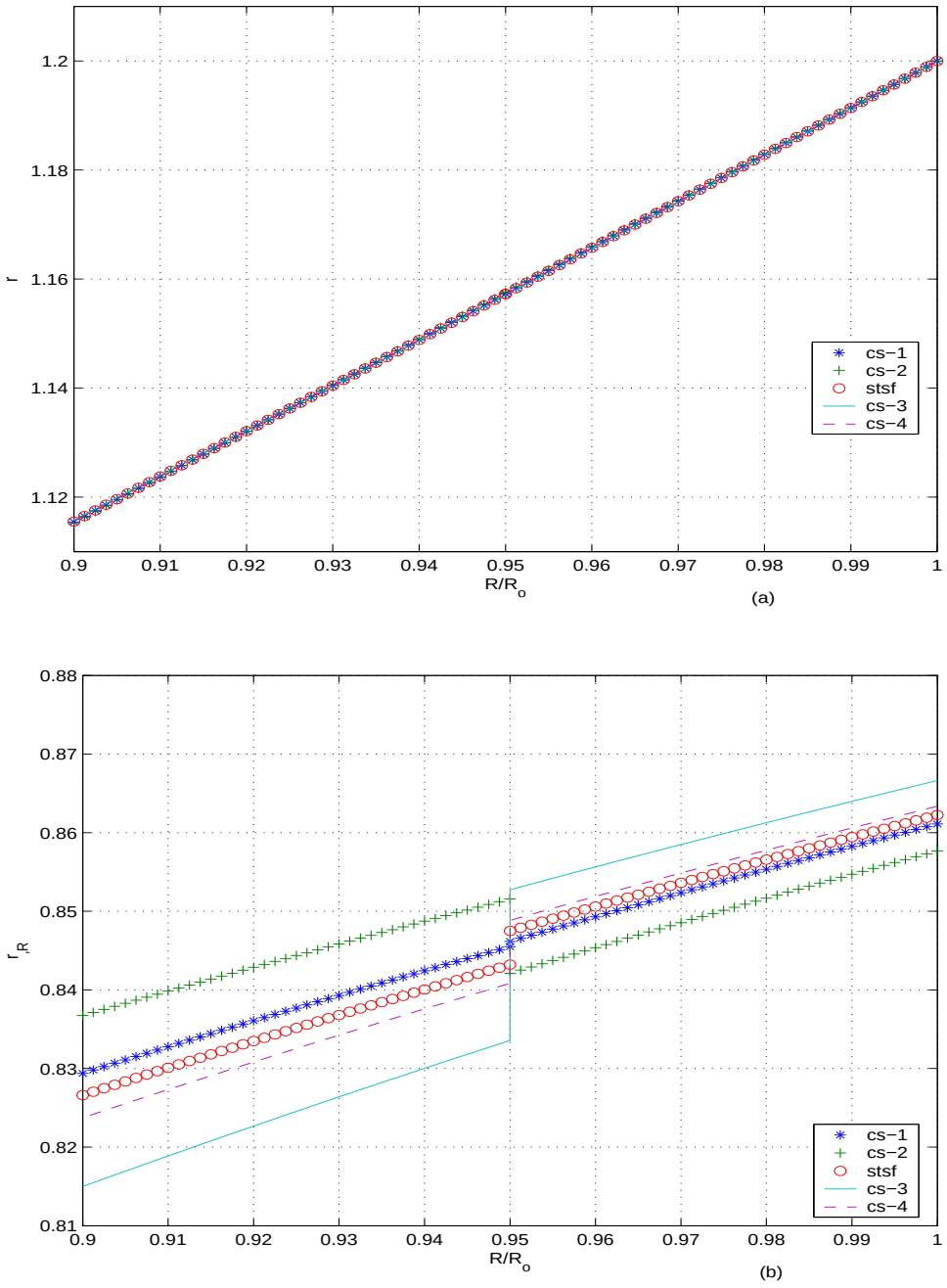

Fig. 34. Plot of (a) r (b) $r_{,R}$ vs. R/R_o in an annular right circular cylinder with $R_o = 1$ and $R_i = 0.9$ made of biological material subjected to inflation with $r_o = 1.2R_o$, for various prestress distributions shown in figure 28 when μ_1 is as shown in figure 29 and $\mu_2 = 0.1$.

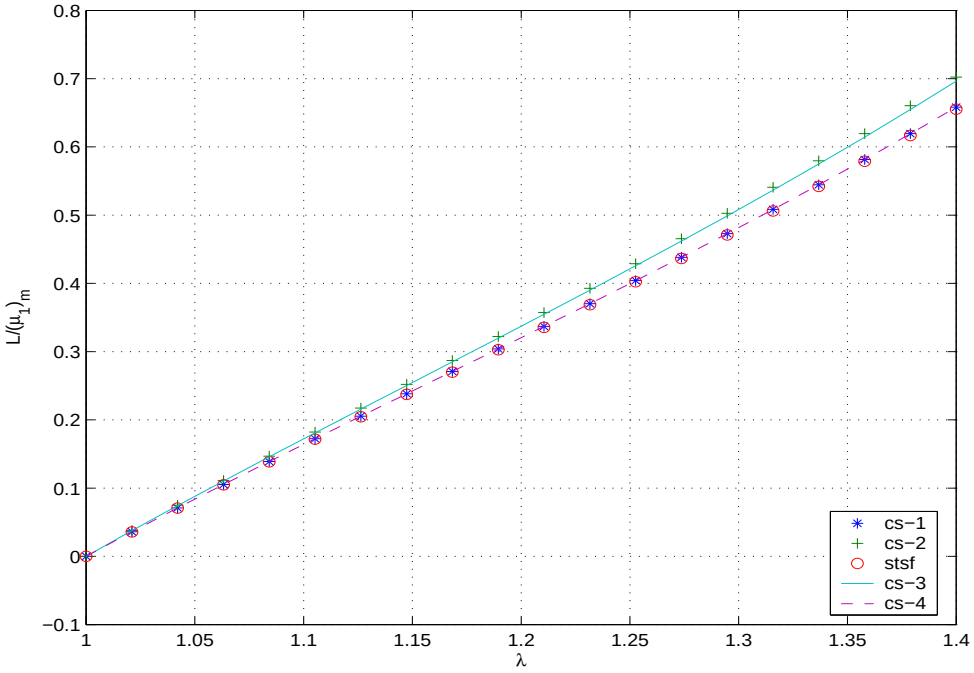

Fig. 35. Plot of $L/(\mu_1)_m$ vs. λ for an annular right circular cylinder with $R_o = 1$ and $R_i = 0.9$ made of biological material for various prestress distributions shown in figure 28 when μ_1 is as shown in figure 29 and $\mu_2 = 0.1$.

As before having specified λ, $T_{rr}(r_i)$, $T_{rr}(r_o)$ and Ω, we study the other boundary traction, namely the axial load, L and the torque, T required along with the boundary deformation r_i and r_o, to realize a given value of Ω. Figures 40 and 41 plot the axial load, the torque and the boundary deformations for various values of twist per unit length, Ω. Figures 42 and 43 plot the radial variation of the non-zero components of the stress field when $\Omega = 0.2$. Figure 44 plots $r(R)$ and $r_{,R}(R)$ for the same value of Ω.

In this case too, the torque, T and the axial load, L required to engender a given twist per unit length and maintain a constant length, varies depending on the magnitude of the prestresses and whether the circumferential prestress is radially

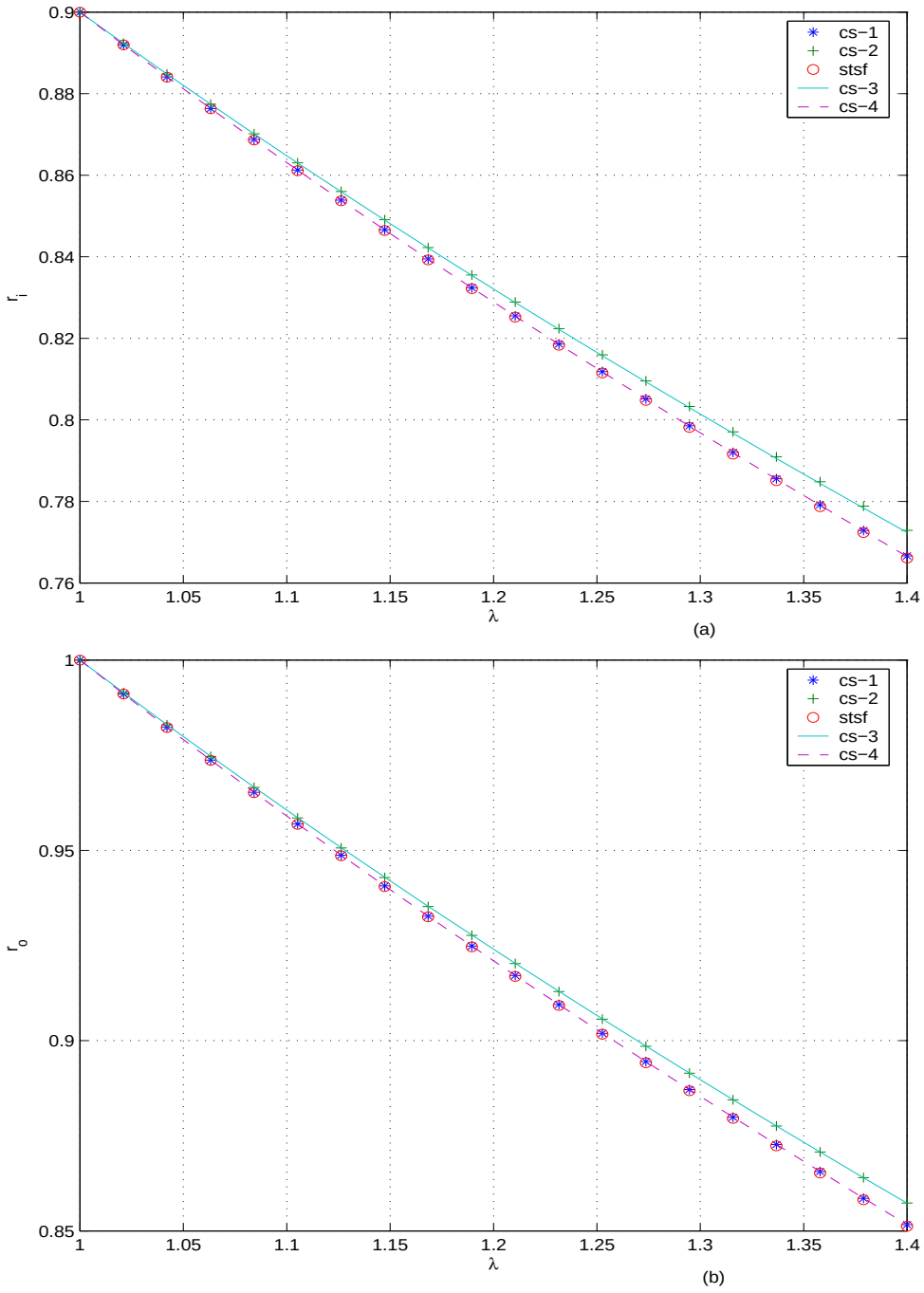

Fig. 36. Plot of (a) r_i (b) r_o vs. λ of an annular right circular cylinder with $R_o = 1$ and $R_i = 0.9$ made of biological material for various prestress distributions shown in figure 28 when μ_1 is as shown in figure 29 and $\mu_2 = 0.1$.

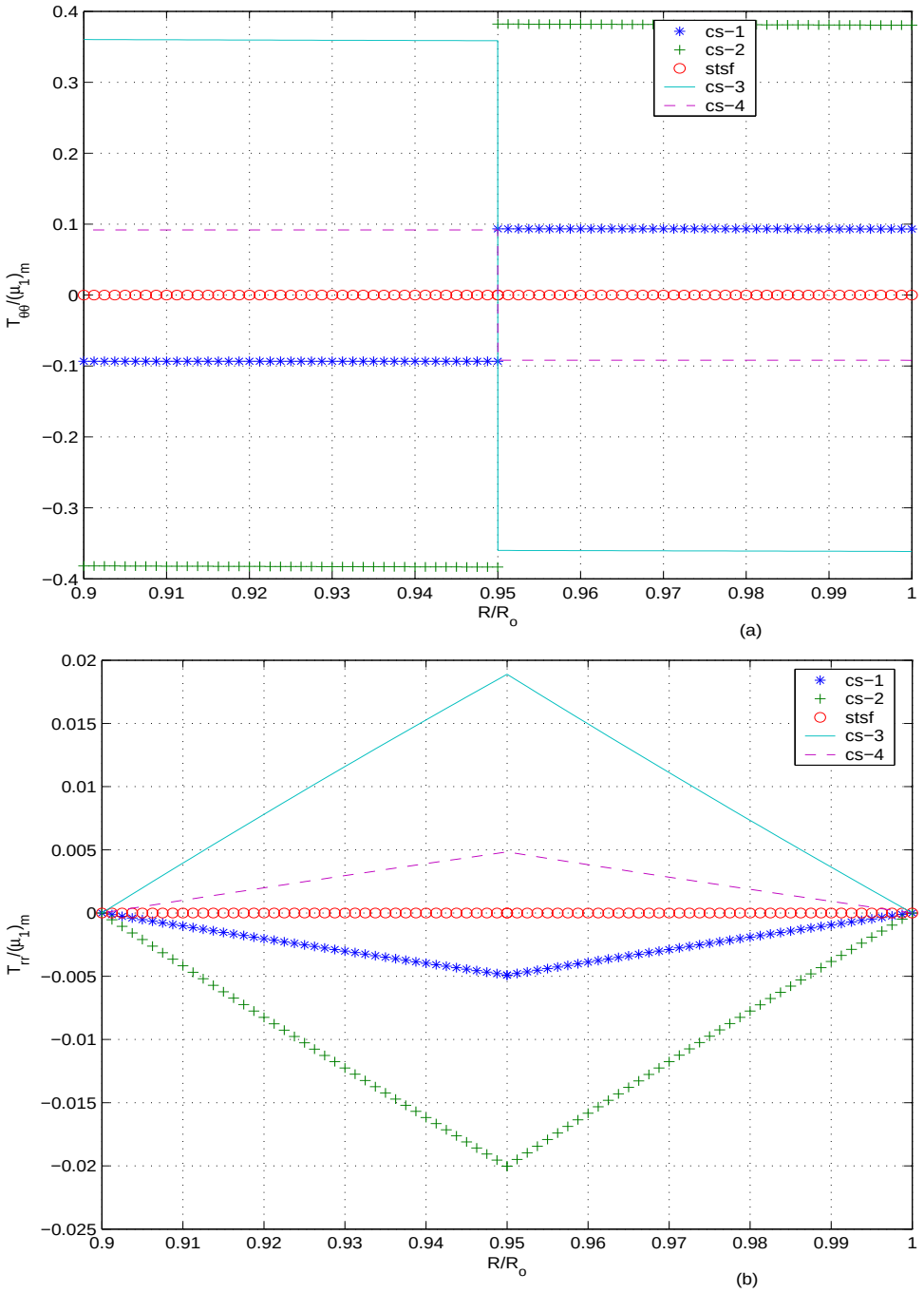

Fig. 37. Plot of stresses (a) $T_{\theta\theta}/(\mu_1)_m$ (b) $T_{rr}/(\mu_1)_m$ vs. R/R_o in an annular right circular cylinder with $R_o = 1$ and $R_i = 0.9$ made of biological material subjected to uniaxial extension with $\lambda = 1.2$ for various prestress distributions shown in figure 28 when μ_1 is as shown in figure 29 and $\mu_2 = 0.1$.

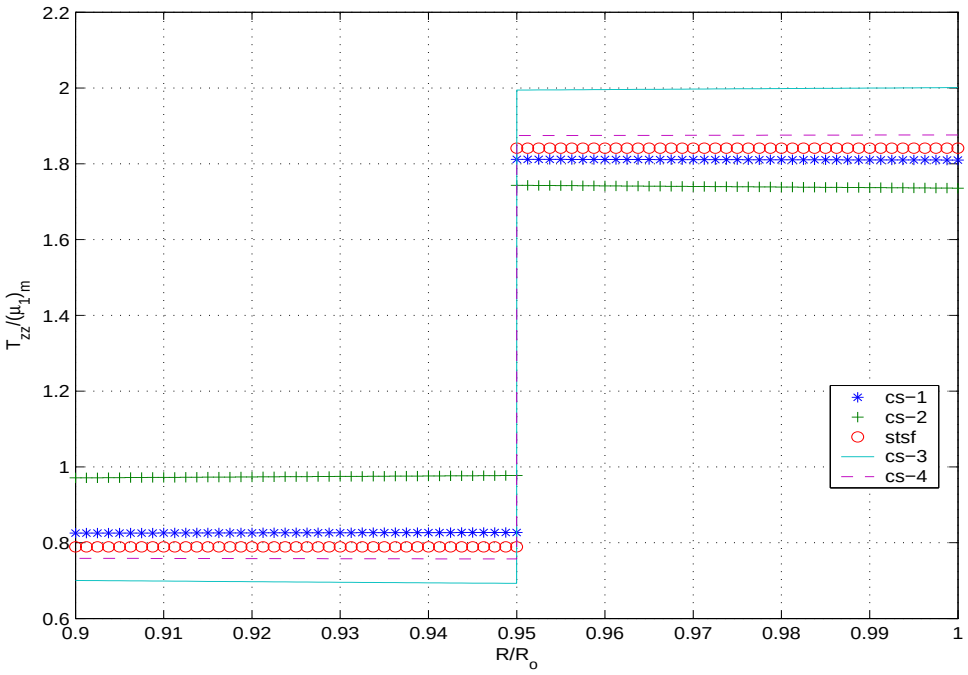

Fig. 38. Plot of stresses $T_{zz}/(\mu_1)_m$ vs. R/R_o in an annular right circular cylinder with $R_o = 1$ and $R_i = 0.9$ made of biological material subjected to uniaxial extension with $\lambda = 1.2$ for various prestress distributions shown in figure 28 when μ_1 is as shown in figure 29 and $\mu_2 = 0.1$.

increasing or decreasing and of course on the magnitude of the twist per unit length. For the cases studied here, the torque varies by as much as 5 percent and the axial load varies by as much as 2 percent as seen in figure 40. Also, the boundary deformations, r_i and r_o, varies less than 1 percent from the stress free body for the cases of prestressed bodies studied here as inferred from figure 41.

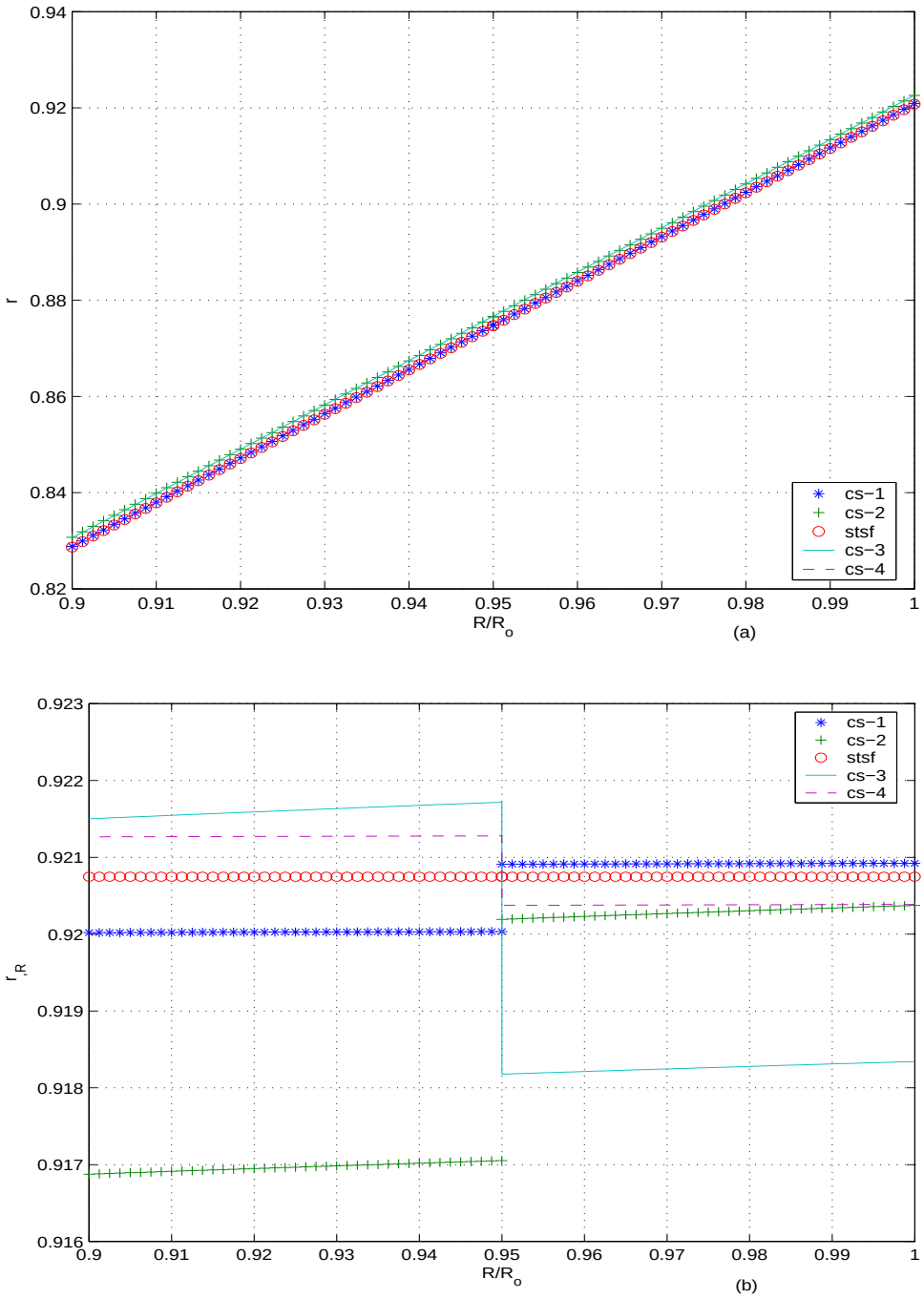

Fig. 39. Plot of (a) r (b) $r_{,R}$ vs. R/R_o in an annular right circular cylinder with $R_o = 1$ and $R_i = 0.9$ made of biological material subjected to uniaxial extension with $\lambda = 1.2$ for various prestress distributions shown in figure 28 when μ_1 is as shown in figure 29 and $\mu_2 = 0.1$.

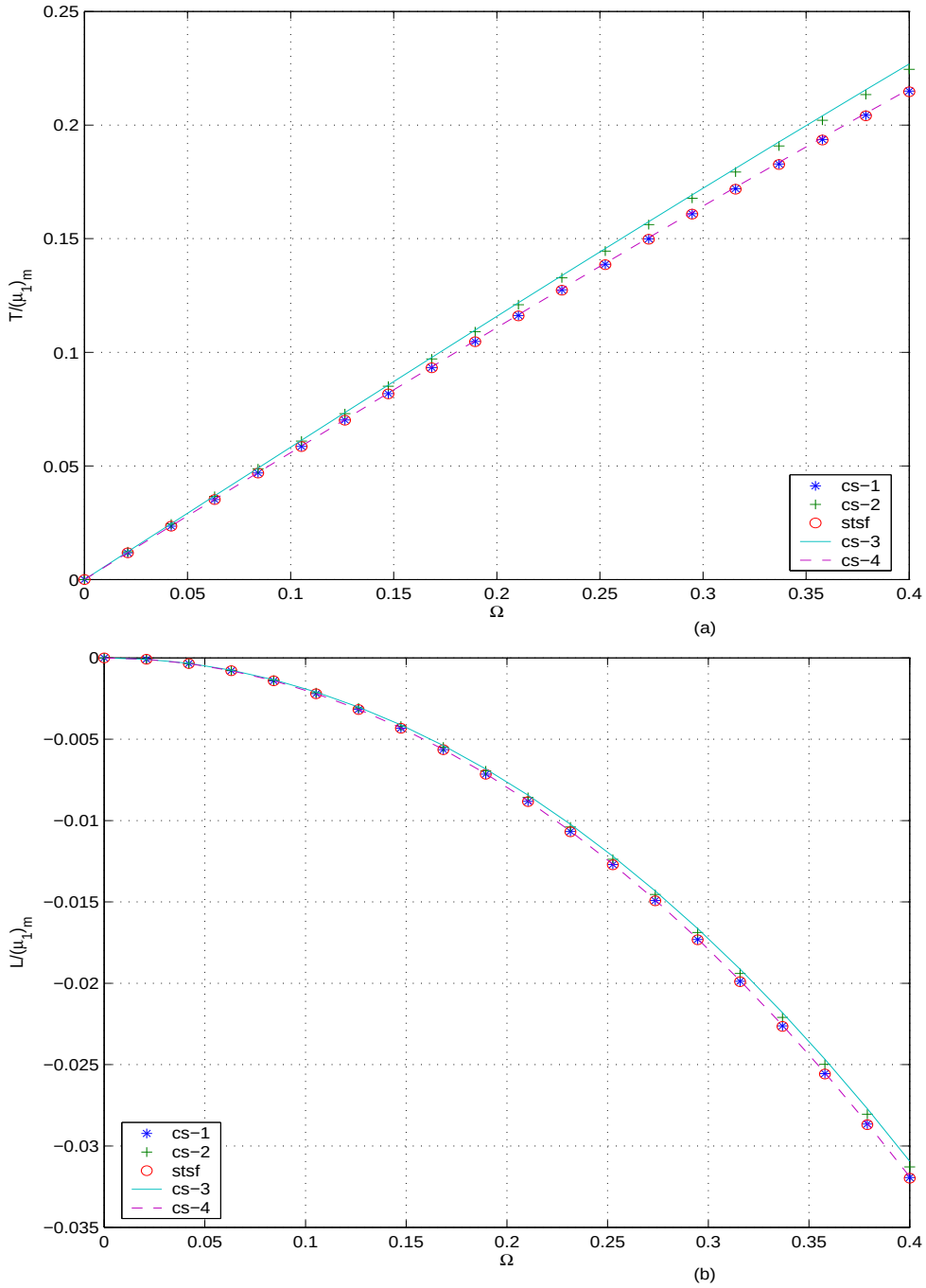

Fig. 40. Plot of (a) $T/(\mu_1)_m$ (b) $L/(\mu_1)_m$ vs. Ω for an annular right circular cylinder with $R_o = 1$ and $R_i = 0.9$ made of biological material for various prestress distributions shown in figure 28 when μ_1 is as shown in figure 29 and $\mu_2 = 0.1$.

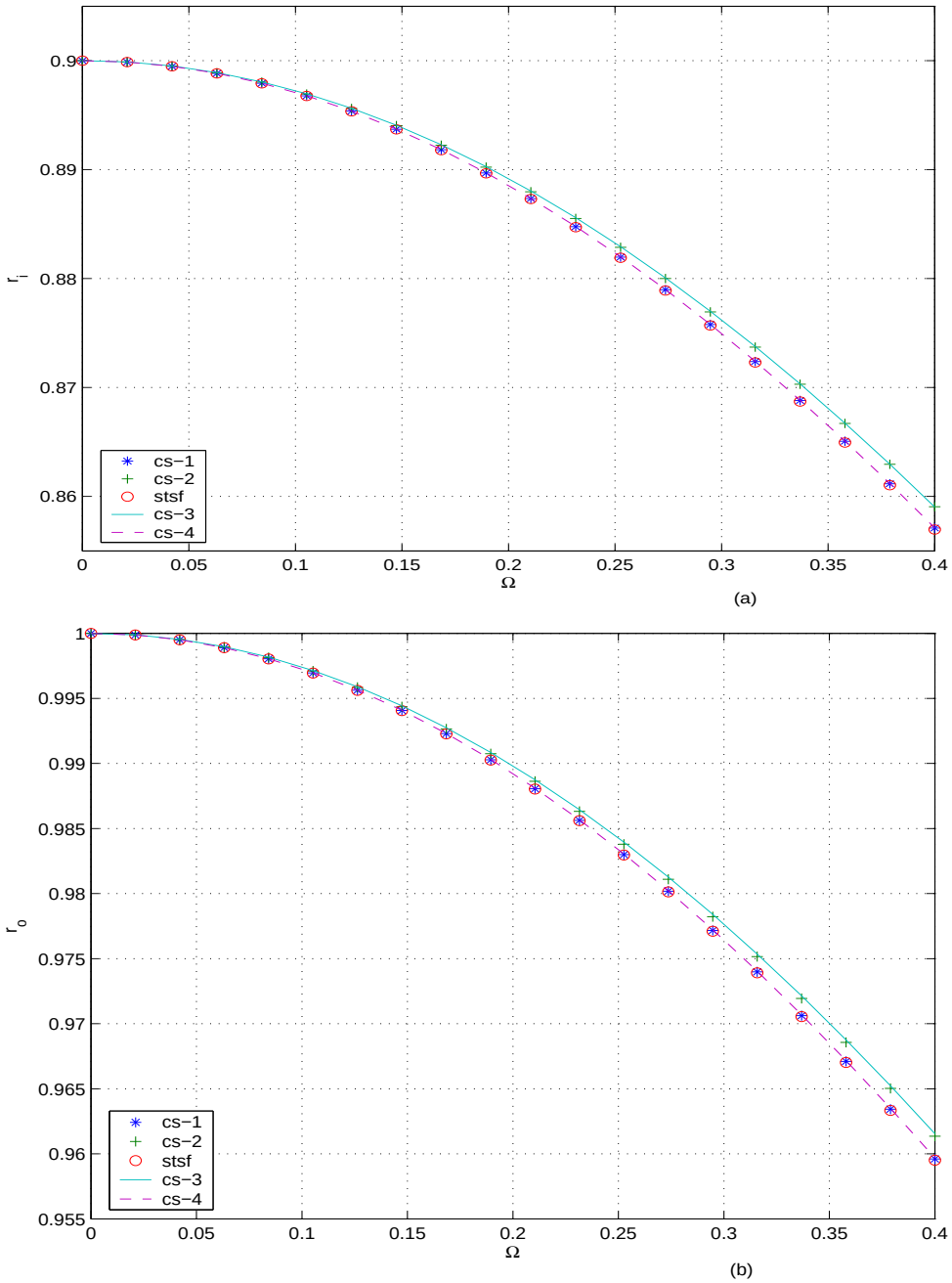

Fig. 41. Plot of (a) r_i (b) r_o vs. Ω of an annular right circular cylinder with $R_o = 1$ and $R_i = 0.9$ made of biological material for various prestress distributions shown in figure 28 when μ_1 is as shown in figure 29 and $\mu_2 = 0.1$.

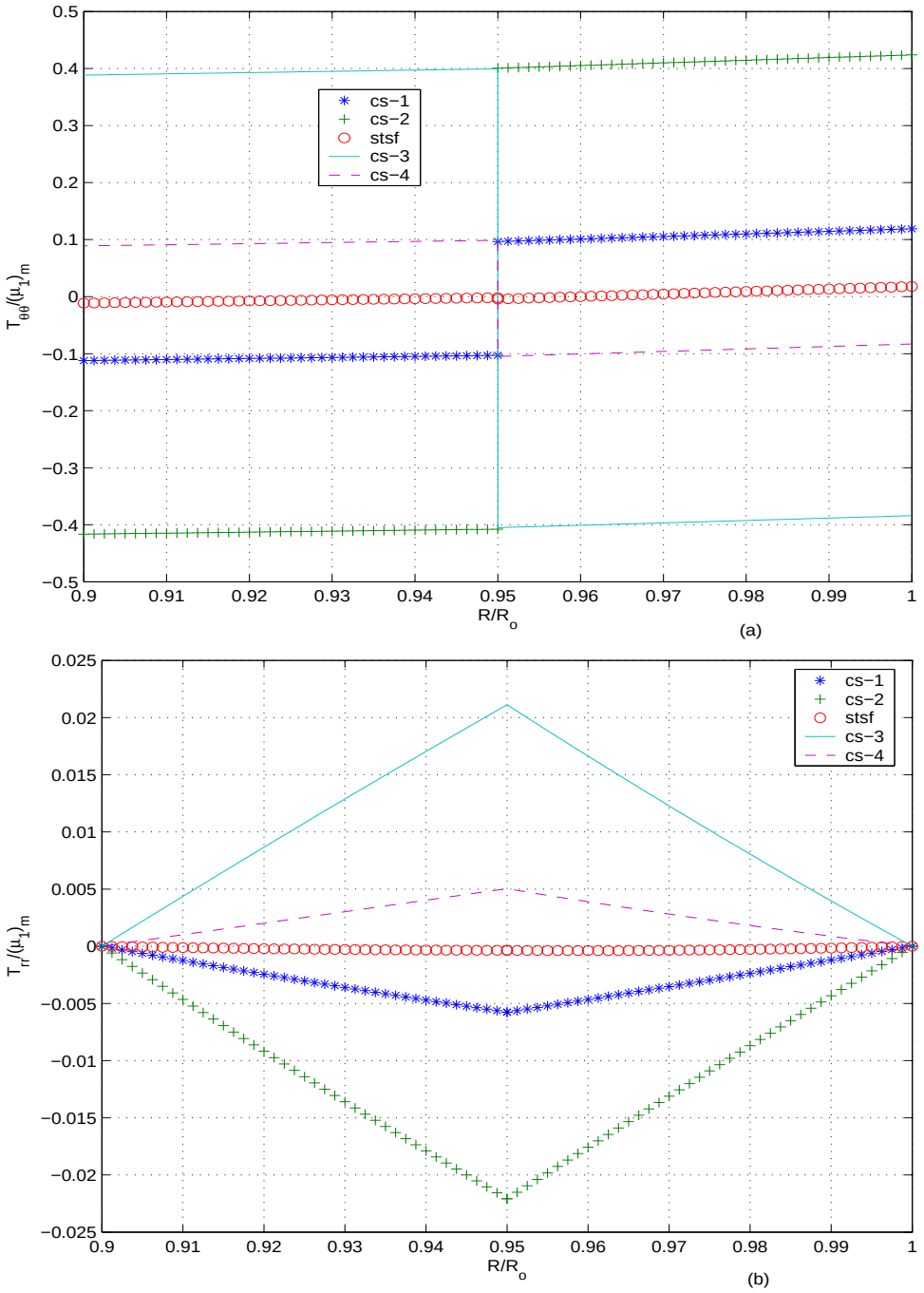

Fig. 42. Plot of stresses (a) $T_{\theta\theta}/(\mu_1)_m$ (b) $T_{rr}/(\mu_1)_m$ vs. R/R_o in an annular right circular cylinder with $R_o = 1$ and $R_i = 0.9$ made of biological material subjected to twisting with $\Omega = 0.2$ for various prestress distributions shown in figure 28 when μ_1 is as shown in figure 29 and $\mu_2 = 0.1$.

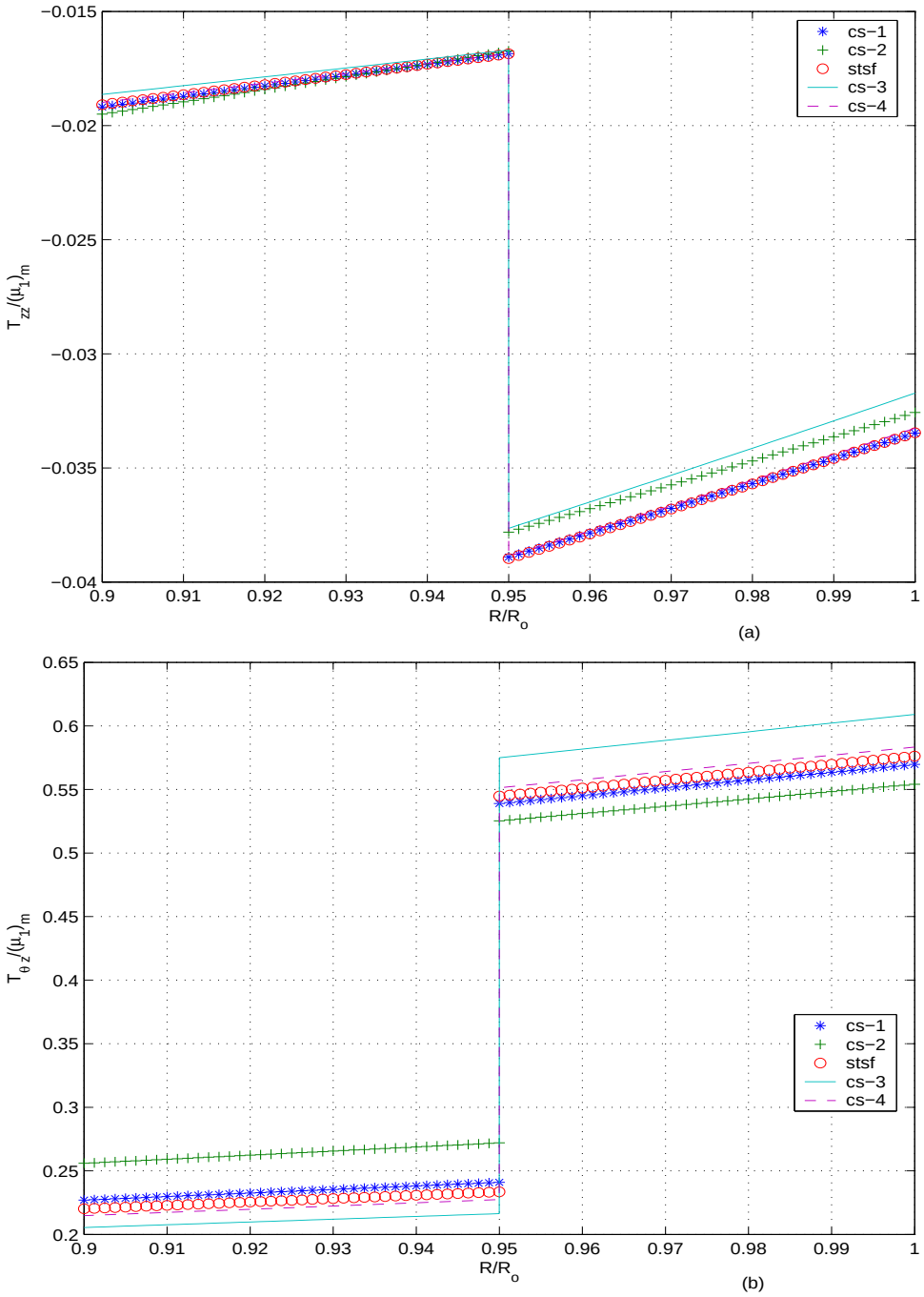

Fig. 43. Plot of stresses (a) $T_{zz}/(\mu_1)_m$ (b) $T_{\theta z}/(\mu_1)_m$ vs. R/R_o in an annular right circular cylinder with $R_o = 1$ and $R_i = 0.9$ made of biological material subjected to twisting with $\Omega = 0.2$ for various prestress distributions shown in figure 28 when μ_1 is as shown in figure 29 and $\mu_2 = 0.1$.

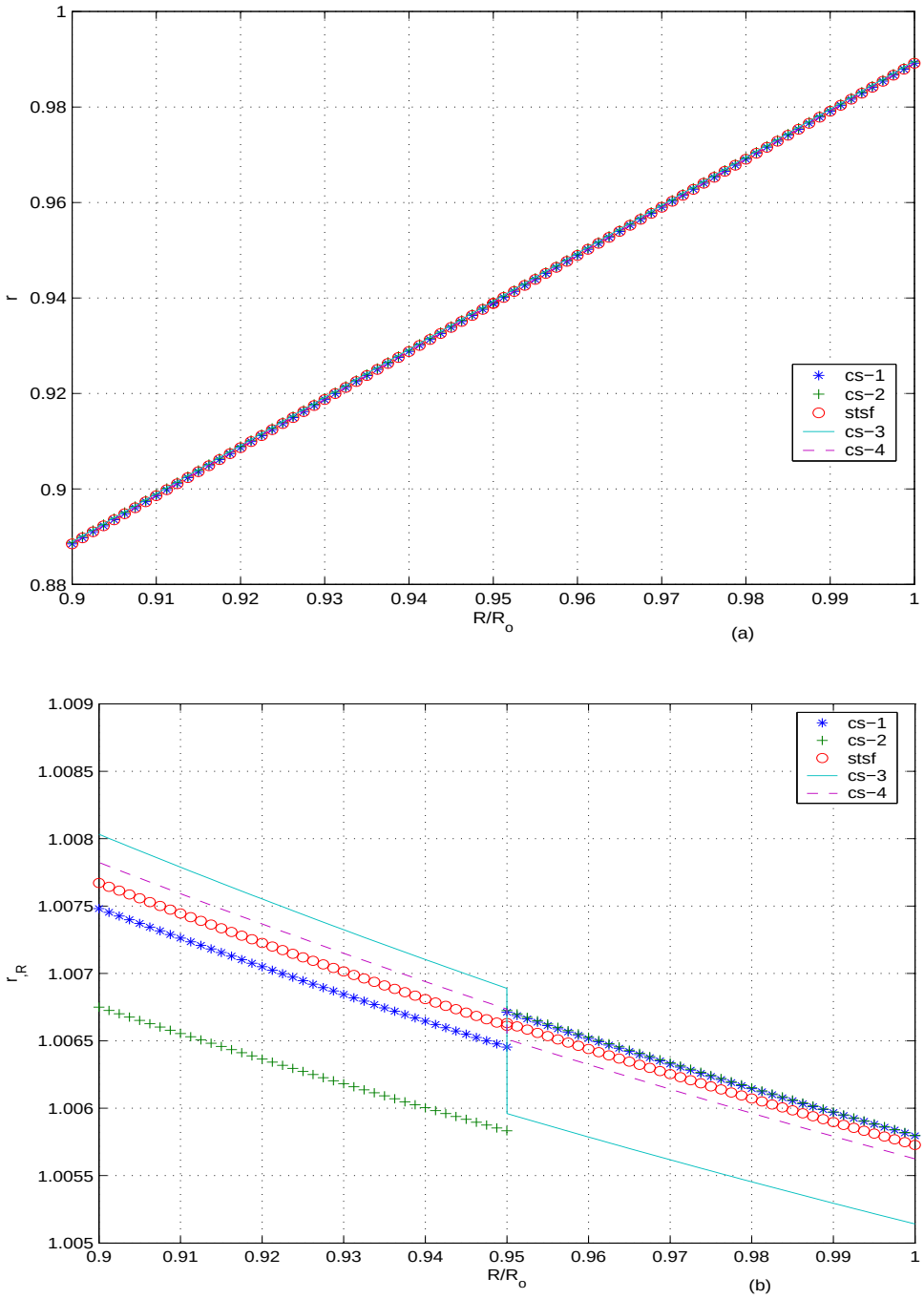

Fig. 44. Plot of (a) r (b) $r_{,R}$ vs. R/R_o in an annular right circular cylinder with $R_o = 1$ and $R_i = 0.9$ made of biological material subjected to twisting with $\Omega = 0.2$ for various prestress distributions shown in figure 28 when μ_1 is as shown in figure 29 and $\mu_2 = 0.1$.

CHAPTER VI

EXPERIMENTS ON CIRCUMFLEX CORONARY ARTERIES FROM NORMOTENSIVE AND HYPERTENSIVE PIGS

In this chapter, we shall apply the above gained knowledge to broaden our understanding of the response of circumflex coronary arteries subjected to inflation at constant length. Despite coronary artery disease being one of the leading causes of mortality in the western world, there are few studies on the mechanics of the circumflex artery. Kang et al. [77] reported finite extension and inflation tests on passive bovine circumflex arteries, but the emphasis was on delineating general characteristics of heat induced changes in behavior and no constitutive relation was proposed. Carmines et al. [78] reported finite inflation tests at three fixed axial extensions, for non-diseased human and porcine LAD arteries. They placed a latex inner tube to prevent leakage from the side branches in the artery and proposed a different stress and strain relationship for low and high strains, each limiting the utility of their study. By far one of the best experimental study of the coronary arteries is by Cox [33]. He used a 1D constitutive relation which accounted for vascular smooth muscle tone but could not capture the non-linear relationship between the stress and strains. However, he deduced the stress and strains based on the assumption that the blood vessel could be approximated as a thin walled homogeneous annular cylinder and that the boundary traction free reference configuration of the body was also stress free. Blood vessels are neither homogeneous nor stress free in a configuration free of boundary traction, thus limiting the applicability of his study.

Here, the aim of performing mechanical tests on arteries is to move a step closer to deducing robust 3D constitutive relations that include vascular smooth muscle tone and to examine whether these constitutive relation changes during the time course of

adaptation and remodelling of arteries due to experimentally induced hypertension. This involves finding a form of the Helmoltz potential[1], i.e., $\psi = \hat{\psi}(\widetilde{J}_{m1}, \widetilde{J}_{m2}, \widetilde{J}_{m3}, \vartheta, \mathbf{P})$ and the prestress field, $\mathbf{T}^o = \hat{\mathbf{T}}^o(\mathbf{P})$ as a function of vascular smooth muscle tone. While one expects the form of Helmoltz potential not to change on sectioning the artery, the prestress field does. Hence, it becomes necessary to perform experiments on the intact blood vessels. This limits the experiments that can be performed. The experiments that can be performed are inflation, extension and twisting of intact blood vessels. A subclass of these experiments were performed in this study on porcine circumflex coronary arteries.

Before further examining, in some detail, the mechanical response of the circumflex artery, let us briefly study its wall structure, as outlined in Humphrey [5], to understand how best it can be approximated. Like other arteries, the circumflex consists of three layers: the tunica intima, tunica media, and tunica adventitia. The tunica intima consist of a monolayer of endothelial cells and a subendothelial layer of connective tissue (i.e., basement membrane consisting of collagen IV and lamina) and axially oriented smooth muscle cells. An internal elastic lamina, considered to be part of media, separates the media and the intima and is essentially a fenestrated sheet of elastin. The media contains smooth muscle cells embedded in an extracellular plexus of elastin and collagen (type I, III and V) and an aqueous ground substance matrix containing proteoglycans. Even though the orientation and distribution of the medial constituents varies with species, the vascular smooth muscle cells tend to be oriented helically, albeit nearly circumferentially in many cases. The smooth muscle appears as a single thick layer that is bounded by a thick internal and less marked external

[1]Here we have suppressed the dependence of the invariants, $\widetilde{J}_{mi}$ and the temperature, ϑ on $\mathbf{P}$ and assume that the functional form of the Helmoltz potential does not change with the material points being considered, but only the material parameters can change.

elastic lamina. Further, the smooth muscle cells are embedded in a loose connective tissue matrix and arranged as a sequence of concentric layers of cells; with many of these layers. The connective tissue augments the structural integrity of the wall, including its ability to generate force, and acts as a scaffolding on which the cells can adhere or move. Finally, the outermost layer, the adventitia, consists primarily of a dense network of type I collagen fibers with admixed elastin and fibroblasts. The adventitial collagen fibers tend to have an axial orientation and are undulated slightly in the basal state. The adventitia, comprising approximately 50% of the circumflex wall, is thought to limit acute over distension, thus serving as a protective sheath. Hence, for understanding the mechanical response of the circumflex artery or more generally, muscular arteries, can be thought of as two layered[2] right circular annular cylinder with the layers being of the same thickness but with different material properties. Here we propose ways to examine whether such an assumption is adequate given the arrangement of the smooth muscle cells which are about $5\mu m$ in diameter, in a wall that is approximately $500\mu m$ thick.

Towards this, we observe that if the deformation is of the form

$$r = r(R), \qquad \theta = \Theta, \qquad z = \lambda Z, \tag{6.1}$$

then the value of the principal invariants is constant[3] on the surface defined by $R = R_o$, a constant. Here (R, Θ, Z) denotes the coordinates of a typical material point in a reference configuration and (r, θ, z) the coordinates of a typical material point in the current configuration; R_o is the outer radius of the artery, assumed to be

[2]The innermost layer, tunica intima is considered to be mechanically insignificant [5].

[3]Note that while the matrix components of the gradient of deformation in cylindrical coordinates is constant on the surface of the cylinder, that of the Cartesian coordinates are not.

an annular right circular cylinder. From the results in the last chapter, it is easy to see that the deformation (6.1) is possible provided $\psi = \hat{\psi}(\widetilde{J}_{m1}, \widetilde{J}_{m2}, \widetilde{J}_{m3}, R)$, $\mathbf{T}^o = \hat{\mathbf{T}}^o(R)$ and $\hat{\psi}(\widetilde{J}_{m1}, \widetilde{J}_{m2}, \widetilde{J}_{m3}, R) \in C^\infty(\omega_a)$ i.e., the blood vessel can be at most radially inhomogeneous and the prestress fields vary at most radially and the Helmoltz potential is a smooth function of the invariants $\widetilde{J}_{mi}$ and piecewise smooth functions of R. It should be emphasized that there can exist other deformations, not of the form (6.1), satisfying the relevant boundary conditions[4] and balance of linear momentum when $\psi = \hat{\psi}(\widetilde{J}_{m1}, \widetilde{J}_{m2}, \widetilde{J}_{m3}, R)$, $\mathbf{T}^o = \hat{\mathbf{T}}^o(R)$. Thus, it can only be concluded that if the deformation was of the form (6.1) then the Helmoltz potential and the prestresses do not vary circumferentially and/or axially. Thus, the first objective is to examine if the principal invariants are constant on the surface of the circumflex artery subjected to inflation at constant length.

Vascular smooth muscle tone is known to modify the mechanical response of the artery [See Cox ([33],[34], [35]), Zulliger et al. [36], Fridez et al. ([37],[38],[39])], to change the "opening angle" in a radially cut short segment of the artery ([41],[79]), and to change the diameter of the artery held at constant length with a constant radial component of the normal stress at its inner surface. In other words, smooth muscle tone alters the stress field in a given configuration, particularly that in the reference configuration. That is, $\mathbf{T}^o$, the stress in the reference configuration depends on the smooth muscle tone and possibly other factors, yet to be identified. In vitro, the smooth muscle tone depends on the concentration of the agonist, temperature and presumably on the mechanical state of the blood vessel [5]. The change in the smooth muscle tone depending on the mechanical stress ([5], [36]) experienced by it is called

[4]The prescribed boundary conditions are $T_{rr}(r_i)$, $T_{rr}(r_o)$, the radial component of the normal stress at the inner and outer surfaces, the axial load, L, defined in (4.72), the torque, T, defined in (4.73), the deformed inner and outer radius, r_i and r_o, the ratio of the deformed length to original length, λ and twist per unit length, Ω.

the myogenic response. However, this dependence is deduced from the assumption that the total stress in the artery is the sum of the active stress (i.e. the stress that arises due to smooth muscle contraction) and the passive stress (i.e. the stress in the arterial wall when the smooth muscles are fully relaxed). It was shown in chapter III that an additive decomposition of the stresses does not hold, in general, when the body undergoes finite deformations. Here we examine if we can provide experimental evidence towards the same.

Finally, we outline the issues that arise while comparing the response of two different inhomogeneous and prestressed bodies. The question here is how to distinguish differences in the mechanical response of the body arising from differences in the geometry of the bodies versus differences in the material that it is made of. Even what we mean by differences in the material is not clear in the case of prestressed bodies. For example, consider two bodies identical in geometry and chemical composition except that one of them has prestresses. Now, the mechanical response of these bodies would in general be different. Therefore, are we to conclude that they are made of different materials? It is difficult to isolate the effects of geometry of the body while experimentally investigating the mechanical response of inhomogeneous and prestressed bodies because, in general, the stress distribution is non-uniform and the deformations are inhomogeneous and it is rarely possible in experiments to determine either of them without making some assumptions. Here it is pertinent to note that deformations that are solutions to balance of linear momentum need not be algebraic functions but might locally be well approximated by algebraic functions. However, caution has to be exercised in such a comparison or approximation, for many different prestress field can result in nearly the same deformation, as was shown in the last chapter (see figures 34, 39 and 44), even though their gradients were relatively markedly different. Thus, we finally provide a possible scheme for comparing the

mechanical response of different inhomogeneous and prestressed bodies.

A. Experimental system

A computer controlled system originally designed and built to test embryonic chick hearts subjected to low pressures, reported in Ling et al. [80], was adapted to test circumflex arteries. A schematic of the experimental system is shown in figure 45. The overall system consists of three main subsystems.

Fist, we consider a video-based system which allows 2D tracking of up to 12 markers. This system consists of a microscope (Olympus SZ60) with an auxiliary viewing port (SZ-PT), a charged couple device (CCD) camera (Javelin JE-7442), a VCR (Sony SVT-S3100), two B&W monitors (Sony SSM-171 for specimen preparation and a Panasonic TR-930B for visualizing the on-line tracking of fiducial markers) and a video frame grabber board (Data Translation DT-2853SQ) that captures 8 bit gray scale images as 512×512 pixel arrays. Markers are tracked online at 30 Hz using the correlation-based algorithm reported in Downs et al. [81]. To maintain focus of the markers on the surface of the artery during "extreme" deformations, a manually controlled focussing mechanism can translate the microscope optics vertically. This was achieved by replacing the rack and pinion microscope stand with a motorized vertical translation stage (Newport Corporation 426 and CMA-25CC 861 controller) mounted on a damped mounting rod (Thorlabs DP14).

Second, the cannulated specimen is held by and loaded through a system as shown in figure 45, so that the artery is submerged in the test chamber, which contains a physiologic solution. The specimen could be axially stretched using a computer controlled actuator (Newport Corp.) through a precision x-y-z stage that allows adjustment of the position of the specimen within the video field of view. The x-y-z

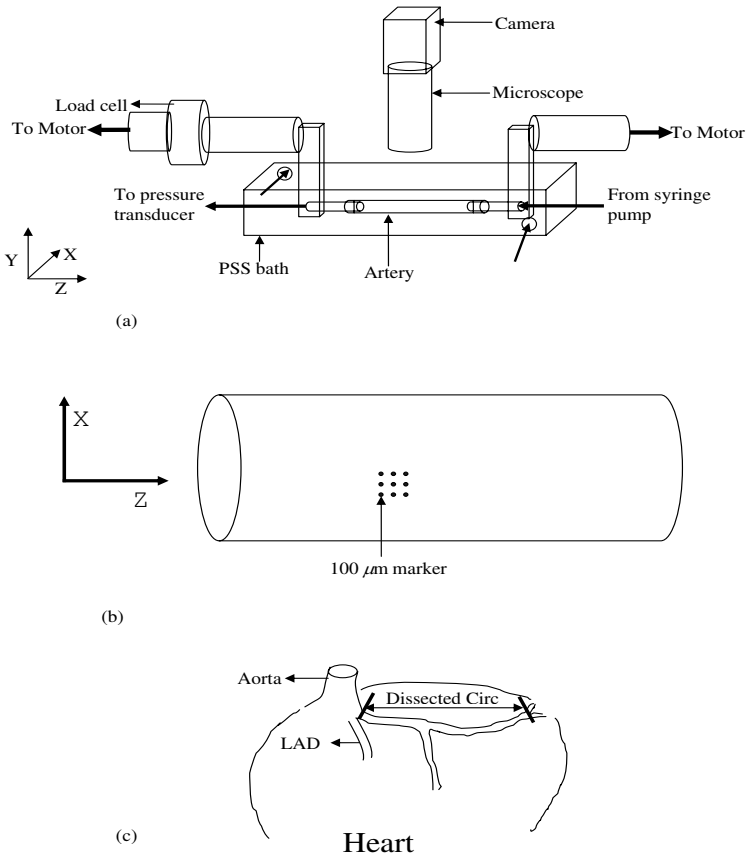

Fig. 45. (a) Schematic of the experimental setup (b) Schematic of the placement of the markers on the dissected circumflex artery (c) Schematic of the location from where the circumflex artery is dissected.

stage is also used to change the length of the artery at which it is held fixed while inflating. Also, one end of the specimen is attached to a computer controlled syringe pump (World Precision Instruments SP210iw) and the other end to a pressure transducer (Sensotec) and load cell (Sensotec), as shown in figure 45. The artery is connected to the syringe pump and pressure transducer using tubes of 2mm inner diameter. The syringe pump is fitted with a 3cc syringe (Hamilton 1705TLL). The pump is controlled by the computer via ASCII commands that allows cyclic pressurization tests over a wide range of infusion rates. The pressure transducer has a sensing range from 0 to 258 mmHg, with a factory reported accuracy of 0.26 mmHg. The load cell, used to measure the axial load, has a sensing range from 0 to 250 gms with a reported accuracy of 0.25 gms. The pressure transducer and the load cell is sampled via a 12-bit analog to digital (A/D) board (Data Translation DT2831) in the computer.

Third, the experiments and data collection (video, axial load and radial component of the normal stress at the inner surface of the artery) are controlled by Keyboard commands via a custom C code running on an Intel Pentium II computer (Compaq Deskpro, RAM reduced to 8MB to accommodate the online tracking algorithm). The stored data is analyzed using custom *matlab* code.

The pressure transducer was calibrated using sphygmomanometer and the load cell using standard weights. The video system was not calibrated because we were interested only in the gradient of the deformation and it is a dimensionless quantity.

B. Computation of deformation gradient

Here, we shall first concern ourself with the problem of computing the gradient of the deformation from the position of 'n' markers at different instances. Towards

this, we first estimate a smooth deformation field from the position of 'n' markers in the reference and current configurations and then compute the gradient of the inferred smooth deformation field. As already noted, in general, it is not possible to experimentally determine the exact deformation field by tracking 'n' markers, we can at most get a reasonable approximation of the deformation field and its gradient locally. In other words, we chose a finite dimensional function space and seek the best approximation of the actual deformation in this space.

To elaborate, let $\boldsymbol{\phi}_i$ be a basis for the chosen finite dimensional function space. Then, the approximate deformation field, $\boldsymbol{\chi}^a$ has a representation[5]

$$(\chi^a)^j = \sum_{i=1}^{m} a_i^j \phi_i^j(X, Y, Z), \tag{6.2}$$

where a_i^j are constants, (X, Y, Z) are Cartesian coordinates of the marker in the reference configuration, m is a finite integer. The constants a_i^j have to be determined from knowing the position of 'n' markers in the current and reference configuration. This can be achieved in couple of ways. In the first case, assuming $m < n$, we choose 'm' markers out of the available 'n' markers such that $\Delta^j \neq 0$ for $j \in \{x, y, z\}$, where $\Delta^j = \det(\mathbf{A}^j)$,

$$\mathbf{A}^j = \begin{pmatrix} \phi_1^j(X_1, Y_1, Z_1) & \phi_2^j(X_1, Y_1, Z_1) & \cdots & \phi_m^j(X_1, Y_1, Z_1) \\ \phi_1^j(X_2, Y_2, Z_2) & \phi_2^j(X_2, Y_2, Z_2) & \cdots & \phi_m^j(X_2, Y_2, Z_2) \\ \vdots & \vdots & \cdots & \vdots \\ \phi_1^j(X_m, Y_m, Z_m) & \phi_2^j(X_m, Y_m, Z_m) & \cdots & \phi_m^j(X_m, Y_m, Z_m) \end{pmatrix} \tag{6.3}$$

(X_k, Y_k, Z_k) are the Cartesian coordinates of k^{th} marker of the chosen m markers

[5]Since we can track only a finite number of markers, at times it might be advantageous to approximate the deformation by functions such as $x = \sqrt{\frac{a_1}{X^2} + a_2}$ or rational functions. In these cases, the constants, a_i can be determined by the method outlined below, albeit with some modifications.

in the reference configuration. Then, we find the constants a_i^j by solving the linear system of equations to be

$$\mathbf{a}^x = (\mathbf{A}^x)^{-1}\mathbf{x}, \qquad \mathbf{a}^y = (\mathbf{A}^y)^{-1}\mathbf{y}, \qquad \mathbf{a}^z = (\mathbf{A}^z)^{-1}\mathbf{z}, \tag{6.4}$$

where

$$\mathbf{a}^j = \begin{Bmatrix} a_1^j \\ a_2^j \\ \vdots \\ a_m^j \end{Bmatrix}, \quad \mathbf{x} = \begin{Bmatrix} x_1 \\ x_2 \\ \vdots \\ x_m \end{Bmatrix}, \quad \mathbf{y} = \begin{Bmatrix} y_1 \\ y_2 \\ \vdots \\ y_m \end{Bmatrix}, \quad \mathbf{z} = \begin{Bmatrix} z_1 \\ z_2 \\ \vdots \\ z_m \end{Bmatrix}, \tag{6.5}$$

(x_k, y_k, z_k) are the Cartesian coordinates of the k^{th} marker of the chosen m markers in the current configuration. The value of the constants $\mathbf{a}^j$ depends on the choice of the m markers, unless the actual deformation is contained in the chosen function space.

Now, let I_1^c, I_2^c and I_3^c denote the principal invariants computed from $(a_i^j)^c$, the value of the constants obtained for the c^{th} choice of 'm' markers. In general, at a given location, we obtain different values for the principal invariants corresponding to different choices of the 'm' markers. These different values of the principal invariants not only reflect the quality of the approximation of the chosen function space of the actual deformation, they in fact carry information about the true spatial variation of the deformation and its gradient, as is evident when the basis of the function space is $\{X, Y, Z, 1\}$. To understand what we mean by this, let us consider a simpler problem. Say we are interested in approximating the function, $f(x)$ by a straight line $a * x + b$. Immediately, we know that unless the function $f(x)$ happens to be a straight line, we could not approximate the function $f(x)$ globally by a straight line with good degree of accuracy. However, we could locally approximate a smooth function $f(x)$ by the

straight line

$$y = \frac{f(x_1) - f(x_2)}{x_1 - x_2} x + \frac{x_1 f(x_2) - x_2 f(x_1)}{x_1 - x_2}, \tag{6.6}$$

fairly accurately in many cases. In fact as x_2 tends to x_1, the approximation becomes better for both the function and its first derivative. But the important observation here is that the value of the constants a and b varies with the choice of x_1 and x_2 in keeping with the changes in the value of the function $f(x)$. Hence, it is worthwhile to study the variation of the principal invariants with the choice 'm' markers. Towards this, we find the following two definitions useful to present our results:

$$I_p = \frac{1}{d} \sum_{c=1}^{d} I_p^c, \qquad I_p^s = \sqrt{\frac{1}{d-1} \sum_{c=1}^{d} (I_p^c - I_p)^2}, \tag{6.7}$$

where $p \in \{1, 2, 3\}$ and d is the total number of different sets of m markers used to infer the invariants, I_p.

Alternatively, when one knows that the function space to which the deformation belongs, we can use the position of all the 'n' markers to find the values of the constants a_i^j such that the errors

$$\begin{aligned} e^x &= \sum_{k=1}^{n} \left[x_k - \sum_{i=1}^{m} a_i^x \phi_i^x(X_k, Y_k, Z_k) \right]^2, \\ e^y &= \sum_{k=1}^{n} \left[y_k - \sum_{i=1}^{m} a_i^y \phi_i^y(X_k, Y_k, Z_k) \right]^2, \\ e^z &= \sum_{k=1}^{n} \left[z_k - \sum_{i=1}^{m} a_i^z \phi_i^z(X_k, Y_k, Z_k) \right]^2, \end{aligned} \tag{6.8}$$

are minimized. This yields

$$\mathbf{a}^x = (\mathbf{D}^x)^{-1} \mathbf{x}^*, \qquad \mathbf{a}^y = (\mathbf{D}^y)^{-1} \mathbf{y}^*, \qquad \mathbf{a}^z = (\mathbf{D}^z)^{-1} \mathbf{z}^*, \tag{6.9}$$

where

$$\mathbf{D}^j = \begin{pmatrix} \sum_{k=1}^n (\hat{\phi}_1^j)^2 & \sum_{k=1}^n \hat{\phi}_1^j \hat{\phi}_2^j & \cdots & \sum_{k=1}^n \hat{\phi}_1^j \hat{\phi}_m^j \\ \sum_{k=1}^n \hat{\phi}_2^j \hat{\phi}_1^j & \sum_{k=1}^n (\hat{\phi}_2^j)^2 & \cdots & \sum_{k=1}^n \hat{\phi}_2^j \hat{\phi}_m^j \\ \vdots & \vdots & \cdots & \vdots \\ \sum_{k=1}^n \hat{\phi}_m^j \hat{\phi}_1^j & \sum_{k=1}^n \hat{\phi}_m^j \hat{\phi}_2^j & \cdots & \sum_{k=1}^n (\hat{\phi}_m^j)^2 \end{pmatrix}, \tag{6.10}$$

$$\mathbf{x}^* = \begin{Bmatrix} \sum_{k=1}^n x_k \hat{\phi}_1^1 \\ \sum_{k=1}^n x_k \hat{\phi}_2^1 \\ \vdots \\ \sum_{k=1}^n x_k \hat{\phi}_m^1 \end{Bmatrix}, \quad \mathbf{y}^* = \begin{Bmatrix} \sum_{k=1}^n y_k \hat{\phi}_1^2 \\ \sum_{k=1}^n y_k \hat{\phi}_2^2 \\ \vdots \\ \sum_{k=1}^n y_k \hat{\phi}_m^2 \end{Bmatrix}, \quad \mathbf{z}^* = \begin{Bmatrix} \sum_{k=1}^n z_k \hat{\phi}_1^3 \\ \sum_{k=1}^n z_k \hat{\phi}_2^3 \\ \vdots \\ \sum_{k=1}^n z_k \hat{\phi}_m^3 \end{Bmatrix}, \tag{6.11}$$

and note that $\hat{\phi}_i^j = \phi_i^j(X_k, Y_k, Z_k)$.

Having determined the constants a_i^j, it is straight forward to compute the gradient of deformation and hence the principal invariants I_1, I_2 and I_3. Note that in this case since we have used all the 'n' markers there is only one set of a_i^j and hence the principal invariants. Here the errors e^j, provides information about how good the deformation was approximated in the chosen function space. However, as shown in the last chapter, even when the deformations are close, their gradients can be far apart and we need a good estimate of the gradient of the deformation because stress depends on it. Hence, if we are not sure of the function space to which the deformation belongs, using this method can result in significant errors in the determined value of the gradient of deformation, which cannot be estimated. But this method is less sensitive than the previous method to the errors in the location of the centroid of the markers.

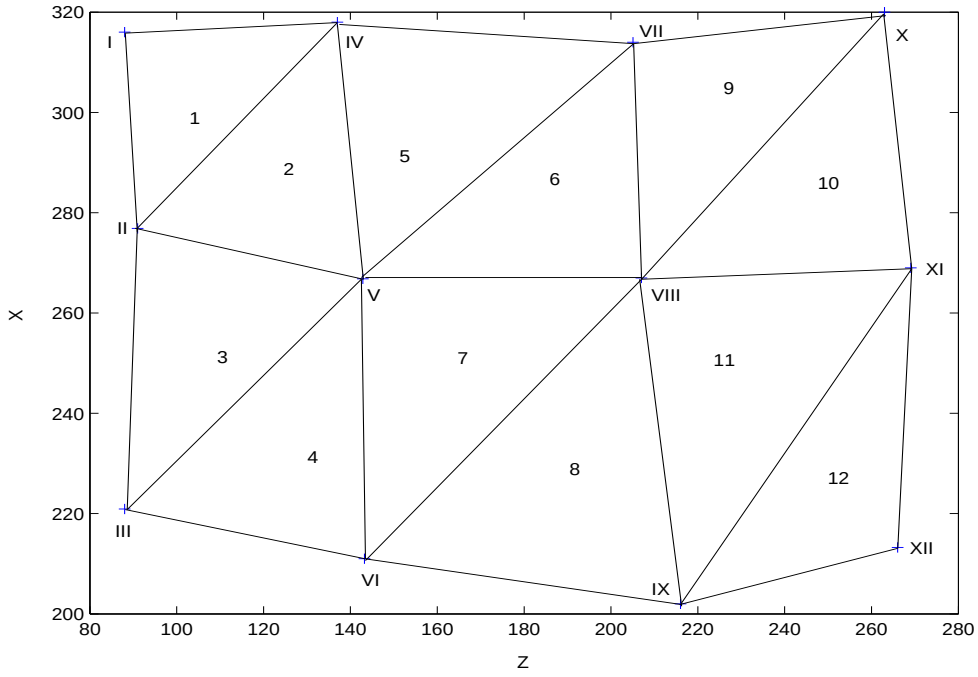

Fig. 46. Selection of triangles (1-12) in the reference configuration to compute the deformation field by tracking 12 markers (I-XII) using (6.12).

1. Illustrative example for markers tracked in 2D

Above we outlined a general scheme for computing the deformation gradient from the position of 'n' markers in the reference and current configuration. Now, we apply the scheme for inferring the deformation gradient when the markers are tracked in 2D.

Let us define the function space as that spanned by the basis $\{X, Z, 1\}$ for both the x coordinate and the z coordinate. Thus, (6.2) can be written as

$$x = a_1^x X + a_2^x Z + a_3^x, \qquad z = a_1^z X + a_2^z Z + a_3^z, \tag{6.12}$$

where a_i^x and a_i^z are constants and we have assumed that the 2D cartesian coordinates of the tracked markers are x and z in the current configuration and X and Z in the reference configuration. Now, if we know the location of three markers in the current

and reference configuration we can obtain $(a_i^x)^c$ and $(a_i^z)^c$, the value of a_i^x and a_i^z corresponding to the c^{th} choice of 3 markers, from solving the linear equations

$$\begin{pmatrix} X_1 & Z_1 & 1 \\ X_2 & Z_2 & 1 \\ X_3 & Z_3 & 1 \end{pmatrix} \begin{Bmatrix} (a_1^x)^c \\ (a_2^x)^c \\ (a_3^x)^c \end{Bmatrix} = \begin{Bmatrix} x_1 \\ x_2 \\ x_3 \end{Bmatrix}, \qquad \begin{pmatrix} X_1 & Z_1 & 1 \\ X_2 & Z_2 & 1 \\ X_3 & Z_3 & 1 \end{pmatrix} \begin{Bmatrix} (a_1^z)^c \\ (a_2^z)^c \\ (a_3^z)^c \end{Bmatrix} = \begin{Bmatrix} z_1 \\ z_2 \\ z_3 \end{Bmatrix}, \tag{6.13}$$

where X_i and Z_i are the coordinates in the reference configuration of the i^{th} marker in the selected 3 markers and x_i and z_i are the coordinates of the same i^{th} marker in the current configuration. It is then straight forward to see that the invariants, $tr(\mathbf{C}^{2D})$ and $det(\mathbf{C}^{2D})$, are given by

$$(I_1^{2D})^c = (a_1^x)^{c2} + (a_2^x)^{c2} + (a_1^z)^{c2} + (a_2^z)^{c2}, \qquad (I_3^{2D})^c = [(a_1^x)^c (a_2^z)^c - (a_2^x)^c (a_1^z)^c]^2. \tag{6.14}$$

Thus, we find $(I_1^{2D})^c$ and $(I_3^{2D})^c$ corresponding to the c^{th} choice of three markers. Figure 46 shows a typical selection of 12 sets of three markers where the markers are at the vertices of each triangle and are numbered using Roman numerals. Here we choose different sets of 3 markers such that the triangles formed with these markers as vertices have no overlapping areas.

Instead of finding the constants a_i^j in (6.12) from the position of three markers we can find them using all the 'n' markers such that the errors

$$e^x = \sum_{i=1}^{n} \left[a_1^x X_i + a_2^x Z_i + a_3^x - x_i\right]^2 \quad \text{and} \quad e^z = \sum_{i=1}^{n} \left(a_1^z X_i + a_2^z Z_i + a_3^z - z_i\right)^2, \tag{6.15}$$

are minimized. This requires

$$\begin{pmatrix} \sum_{i=1}^n X_i^2 & \sum_{i=1}^n X_i Z_i & \sum_{i=1}^n X_i \\ \sum_{i=1}^n X_i Z_i & \sum_{i=1}^n Z_i^2 & \sum_{i=1}^n Z_i \\ \sum_{i=1}^n X_i & \sum_{i=1}^n Z_i & n \end{pmatrix} \begin{Bmatrix} a_1^x \\ a_2^x \\ a_3^x \end{Bmatrix} = \begin{Bmatrix} \sum_{i=1}^n x_i X_i \\ \sum_{i=1}^n x_i Z_i \\ \sum_{i=1}^n x_i \end{Bmatrix}, \tag{6.16}$$

$$\begin{pmatrix} \sum_{i=1}^n X_i^2 & \sum_{i=1}^n X_i Z_i & \sum_{i=1}^n X_i \\ \sum_{i=1}^n X_i Z_i & \sum_{i=1}^n Z_i^2 & \sum_{i=1}^n Z_i \\ \sum_{i=1}^n X_i & \sum_{i=1}^n Z_i & n \end{pmatrix} \begin{Bmatrix} a_1^z \\ a_2^z \\ a_3^z \end{Bmatrix} = \begin{Bmatrix} \sum_{i=1}^n z_i X_i \\ \sum_{i=1}^n z_i Z_i \\ \sum_{i=1}^n z_i \end{Bmatrix}. \tag{6.17}$$

We solve the above linear equations to obtain the unknown a_i^x's and a_i^z's. Then we compute the invariants I_1^{2D} and I_3^{2D} from

$$I_1^{2D} = (a_1^x)^2 + (a_2^x)^2 + (a_1^z)^2 + (a_2^z)^2, \qquad I_3^{2D} = [(a_1^x)(a_2^z) - (a_2^x)(a_1^z)]^2. \tag{6.18}$$

Instead of projecting deformation on to a function space spanned by $\{X, Z, 1\}$, we could project it to a function space spanned by $\{X, Z, XZ, 1\}$. Thus, (6.2) for this case can be written as

$$x = a_1^x X + a_2^x Z + a_3^x XZ + a_4^x, \qquad z = a_1^z X + a_2^z Z + a_3^z XZ + a_4^z. \tag{6.19}$$

As before in this case too we can determine the constants a_i^x and a_i^z from the position of only 4 markers or from all the 'n' markers. When only 4 markers are used to infer the deformation field, we compute

$$\begin{aligned} (I_1^{2D})^c &= [(a_1^x)^c + (a_3^x)^c Z_c]^2 + [(a_2^x)^c + (a_3^x)^c X_c]^2 + [(a_1^z)^c + (a_3^z)^c Z_c]^2 \\ &\quad + [(a_2^z)^c + (a_3^z)^c X_c]^2, \\ (I_3^{2D})^c &= \{[(a_1^x)^c + (a_3^x)^c Z_c][(a_2^z)^c + (a_3^z)^c X_c] - [(a_2^x)^c + (a_3^x)^c X_c][(a_1^z)^c + (a_3^z)^c Z_c]\}^2, \end{aligned}$$

where

$$X_c = \frac{1}{n}\sum_{j=1}^n X_j, \qquad Z_c = \frac{1}{n}\sum_{j=1}^n Z_j, \tag{6.20}$$

and $(a_i^x)^c$ and $(a_i^z)^c$ are the value of a_i^x and a_i^z computed from the c^{th} choice of 4 markers. On the other hand when all 'n' markers are used to infer the deformation

then

$$\begin{aligned} I_1^{2D} &= (a_1^x + a_3^x Z_c)^2 + (a_2^x + a_3^x X_c)^2 + (a_1^z + a_3^z Z_c)^2 + (a_2^z + a_3^z X_c)^2, \\ I_3^{2D} &= \left[(a_1^x + a_3^x Z_c)(a_2^z + a_3^z X_c) - (a_2^x + a_3^x X_c)(a_1^z + a_3^z Z_c)\right]^2 . \end{aligned}$$

We record the above cases for their use later.

2. A study on the quality of approximation

Next, let us study in some detail the consequences of approximating the deformation (6.1) using a linear polynomial, (6.12). Let (R_o, Θ_1, Z_1), (R_o, Θ_2, Z_2), (R_o, Θ_3, Z_3) denote the cylindrical polar coordinates of three markers in the reference configuration and (r_o, θ_1, z_1), (r_o, θ_2, z_2), (r_o, θ_3, z_3) the cylindrical polar coordinates of the same markers in the current configuration. Now, (6.13) becomes

$$\begin{aligned} \begin{pmatrix} R_o\cos(\Theta_1) + x_o & Z_1 & 1 \\ R_o\cos(\Theta_2) + x_o & Z_2 & 1 \\ R_o\cos(\Theta_3) + x_o & Z_3 & 1 \end{pmatrix} \begin{Bmatrix} a_1^x \\ a_2^x \\ a_3^x \end{Bmatrix} &= \begin{Bmatrix} r_o\cos(\theta_1) + x_o \\ r_o\cos(\theta_2) + x_o \\ r_o\cos(\theta_3) + x_o \end{Bmatrix}, \\ \begin{pmatrix} R_o\cos(\Theta_1) + x_o & Z_1 & 1 \\ R_o\cos(\Theta_2) + x_o & Z_2 & 1 \\ R_o\cos(\Theta_3) + x_o & Z_3 & 1 \end{pmatrix} \begin{Bmatrix} a_1^z \\ a_2^z \\ a_3^z \end{Bmatrix} &= \begin{Bmatrix} z_1 \\ z_2 \\ z_3 \end{Bmatrix}, \end{aligned} \tag{6.21}$$

where $r_o = r(R_o)$, x_o shifts the origin from the axis of the annular cylinder to some point outside the cylinder, as it happens when local coordinates of the frame grabber board is used. Solving the above equations for a_i^x and a_i^z and using $\Theta = \theta$ and $z = \lambda Z$, we obtain $a_1^x = r_o/R_o$, $a_2^x = 0$, $a_3^x = (R_o - r_o)x_o/R_o$, $a_1^z = a_3^z = 0$ and $a_2^z = \lambda$. Thus, the value of the constants a_i^j are independent of the choice of the three markers

selected to compute them. Hence, the value of

$$I_1^{2D} = \left(\frac{r_o}{R_o}\right)^2 + \lambda^2 \qquad \text{and} \qquad I_3^{2D} = \left(\frac{r_o}{R_o}\lambda\right)^2, \tag{6.22}$$

are constant when inferred from tracking markers on the surface of the artery, assumed to be a right circular annular cylinder and the actual deformation is given by (6.1). In fact, if we assume that the material is incompressible we could obtain

$$I_1 = \lambda^2 + \left(\frac{r_o}{R_o}\right)^2 + \left(\frac{R_o}{\lambda r_o}\right)^2, \qquad I_2 = \frac{1}{\lambda^2} + \left(\frac{R_o}{r_o}\right)^2 + \left(\frac{\lambda r_o}{R_o}\right)^2, \qquad I_3 = 1, \tag{6.23}$$

where I_i's are the principal invariants of $\mathbf{C}$ in 3D. Thus, the proposed method for computing the deformation field and its gradient are robust at least when the actual deformation is as given by (6.1). Also, it is pertinent here to point out that the basis function corresponding to rigid body translation, $\{1\}$, allows shifting of the origin from the axis of the artery to that of the local coordinates on the frame grabber board. It is this constancy of the principal invariants that we propose to verify.

C. Experimental methods

1. Sample preparation

Hypertension was induced in a set of mature micro-mini pigs (Panapinto Micro Minipigs; Mansonville, CO) by controllable suprarenal aortic coarctation as described in detail in Fossum et al. [82]. Animal care in this study conformed to the guidelines of the University Laboratory Animal Care Committee, Texas A&M University. Briefly, a balloon occluder was placed around the suprarenal aorta proximal to the diaphragm by performing a thoracotomy. In addition telemetry units for measuring blood pressure and heart rate and vascular access ports for drawing blood samples were implanted. The occluder was then inflated over a period of two weeks to induce

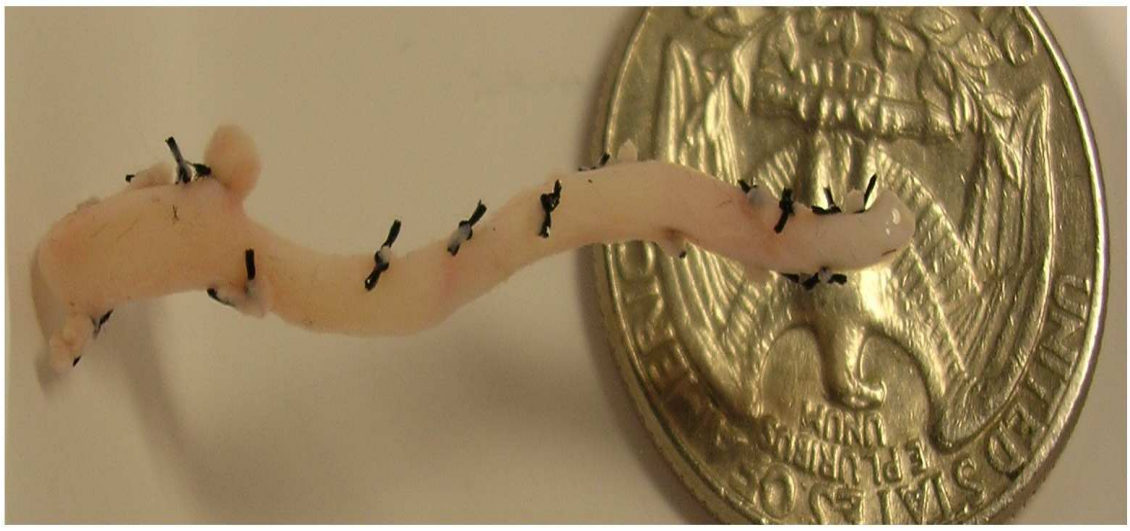

Fig. 47. A dissected circumflex coronary artery.

aortic coarctation and hence to gradually raise the mean proximal arterial blood pressure to 150 mm Hg or more. For another set of pigs, called the normotensive, while the occluder, telemetry units and vascular access ports was placed, hypertension was not induced, i.e., the occluder was not inflated. For the third set of pigs, called true control, no thoracotomy was performed but telemetry units and vascular access ports were implanted. Thus, the true control pigs are also normotensive. The pigs were euthanized 2, 4, 6 and 8 week post attainment of the targeted blood pressure. Their hearts were harvested and transported in ice-cold normal saline. Segments 2 to 4 cm in length of the circumflex artery from its origin at the left coronary artery were dissected (see figure 45c) and its side branches were ligated using 2-0 or 3-0 nylon braided sutures, depending on the size of the branches. Figure 47 shows a typical dissected circumflex artery. The excised circumflex artery is mounted on two stainless steel cannulae, with outer diameters nearly equalling the inner diameter of the circumflex artery, with care being exercised to ensure that the artery does not get

twisted. The length of the vessel is fixed so that the axial load increases with inflation on extending the artery by 10%. That is, the length of the vessel is within 10% of its length at which the axial load remains constant on inflation. Let this length of the artery be denoted by L_o. It should be pointed that in vivo length of the circumflex changes with the inflation and deflation of the heart and hence is not well defined. If the length of the artery were fixed at its no load value, the bending of the artery while inflation posed difficulty in tracking the markers. Then 100 μm diameter black spheres (Interactive Medical Technologies) made of polystyrene divinylbenzene were placed on the surface of the artery as shown in figure 45b using fine tipped forceps and glued (Permabond) using a glass micropipet (WPI PG52150-4) which is formed using a pipet puller (World Precision Instruments PUL-1) and by grinding it down to the desired diameter of 50 μm. The location chosen for placing markers is such that it is approximately at the center of the artery and as best possible not near the ligations. The artery is then placed in normal saline (154 mM $NaCl$) until activated.

2. Protocols

In this study we report the results of the experiments conducted from 2002 through 2004. In total we report the results from 43 different specimens. Table I gives the number of specimens tested in various categories. For the specimens tested from 2002 through 2003 the following protocols were performed on each of the specimen.

1. The location of the markers on the outer surface of the body, in a configuration free of radial component of the normal stress at the inner surface were recorded under quiescent conditions. This recording was used to obtain the reference configuration. Thus, this reference configuration is not free of traction on the boundary; there exists axial component of the normal stress at the of the artery.

Table I. Specimen statistics: HT-hypertensive, NT-normotensive, P-number of specimens tested in passive state, A-number of specimens tested in activated state, N-number of specimens tested in native state.

Duration of HT	HT/NT	P	A	N
2 week	HT	4	2	4
	NT	6	1	0
4 week	HT	6	6	6
	NT	4	1	0
6 week	HT	4	4	4
	NT	2	1	1
8 week	HT	4	3	3
	NT	3	3	3

We call this the native reference configuration and the invariants, I_1^{2D} and I_3^{2D}, are computed using this as the reference configuration unless otherwise stated.

2. The body was translated manually along the x direction using the actuators in the precision x-y-z stage and the motion of the markers were tracked. This protocol was performed to get an estimate of the error in the video tracking system.

3. The microscope was translated vertically using a motorized actuator, described before and the motion of the markers tracked. This protocol was performed to get an estimate of the error in the video tracking system due to changing focus.

4. The artery was inflated cyclically for 5 cycles at constant length in a normal saline bath (154 mM $NaCl$). We call this the response of the artery in its native

state i.e., the state in which it is isolated from natural or artificial hormonal and neural stimuli.

5. Then, in 21 of the cases, the artery was activated, i.e., the smooth muscle cells were made to contract, by changing the solution in which the artery is perfused from normal saline to a solution high in KCl, called the active solution which contains 22.5 mM $NaHCO_3$, 1.2 mM NaH_2PO_4, 2.4 mM Na_2SO_4, 1.2 mM $MgSO_4.7H_2O$, 21 mM $NaCl$, 100 mM KCl, 2.5 mM $CaCl_2$, 5.6 mM Dextrose. The active solution is bubbled continuously with oxygen (95% O_2 and 5% CO_2) and maintained at a constant temperature of 37 degrees Celsius. The artery is perfused with this solution for one hour and during the same time a constant pressure[6] of 70 mm Hg is applied at the inner surface of the artery.

6. At the end of one hour period, the smooth muscles are assumed to have contracted the maximum possible under the given conditions and the following protocols were performed in the same order for all the specimens:

   (a) Cyclic inflation from 0 to 120 mm Hg (or up to 150 mm Hg when possible) at constant length, L_o by infusing the active solution at the rate of 15 $\mu l/sec$.

   (b) The location of the markers in the body free of radial component of the normal stress at the inner surface were recorded under quiescent conditions. As before, this recording is used to obtain a reference configuration called the active reference configuration.

   (c) Cyclic inflation from 0 to 120 mm Hg (or up to 150 mm Hg when possible) at constant length, $1.1L_o$ by infusing the active solution at the rate of 15

[6]By pressure we mean the radial component of the normal stress.

$\mu l/sec$.

(d) Cyclic stretching at the rate of 24 $\mu m/sec$ from L_o to $1.1L_o$ at a constant pressure of 60 mm Hg at the inner surface of the artery.

In all the above cases, the artery was subjected to 5 cycles of loading and unloading and during all the 5 cycles the 2D location of the markers, the pressure and axial load were recorded. All the above protocols were performed within 1 hour of activation and the artery was immersed in the circulating active solution during the entire period of mechanical testing with the solution still being perfused with oxygen and maintained at 37 degree Celsius.

7. After testing the artery in active solution, the solution was drained and the system washed using normal saline. Then, the artery was perfused with passive solution: containing 116.5 mM $NaCl$, 22.5 mM Na_2HCO_3, 1.2 mM NaH_2PO_4, 2.4 mM Na_2SO_4, 4.5 mM KCl, 1.2 mM $MgSO_4$, 1.5 mM $CaCl_2$ and 5.6 mM dextrose and the solution was oxygenated for 20 minutes but its temperature was not controlled. The artery was allowed to equilibrate in the passive solution for 1 hour with a pressure of 70 mm Hg being applied at the inner surface of the artery.

8. After equilibrating for one hour, the smooth muscle cells are presumed to be relaxed the maximum possible under the given conditions and the following mechanical tests were performed in the same order on all the specimens

   (a) The location of the markers in the body free of radial component of the normal stress at the inner surface were recorded under quiescent conditions. As before, we call this the passive reference configuration.

   (b) Cyclic inflation from 0 to 120 mm Hg (or up to 150 mm Hg when possible)

at constant length, L_o by infusing the passive solution at the rate of 15 $\mu l/sec$.

(c) Cyclic inflation from 0 to 120 mm Hg (or up to 150 mm Hg when possible) at constant length, $1.1L_o$ by infusing the passive solution at the rate of 15 $\mu l/sec$.

(d) Cyclic stretching at the rate of 24 $\mu m/sec$ from L_o to $1.1L_o$ at a constant pressure of 60 mm Hg.

In all the above cases the artery was subjected to 5 cycles of loading and unloading and during all the 5 cycles the 2D location of the markers, the pressure and axial load were recorded. All the above protocols were performed within 1 hour of passivation and during this period the artery was just immersed in the passive solution; the solution was not perfused with oxygen nor its temperature maintained at 37 degree Celsius.

9. Then on some specimens, one end was held fixed the other end was rotated so that the twist per unit length, Ω is 1 degree/mm and the artery was cyclically inflated for 5 cycles from 0 to 120 mm Hg holding the length constant at $1.1L_o$ by infusing passive solution at the rate of 15 $\mu L/sec$. This was followed by recording the configuration of the markers in which the body is free of radial component of the normal stress at the inner surface but was extended and twisted. We call this the twisted reference configuration.

10. Finally, the artery was fixed in formalin for histological studies and obtaining geometrical information.

All the mechanical tests were completed within eight hours of harvesting the heart.

For specimens tested in 2004 only protocols 8a to 8c were performed for reasons discussed in section F.

3. Uncertainty analysis

Any experimental measurement has some error associated with it and efforts have to be made to examine if the error can be estimated. Towards this, we first consider the video system. Here we start with examining the error associated with determining the location of the centroid of each marker. That is, the determined location of marker will usually be within only certain number of pixels of the actual location thereby inducing an error. Further, the location of the marker while tracking them can change only discretely, as opposed to continuous variation in reality. In order to get an estimate of these errors, three protocols elaborated above are used.

In the first case, repeated recording of a static configuration of the markers, as done while recording the reference configuration is used. As always, we take the mean of all the repeated recordings of the location of the marker to compute their location in the reference configuration. Now, for the location of the markers in the current configuration, we use the same readings obtained while recording the static configuration of the markers. Hence, ideally $(I_1^{2D})^c = 2$ and $(I_3^{2D})^c = 1$ and any deviation from this value signifies the error in their measurement. The deviation occurs because the centroid of the markers are determined with an accuracy of $\pm a$ pixels only and hence the inferred location of a static configuration of markers is not constant. A representative plot of these errors is shown in figure 48 when the deformation is approximated by a linear polynomial (6.12) which is determined using three markers, as discussed before. This error is sensitive to number of readings, 'b', over which the averaged location of the markers is computed in the current configuration, the polynomial used to approximate the deformation, and the particular selection of the markers. This

error decreases as the number of readings over which the marker location is averaged increases. This error, in the present case, also decreases as the area subtended by the markers used to estimate it increases. However, as the area subtended by the markers increases, the quality of the approximation of the deformation and its gradient by linear polynomial decreases when the actual deformation is not a linear polynomial. Hence, a balance has to be maintained.

In the second case, the protocol 1, repeated recording of a static configuration of the markers is used to find the location of the markers in the reference configuration and the protocol 2, in which the markers were translated as a rigid body along the x direction is used for the location of the markers in the current configuration and the invariants computed for this case. As before ideally, $(I_1^{2D})^c = 2$, $(I_3^{2D})^c = 1$. A representative plot of these errors is shown in figure 49 when the deformation is approximated by a linear polynomial, (6.12) which is determined using three markers and when the markers are manually translated by 300 pixels along the x direction in 18 seconds[7]. This error is also sensitive to the number of readings over which the averaged location of the markers is computed and the particular selection of the markers. From this study, it was concluded that averaging over 10 readings of the marker location was preferred.

Finally, the protocol three is used to obtain the error introduced due to changing focus. In this case, the reference configuration of the markers is inferred from the recordings in the protocol-1 and the current configuration of the markers is inferred from the recordings in the protocol-3 and the invariants computed as before. Again, ideally $(I_1^{2D})^c = 2$ and $(I_3^{2D})^c = 1$. A representative plot of these errors is shown in figure 50 when the deformation is approximated by a linear polynomial which is

[7]Typically, while inflating the artery the markers translate 300 pixels along the x direction in 32 seconds

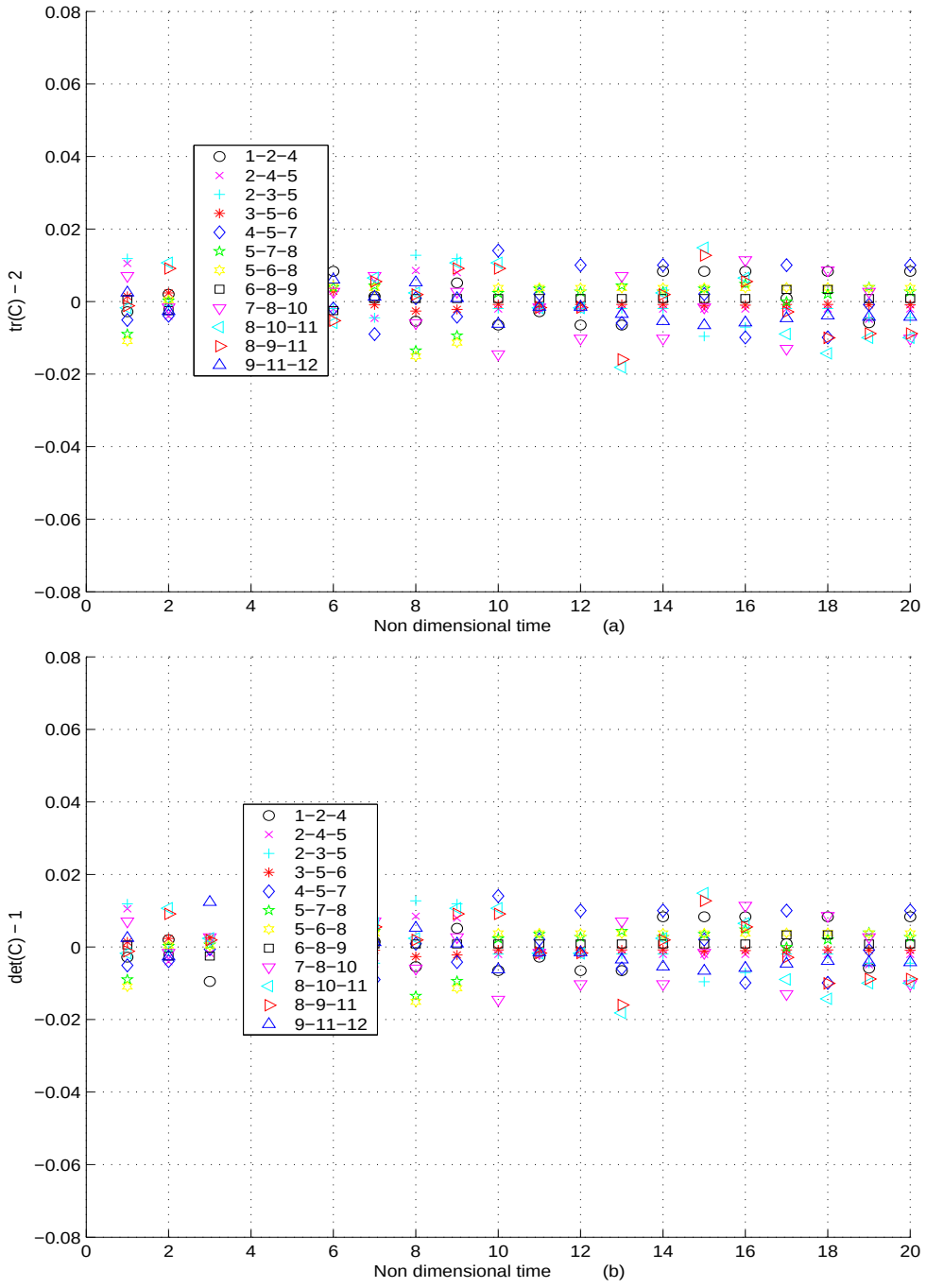

Fig. 48. Plot of (a) $(I_1^{2D})^c - 2$ (b) $(I_3^{2D})^c - 1$ under quiescent conditions.

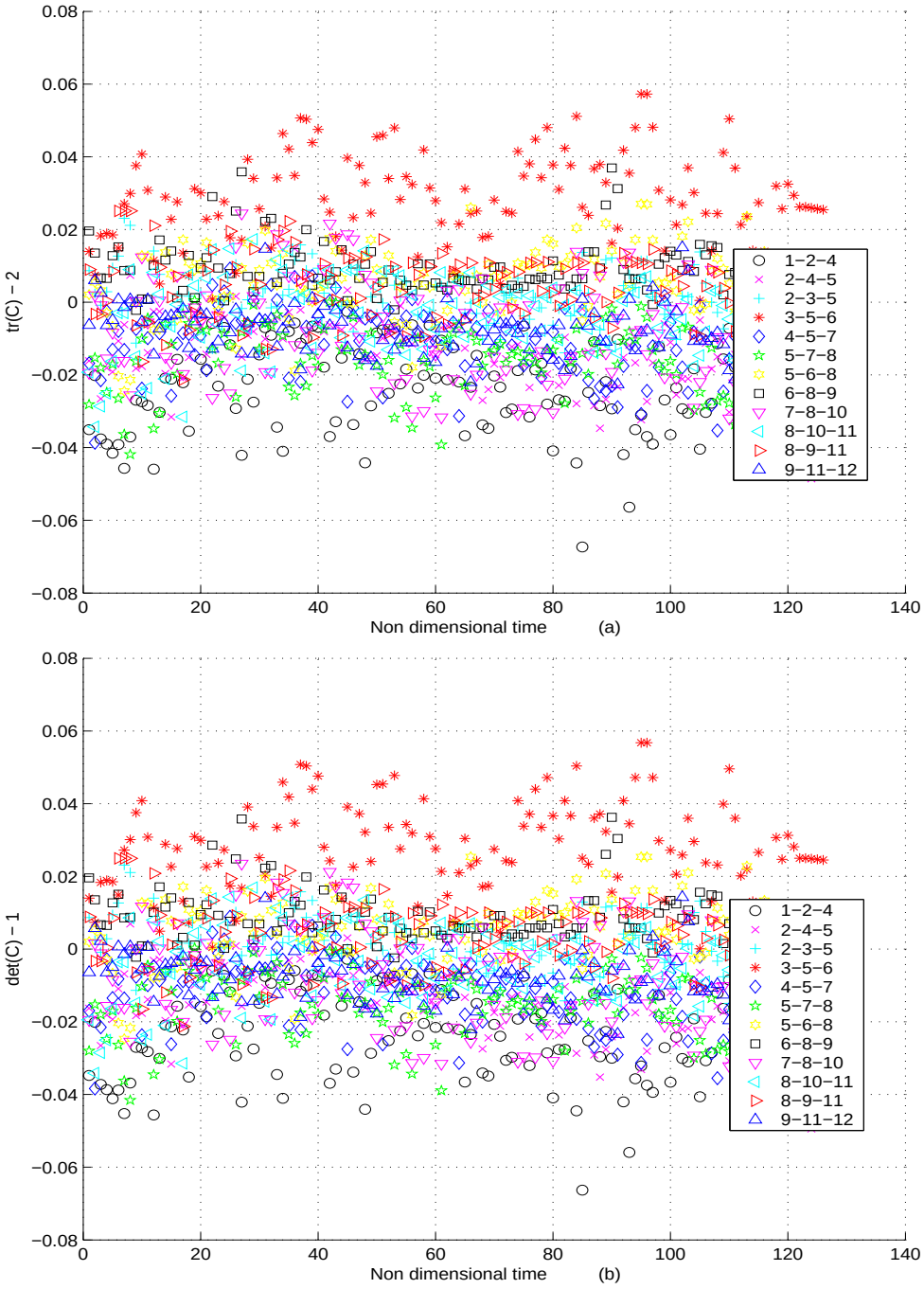

Fig. 49. Plot of (a) $(I_1^{2D})^c - 2$ (b) $(I_3^{2D})^c - 1$ while translating the artery along the x direction as a rigid body.

determined using three markers and when the microscope is translated by ± 1250 μm. This error is sensitive to the same variables described above and changes in the same manner. From these studies it was concluded that the error in the estimated invariants is ± 0.05.

Next, we examine the gross error associated with 2D tracking of the markers. First, we note that the markers placed on the surface of the artery do not lie on a plane. Further, as the artery deforms, if the deformation is not of the form (6.1) significant errors are introduced due to out-of-plane motion of the markers. To get an estimate of the error, a numerical stimulation was performed. The artery was given a rigid body rotation about its axis, i.e., the artery was assumed to deform as

$$r = R, \qquad \theta = \beta + \Theta, \qquad z = Z, \tag{6.24}$$

and the value of the invariants computed theoretically under the assumption that the markers were tracked in 2D using (6.21). The results are plotted in figure 51. We find that the value of the invariants are far off from their expected values, $(I_1^{2D})^c = 2$ and $(I_3^{2D})^c = 1$. Thus, while this experimental set up is ideal to test if the artery deforms as given by (6.1), caution has to be exercised on interpreting the data when the deformation differs.

Next, we turn our focus to errors that are more difficult to quantify. While mounting the artery, inadvertently, some twist could be introduced and the effect of this on the deformation of the artery while inflating requires quantification. Towards this, holding one end fixed, the other end of the artery was rotated manually so that the twist per unit length, Ω is approximately 1 deg/mm and then the response of the artery to inflation is studied. Figures 52 and 53 plot $(I_1^{2D})^c$ and $(I_3^{2D})^c$ respectively for combined inflation at a fixed extension and twist of the artery when the passive reference configuration is used. In the same figures the response of the artery when

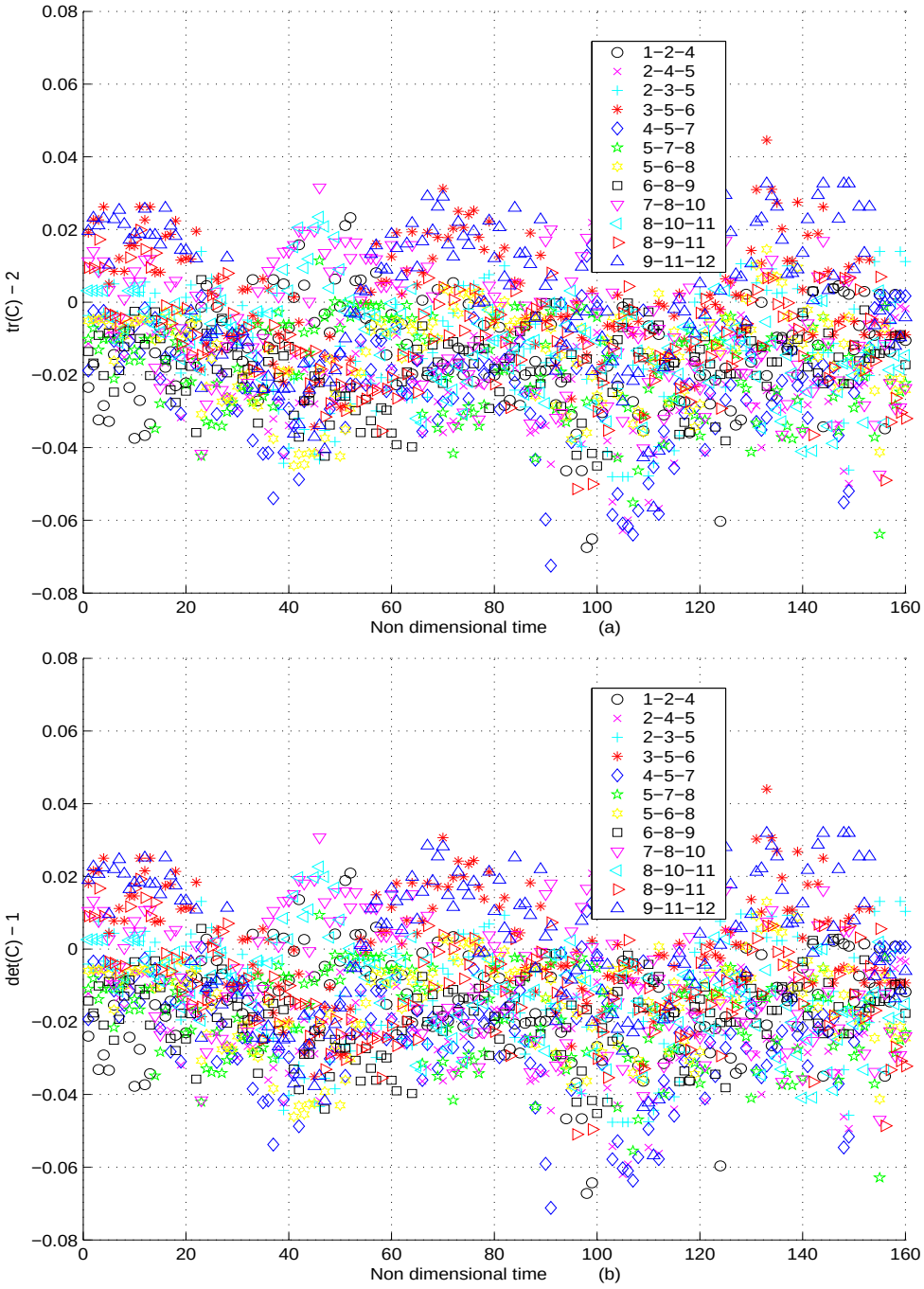

Fig. 50. Plot of (a) $(I_1^{2D})^c - 2$ (b) $(I_3^{2D})^c - 1$ while changing the focus of the microscope.

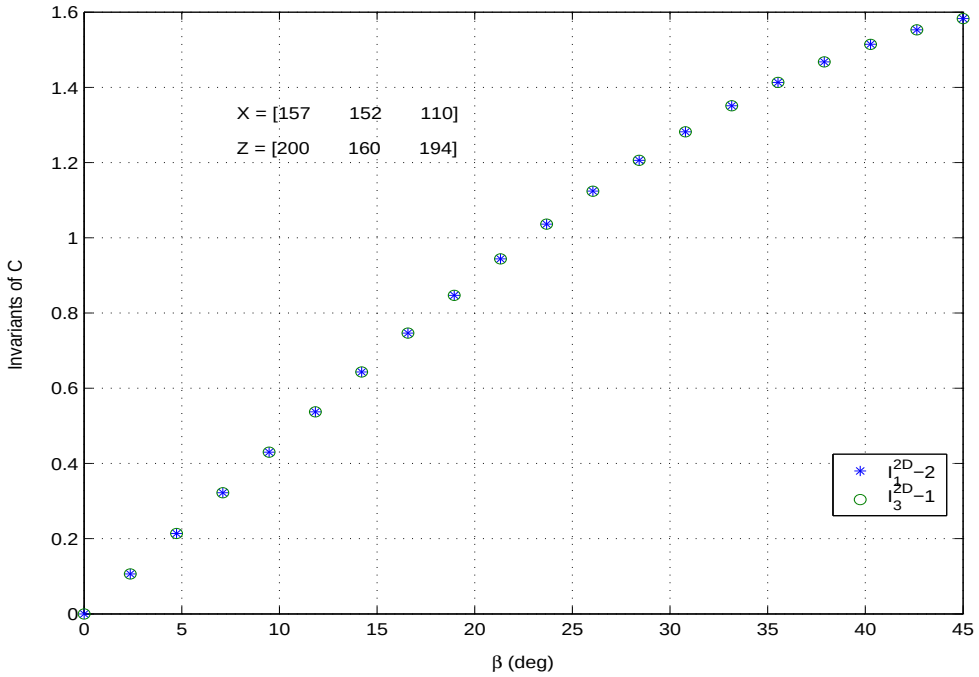

Fig. 51. Theoretically computed plot of $I_1^{2D} - 2$ and $I_3^{2D} - 1$ when the deformation of the artery is given by (6.24) for various values of β.

there is no twist is presented for comparison. The presence of twist not only increases the value of the invariants for a given radial component of the normal stress at the inner surface, as it should, but also the variation is larger when evaluated at different locations on the surface of the artery. This dependence of the invariants on the location on the outer surface at which they are evaluated is expected because twisting causes out of plane deformation of the markers which the 2D tracking system is unable to capture correctly. Figure 54 computes the invariants when the artery is inflated by applying a radial component of the normal stress at its inner surface from the twisted reference configuration. In other words, the only difference between figure 54 and figures 52b and 53b is the reference configuration used to compute the value of the invariants. This is the scenario when the artery is mounted incorrectly, i.e.,

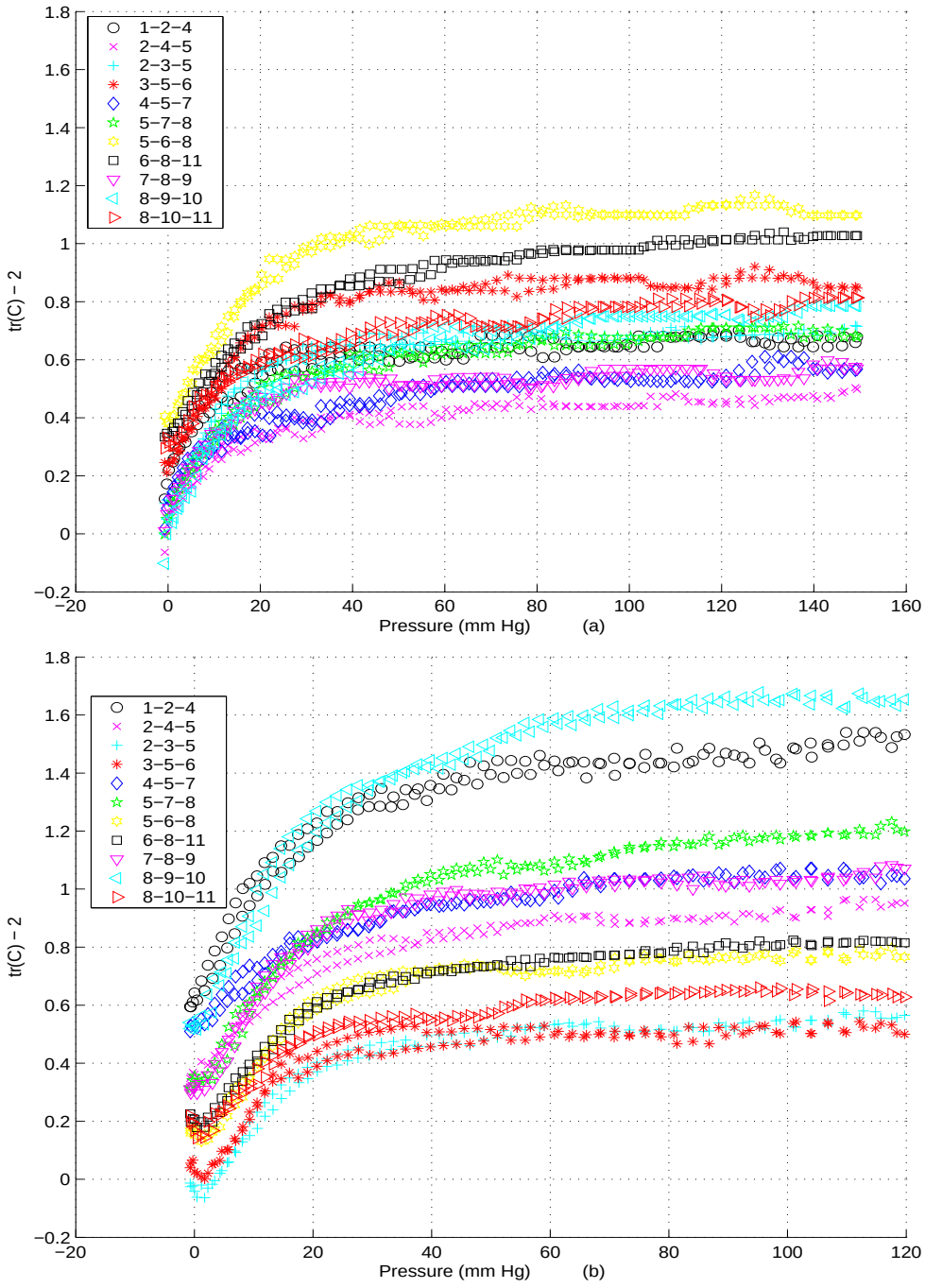

Fig. 52. Plot of $(I_1^{2D})^c - 2$ when $\lambda = 1.1$ (a) $\Omega = 0$ (b) $\Omega = 1 deg/mm$ and inflating the artery by applying a radial component of the normal stress at the inner surface.

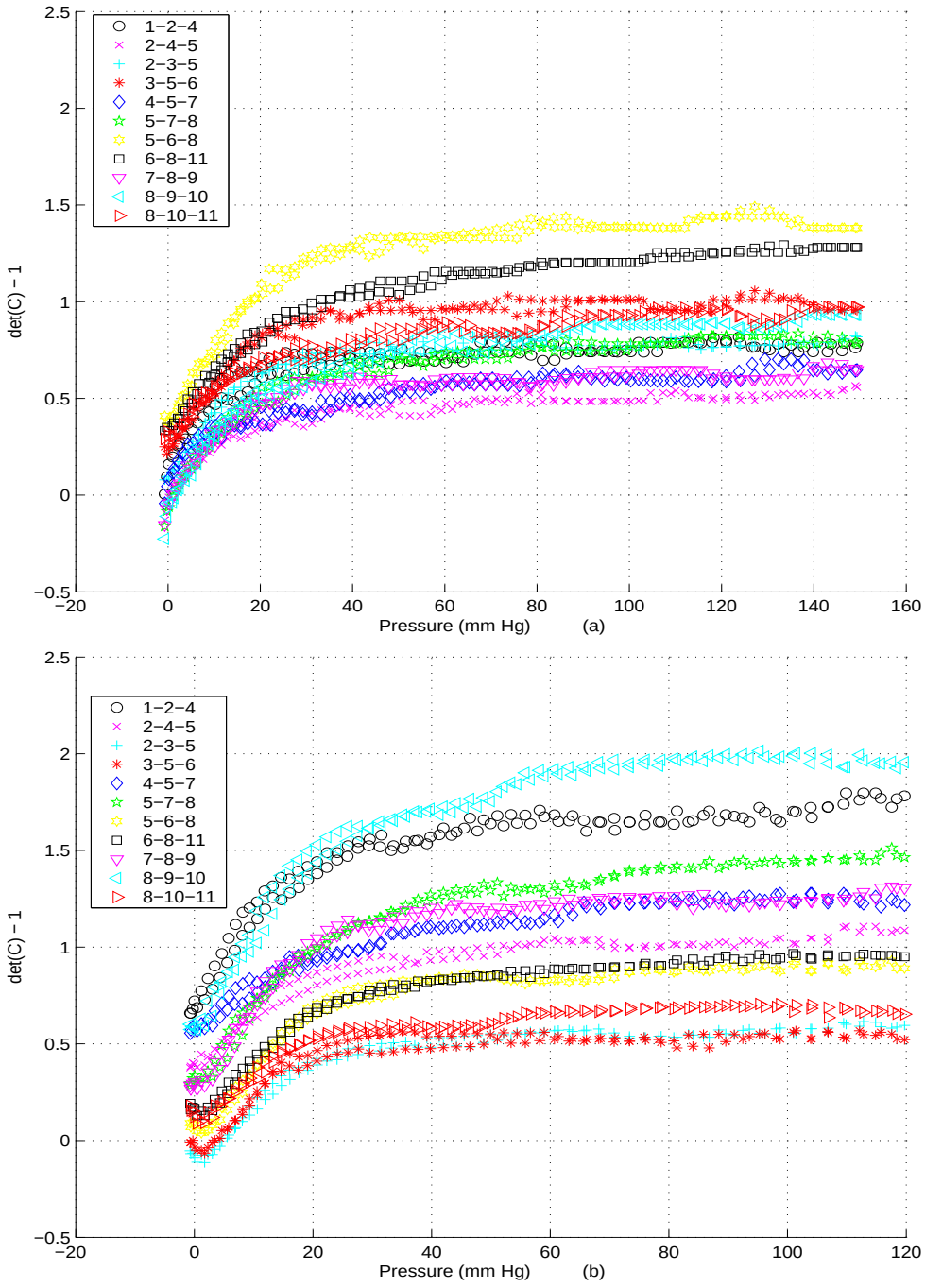

Fig. 53. Plot of $(I_3^{2D})^c - 1$ when $\lambda = 1.1$ (a) $\Omega = 0$ (b) $\Omega = 1 deg/mm$ and inflating the artery by applying a radial component of the normal stress at the inner surface.

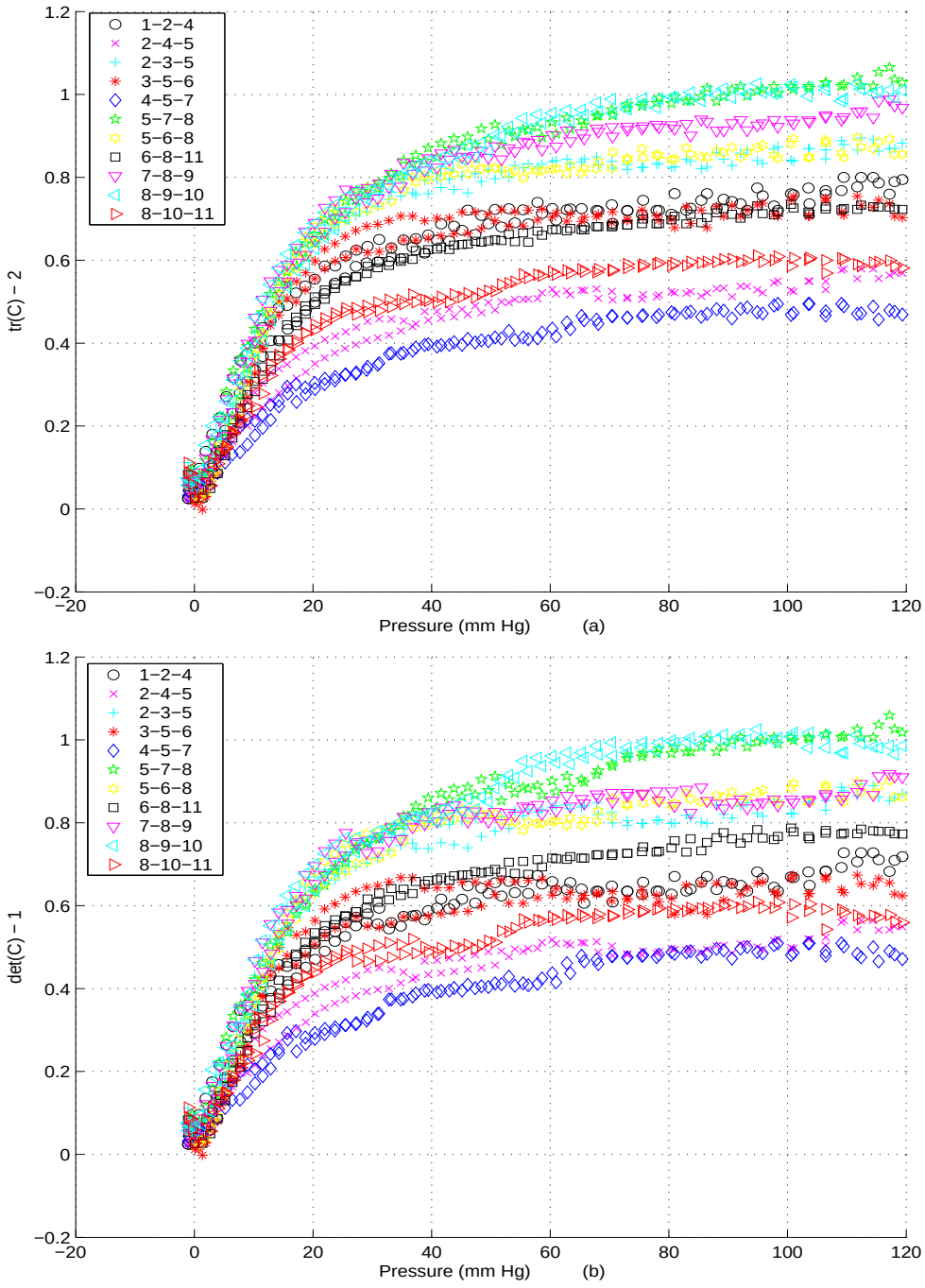

Fig. 54. Plot of (a) $(I_1^{2D})^c - 2$ (b) $(I_3^{2D})^c - 1$ when $\lambda = 1$, $\Omega = 1 deg/mm$ and inflating the artery by applying a radial component of the normal stress at the inner surface.

with a twist. Comparing figure 54 with figures 52a and 53a we find that while the magnitude of the invariants are comparable when accounted for the axial extension, their variation with the choice of the markers is different for lower pressures. This is because in the later case the invariants are constrained to be $(I_1^{2D})^c = 2$ and $(I_3^{2D})^c = 1$ when the pressure is 0.

Next, we explore the quality of approximation of the invariants by linear deformation, (6.12). Towards this, we approximate a given deformation of the artery using different approaches and study the result. Figure 55 plots a representative result of one such study. In the first case, we approximate the deformation by (6.12) and use the c^{th} selection of three markers to compute the invariants, $(I_p^{2D})^c$. We repeat this for various choices of three markers[8] and plot the mean of $(I_p^{2D})^c$ and denote this curve as '3mhomog'. In the second case, we still use (6.12) to approximate the deformation but now use all the 'n' available markers to find I_p^{2D} as described in section B and call this curve 'nmhomog'. For the next case, we approximate the deformation by (6.19) and use the c^{th} selection of four markers to compute $(I_p^{2D})^c$. We repeat this for various choices of four markers, selected such that the area subtended by the quadrilateral formed with these four markers as their vertices does not overlap and plot the mean of $(I_p^{2D})^c$ computed at the centroid of all the markers and denote this curve as '4mbilin'. Finally, we again use (6.19) to approximate the deformation but now use all the 'n' markers to estimate the invariants and denote this estimate as 'nmbilin'. It can be seen from figure 55 that these various methods of approximating the invariants results in nearly the same result.

Finally, gluing of the markers onto the surface of the artery introduces some error in the measured deformation. The motion of the markers would also be influenced

[8]Here we choose the three markers such that the area subtended by the triangle formed with these three markers as their vertices does not overlap.

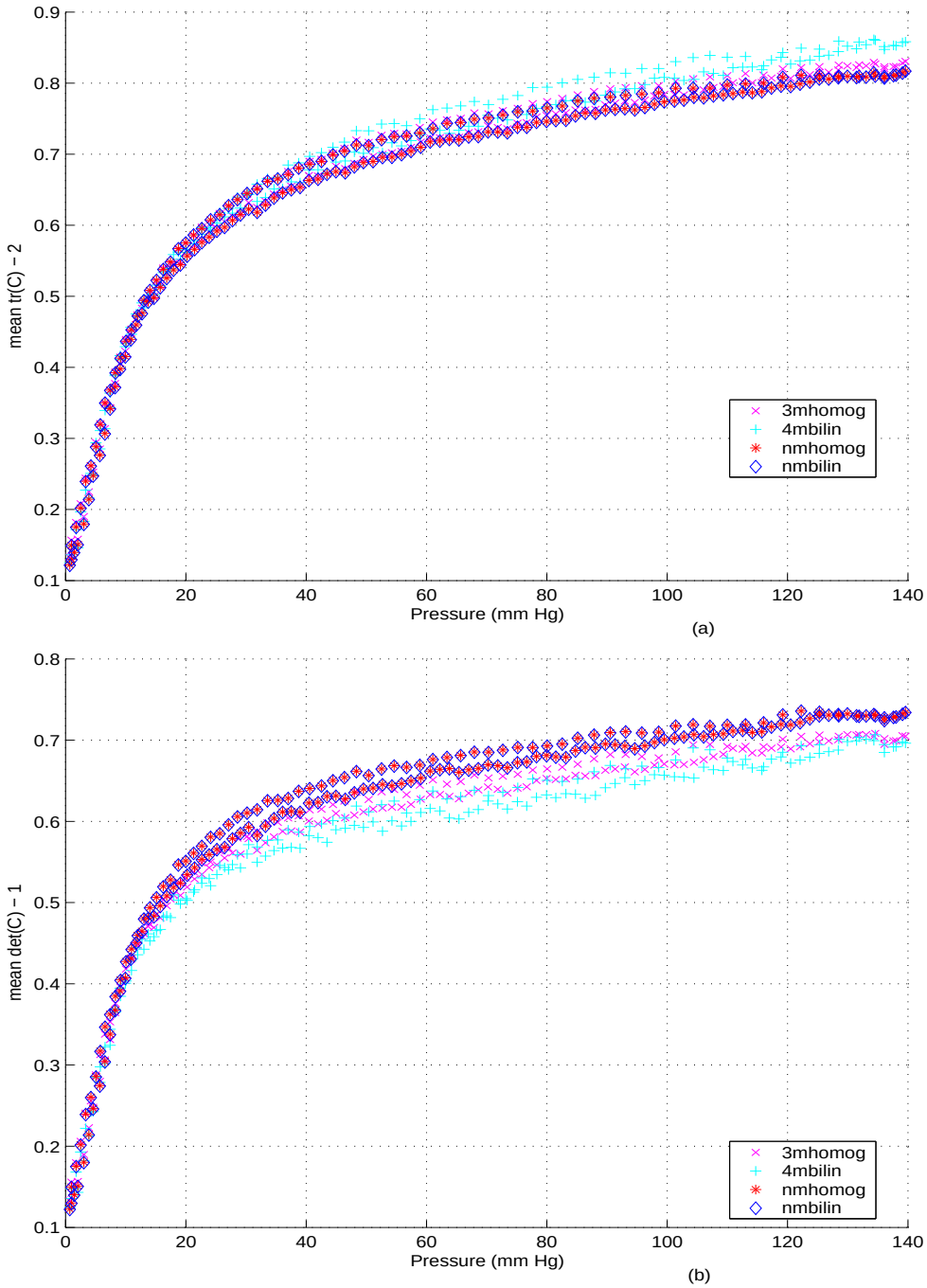

Fig. 55. Plot of (a) $I_1^{2D} - 2$ (b) $I_3^{2D} - 1$ computed for various approximation of the deformation of a 8 week NT circumflex artery in native state inflated at constant length, L_o.

by the ligations of the side branches. Because of their inherent difficulty, these errors could not be quantified here. However, these can be viewed as perturbations that is necessary with the experimental measurement of any quantity.

D. Results

Figures 56 through 65 plot typical pressure versus invariants computed from the native reference configuration for various cases corresponding to the 4^{th} cycle of loading and unloading. Figures 56 to 60 correspond to data from the same 4 week hypertensive specimen and figures 61 to 65 from the same 8 week normotensive specimen. In all these figures the invariants are computed from native reference configuration assuming that the deformation is given by (6.12) for various sets of three markers. Contrary to the expectation, we see from the figures that the invariants seem to vary spatially. The spatial variation of the invariants is far more than that can be accounted by the error in the location of their centroid which was estimated to cause a deviation of ± 0.05 in the value of the invariants. Hence, the deformation of the artery subjected to inflation at constant length is not given by (6.1). In fact, during the experiments one can observe bending and twisting of the artery when inflated holding the length constant. Since this results in the out-of-plane deformation of the markers, the other results herein have to be viewed with caution.

In spite of the above observation, the following remarks can be made from studying these figures. Comparing figures 56 through 60 with figures 61 through 65 the marked difference in the deformation, reflected by how the invariants vary with the choice of the markers, is obvious. In fact, the variation of the invariants with the choice of the markers seem to have some correlation with the set to which the specimen belongs. The standard deviation of $(I_p^{2D})^c$ or range of $(I_p^{2D})^c$ quantifies this. Here

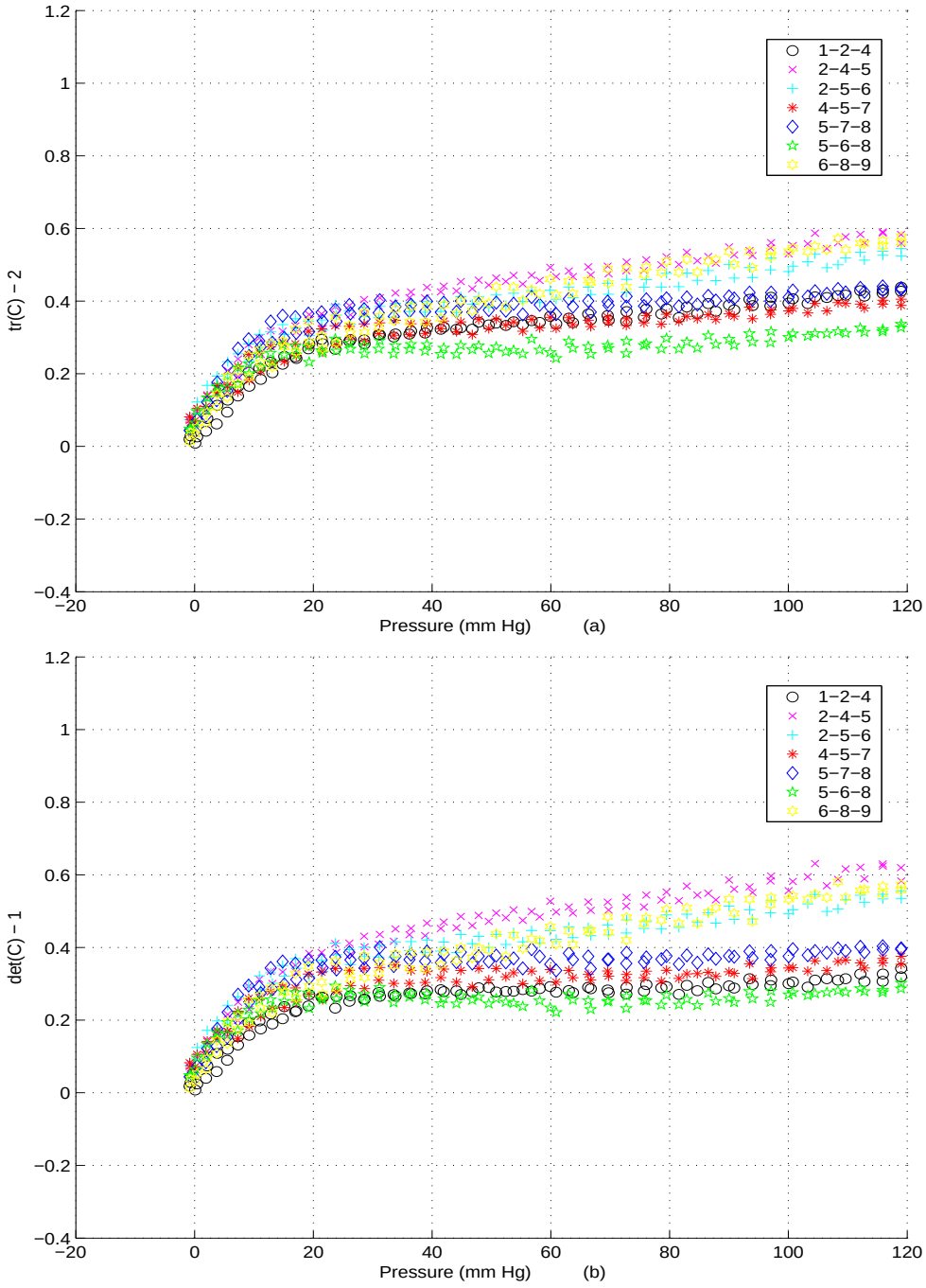

Fig. 56. Plot of (a) $(I_1^{2D})^c - 2$ (b) $(I_3^{2D})^c - 1$ computed for various marker sets while inflating the circumflex artery from 4 week HT pig, in the native state at constant length, L_o.

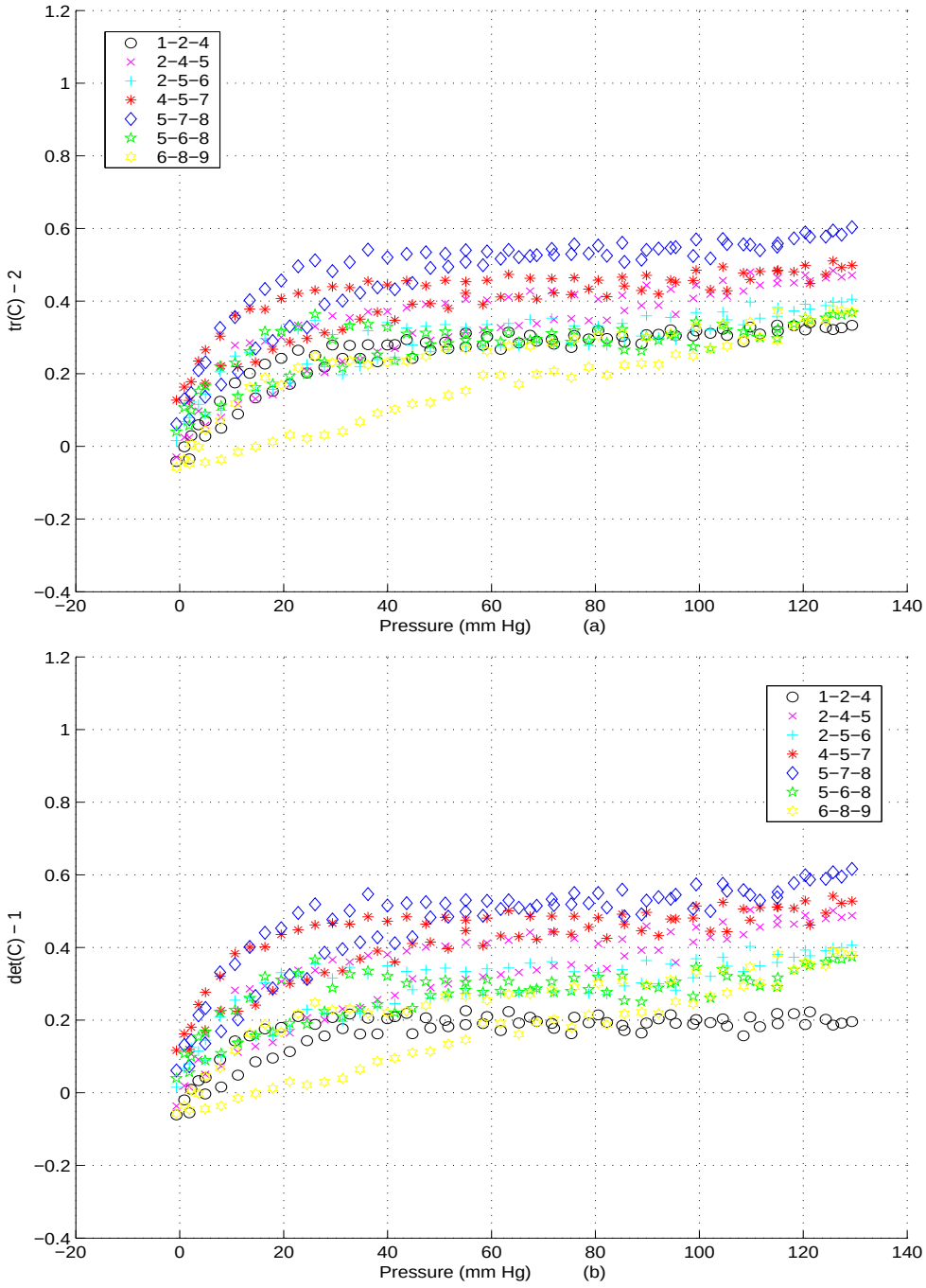

Fig. 57. Plot of (a) $(I_1^{2D})^c - 2$ (b) $(I_3^{2D})^c - 1$ computed for various marker sets while inflating the circumflex artery from 4 week HT pig, in the active state at constant length, L_o.

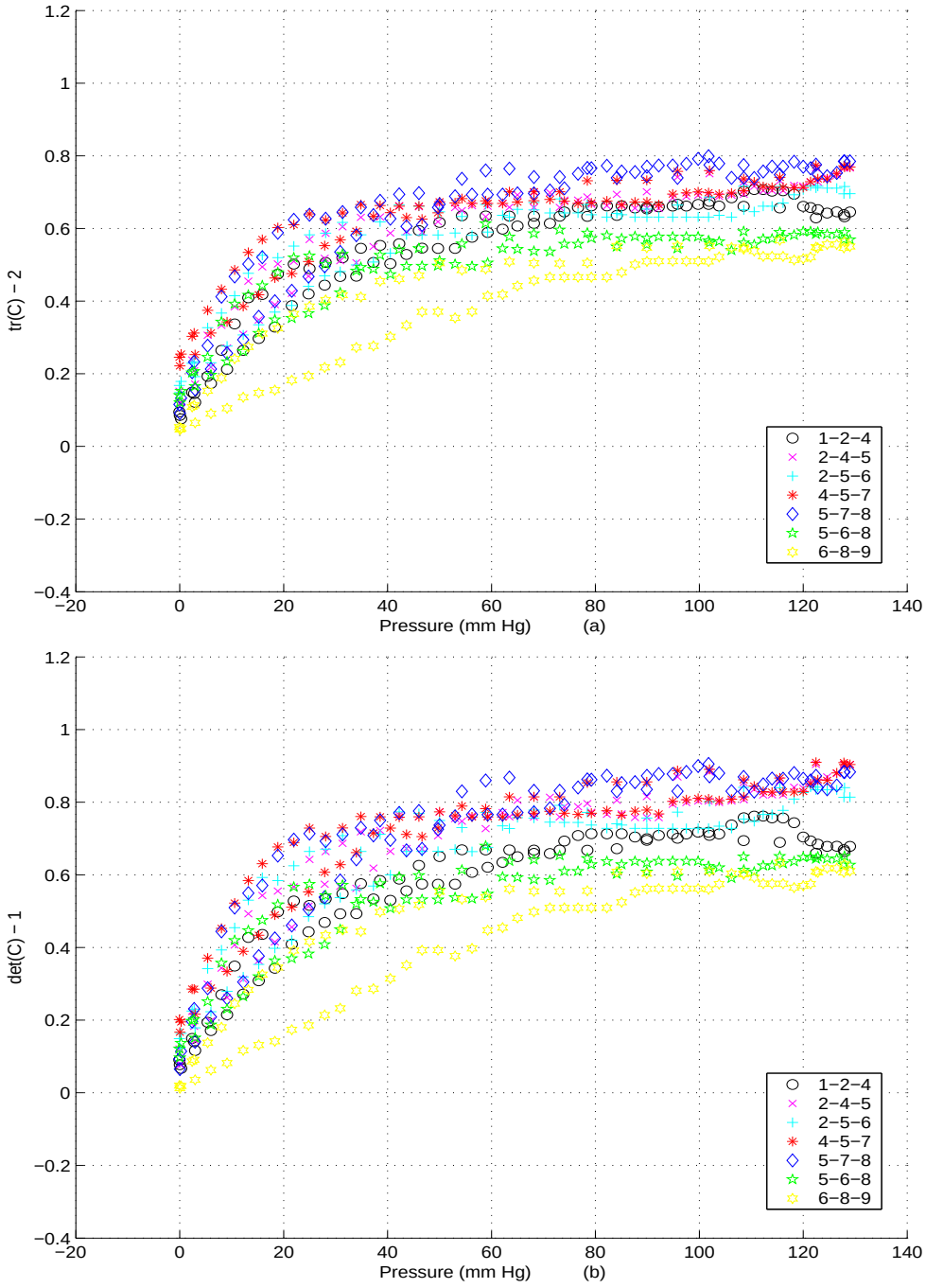

Fig. 58. Plot of (a) $(I_1^{2D})^c - 2$ (b) $(I_3^{2D})^c - 1$ computed for various marker sets while inflating the circumflex artery from 4 week HT pig, in the active state at constant length, $1.1L_o$.

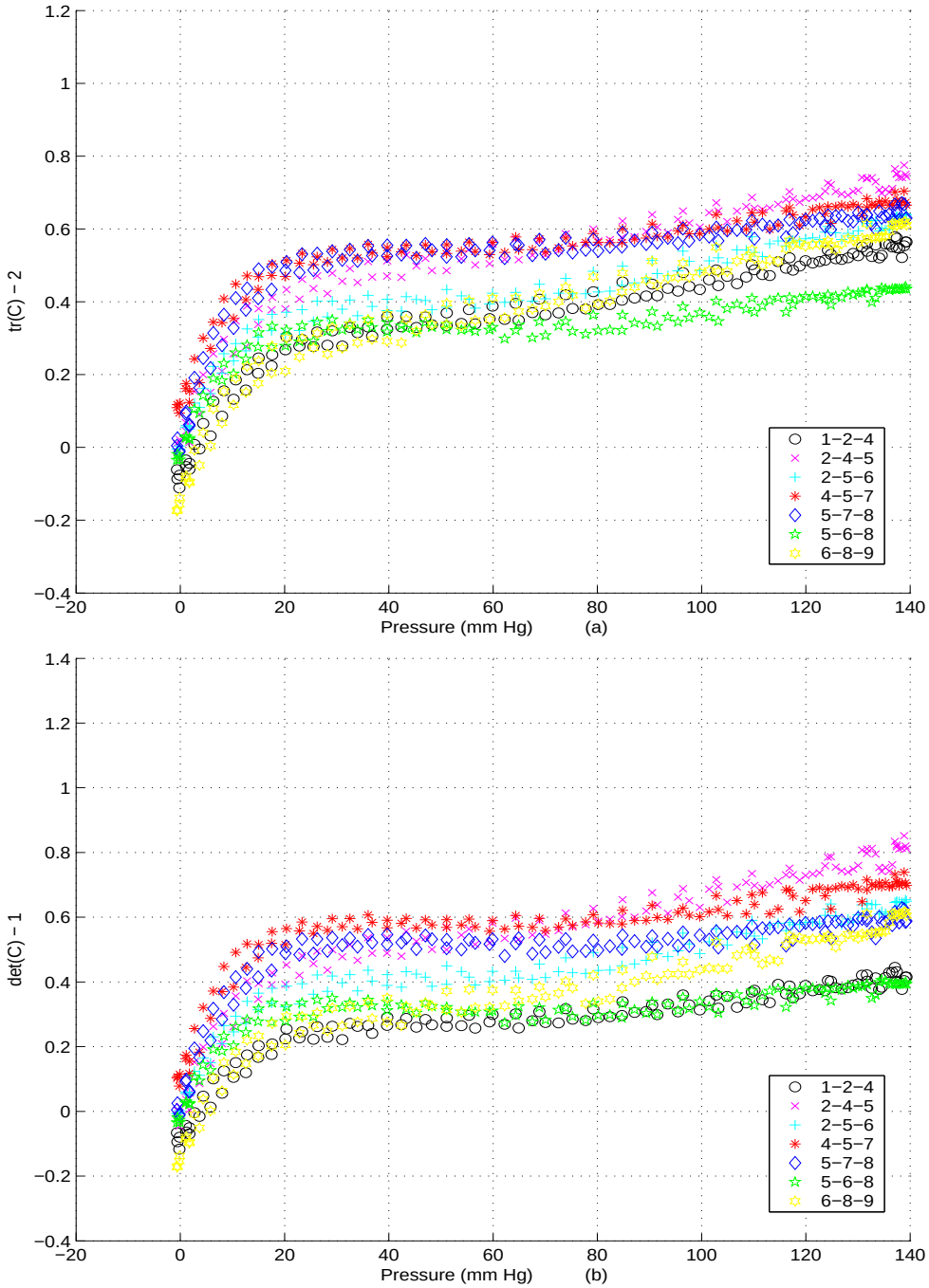

Fig. 59. Plot of (a) $(I_1^{2D})^c - 2$ (b) $(I_3^{2D})^c - 1$ computed for various marker sets while inflating the circumflex artery from 4 week HT pig, in the passive state at constant length, L_o.

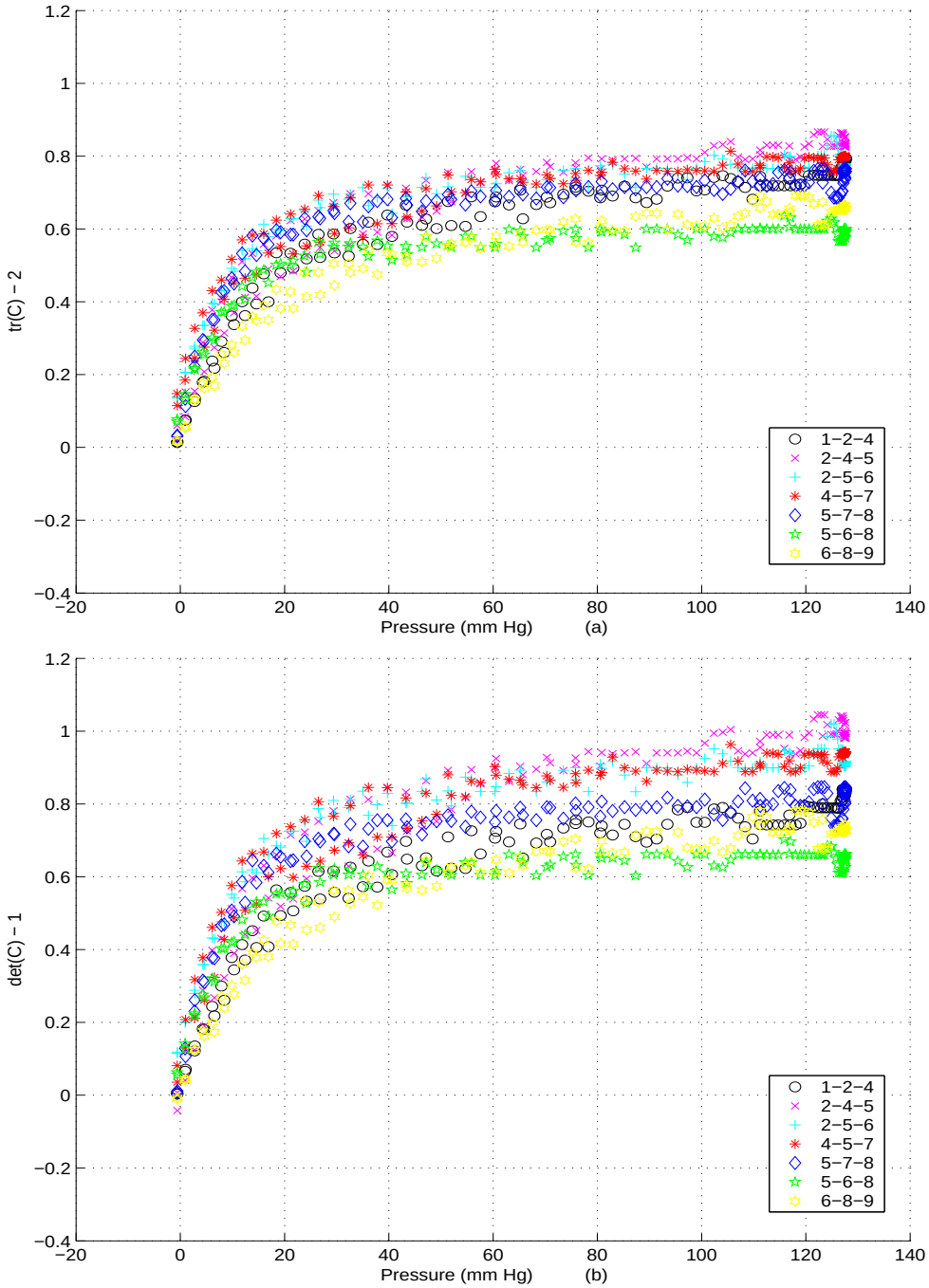

Fig. 60. Plot of (a) $(I_1^{2D})^c - 2$ (b) $(I_3^{2D})^c - 1$ computed for various marker sets while inflating the circumflex artery from 4 week HT pig, in the passive state at constant length, $1.1L_o$.

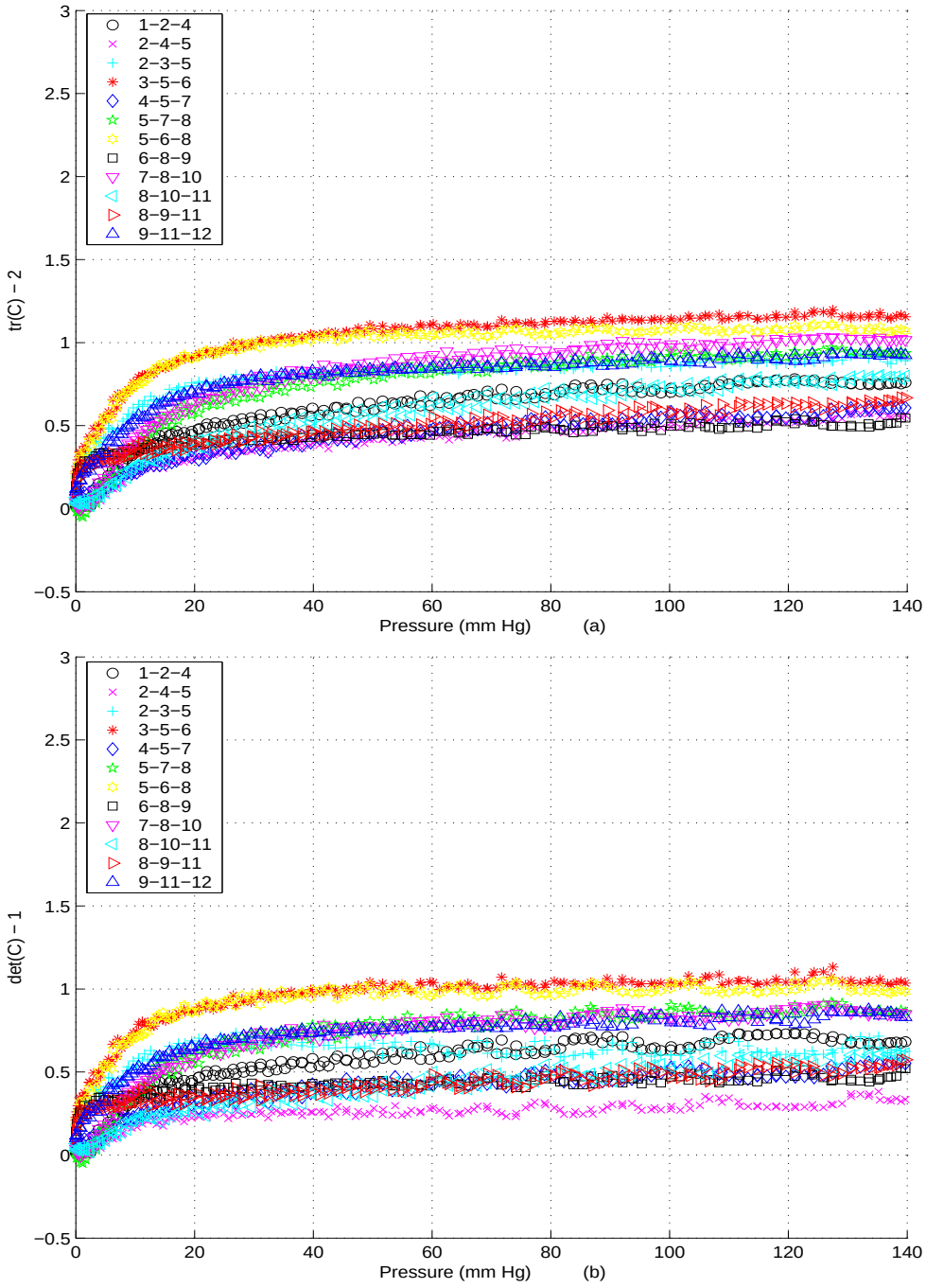

Fig. 61. Plot of (a) $(I_1^{2D})^c - 2$ (b) $(I_3^{2D})^c - 1$ computed for various marker sets while inflating the circumflex artery from 8 week NT pig, in the native state at constant length, L_o.

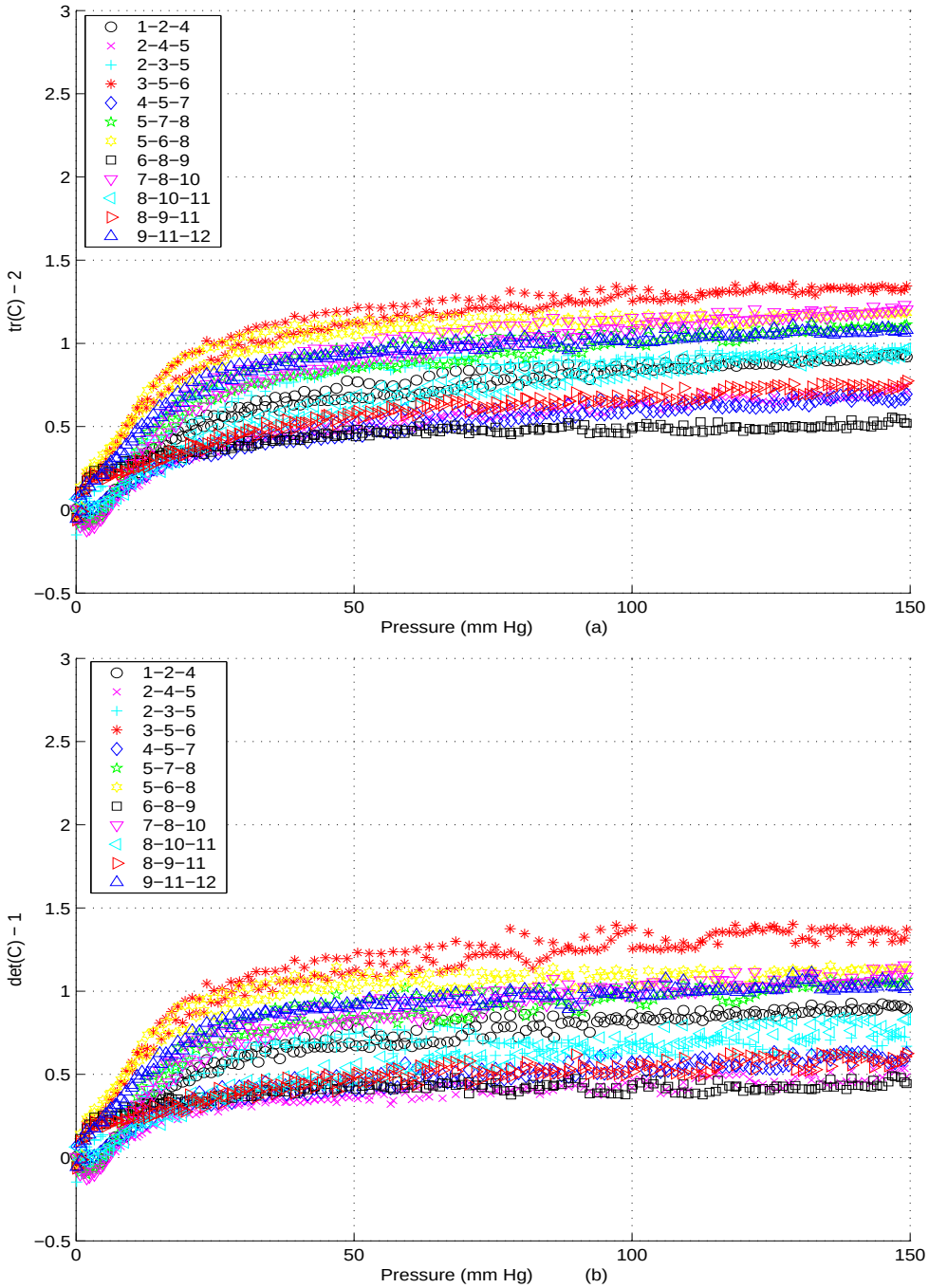

Fig. 62. Plot of (a) $(I_1^{2D})^c - 2$ (b) $(I_3^{2D})^c - 1$ computed for various marker sets while inflating the circumflex artery from 8 week NT pig, in the active state at constant length, L_o.

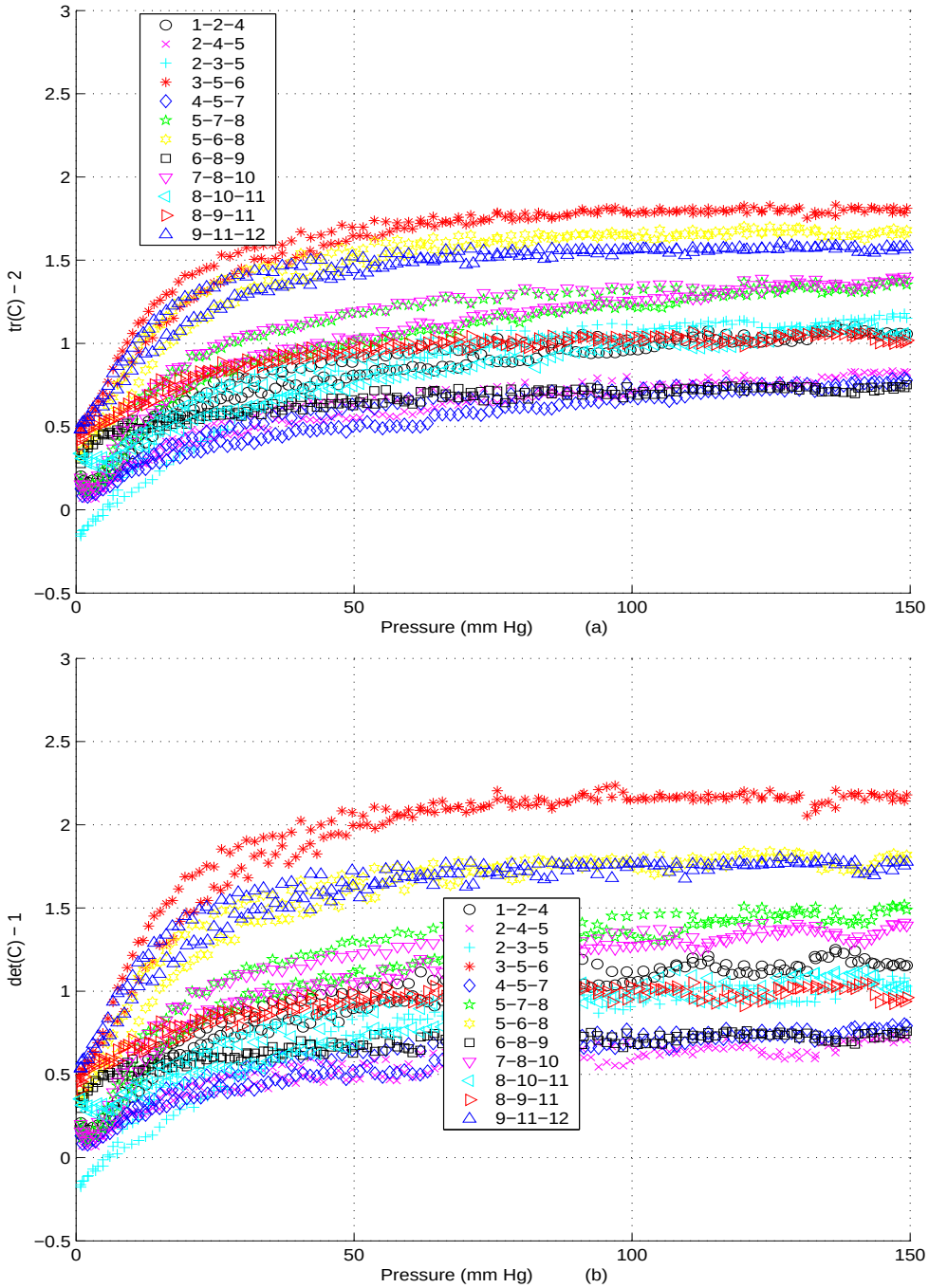

Fig. 63. Plot of (a) $(I_1^{2D})^c - 2$ (b) $(I_3^{2D})^c - 1$ computed for various marker sets while inflating the circumflex artery from 8 week NT pig, in the active state at constant length, $1.1L_o$.

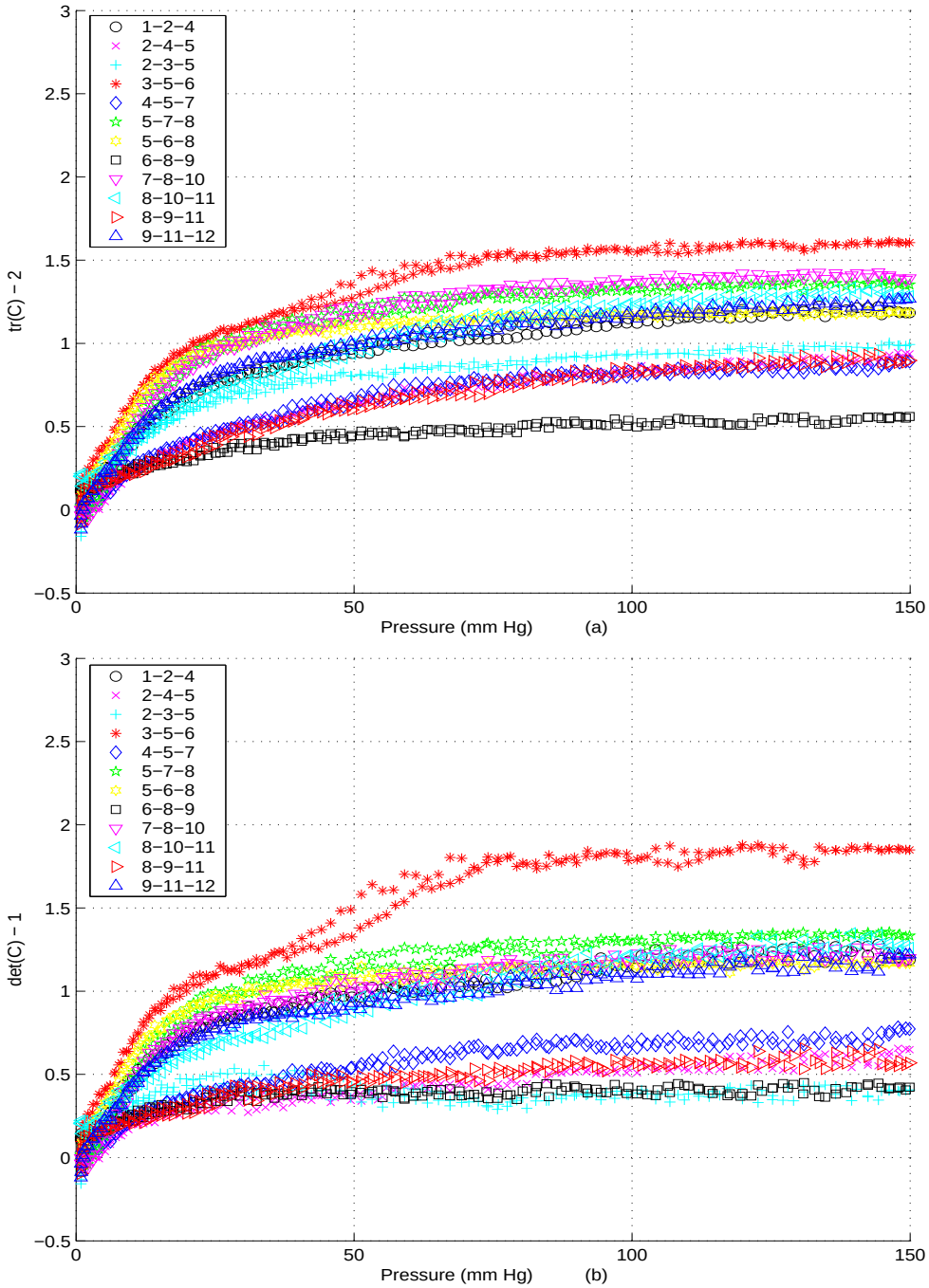

Fig. 64. Plot of (a) $(I_1^{2D})^c - 2$ (b) $(I_3^{2D})^c - 1$ computed for various marker sets while inflating the circumflex artery from 8 week NT pig, in the passive state at constant length, L_o.

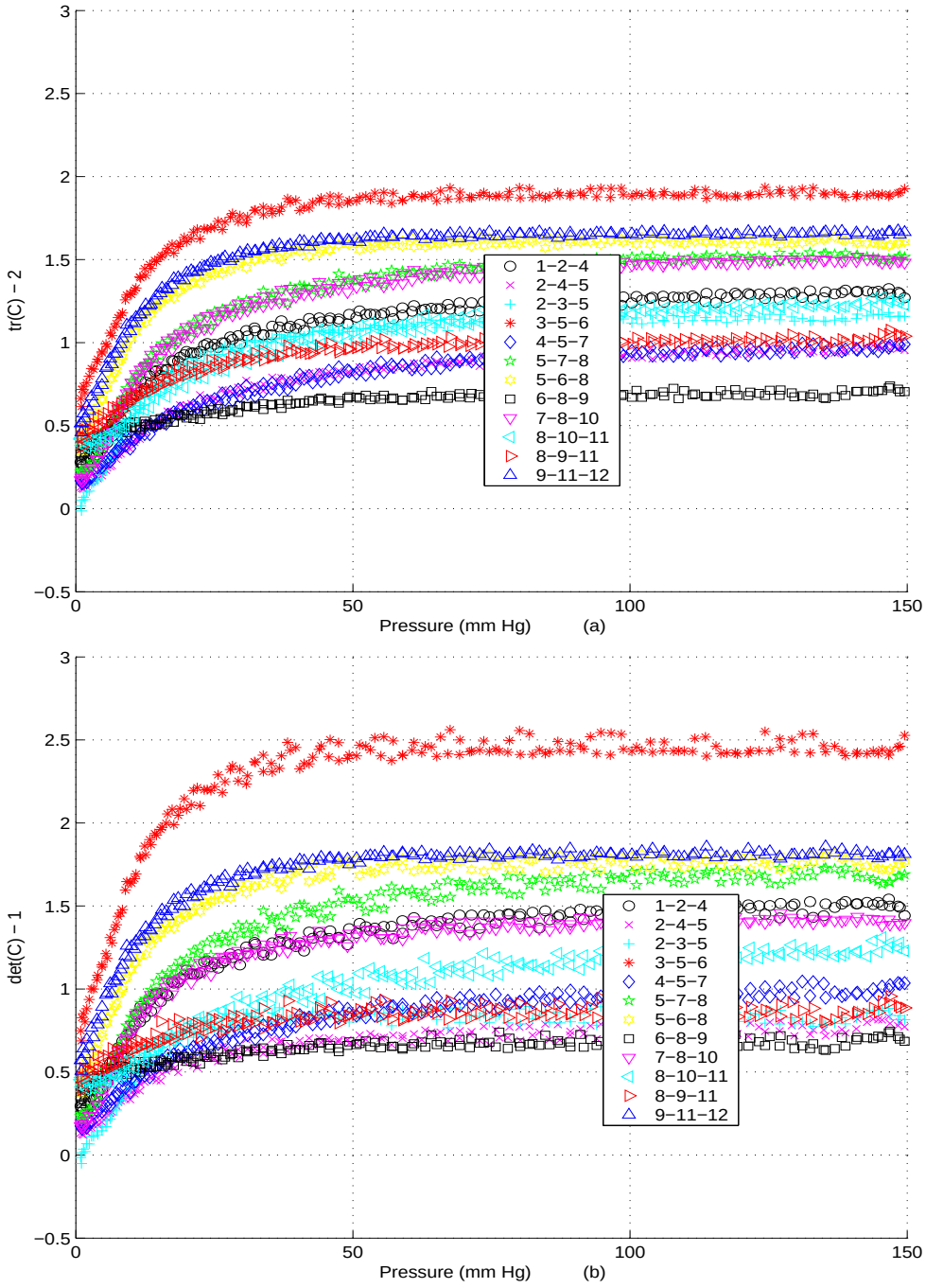

Fig. 65. Plot of (a) $(I_1^{2D})^c - 2$ (b) $(I_3^{2D})^c - 1$ computed for various marker sets while inflating the circumflex artery from 8 week NT pig, in the passive state at constant length, $1.1L_o$.

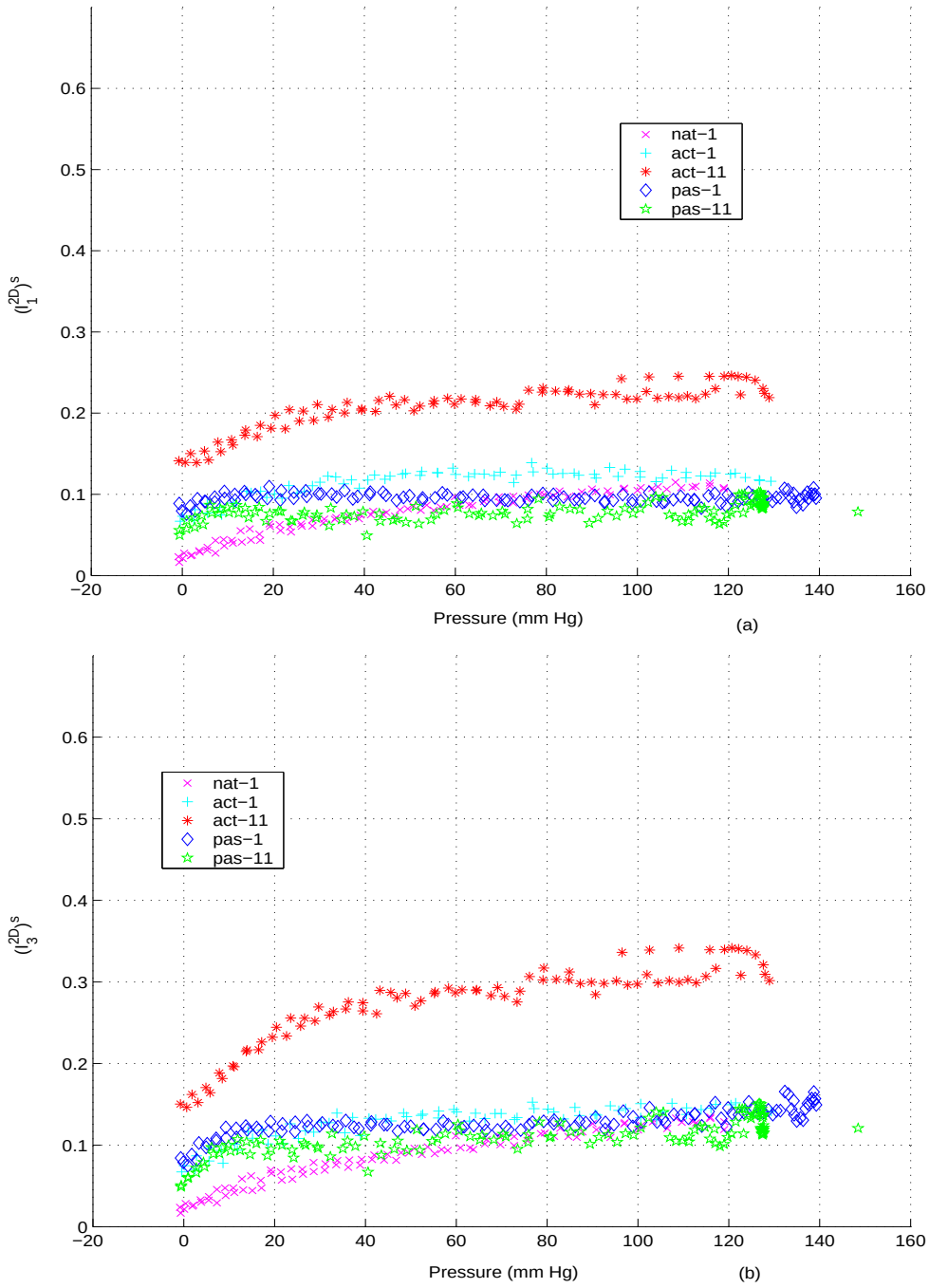

Fig. 66. Plot of (a) $(I_1^{2D})^s$ (b) $(I_3^{2D})^s$ while inflating the circumflex artery from 4 week HT pig under various smooth muscle tone and constant length.

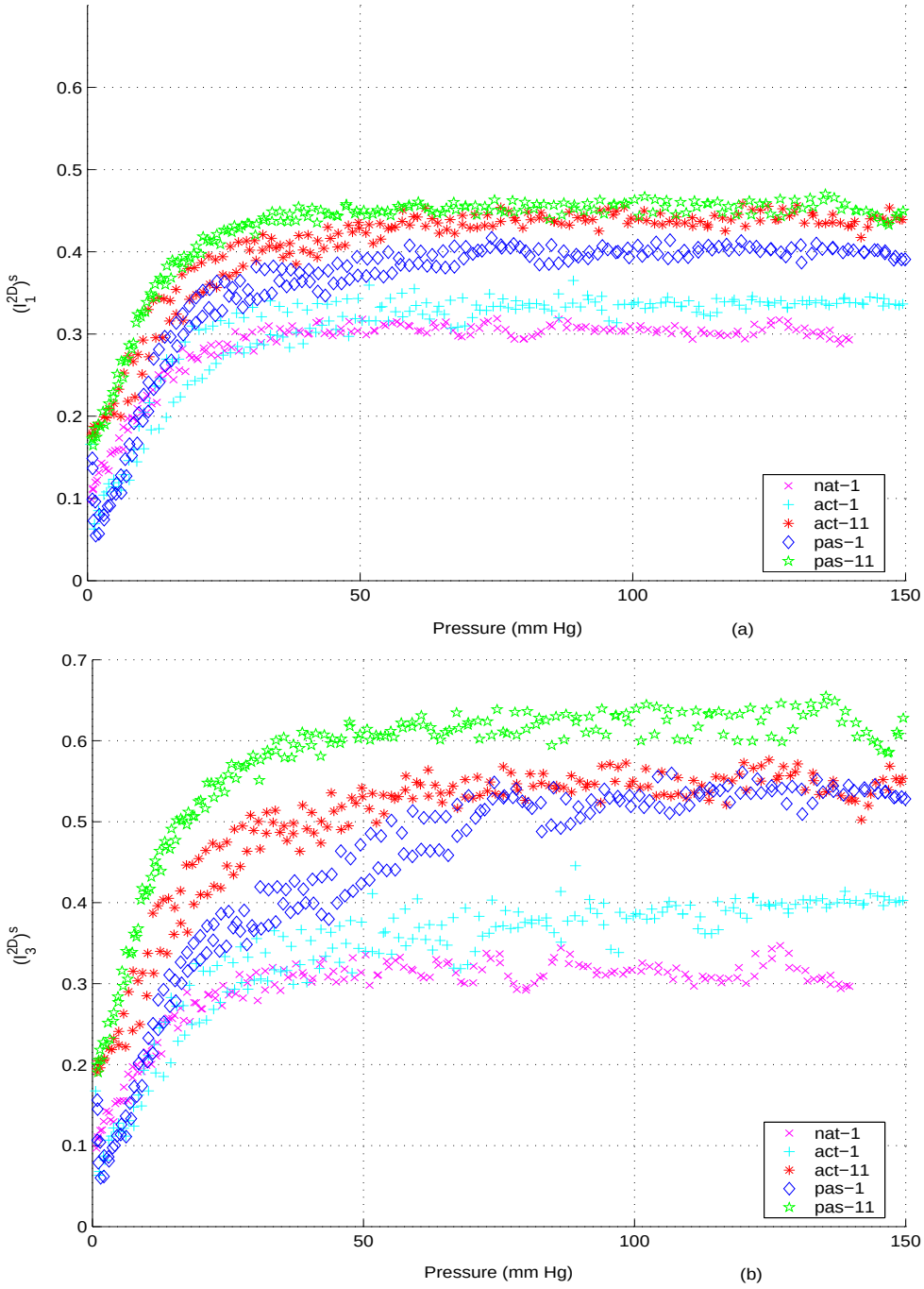

Fig. 67. Plot of (a) $(I_1^{2D})^s$ (b) $(I_3^{2D})^s$ while inflating the circumflex artery from 8 week NT pig under various smooth muscle tone and constant length.

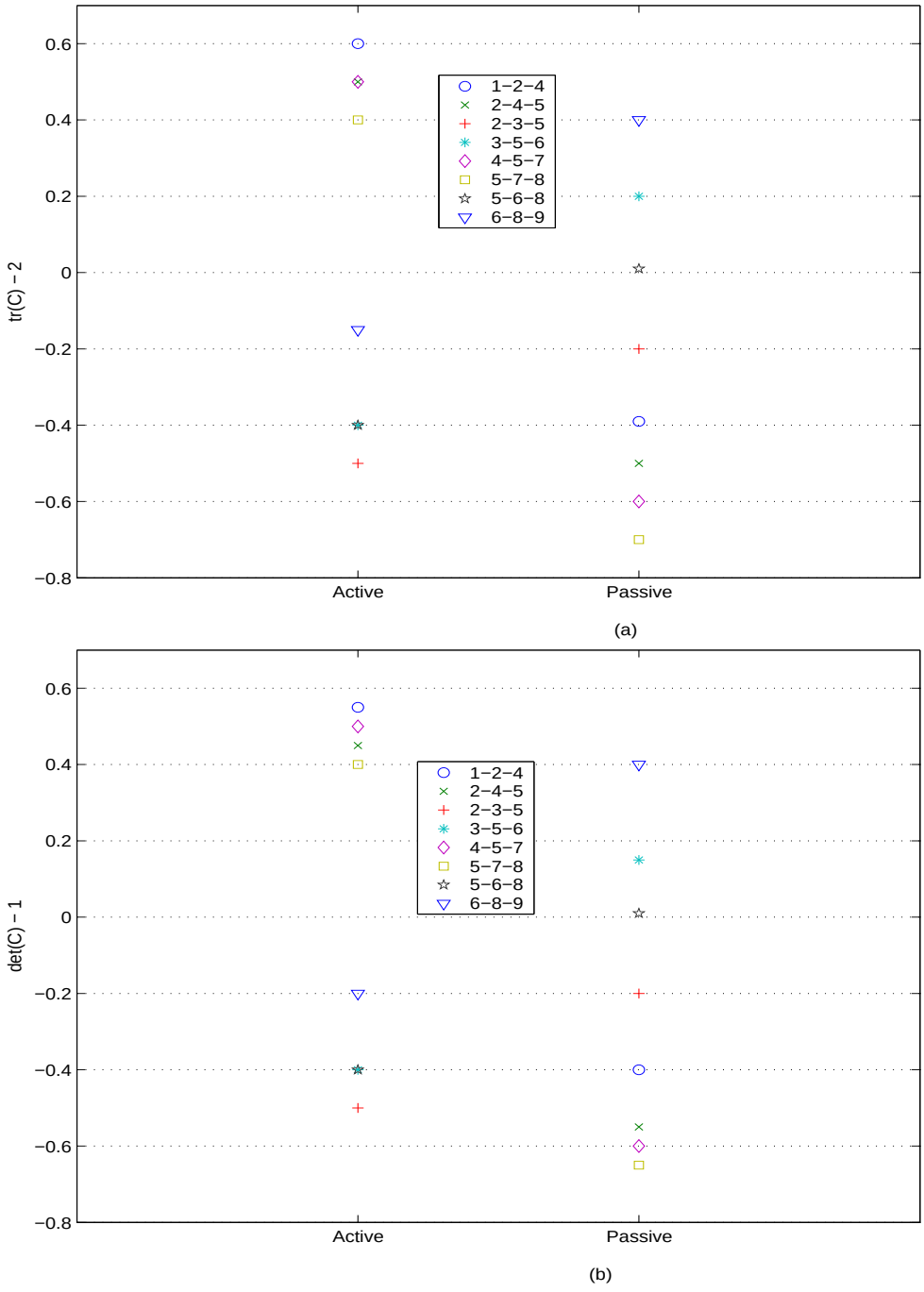

Fig. 68. Plot of (a) $(I_1^{2D})^c - 2$ (b) $(I_3^{2D})^c - 1$ computed for various marker sets while the circumflex artery from 6 week NT pig is in the active and passive state free of radial component of the normal stress at the inner surface and at a length of L_o.

we use standard deviation. Comparing figure 66 and 67 we immediately realize the marked difference in the deformation of these two sets. Here 'nat-1' is a mnemonic for the artery in native state held at a constant length of L_o, 'act-1' for the artery in activated state held at a constant length of L_o, 'act-11' for the artery in activated state held at a constant length of $1.1L_o$, 'pas-1' for the artery in passivated state held at a constant length of L_o, 'pas-11' for the artery in passivated state held at a constant length of $1.1L_o$. This difference in the variation of the invariants is a reflection of the changes in the structure of the artery.

Comparison between the mechanical response of the same specimen in various smooth muscle tones can be made in two ways. One, the value of the invariants computed using a single set of markers can be compared for various smooth muscle tones. It can be seen from figures 56 and 57 that one would reach different conclusions on comparing various set of markers. For example, while the value of $(I_1^{2D})^c$ computed using markers with marker id $(6, 8, 9)$[9] decreases on activation from the native state, it increases when computed using markers with marker id $(5, 7, 8)$. This indicates that activation induces non-axisymmetric deformation. This can also be seen from the evolution of the reference configuration from the native to the activated state (see figure 68[10]). Two, one can use the mean of the invariants computed from various choices of the set of three markers, $(I_i^{2D})^c$, to compare the responses of a given artery to various smooth muscle tones and/or axial stretch. Understanding that this is a gross simplification, the comparative studies, to our knowledge, did not yield any discernable pattern. In one 4 week hypertensive specimen the artery in the native

[9]See Figure 46 for the numbering of the markers.

[10]We note that the value of $(I_1^{2D})^c - 2$ and $(I_3^{2D})^c - 1$ varies from all being negative to all being positive to the one shown in the figure, for the specimens belonging to the same set. Hence figure 68 is not a representative figure.

state would be softer[11] than the artery in the activated state and in the another 4 week hypertensive specimen we observe the opposite. Stretching the artery should result in an increase in the value of the 2D principal invariants and hence one would expect the extended artery to be softer than an unextended artery. However, even this does not hold in all cases.

E. Illustrative data

In this section, we discuss ways to compare the mechanical response of different specimens for the collected data. In homogeneous bodies subjected to homogeneous deformations, it is easy to obtain stress vs. (some measure of) strain plot and compare them for different specimens. In case of bodies subjected to inhomogeneous deformations, like inflation of an annular cylinder, then the boundary traction or the integrated boundary traction is compared with the corresponding boundary displacement, for example radial component of the normal stress at the inner surface to engender a given outer diameter of the annular cylinder could be compared. As noted in chapter IV, in this later case, all the (integrated) boundary traction on various surfaces has to be compared with the corresponding boundary displacement. Thus, in the case of inflation of an annular cylinder at constant length, apart from comparing the radial component of the normal stress at the inner surface required to engender a given outer diameter, it is also necessary to compare the variation of the inner diameter and the axial load with pressure. Otherwise, there could be more than one constitutive relation for stress that could satisfy the limited data for a given

[11]Hence forth by 'A being softer than B' we mean that the value of the invariant for the case A at a given pressure is greater than the value of the invariant for the case B at the same pressure. We caution that here the use of the term "softer" though is in agreement with the physical connotations that goes with it in many cases, it blatantly doesn't in some other cases, as will become evident from the examples that we discuss.

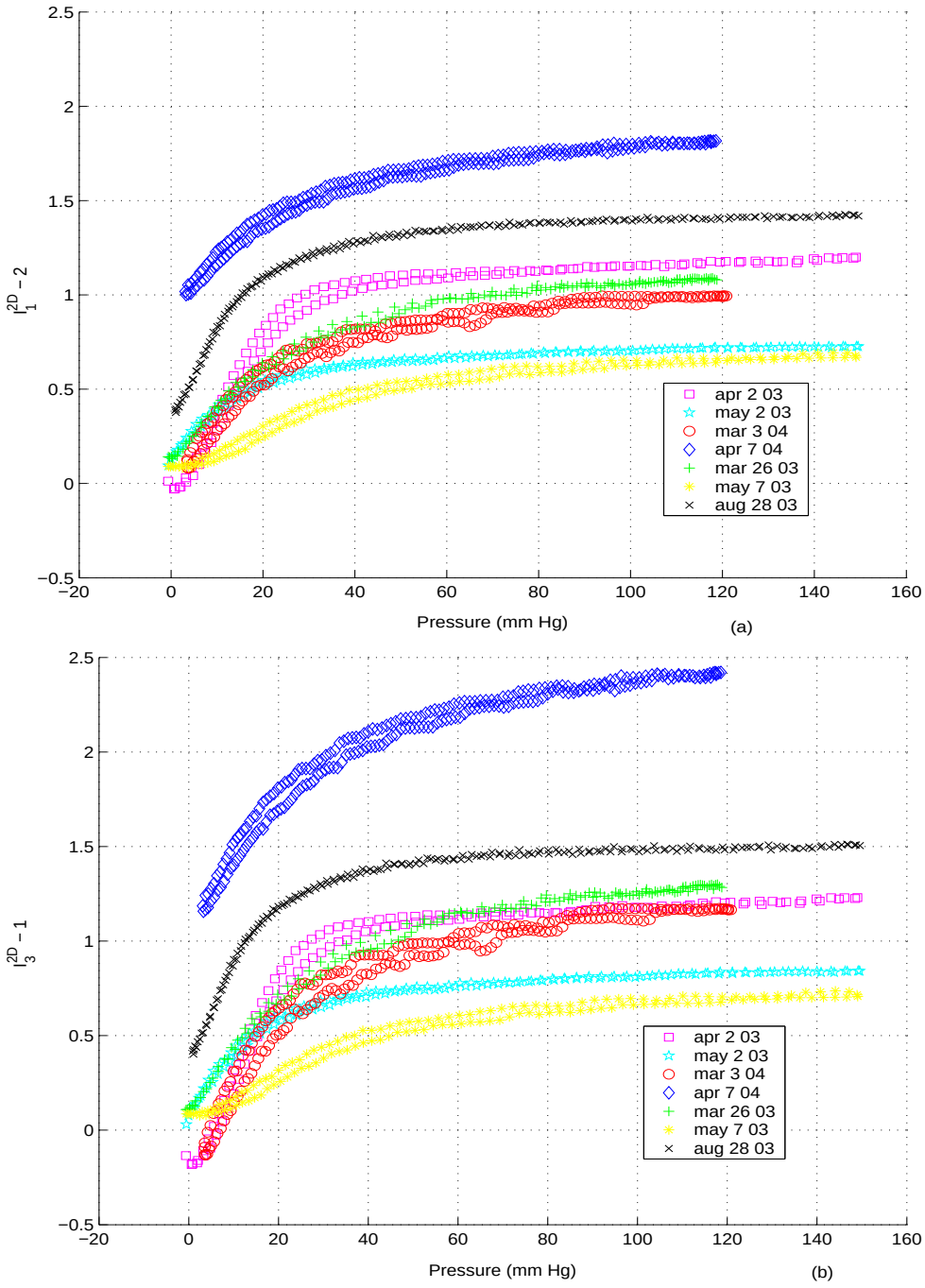

Fig. 69. Plot of (a) $I_1^{2D} - 2$ (b) $I_3^{2D} - 1$ while inflating the circumflex artery in passive state at constant length, $1.1L_o$ from various 8 week NT and HT pigs. Solid symbols - mar 26 03, may 7 03 and aug 28 03 - are NT open symbols are HT.

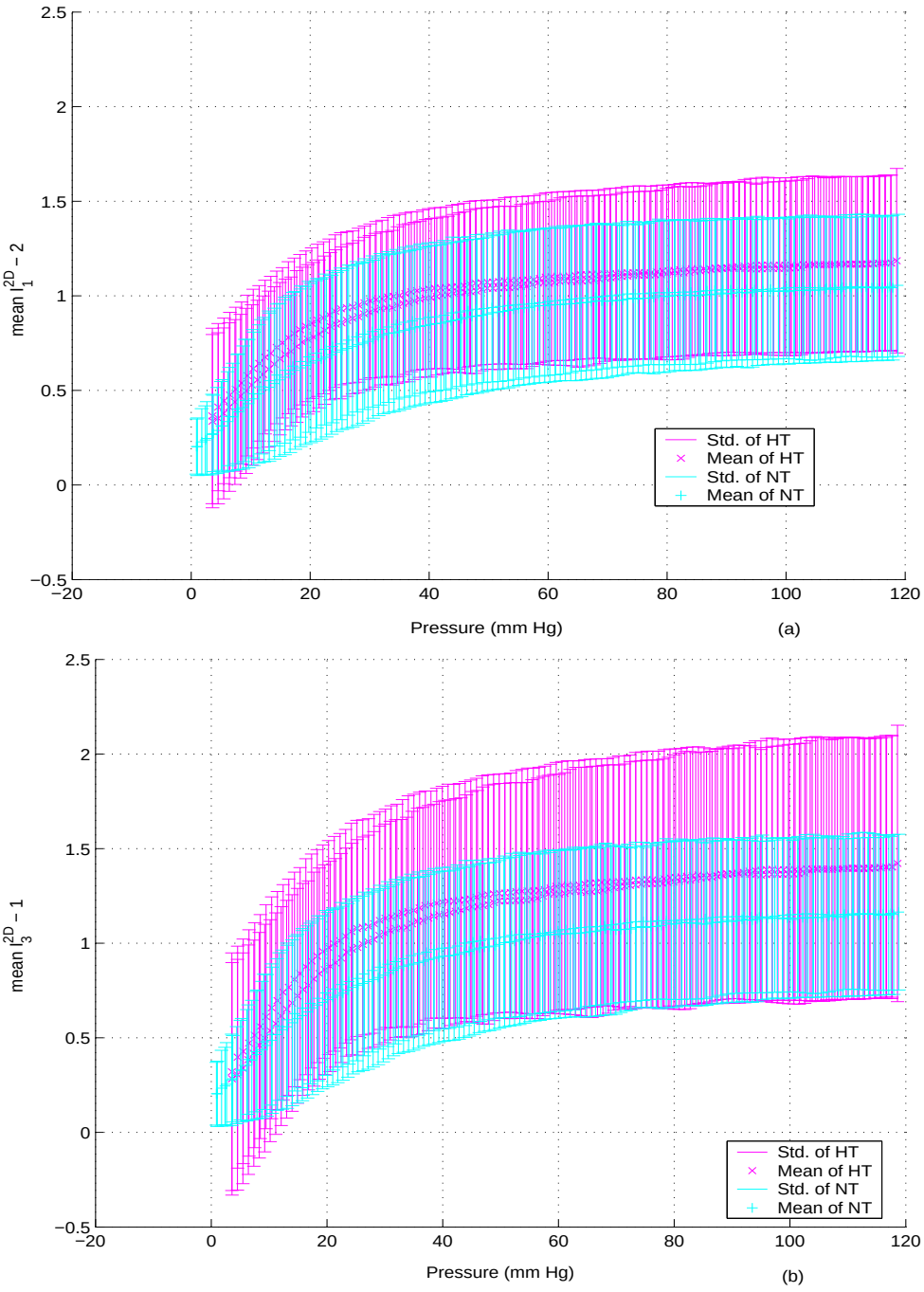

Fig. 70. Plot of mean and standard deviation of (a) $I_1^{2D} - 2$ (b) $I_3^{2D} - 1$ while inflating the circumflex artery in passive state at constant length, $1.1L_o$ from 8 week NT and HT pigs.

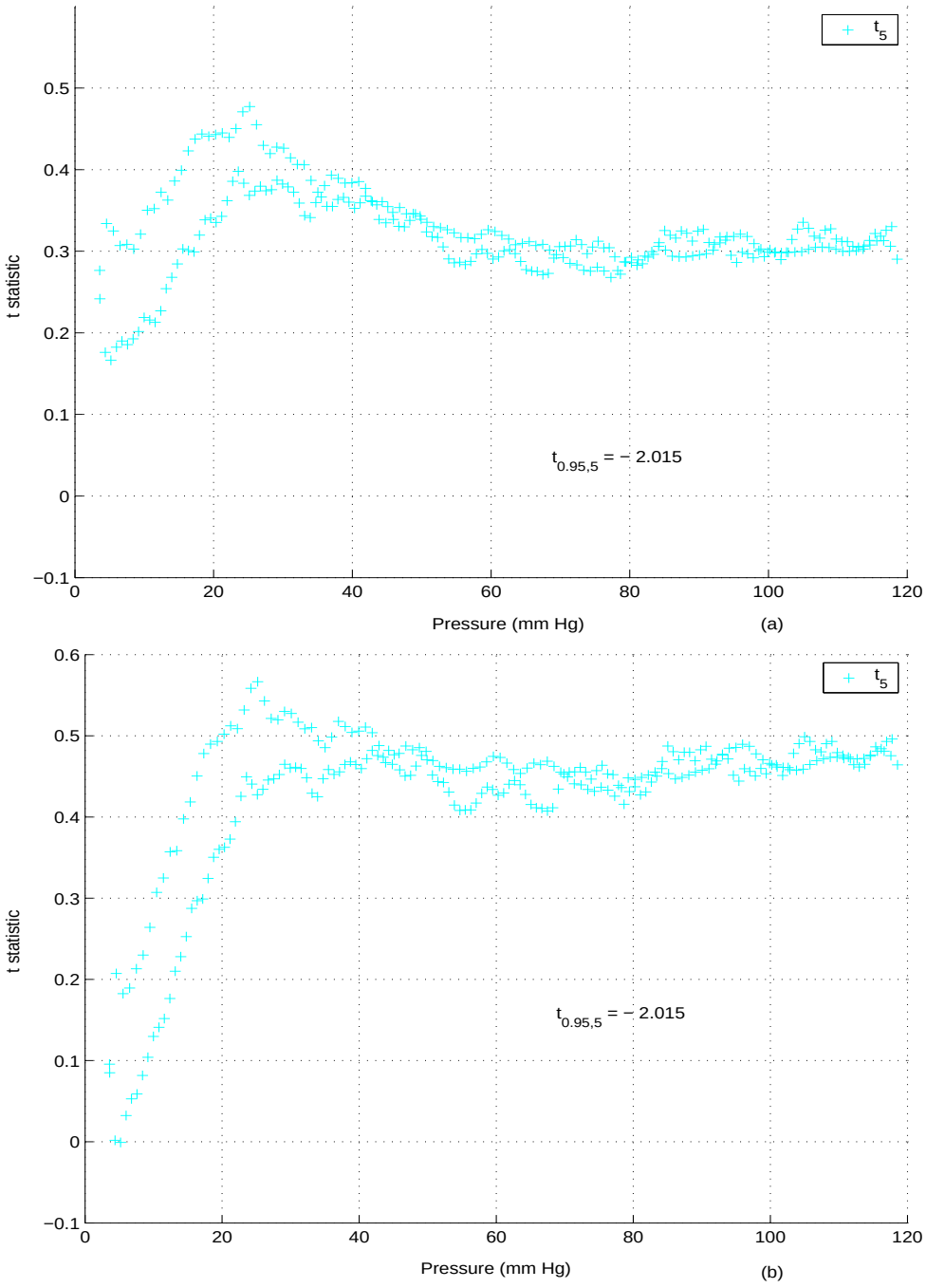

Fig. 71. Plot of t statistic for testing the hypothesis that (a) I_1^{2D} (b) I_3^{2D} is greater in the case of NT artery in comparison with the HT artery in passive state when inflated at constant length, $1.1L_o$.

body. It is worthwhile to point out that while the stress vs. strain plot does not depend on geometry of the body, the plot of radial component of the normal stress at the inner surface of the annular cylinder versus outer diameter does.

In chapter IV, it was also pointed out that the form of the deformation must be established. The design of experiments here was to establish the form of the deformation when an artery is inflated at constant length. As elaborated in section B.2, if the deformation was of the assumed form (6.1), then the boundary displacement could be inferred from the motion of the markers alone. Since the deformation is not of the assumed form, the boundary deformation cannot be inferred from the motion of the markers alone and hence, now the question is how best can we compare the response of different specimens from the available information.

Here the following procedure was adopted to compare the mechanical response of different specimens subjected to inflation at constant length.

1. Approximating the deformation by (6.12), we first compute $(I_p^{2D})^c$ for various choices of three markers for a given protocol of a particular specimen.

2. From the results of step 1, we compute I_p^{2D} and $(I_p^{2D})^s$ which are defined in equation (6.7).

3. Steps 1 and 2 are repeated for various specimens and various protocol.

4. The results of step 3 were grouped according to the different sets of specimens for a given protocol and plot of I_p^{2D} vs. pressure, similar to those reported in figure 69 were obtained.

5. Then, for equally spaced pressure varying from 0 to 120 mm Hg, I_p^{2D} is computed using nearest neighbor cubic spline interpolation from the data obtained in step 3. Using this, the mean and standard deviation of I_p^{2D} for a given group, as

a function of pressure, is obtained and plotted. See figure 70 for example. Interpolation is necessary to ensure that the statistics of I_p^{2D} is obtained for the same pressure.

6. At each pressure using the results computed in step 5, the hypothesis that I_p^{2D} for group A is less than that of group B is tested using t statistic assuming that both the groups are statistically independent but have same variance following methods outlined in [83]. A sample plot of the obtained t-statistic is shown in figure 71. If for a given pressure the obtained t-statistic is greater than $t_{crtical}$, then the null hypothesis that I_p^{2D} for group A is equal to that of group B is not rejected. If the null hypothesis was rejected for nearly all the range of values of pressure considered then it was concluded that I_p^{2D} for group A is less than that of group B. Table II through table IV summarizes the results obtained for various hypothesis tested. We note that for all the hypothesis tested there was no evidence that the variances of the groups tested were different. The null hypothesis that the variances are equal was tested using f-statistic, following methods outlined in [83].

In tables II through IV, 'sig.' stands for statistical significance, 'Y' stands for the hypothesis being statistically significant with $p < 0.05$, 'Y^*' stands for the hypothesis being statistically significant with $p < 0.1$, 'Y^+' stands for the hypothesis being statistically significant with $p < 0.01$, 'N' stands for the hypothesis being statistically insignificant, 'N^*' for the hypothesis being close to significant, N^+ for the t statistic being close to 0 and hence the hypothesis being statistically insignificant, '$-$' indicates that statistical significance was not examined because data are not available for more than two specimens. This happens because the corresponding protocols was not performed for the specimens tested in 2004, due to reasons outlined in section F.

Table II. Comparison between NT and HT specimens subjected to various protocols.'NsH' is an acronym for NT is softer than HT, 'HsN' for HT is softer than NT and '−' stands for no data.

Hypothesis	I_i^{2D}	2 week		4 week		6 week		8 week	
		trend	sig.	trend	sig.	trend	sig.	trend	sig.
NsH @ L_o	I_1^{2D}	HsN	N	NsH	Y^*	NsH	Y	HsN	N^+
in passive	I_3^{2D}	HsN	N	NsH	N^*	NsH	Y^+	HsN	N^+
NsH @ L_o	I_1^{2D}	HsN	−	NsH	−	NsH	−	HsN	N
in active	I_3^{2D}	HsN	−	NsH	−	NsH	−	HsN	N
NsH @ L_o	I_1^{2D}	−		−		NsH	−	HsN	N^+
in native	I_3^{2D}	−		−		NsH	−	HsN	N^+
NsH @ $1.1L_o$	I_1^{2D}	HsN	N	NsH	Y^*	NsH	−	HsN	N
in passive	I_3^{2D}	HsN	N	NsH	N^*	NsH	−	HsN	N
NsH @ $1.1L_o$	I_1^{2D}	−		−		NsH	−	NsH	N^+
in active	I_3^{2D}	−		−		NsH	−	NsH	N^+

It transpires from the table II that while NT specimens are softer than HT specimens at 4 and 6 weeks into hypertension, there is little difference between the two sets 2 or 8 weeks into hypertension. The above seem to hold for all the protocols studied here. This kind of response is consistent with the observations of Cox ([84],[34]). However, his observations were based on the mechanics of rat carotid artery, with the hypertension being induced by renal artery stenosis or deoxycorticosterone. Moreover, his conclusions were based on the comparison of the pressure required to engender a given outer diameter.

We infer from table III that there is no evidence that the value of invariants increases on superposing a fixed axial stretch on a vessel being inflated. This is because

Table III. Comparison of the response of the circumflex artery to inflation at various fixed lengths.'LsLo' is an acronym for the artery stretched to $1.1L_o$ is softer than at L_o, 'LosL' for the artery at length L_o is softer than $1.1L_o$ and '$-$' stands for no data.

Hypothesis	I_i^{2D}	2 week		4 week		6 week		8 week	
		trend	sig.	trend	sig.	trend	sig.	trend	sig.
LsLo for HT	I_1^{2D}	LsLo	N	LsLo	N	LsLo	N	LsLo	N
in passive	I_3^{2D}	LsLo	N	LsLo	N	LsLo	N	LsLo	N
LsLo for HT	I_1^{2D}	LosL	N	LsLo	N^*	LsLo	N^+	LsLo	N^+
in active	I_3^{2D}	LosL	N	LsLo	N^*	LsLo	N^+	LsLo	N^+
LsLo for NT	I_1^{2D}	LosL	N^+	LsLo	N	LosL	$-$	LsLo	N
in passive	I_3^{2D}	LosL	N^+	LsLo	N	LosL	$-$	LsLo	N
LsLo for NT	I_1^{2D}	$-$		$-$		LosL	$-$	LsLo	N
in active	I_3^{2D}	$-$		$-$		LosL	$-$	LsLo	N

the increase in the value of invariants due to axial stretch is small in comparison to that due to inflation and the increase is likely compensated by the associated decrease in the circumferential stretch due to inflation as well as stretching. Thus, since invariants reflect the sum total of different effects; they being greater does not mean that the material is softer, in the physical sense.

For the data in table IV, one would expect that the artery in the passive state to be softer than the native and the active to be the stiffest. This is because the activation reduces the circumferential stretch. While there was some evidence towards this in 4 week HT, there was little to no evidence in 2, 6 and 8 week HT and NT. Here it is pertinent to point out that Cox [33] reports just a marginal change in the pressure required to engender a given outer diameter of the coronary artery from healthy canines on activation.

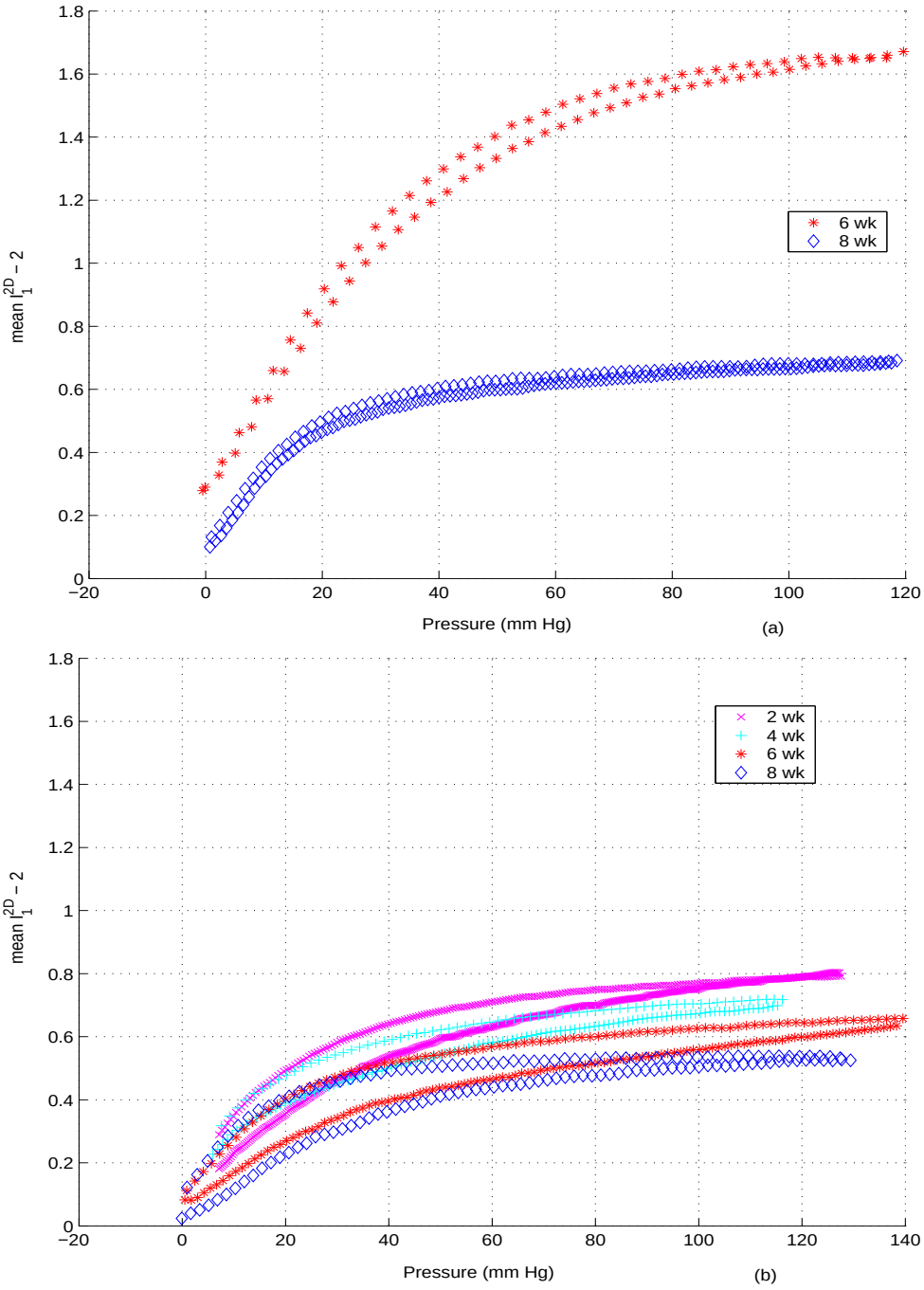

Fig. 72. Plot of mean of $I_1^{2D} - 2$ obtained for various (a) NT (b) HT pigs, while inflating the circumflex artery in native state at constant length, L_o.

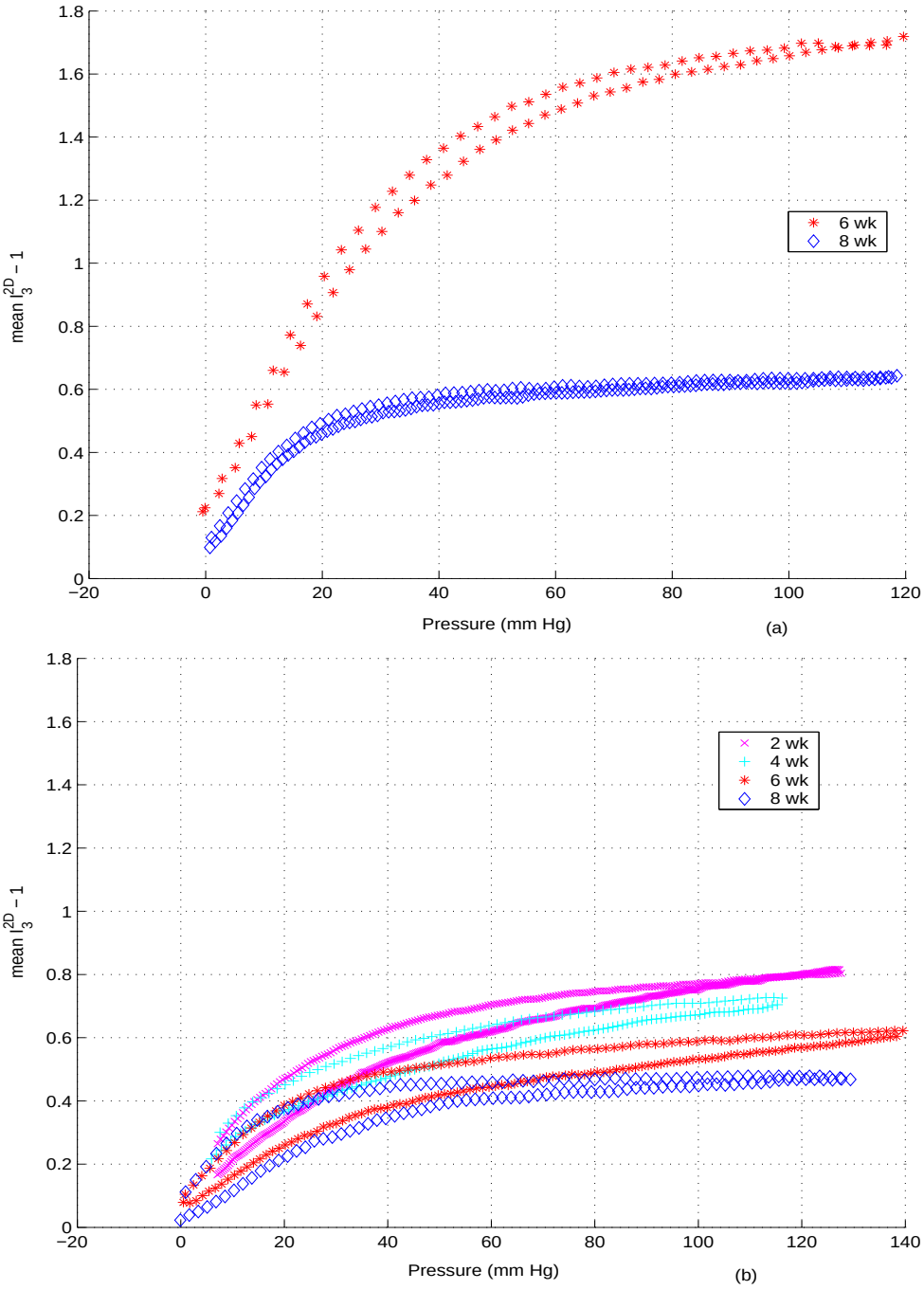

Fig. 73. Plot of mean of $I_3^{2D} - 1$ obtained for various (a) NT (b) HT pigs, while inflating the circumflex artery in native state at constant length, L_o.

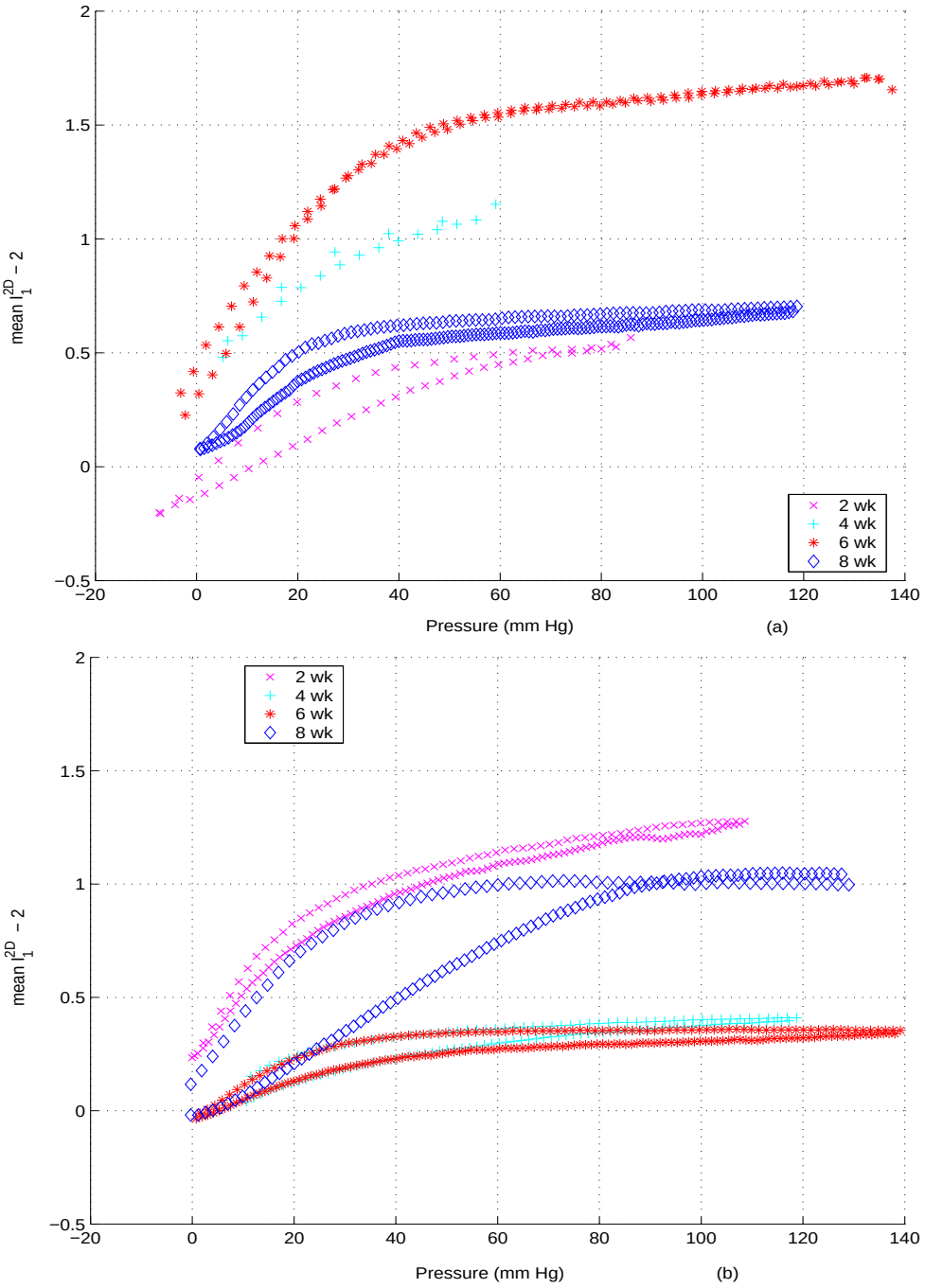

Fig. 74. Plot of mean of $I_1^{2D} - 2$ obtained for various (a) NT (b) HT pigs, while inflating the circumflex artery in activated state at constant length, L_o.

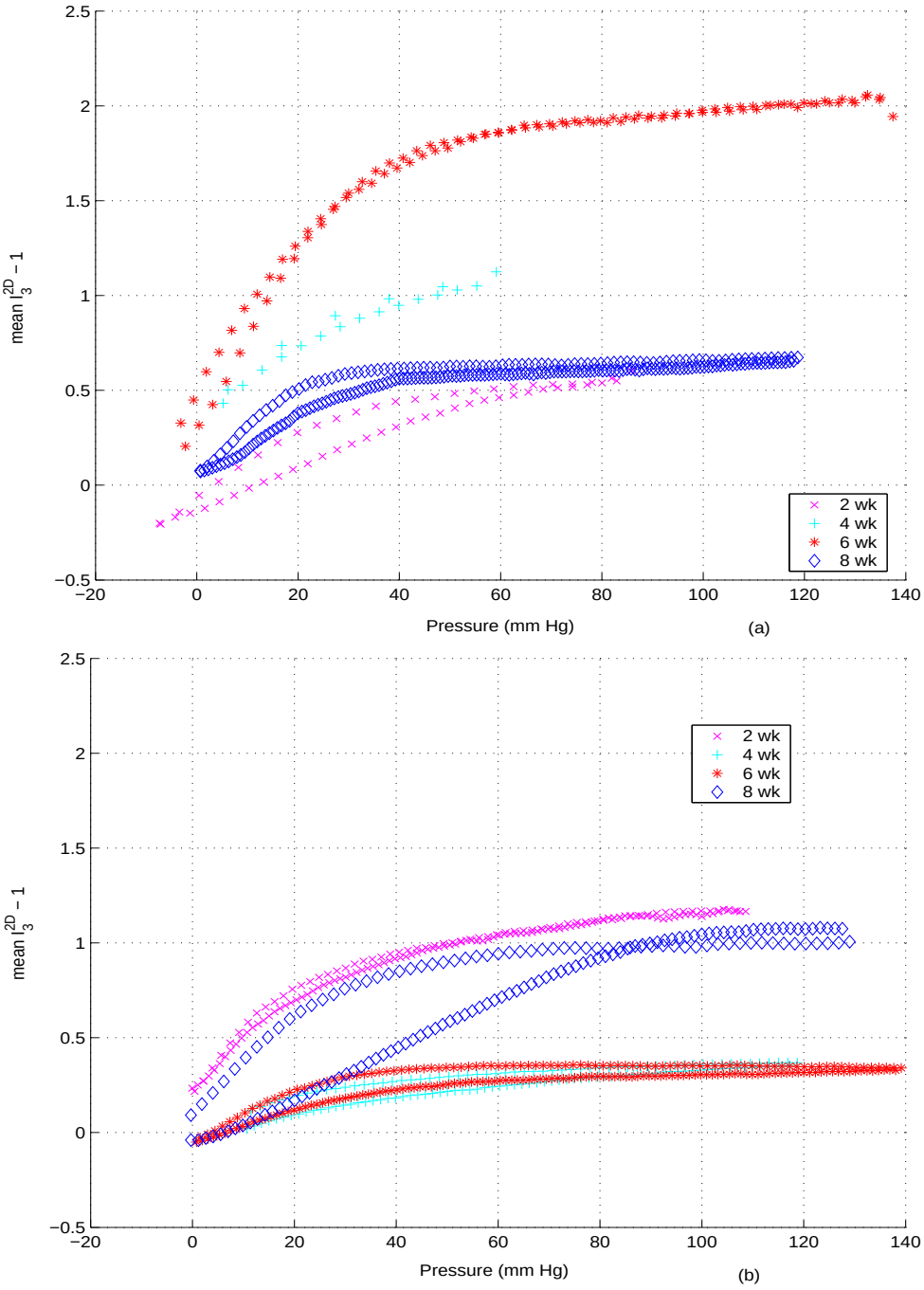

Fig. 75. Plot of mean of $I_3^{2D} - 1$ obtained for various (a) NT (b) HT pigs, while inflating the circumflex artery in activated state at constant length, L_o.

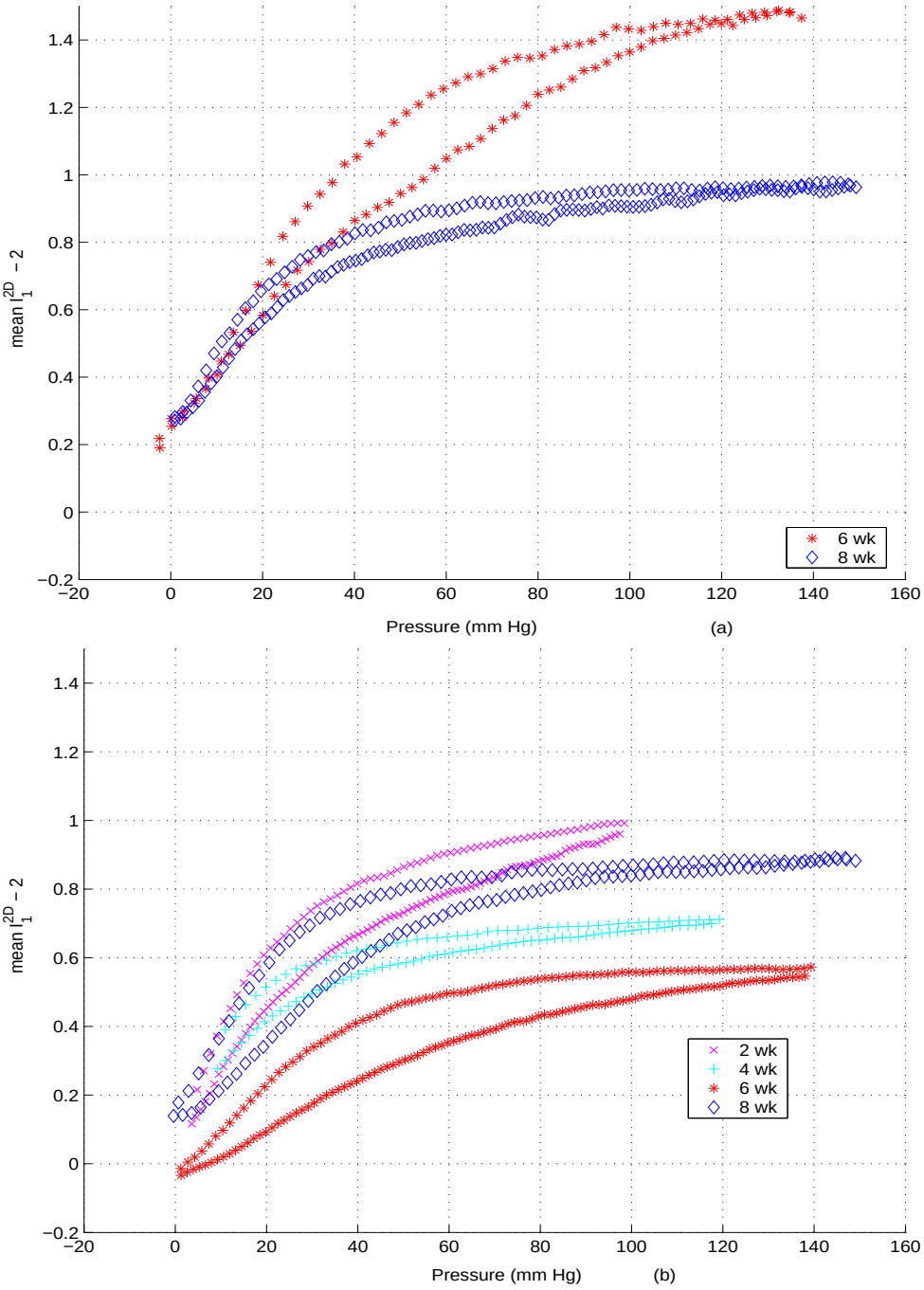

Fig. 76. Plot of mean of $I_1^{2D} - 2$ obtained for various (a) NT (b) HT pigs, while inflating the circumflex artery in activated state at constant length, $1.1L_o$.

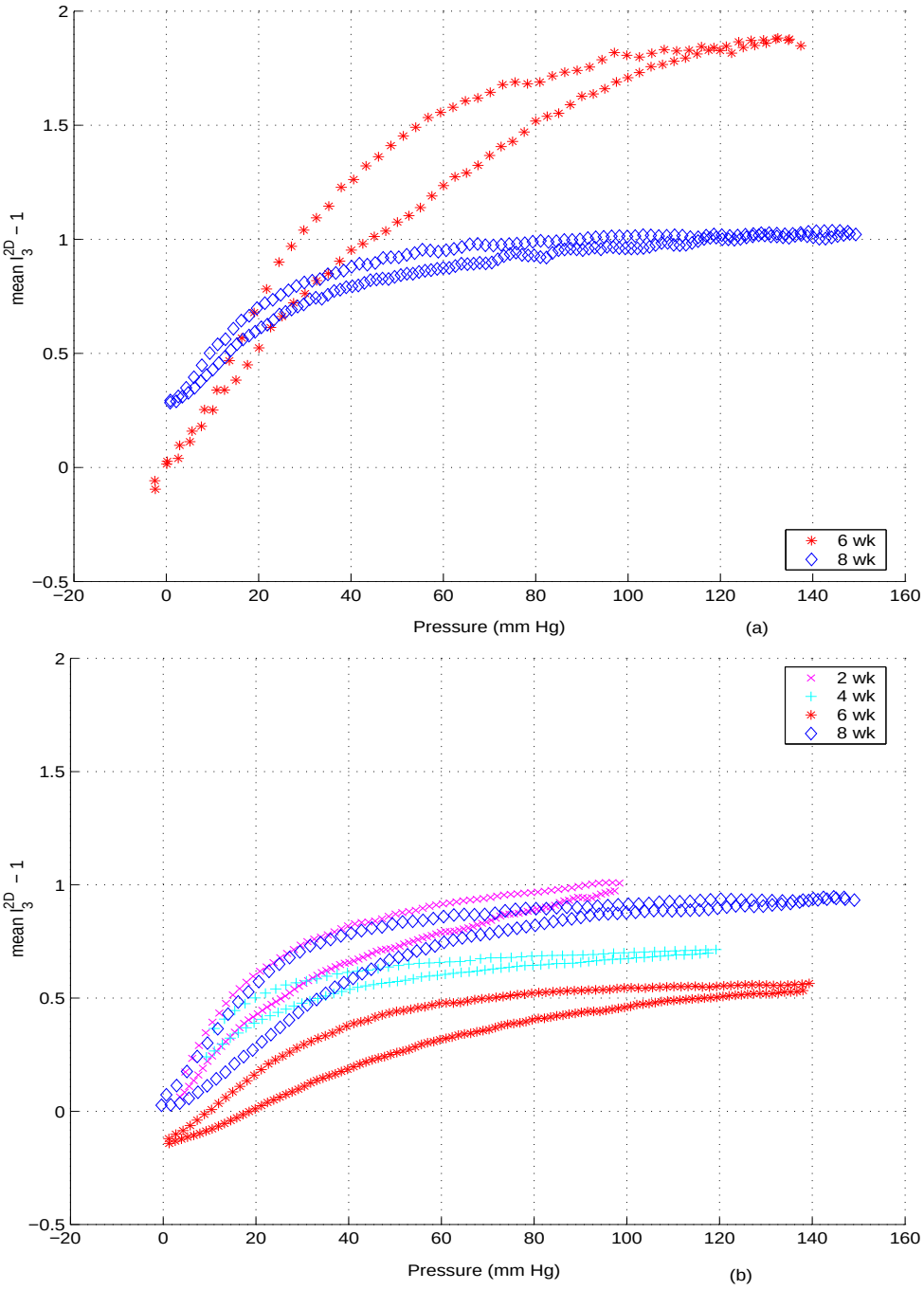

Fig. 77. Plot of mean of $I_3^{2D} - 1$ obtained for various (a) NT (b) HT pigs, while inflating the circumflex artery in activated state at constant length, $1.1L_o$.

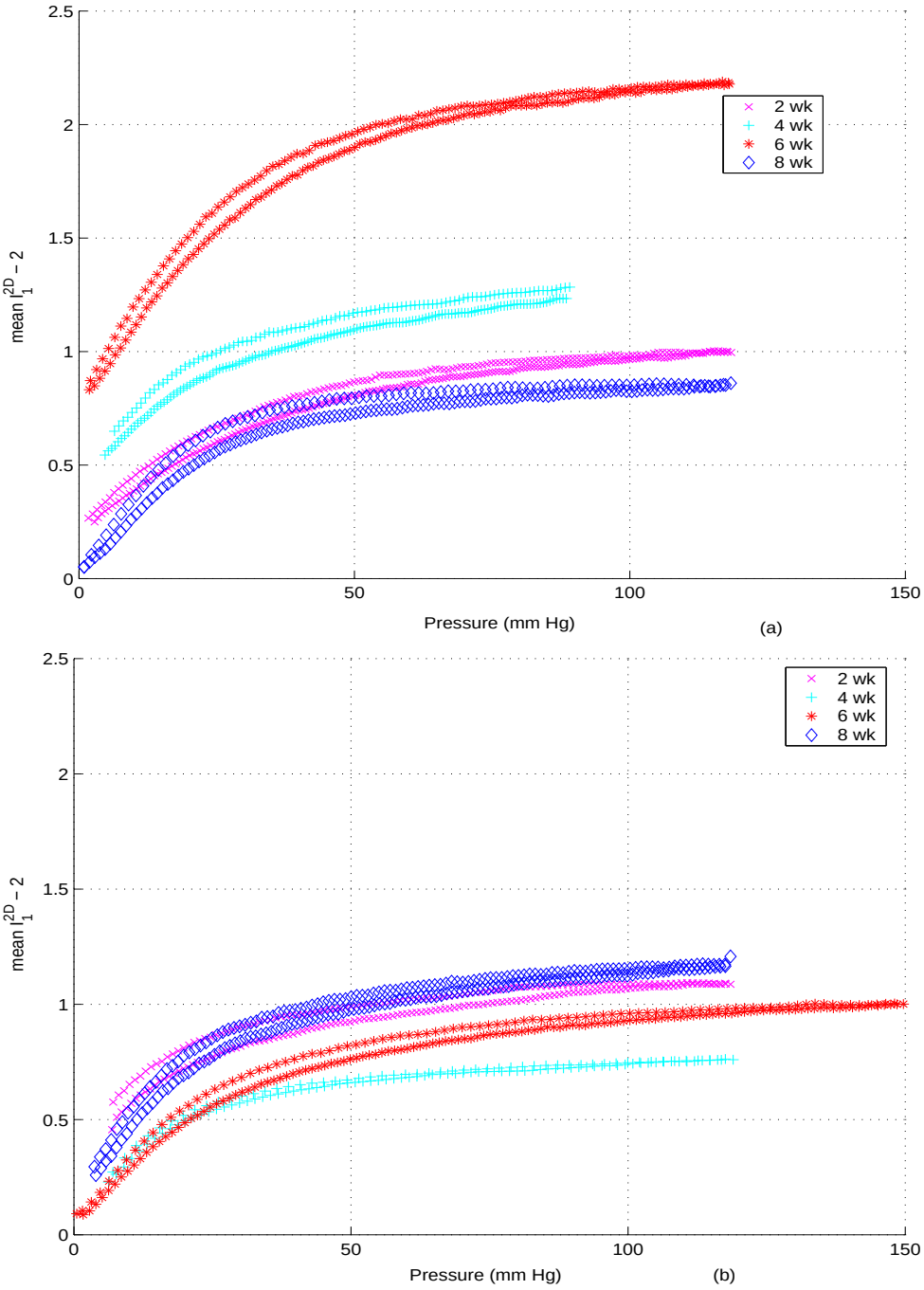

Fig. 78. Plot of mean of $I_1^{2D} - 2$ obtained for various (a) NT (b) HT pigs, while inflating the circumflex artery in passive state at constant length, L_o.

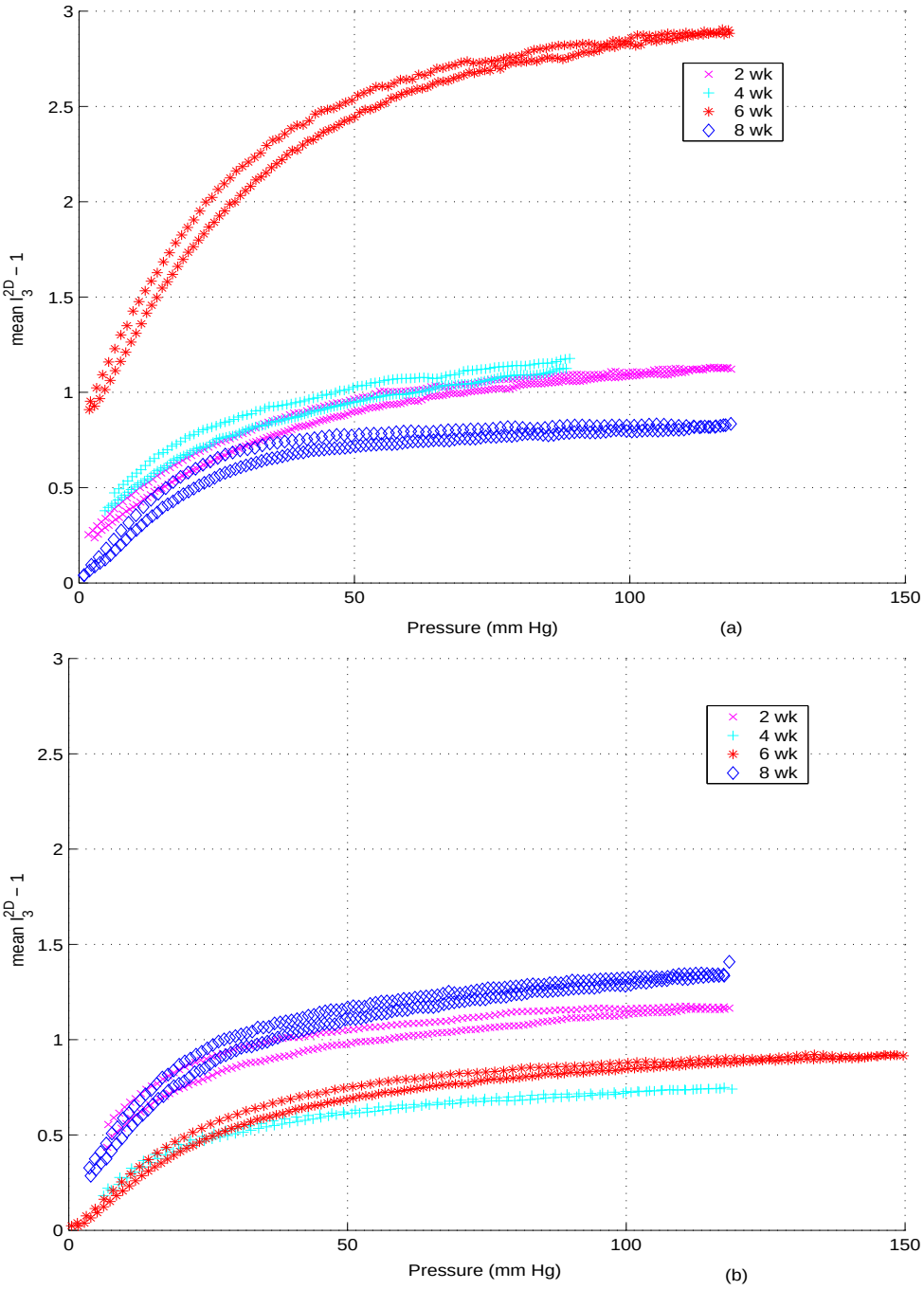

Fig. 79. Plot of mean of $I_3^{2D} - 1$ obtained for various (a) NT (b) HT pigs, while inflating the circumflex artery in passive state at constant length, L_o.

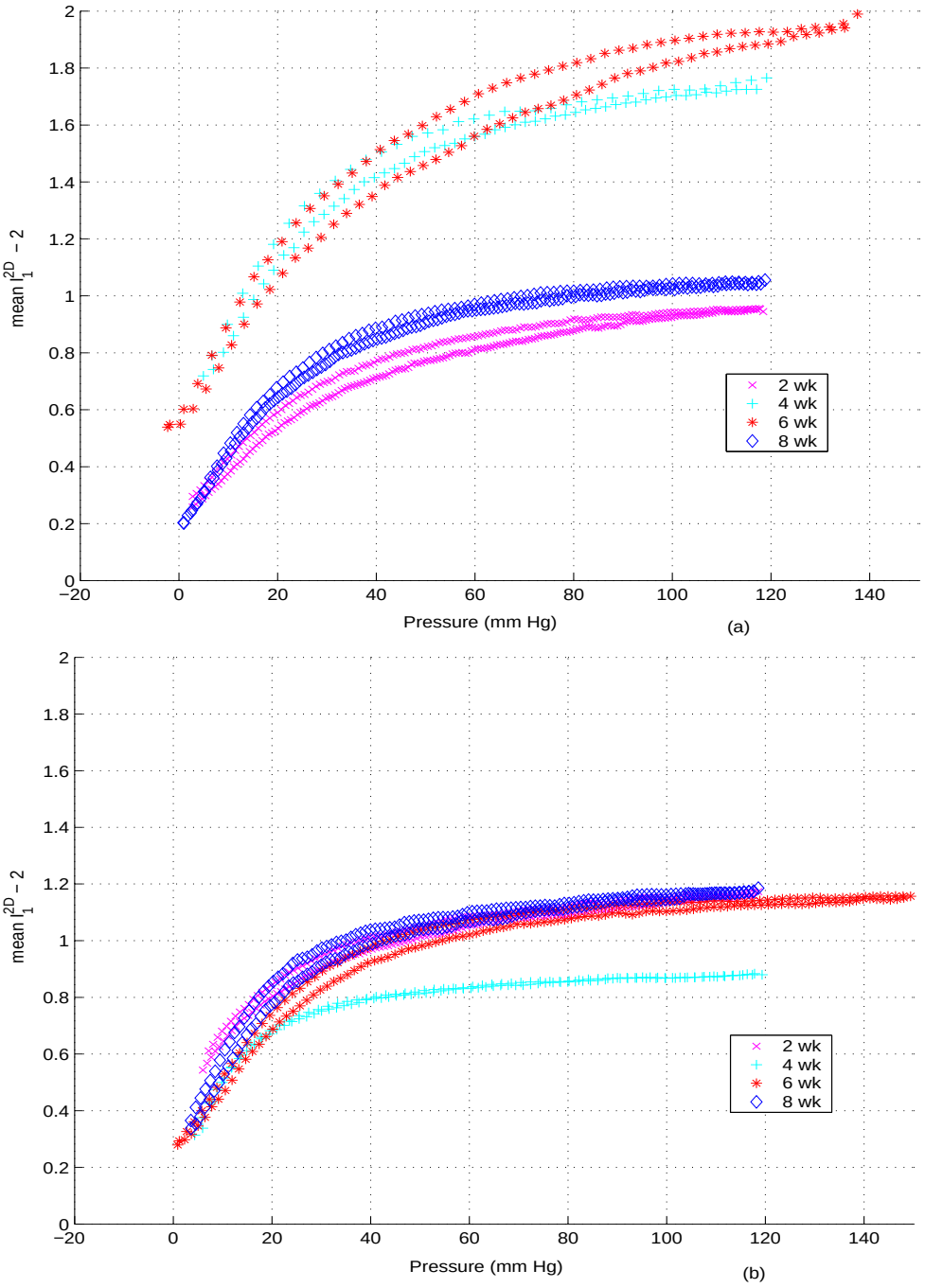

Fig. 80. Plot of mean of $I_1^{2D} - 2$ obtained for various (a) NT (b) HT pigs, while inflating the circumflex artery in passive state at constant length, $1.1L_o$.

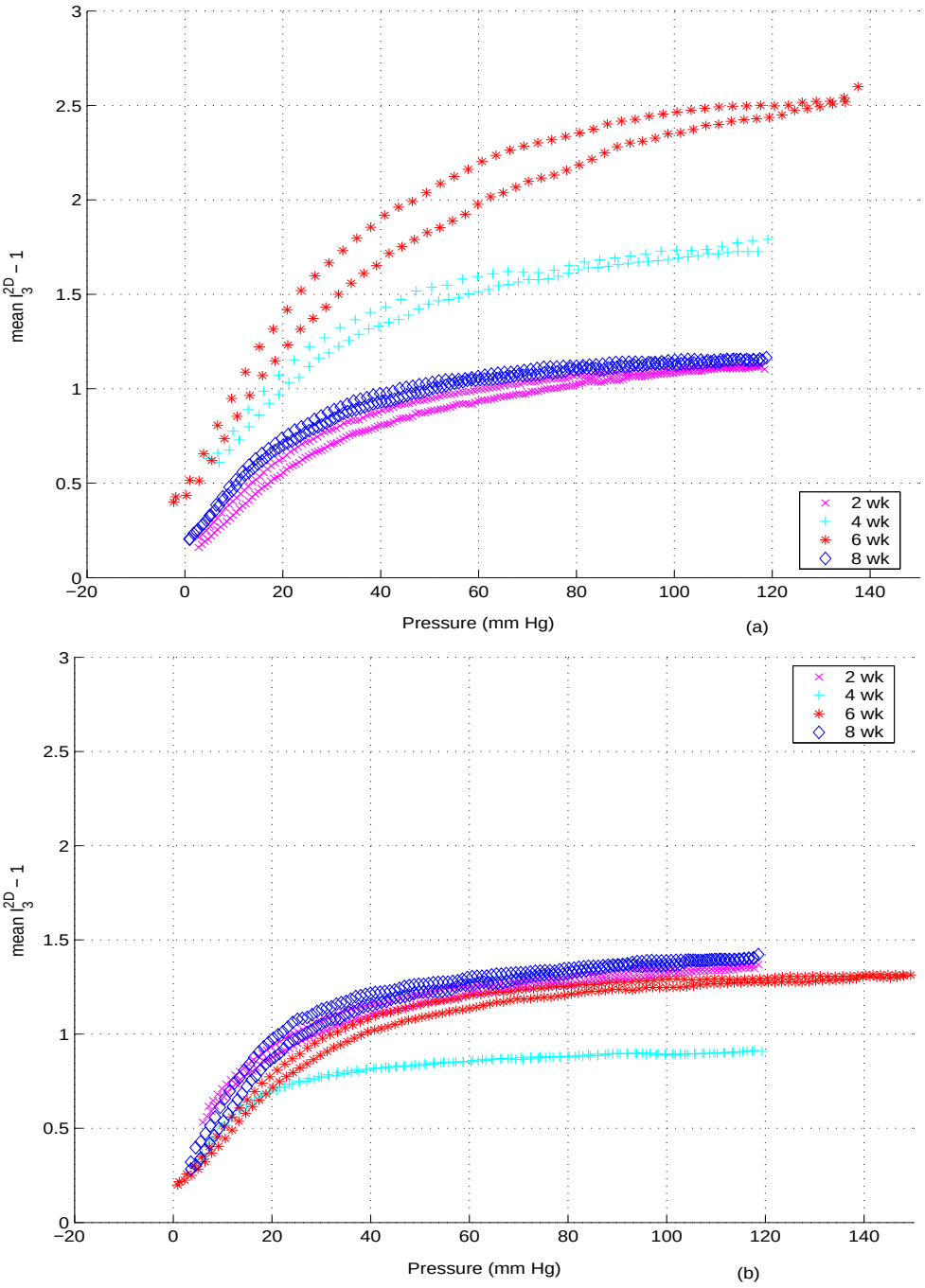

Fig. 81. Plot of mean of $I_3^{2D} - 1$ obtained for various (a) NT (b) HT pigs, while inflating the circumflex artery in passive state at constant length, $1.1L_o$.

Table IV. Comparison of the response of the circumflex artery to inflation for various smooth muscle tone. 'nsa' is an acronym for the native state of the artery being softer than that in the active state, 'asn' stands for the activated state of the artery is softer than that in the native state, 'psn' is an acronym for the passivated artery is softer than that in the native state, 'nsp' denotes that the artery in the native state is softer than that in the passive state 'psa' stands for passivated artery is softer than the artery in the active state, 'asp' denotes that the activated artery is softer than the passivated artery and '−' for no data.

Hypothesis	I_i^{2D}	2 week		4 week		6 week		8 week	
		trend	sig.	trend	sig.	trend	sig.	trend	sig.
nsa for HT	I_1^{2D}	asn	N	nsa	N^*	nsa	N	asn	N
@ L_o	I_3^{2D}	asn	N	nsa	Y^*	nsa	N	asn	N
psa for HT	I_1^{2D}	asp	N^+	psa	N^*	psa	N	psa	N
@ L_o	I_3^{2D}	asp	N^+	psa	N^*	psa	N	psa	N
psn for HT	I_1^{2D}	psn	N	psn	N^+	psn	N	psn	N^*
@ L_o	I_3^{2D}	psn	N	psn	N^+	psn	N	psn	Y^*
nsa for NT	I_1^{2D}	−		−		nsa	−	nsa	N^+
@ L_o	I_3^{2D}	−		−		nsa	−	nsa	N^+
psa for NT	I_1^{2D}	asp	−	psa	−	psa	−	psa	N
@ L_o	I_3^{2D}	asp	−	psa	−	psa	−	psa	N
psn for NT	I_1^{2D}	−		−		psn	−	psn	N
@ L_o	I_3^{2D}	−		−		psn	−	psn	N

Figures 72 through 81 plot the mean value of I_p^{2D} obtained for various groups, namely 2,4,6 and 8 week NT and HT pigs, while inflating the circumflex artery in various states. It is the information contained in these figures, that were summarized in tables II through IV.

Figures 82 through 91 plot the mean value of $(I_p^{2D})^s$ obtained for various groups, namely 2,4,6 and 8 week NT and HT pigs, while inflating the circumflex artery in various states. From these figures we study if there is any relationship between the spatial variation of $(I_p^{2D})^c$ and the group to which the specimen belonged. As before, $(I_p^{2D})^c$ is obtained by approximating the actual deformation by (6.12) and determined using three markers. It could be seen from these figures that while the 4 week HT specimens have the least value of $(I_p^{2D})^s$, 6 week NT specimens have the largest value of $(I_p^{2D})^s$. Also, except for 2 week HT specimens the $(I_p^{2D})^s$ for the other HT specimens is smaller than or equal to the corresponding age matched NT specimens in passive state. This information could potentially provide insight about the changes in the underlying structure of the artery and/or its prestress distribution due to hypertension and/or aging.

F. Discussion

In constitutive modelling one is required to specify the Helmoltz potential and the prestresses and it is the aim of the experiments to determine the same. Here we designed experiments to determine the spatial variation of the prestresses and the material parameters in Helmoltz potential. We hypothesized that the prestresses and material parameters vary only radially. As described above, we could not get sufficient evidence to substantiate this hypothesis. Given the microstructure of the artery and its mechanical response being dependent on the vascular smooth muscle

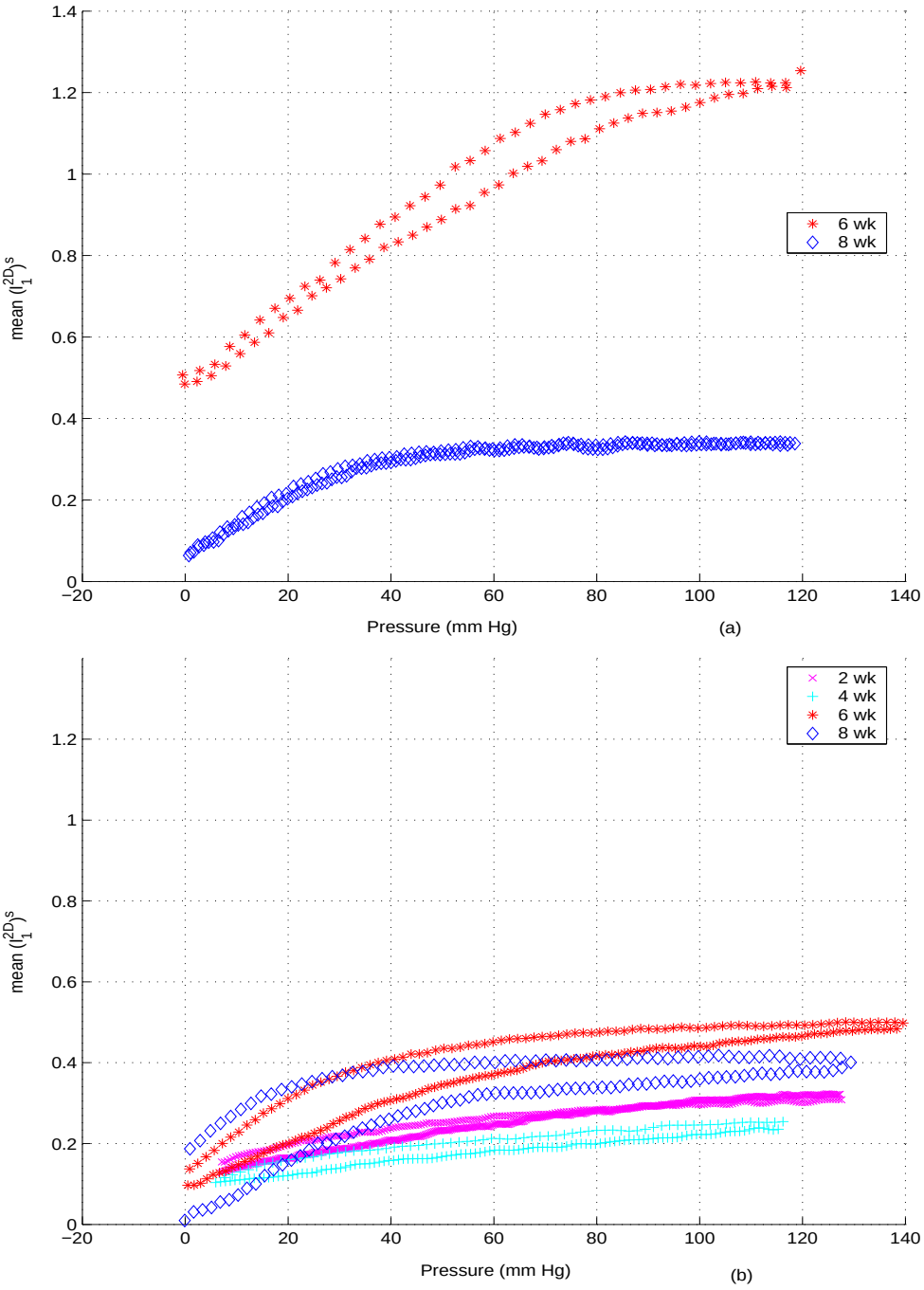

Fig. 82. Plot of mean of $(I_1^{2D})^s$ obtained for various (a) NT (b) HT pigs, while inflating the circumflex artery in native state at constant length, L_o.

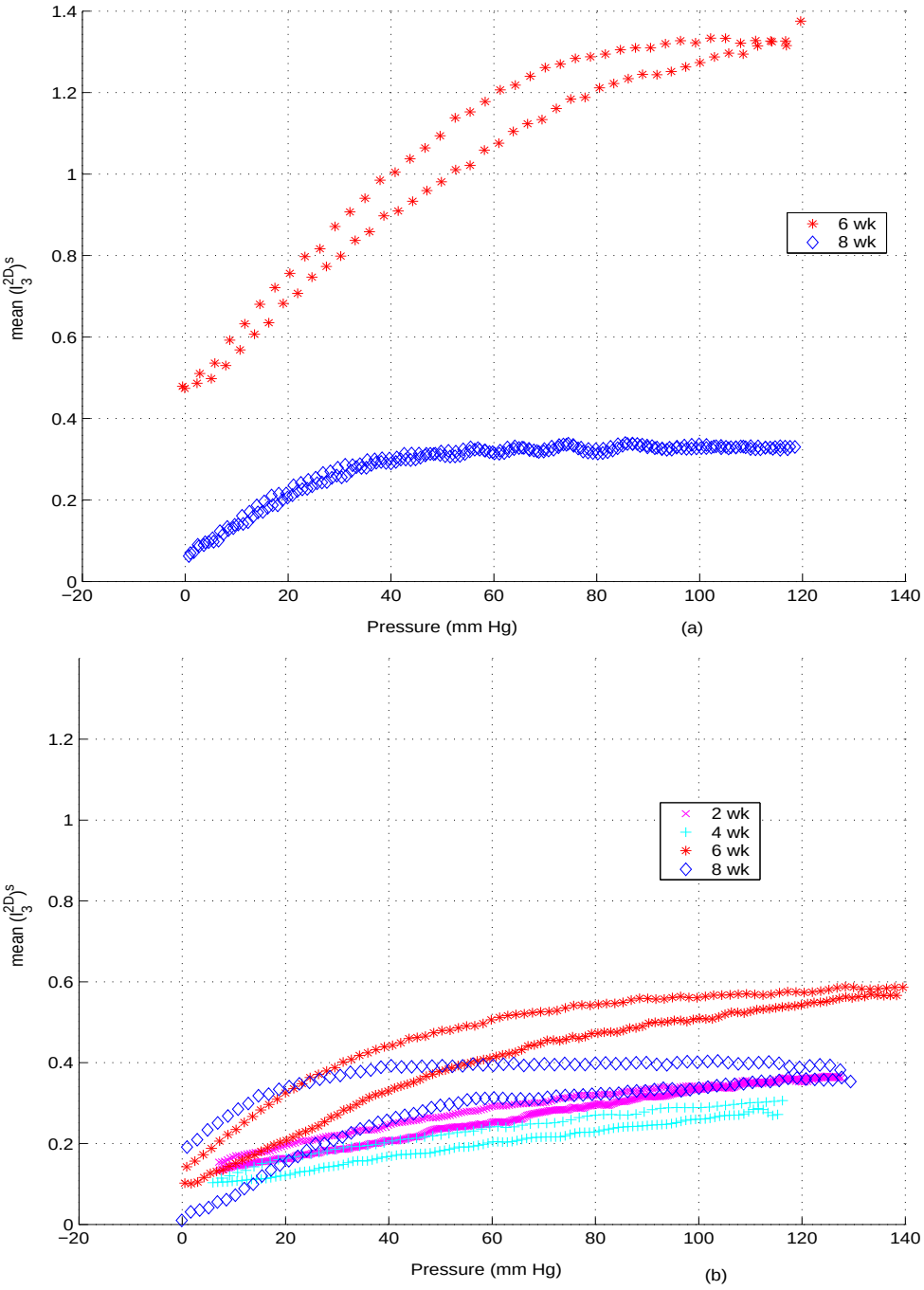

Fig. 83. Plot of mean of $(I_3^{2D})^s$ obtained for various (a) NT (b) HT pigs, while inflating the circumflex artery in native state at constant length, L_o.

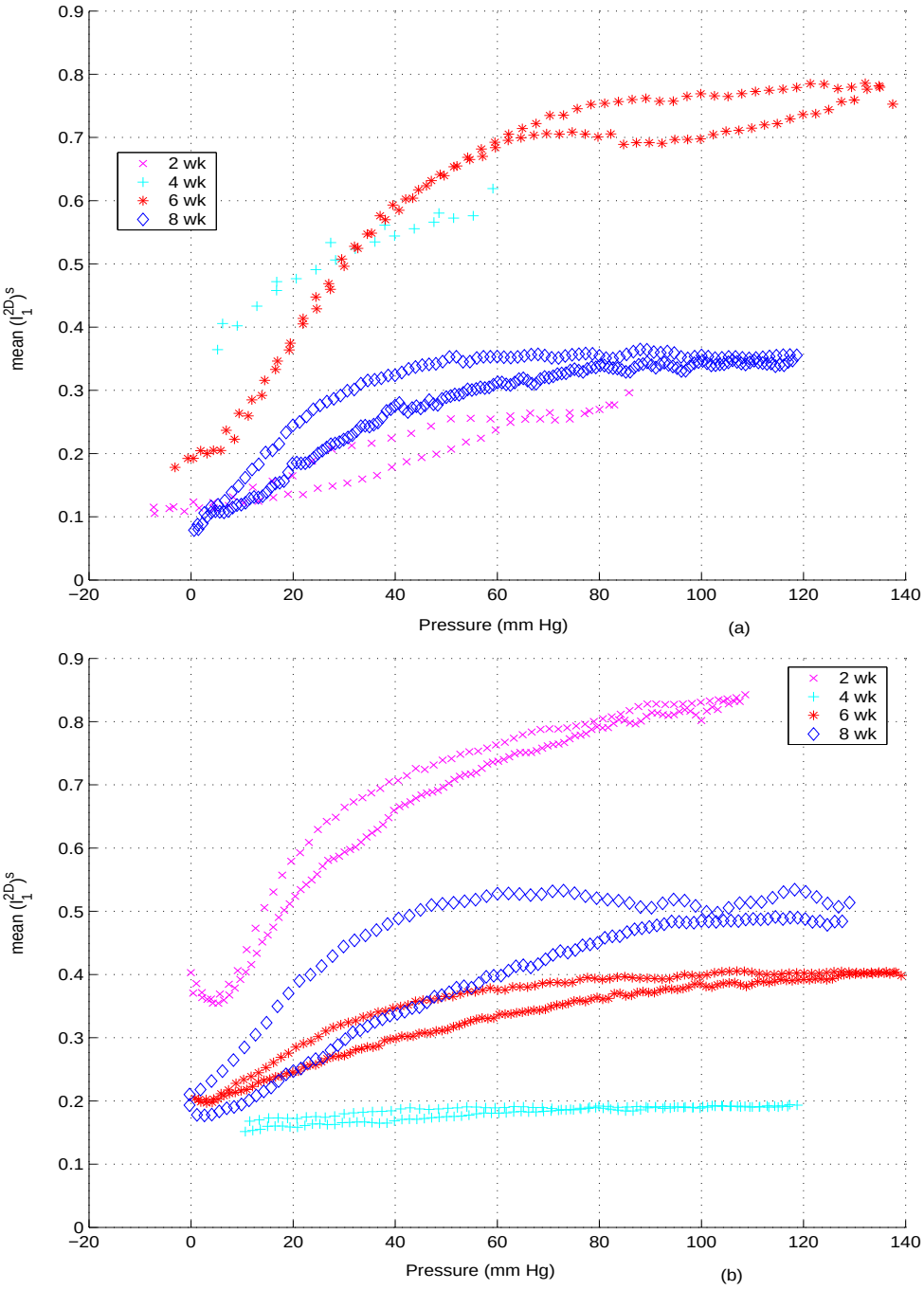

Fig. 84. Plot of mean of $(I_1^{2D})^s$ obtained for various (a) NT (b) HT pigs, while inflating the circumflex artery in activated state at constant length, L_o.

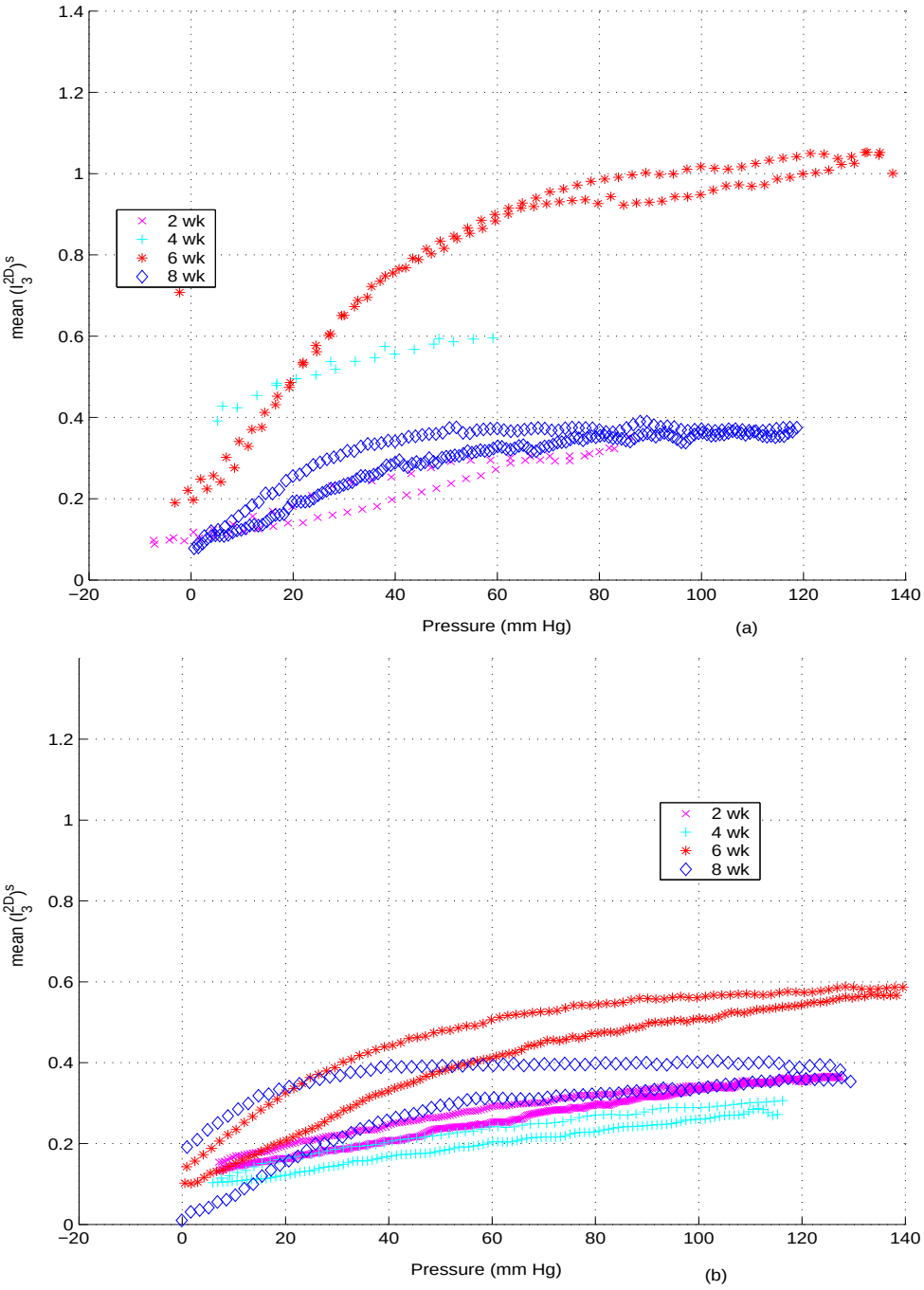

Fig. 85. Plot of mean of $(I_3^{2D})^s$ obtained for various (a) NT (b) HT pigs, while inflating the circumflex artery in activated state at constant length, L_o.

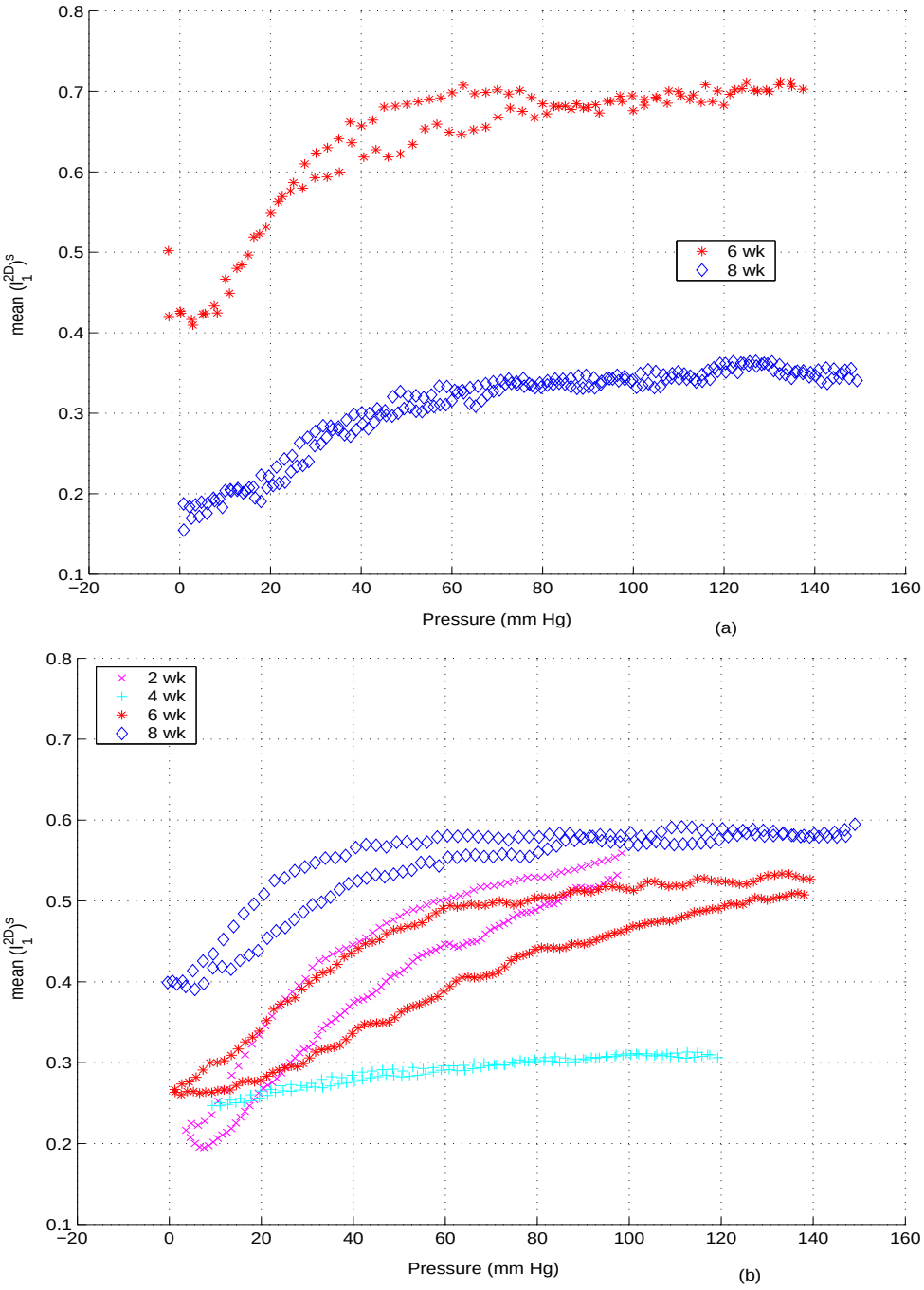

Fig. 86. Plot of mean of $(I_1^{2D})^s$ obtained for various (a) NT (b) HT pigs, while inflating the circumflex artery in activated state at constant length, $1.1L_o$.

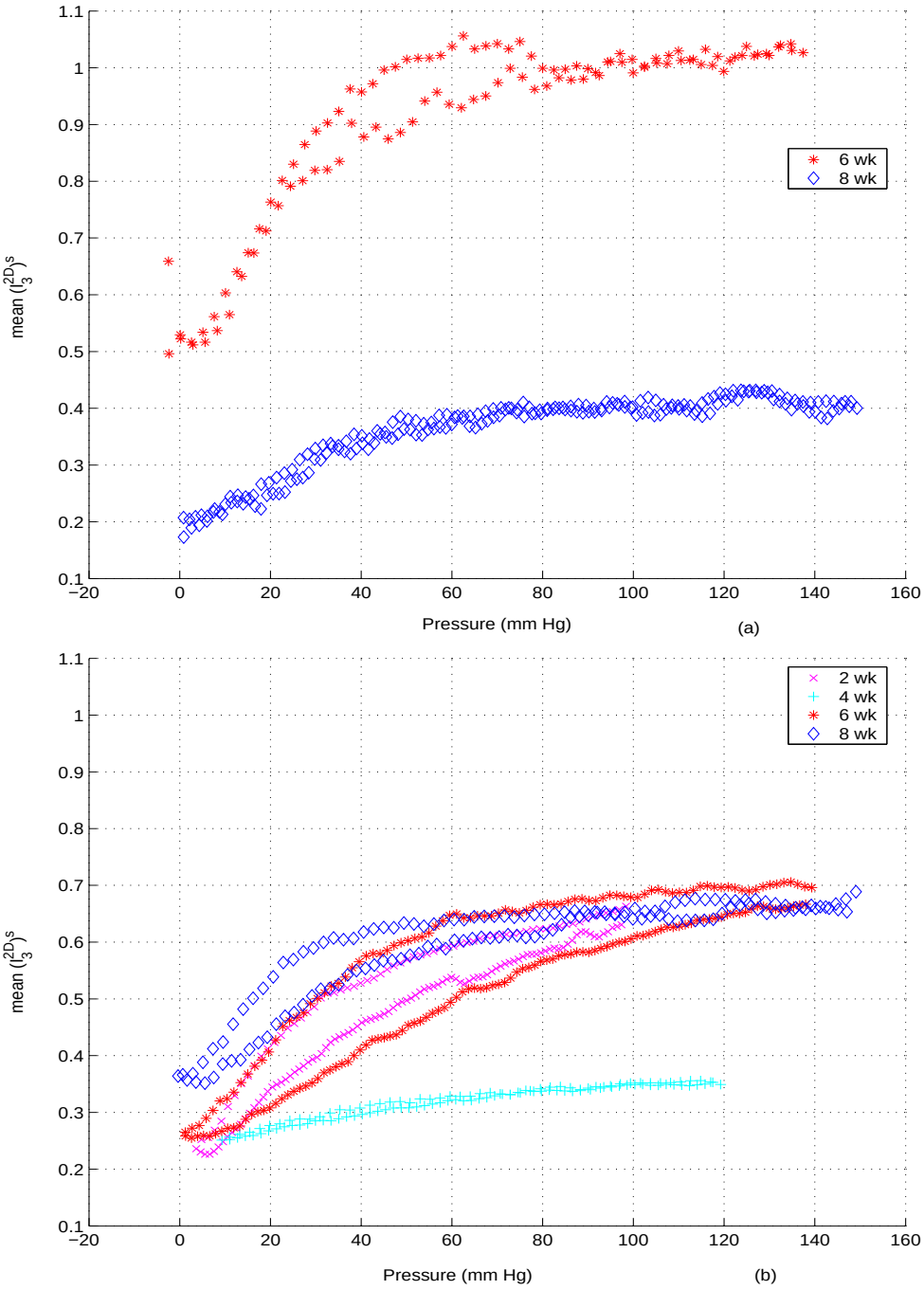

Fig. 87. Plot of mean of $(I_3^{2D})^s$ obtained for various (a) NT (b) HT pigs, while inflating the circumflex artery in activated state at constant length, $1.1L_o$.

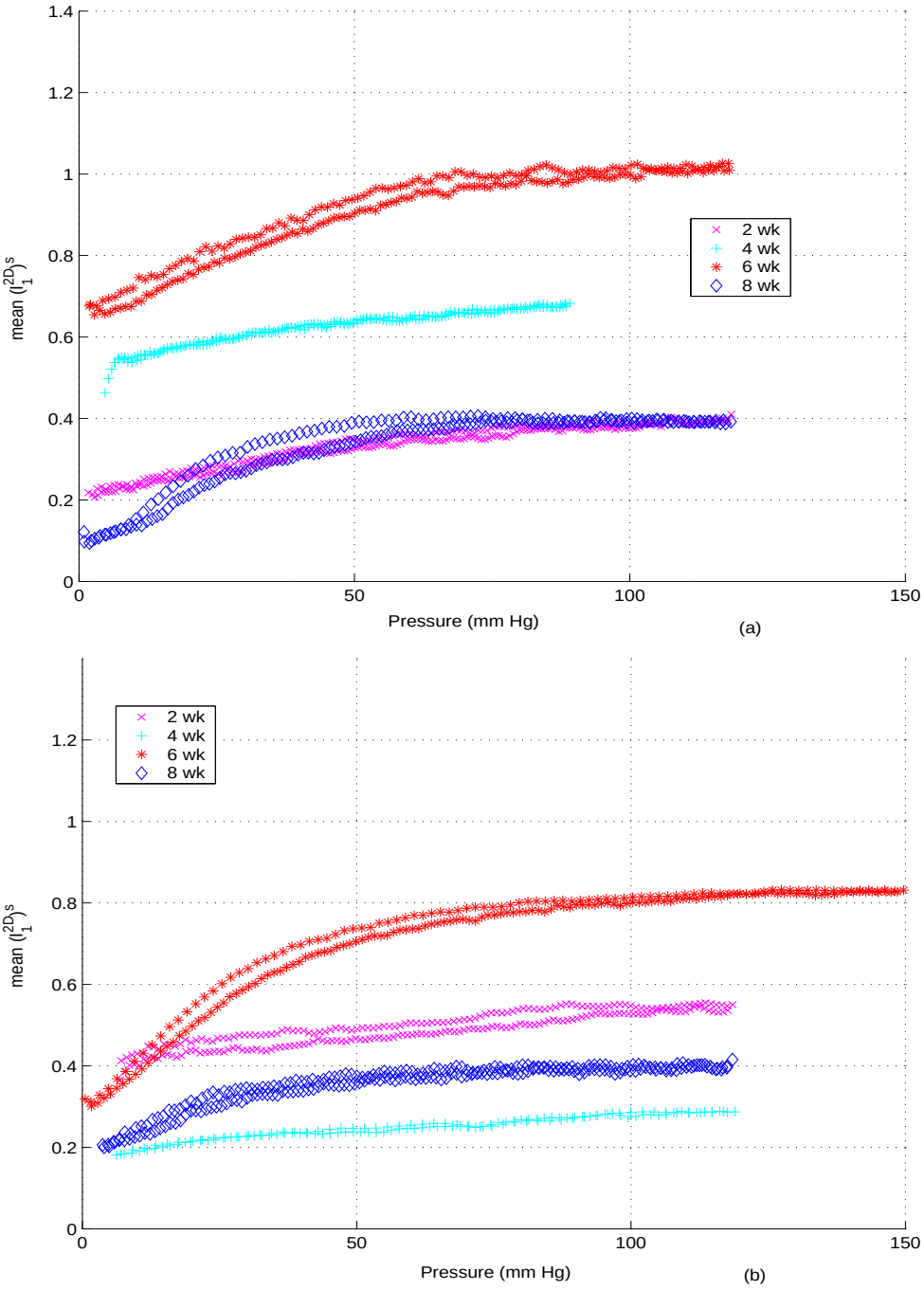

Fig. 88. Plot of mean of $(I_1^{2D})^s$ obtained for various (a) NT (b) HT pigs, while inflating the circumflex artery in passive state at constant length, L_o.

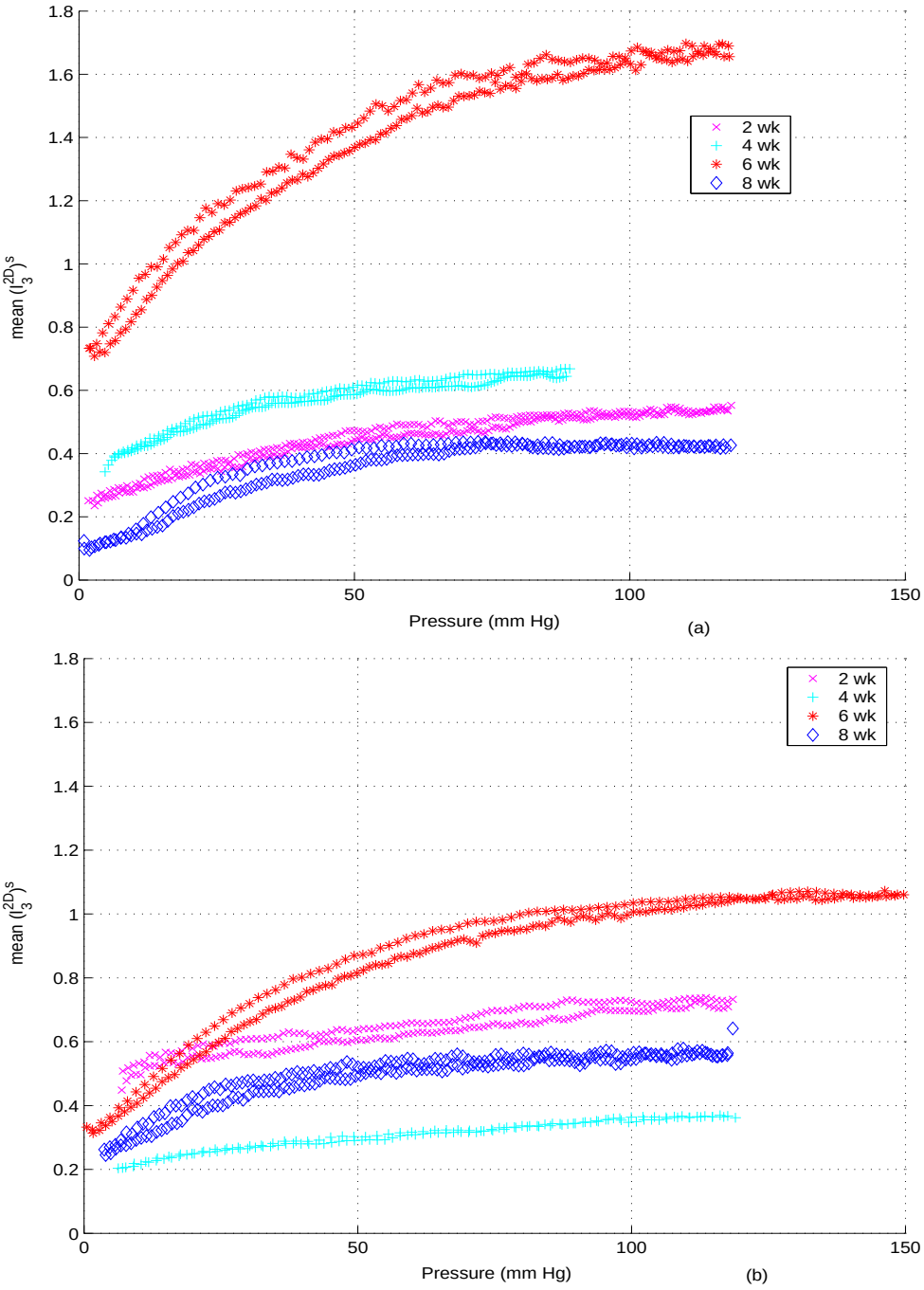

Fig. 89. Plot of mean of $(I_3^{2D})^s$ obtained for various (a) NT (b) HT pigs, while inflating the circumflex artery in passive state at constant length, L_o.

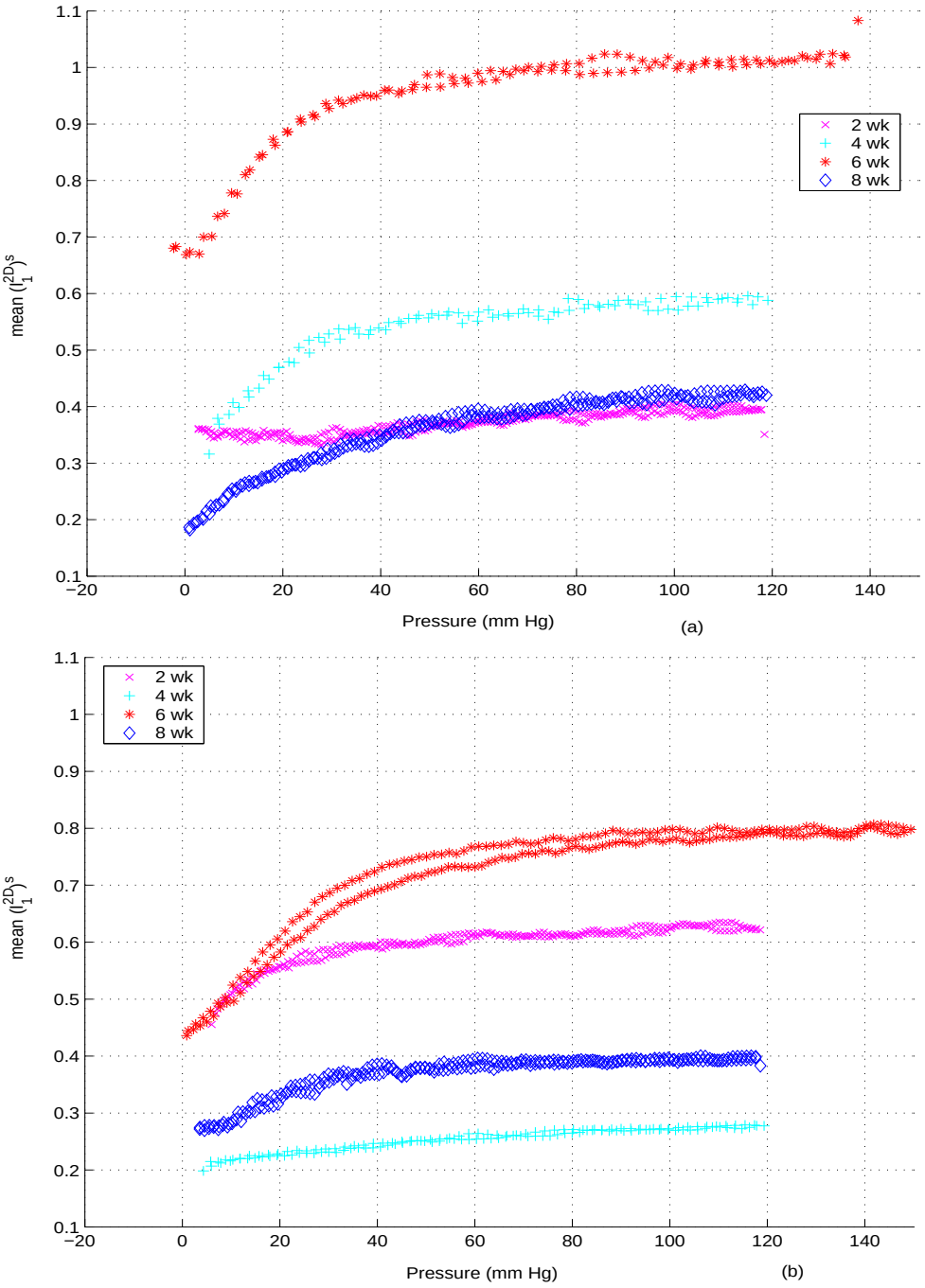

Fig. 90. Plot of mean of $(I_1^{2D})^s$ obtained for various (a) NT (b) HT pigs, while inflating the circumflex artery in passive state at constant length, $1.1L_o$.

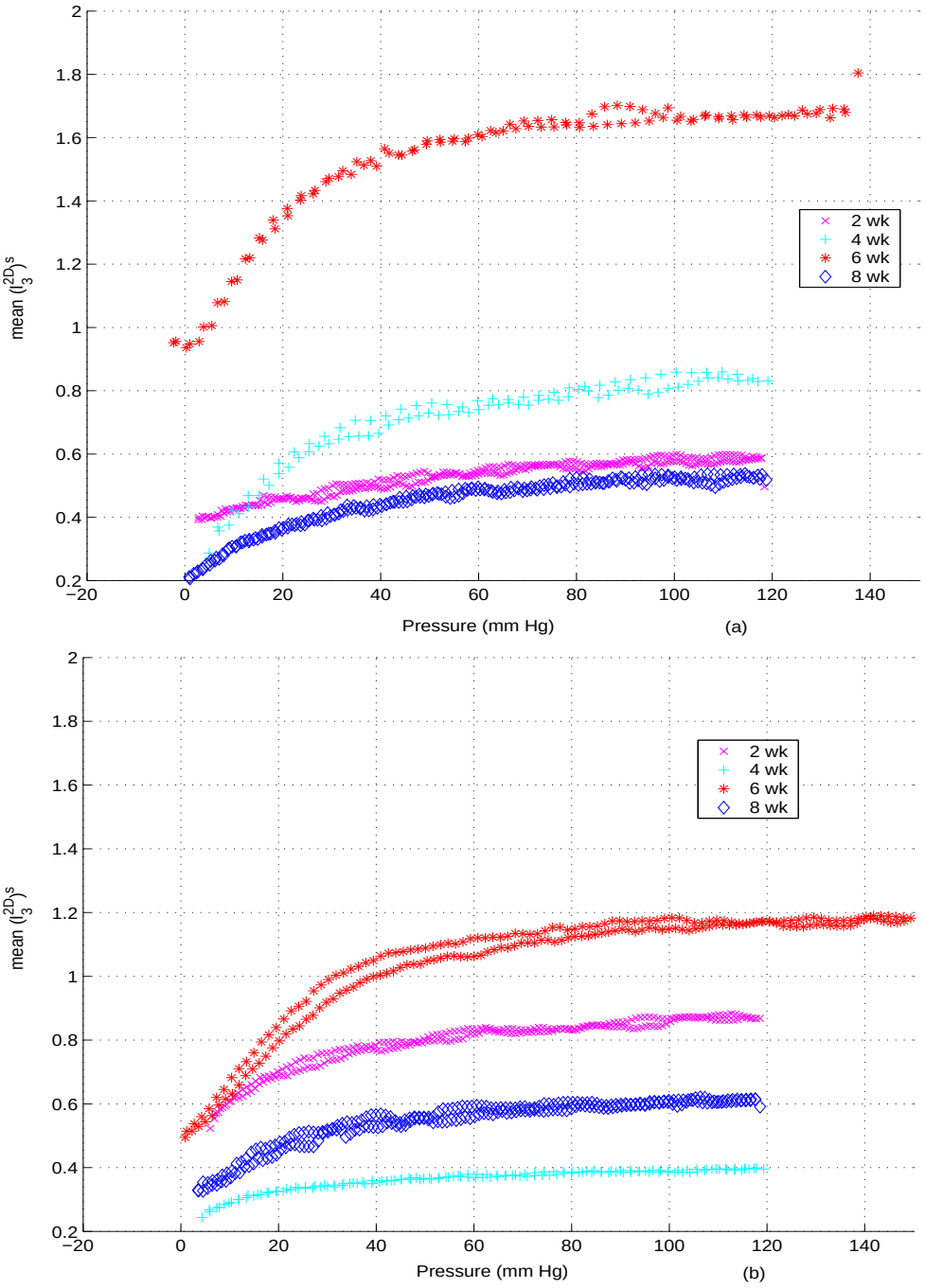

Fig. 91. Plot of mean of $(I_3^{2D})^s$ obtained for various (a) NT (b) HT pigs, while inflating the circumflex artery in passive state at constant length, $1.1L_o$.

tone, this is to be expected. Further, Pao et al.[85] has shown that in vivo, the coronary artery tree bends and twists, in keeping with the changes in the size and shape of the heart in the course of a heart beat. Here too we observed bending and twisting of the circumflex artery while inflating in vitro. Unfortunately, the 2D tracking system could not capture this motion accurately, due to the out of plane motions of the markers being tracked. Hence, it remains an open question as to what causes this bending and twisting of the circumflex artery when subjected to inflation. Whatever the cause may be, this twisting moment is implicated in the development of atherosclerotic lesions [30]. Hence, it is necessary to investigate this nexus between the structure of the circumflex artery and its deformation when subject to inflation. Also, it remains to be investigated whether the other muscular and elastic arteries deform as given by (6.1) while inflating.

It is pertinent to note that Han and Fung [86] while investigating the residual strain in porcine aorta by introducing a radial cut on a transverse section, also report circumferential variation of the components of the residual strain apart from the radial variation (see their figure 3), locally, that is for small variations in the circumferential and radial location. However, globally the circumferential variation was not statistically significant[12]. Here the reported variations are local and we do not have information about global variations, which may prove valuable.

The value of the invariants obtained for a given pressure is less when compared with those reported in the literature ([33],[77]). For example, according to the data in the literature a pressure of 120 mm Hg results in the outer diameter of the vessel

[12]This just means that the deformation is a non-linear function of the radial location contrary to the assumption made while computing the strain from the location of the markers in the current and reference configuration. In fact, theoretically determined deformation field, as reported by them, is a non-linear function of 'R', the radial location

increasing to 1.6 times its original value, yielding a value of 1.56 for both $I_1^{2D} - 2$ and $I_3^{2D} - 1$, assuming an axial stretch ratio of 1 and that the actual deformation is given by (6.1). In the present study, this value is exceeded by only 6 week NT specimens. The reason for this lower value can be determined only when the value of the invariants inferred from 3D tracking of the markers is available. Thus, when the deformation of the artery is given by (6.1), $I_1^{2D} - 2 = I_3^{2D} - 1 = (r_o/R_o)^2 - 1$, assuming $\lambda = 1$. This equality of the principal invariants seem to prevail in the observed deformation as well, see figures 72 through 75 and figures 78 and 79.

As seen in figure 70 the specimen to specimen variation, even when they belonged to the same group, is large in comparison to those reported in the literature based on the measurement of the outer diameter. This may be because of the uncertainty in the estimated value of I_p^{2D}, due to the spatial variation of the invariants. This specimen to specimen variation could not be attributed to differences in the configuration used as reference, namely the length, L_o at which the artery was held fixed, because an axial extension of $1.1L_o$ did not produce a significant difference in the response of the artery to inflation and the arteries were rarely stretched more than ten percent from their no load length to obtain L_o.

For the above reasons, it is essential that the experiments concerning the inflation of the arteries be carried out by tracking the markers in 3D.

Finally, we like to caution that requiring nearly the same value of the radial component of the normal stress to engender a given outer diameter or principal invariants does not mean that the constitutive relation for the two sets being compared is same, unless the geometry of the corresponding vessels is also the same. Thus, even though the response of the 8 week HT and NT vessels are the same, since their geometries are likely to be different with the HT specimens being thicker, it does not mean that their constitutive relations are the same. Similarly, requiring a different

pressure at the inner surface to engender a different outer diameter or principal invariants does not mean that their constitutive relations are different; it could be just a consequence of differing geometries. Hence, there is a dire need to fit these data to a robust 3D constitutive relation that accounts for vascular smooth muscle tone so that we could study the evolution of the prestress fields and/or that of the material with the duration of hypertension.

Here we present no data corresponding to axial extension at constant pressure or the variation of the axial load while inflating because the measured axial load was sensitive to small perturbations of the experimental setup. Also, since by the end of 2003, it was satisfactorily established that the deformation of the artery did not correspond to (6.1) and 2D tracking of the markers insufficient, only protocols 8a to 8c were performed on specimens tested after 2003.

CHAPTER VII

CONCLUSION

The aim of this work was to develop a framework to study the mechanical response of prestressed bodies subjected to finite elastic deformations. The prestresses in many cases are believed to arise from misfit of subparts of the body and hence the main issue with these bodies is that there exist no single placer for the entire body in the Euclidean space in which it is free of stresses. Consequently, one should either model the processes that cause misfit and subsequently infer the prestress or take cognizance of the fact that the configuration used as reference is not stress free, contrary to the assumption made while obtaining a representation for stress and constitutively prescribe the prestresses. That is, constitutive prescriptions have to be made about the misfits or the prestresses. Here we prescribe the prestresses. There are many reasons to take this viewpoint. Firstly, while there are no restrictions on how misfits can arise, the prestress fields have to satisfy the balance of linear momentum under static conditions and traction free boundary conditions, providing valuable restrictions on the constitutive prescription. Secondly, almost always the experimentalist has access only to stressed configurations due to the ever present gravity and atmospheric pressure (unless the experiments are conducted in vacuum) apart from the prestresses. Thirdly, it is difficult to obtain the prestress field from the misfits except in idealized cases. Hence, we sought a representation for stress from a stressed configuration as reference, in terms of the stress in the reference configuration and gradient of motion, with the motion being inferred from this stressed reference configuration. We accomplished this by recognizing that the value of stress in the current configuration is independent of the choice of the reference configuration. However, we require the existence of a piecewise smooth motion field from the stress free configuration to the stressed

reference configuration. This places some additional restrictions on the admissible prestress fields. But we are unable to identify these restrictions. Consequently, we assumed that all the prestress fields prescribed here satisfied these requirements. This needs to be verified. Further, here we do not concern ourselves with the process that resulted in the development of the prestresses but just acknowledge their presence by constitutively prescribing them. This standpoint was adopted because the process that cause the development of the prestresses is poorly understood in some cases, as in biological bodies. Moreover, we study only processes in which the prestresses do not change and call such a process elastic. The framework needs to be generalized on this count.

However, the above study helped identify four issues. First, it helped identify restrictions on the constitutive relations for stress so that a hydrostatic state of stress does not result in extension along one direction and compression along the other two or vice versa. That is, we identified restrictions so that whenever the algebraic multiplicity of the eigen values of stress is three, the algebraic multiplicity of the eigen values of left Cauchy-Green stretch tensor is also three. Second, we find that when we linearize the representation of the stress from a stressed configuration, the apparent value[1] of the shear modulus depends on the stress in the reference configuration. While there exist scenarios where the value of the shear modulus may not change significantly, they do change. In fact, we show that the stressed body can shear soften or harden depending on the value of certain parameters which are not visible within the framework of classical linearized elasticity. Thus, models for prestresses within the context of linearized elasticity, that appeal to superposition of the prestresses with

[1]That is the apparent shear modulus, $\mu_a = \mu - \mu_e$, where μ is the shear modulus in a stress free configuration, μ_e is the correction to the shear modulus whose value depends on the stress in the reference configuration, among other variables.

the stresses due to service loads can under estimate or over estimate the total stresses. The next observation concerns material properties, that is certain constants in the constitutive equation like the shear modulus, μ_1 and the exponent, μ_3 in the Blatz-Ko constitutive relation, whose value depends only on chemical composition of the body. Two bodies identical in geometry and made up of the same material, chemically, but having different prestress fields may respond differently i.e., say, the magnitude of the boundary displacement to the application of the same boundary traction is different, but the value of these material parameters are preserved[2]. The issue here is to find the appropriate metrics that is experimentally measurable and reflects the invariance of these material parameters. Of course, when one fits a constitutive relation to any of the experimentally measured quantities this invariance would be revealed. The last issue concerns with that of material symmetry. A deformation of the body is said to belong to its symmetry group, if the deformed and the initial configuration of the body are indistinguishable. Then, the issue is how to experimentally determine whether the two given configurations are distinguishable. Towards this, we showed that using the traction required to engender a given uniaxial stretch to identify if the rotated and initial configuration of the body are distinguishable to be unsatisfactory. Wineman et. al. [26] showed that when an isotropic body is uniaxially or equi-biaxially stretched then the symmetry group for the deformed configuration contains non-orthogonal but unimodular elements. That is two micro-structures not related by rigid body rotation can be in the same mechanical state. Hence, micro-structure also cannot be used to infer material symmetry for the body's mechanical response. Further, Hoger [63] showed that a prestressed body cannot be isotropic, in fact a body in a stressed state different from that of hydrostatic stresses has to be

[2]This is more transparent than in the case of linearized equations considered above.

anisotropic. Burghoff and Bohlen [87] have shown that the directional properties of 68-32 brass strip depends on the amount of cold-work. From which we can infer that the prestresses developed during inelastic deformation contributes to the directional properties of the brass strip. Hence, we postulate that the state of stress in a given configuration determines the material symmetry in that configuration when attention is restricted to the mechanical response of the body.

It was then argued that for boundary conditions, both the traction and the displacement of the boundary should be prescribed for the entire boundary when the constitutive relations are not known or the form of the deformation is not known. However, in stimulations like the present study, when assumptions are made about both the constitutive relation and the form of the deformation, a subset of the above boundary conditions suffices. But as was shown in Saravanan [70] different forms of the deformation could satisfy the limited boundary condition that is prescribed. To elaborate, while studying the homogeneous deformation of homogeneous, isotropic bodies, it may suffice to prescribe the boundary traction for the boundary conditions. However, as it was shown here (section F in chapter II) and in Saravanan [70] that different forms of the deformation, which do not differ just by a rigid body rotation, can satisfy the limited boundary conditions.

We then outlined a constructive proof for showing the existence of deformation of a certain form for a given constitutive relation when both the deformation, $\widetilde{\boldsymbol{\chi}}$ and its gradient, $\mathbf{H}_t$ are known at the same point. We illustrated the working of the constructive proof through a number of examples. In the process, we studied inflation of a spherical shell and inflation, extension and torsion of an annular right circular cylinder in some detail. It transpires from these studies that while the local measures - like the stress - differ significantly for the stress free and a prestressed body, global measures - like the axial load required to engender a given stretch differs

insignificantly, for reasonable magnitudes and type of the prestresses studied here. Even the deformation and its gradient differ insignificantly, making it difficult to infer the prestress fields from the mechanical experiments conducted on intact bodies.

Finally, we sought to apply the above gained knowledge to understand the mechanics of circumflex arteries. Here we investigated whether the deformation of the circumflex artery subjected to inflation at constant length corresponds to $r = r(R)$, $\theta = \Theta$, $z = \lambda Z$, with the symbols having their usual meaning. We found this not to be the case. In fact, the artery bends and twists when inflated. Since, in vivo the artery bends and twists along with the deforming heart this is at the least surprising. It would have been interesting to investigate the nexus between the prestress distribution or the inhomogeneity that causes this peculiar deformation of the artery when inflated. However, the experimental system used could track the markers only along two dimensions which we find to be insufficient to capture the actual deformation. Therefore, there is a need to design experimental system that could track the markers in 3D so that the cause of bending and twisting of the artery can be investigated. This is important especially since, the twisting of the artery is implicated in the development of atherosclerotic lesions [30].

Notwithstanding the above limitation, the general characteristics of the response of the artery subjected to inflation at constant length were preserved. Hence, comparisons were made between the response of the arteries at various vascular smooth muscle tone and stretch ratio, λ as well as between hypertensive and normotensive specimens, using statistical methods. We find that 4 and 6 weeks into the study, the value of the principal invariants for a given radial component of the normal stress at the inner surface of normotensive specimens are greater than that of hypertensive specimens in passive state. On the other hand there were no significant differences between the hypertensive and normotensive specimens 2 or 8 weeks into the study.

Other comparisons also did not result in significant differences.

Thus, this study made some strides towards understanding the response of pre-stressed and inhomogeneous bodies subjected to an idealized process called elastic.

REFERENCES

[1] Rivlin, R.S. Large elastic deformations of isotropic materials - VI further results in the theory of torsion, shear and flexure. *Philosophical Transactions of the Royal Society of London, A*, 242, 173–195 (1949).

[2] Gent, A.N. and Rivlin, R.S. Experiments on the mechanics of rubber I. Eversion of tube. *Proceedings of the Physical Society of London, B*, 65, 118–121 (1952).

[3] Withers, P.J. and Bhadesia, H.K.D.H. Residual stress part 2 - nature and origins. *Material Science and Technology*, 17, 366–375 (2001).

[4] Fung, Y.C. *Biomechanics: Motion, Flow, Stress and Growth.* Springer-Verlag, New York, 1990.

[5] Humphrey, J.D. *Cardiovascular Solid Mechanics: Cells, Tissues, and Organs.* Springer, New York, 2002.

[6] Skalak, R., Zargaryan, S., Jain, R.K., Netti, P.A. and Hoger A. Compatibility and the genesis of residual stress by volumetric growth. *Journal of Mathematical Biology*, 34, 889–913 (1995).

[7] Rodriguez, E., Hoger, A., and McCulloch, A.D. Stress-dependent finite growth in soft elastic tissues. *Journal of Biomechanics*, 27(4), 455–467 (1994).

[8] Love, A.E.H. *A Treatise on the Mathematical Theory of Elasticity.* Dover Publications, New York, 1944.

[9] Withers, P.J. and Bhadesia, H.K.D.H. Residual stress part 1 - measurement and techniques. *Material Science and Technology*, 17, 355–365 (2001).

[10] Hahn, H.T. Residual stress in polymer matrix composite laminates. *Journal of Composite Materials*, 10, 266–278 (1976).

[11] Krawietz, R., Bobeth, M., Pompe, W., Wersing, W., and Winkler, B. Modelling of residual stress development in electronic materials and devices. *Advanced Engineering Materials*, 4(8), 565–571 (2002).

[12] Nagayoshi, H. Morinaka, K., Kamisako, K., Shimada, T. and Tarui, Y. Residual stress of a $si_{1-x}n_x : h$ films prepared by afterglow plasma chemical vapor deposition techniques. *Japanese Journal of Applied Physics*, 31(part 2), L867–L869 (1992).

[13] Fung, Y.C. and Liu, S.Q. Change of residual strains in arteries due to hypertrophy caused by aortic constriction. *Circulation Research*, 65, 1340–1349 (1989).

[14] Smith, G.F. and Rivlin, R.S. Photoelasticity with finite deformation. *Zeitschrift fur Angewandte Mathematik und Physik*, 21, 101–115 (1970).

[15] Boulanger, P. and Hayes, M. Some remarks on photoelasticity. *Archive for Rational Mechanics and Analysis*, 116, 199–222 (1991).

[16] Ieşan, D. *Prestressed Bodies*, volume 195 of *Pitman Research Notes in Mathematics Series*. Longman Scientific and Technical, Essex, UK, 1989.

[17] Lu, J., editor *Handbook of Measurement of Residual Stresses,* Society for Experimental Mechanics, Inc., New York, 1996.

[18] Chuong, C.J. and Fung, Y.C. On residual stress in arteries. *Journal of Biomechanical Engineering*, 108, 189–192 (1986).

[19] Vossoughi, J., Hedjazi, Z., and Borris, F.S. Intimal residual stress and strain in large arteries. *ASME Advances in Bioengineering*, 434–437 (1993).

[20] Greenwald, S.E., Moore, J.E., Rachev, A., Kane, T.P.C., and Meister, J.J. Experimental investigation of the distribution of residual strains in the artery wall. *Journal of Biomechanical Engineering*, 119, 438–444 (1997).

[21] Green, A.E., Rivlin, R.S., and Shield, R.T. General theory of small elastic deformations superposed on finite elastic deformations. *Proceedings of the Royal Society of London, A*, 211, 128–154 (1952).

[22] Truesdell, C. and Noll, W. *The Nonlinear Field Theories*, in *Handbuch der Physik, Volume III/3*. Springer-Verlag, Berlin, 1965.

[23] Biot, M.A. *Mechanics of Incremental Deformations*. John Wiley & Sons, New York, 1965.

[24] Johnson, B.E. and Hoger, A. The use of a virtual configuration in formulating constitutive equations for residually stresses elastic materials. *Journal of Elasticity*, 41, 177–213 (1995).

[25] Hoger, A. Virtual configurations and constitutive equations for residually stressed bodies with material symmetry. *Journal of Elasticity*, 48, 125–146 (1997).

[26] Wineman, A.S., Rajagopal, K.R., and Negahban, M. Changes in material symmetry associated with deformation - uniaxial extension. *International Journal of Engineering Science*, 26(12), 1307–1318 (1988).

[27] Denis, S., Archambault, P., Gautier, E., Simon, A., and Beck, G. Prediction of residual stress and distortion of ferrous and non-ferrous metals: current status and future developments. *Journal of Materials Engineering and Performance*, 11(1), 92–102 (2002).

[28] Humphrey, J.D. Continuum biomechanics of soft biological tissues. *Proceedings of the Royal Society of London Series A*, 459, 3–46 (2003).

[29] Holzapfel, G.A., Gasser, T.C., and Ogden, R.W. A new constitutive framework for arterial wall mechanics and a comparative study of material models. *Journal of Elasticity*, 61, 1–48 (2000).

[30] Osol, G. Mechanotransduction by vascular smooth muscle. *Journal of Vascular Research*, 32, 275–292 (1995).

[31] Driessen, N.J.B, Wilson, W., Bouten, C.V.C, and Baaijens, F.P.T. A computational model for collagen fiber remodelling in the arterial wall. *Journal of Theoretical Biology*, 226, 53–64 (2004).

[32] Roy, C.S. The elastic properties of the arterial wall. *Philosophical Transactions of the Royal Society of London Series B*, 99, 1–31 (1880).

[33] Cox, R.H. Regional variation of series elasticity in canine arterial smooth muscle. *American Journal of Physiology*, 234(5), H542–H551 (1978).

[34] Cox, R.H. Alterations in active and passive mechanics of rat carotid artery with experimental hypertension. *American Journal of Physiology*, 237(5), H597–H605 (1979).

[35] Cox, R.H. Comparison of arterial wall mechanics in normotensive and spontaneously hypertensive rats. *American Journal of Physiology*, 237(2), H159–H167 (1979).

[36] Zulliger, M.A., Kwak, T.M.R., Tsapikouni, T., and Stergiopulos, N. Effects of longitudinal stretch on VSM tone and distensibility of muscular conduit arter-

ies. *American Journal of Heart and Circulation Physiology*, 283, H2599–H2605 (2002).

[37] Fridez, P., Makino, A., Miyazaki, H., Meister, J.J., Hayashi, K., and Stergiopulos, N. Short-term biomechanical adaptation of the rat carotid to acute hypertension: Contribution of smooth muscle. *Annals of Biomedical Engineering*, 29, 26–34 (2001).

[38] Fridez, P., Makino, A., Kadoi, D., Miyazaki, M., Meister, J. J., Hayashi, K., and Stergiopulos, N. Adaptation of conduit artery vascular smooth muscle tone to induced hypertension. *Annals of Biomedical Engineering*, 30, 905–916 (2002).

[39] Fridez, P., Zulliger, M., Bobard, F., Montorzi, G., Miyazaki, H., Hayashi, K., and Stergiopulos, N. Geometrical, functional, and histomorphometric adaptation of rat carotid artery in induced hypertension. *Journal of Biomechanics*, 36, 671–680 (2003).

[40] Fridez, P. *The role of vascular smooth muscle in biomechanical adaptation of the arterial wall to induced hypertension.* PhD thesis, Swiss Federal Institute of Technology, Lausanne, 2000.

[41] Matsumoto, T. and Hayashi, K. Stress and strain distribution in hypertensive and normotensive rat aorta considering residual strain. *Journal of Biomechanical Engineering*, 118, 62–73 (1996).

[42] Zeller, P.J. and Skalak, T.C. Contribution of individual structural components in determining the zero-stress state in small arteries. *Journal of Vascular Research*, 35, 8–17 (1998).

[43] Vito, R.P. and Dixon, S.A. Blood vessel constitutive models 1995-2002. *Annual Review of Biomedical Engineering*, 5, 413–439 (2003).

[44] Humphrey, J.D. Mechanics of arterial wall: Review and directions. *Critical Review in Biomedical Engineering*, 23, 1–161 (1995).

[45] Holzapfel, G.A., Gasser, T.C., and Stadler, M. A structural model for the viscoelastic behavior of arterial walls: Continuum formulation and finite element analysis. *European Journal of Mechanics A/Solids*, 21, 441–463 (2002).

[46] Rachev, A. and Hayashi, K. Theoretical study of the effects of vascular smooth muscle contraction on strain and stress distribution in arteries. *Annals of Biomedical Engineering*, 27, 459–468 (1999).

[47] Zulliger, M.A., Rachev, A. and Stergiopulos, N. A constitutive formulation of arterial mechanics including vascular smooth muscle tone. *American Journal of Physiology*, 287, H1335–H1343 (2004).

[48] Von Maltzahn, W.W., Besdo, D., and Wiemer, W. Elastic properties of arteries: A nonlinear two layered approach. *Journal of Biomechanics*, 14, 389–397 (1981).

[49] Von Maltzahn, W.W., Warriyar, R.G., and Keitzer, W.F. Experimental measurements of elastic properties of media and adventitia of bovine carotid arteries. *Journal of Biomechanics*, 17, 839–847 (1984).

[50] Demiray, H. and Vito, R.P. A layered cylindrical shell model for an aorta. *International Journal for Engineering Sciences*, 29, 47–54 (1991).

[51] Zulliger, M.A., Fridez, P., Hayashi, K., and Stergiopulos, N. A strain energy function for arteries accounting for wall composition and structure. *Journal of Biomechanics*, 37, 989–1000 (2004).

[52] Olivetti, G.P., Anversa, P., Melissari, M., and Loud, A.V. Morphometry of medial hypertrophy in the rat thoracic aorta. *Laboratory Investigation*, 42, 559–565 (1980).

[53] Owens, G.K. and Reidy, M. Hyperelastic growth response of vascular smooth muscle cells following induction of acute hypertension in rats by aortic coarctation. *Circulation Research*, 51, 280–289 (1985).

[54] Liu, S.Q. and Fung, Y.C. Relationship between hypertension, hypertrophy and opening angle of zero-stress state of arteries following aortic coarctation. *Journal of Biomechanical Engineering*, 111, 325–335 (1989).

[55] Truesdell, C. and Rajagopal, K.R. *An Introduction to the Mechanics of Fluids*. Birkhäuser, Boston, 2000.

[56] Gurtin, M.E. *An Introduction to Continuum Mechanics*, volume 158 of *Mathematics in Science and Engineering*. Academic Press, San Diego, 1970.

[57] Halmos, P.R. *Finite Dimensional Vector Spaces*. Van Nostrand Company, Inc., New York, 1958.

[58] Kellogg, O.D. *Foundations of Potential Theory*. Verlag von Julius Springer, Berlin, 1929.

[59] Truesdell, C. *A First Course in Rational Continuum Mechanics*. Academic Press, New York, 1991.

[60] Ogden, R.W. *Non-linear Elastic Deformations*. Dover Publications, New York, 1997.

[61] Noll, W. A mathematical theory of the mechanical behavior of continuous media. *Archive for Rational Mechanics and Analysis*, 2, 197–226 (1958).

[62] Coleman, B.D. and Noll, W. Material symmetry and thermostatic inequalities in finite elastic deformations. *Archive for Rational Mechanics and Analysis*, 15, 87–111 (1964).

[63] Hoger, A. On the residual stress possible in an elastic body with material symmetry. *Archive for Rational Mechanics and Analysis*, 88, 271–290 (1985).

[64] Serrin, J. The derivation of stress-deformation relations for a stokesian fluid. *Journal of Mathematics and Mechanics*, 8(4), 459–469 (1959).

[65] Rivlin, R.S. and Ericksen, J.L. Stress deformation relation for isotropic materials. *Journal for Rational Mechanics and Analysis*, 4, 323–425 (1955).

[66] Blatz, P.J. and Ko, W.L. Application of finite elastic theory to the deformation of rubbery materials. *Transactions of the Society of Rheology*, VI, 223–251 (1962).

[67] Fung, Y.C. Elasticity of soft tissues in elongation. *American Journal of Physiology*, 213, 1532–1544 (1967).

[68] Beatty, M.F. Topics in finite elasticity: Hyperelasticity of rubber, elastomers, and biological tissues - with examples. *Applied Mechanics Review*, 40(12 Part 1), 1699–1733 (1987).

[69] Horgan, C.O. Remarks on the generalized Blatz-Ko constitutive model for a compressible nonlinearly elastic solid. *Journal of Elasticity*, 42, 165–176 (1996).

[70] Saravanan, U. *A study on the isothermal elastic response of inhomogeneous materials for certain classes of boundary value problems.* Master's thesis, Texas A&M University, College Station 2001.

[71] Saravanan, U. and Rajagopal, K.R. On the role of inhomogeneities in the deformation of elastic bodies. *Mathematics and Mechanics of Solids*, 8, 349–376 (2003).

[72] Saravanan, U. and Rajagopal, K.R. Inflation, extension, torsion and shearing of compressible, inhomogeneous annular cylinder. *Mathematics and Mechanics of Solids*, (in press).

[73] Hoger, A. On the determination of residual stress in an elastic body. *Journal of Elasticity*, 16, 303–324 (1986).

[74] Gurtin, M.E. *The Linear Theory of Elasticity,* in *Handbuch der Physik, Volume VIa/2*. Springer-Verlag, Berlin, 1972.

[75] Chung, D.T., Horgan, C.O., and Abeyratane, R. The finite deformation of internally pressurized hollow cylinders and spheres for a class of compressible elastic materials. *International Journal of Solids and Structures*, 22, 1557 (1986).

[76] Ericksen, J.L. Deformations possible in every compressible isotropic perfectly elastic material. *Journal of Mathematics and Physics*, 34, 126–128 (1955).

[77] Kang, T., Resar, J., and Humphrey, J.D. Heat induced changes in the mechanical behavior of passive coronary arteries. *Journal of Biomechanical Engineering*, 117, 86–93 (1995).

[78] Carmines, D.V., McElhaney, J.H., and Stack, R. A piecewise nonlinear elastic stress expression of human and pig coronary arteries tested in vitro. *Journal of Biomechanics*, 24, 899–906 (1991).

[79] Matsumoto, T., Tsuchida, M., and Sato, M. Change in intramural strain distribution in rat aorta due to smooth muscle contraction and relaxation. *American*

Journal of Physiology, 271, H1711–H1716 (1996).

[80] Ling, P., Taber, L.A., and Humphrey, J.D. Approach to quantify the mechanical behavior of the intact embryonic chick heart. *Annals of Biomedical Engineering*, 30, 636–645 (2002).

[81] Downs, J., Halperin, H.R., Humphrey, J.D., and Yin, F.C.P. An improved video based computer tracking system for soft biomaterial testing. *IEEE Transactions in Biomedical Engineering*, 37, 903–907 (1990).

[82] Fossum, T.W., Baltzer, W.I., Miller, M.W., Aguirre, M., Miller, M.W., Whitlock, D., Solter, P, Makarski, L.A., McDonald, M.M., An, M.Y., and Humphrey, J.D. A novel aortic coarctation model for studying hypertension in the pig. *Journal of Investigative Surgery*, 16, 35–44 (2003).

[83] Dowdy, S, Weardon, S, and Chilko, D. *Statistics for Research*, volume 1345 of *Wiley Series in Probability and Statistics*. John Wiley & Sons, New Jersey, 2004.

[84] Cox, R.H. Carotid artery mechanics and composition in renal and DOCA hypertension in the rat. *Cardiovascular Medicine*, 2, 761–766 (1977).

[85] Pao, Y.C., Lu, J.T., and Ritman, E.L. Bending and twisting of an in vivo coronary artery at a bifurcation. *Journal of Biomechanics*, 25(3), 287–295 (1992).

[86] Han, C.H. and Fung, Y.C. Direct measurement of transverse residual strains in aorta. *American Journal of Physiology*, 270, H750–H759 (1996).

[87] Burghoff, H.L. and Bohlen, E.C. Directional properties of 68-32 brass strip. *Transactions of AIME*, 147, 144–163 (1942).

[88] Rivlin, R.S. Large elastic deformations of isotropic materials ii. some uniqueness theorems for pure homogeneous deformations. *Philosophical Transactions of the Royal Society*, 240, 419–508 (1948).

[89] Rivlin, R.S. Stability of pure homogeneous deformations of an elastic cube under dead loading. *Quarterly of Applied Mathematics*, 32, 265–272 (1974).

[90] Rivlin, R.S. Some thoughts on material stability. In *Proceedings of the IUTAM Symposium on Finite Elasticity*, Lehigh University, 1982.

APPENDIX A

NON-UNIQUENESS OF SOLUTIONS FOR A COMPRESSIBLE BODY SUBJECTED TO HYDROSTATIC STRESSES

Rivlin ([88], [89], [90]) has shown that for an incompressible neo-hookean cube subjected to hydrostatic pressure there exist solutions other than, $\mathbf{B} = \mathbf{1}$. Here we examine if a compressible stress free body subjected to hydrostatic pressure, i.e., $\mathbf{T} = p\mathbf{1}$ admits solutions other than $\mathbf{B} = \lambda\mathbf{1}$, especially when p is given by (3.24). Since, we find that multiple solutions are possible for this sub-class of hydrostatic pressures, uniqueness is not ensured for the general hydrostatic pressure loading as well.

As shown in chapter II, one of the general representations for stress when a stress free configuration is used as reference is given by

$$\mathbf{T} = \alpha_0\mathbf{1} + \alpha_1\mathbf{B} + \alpha_2\mathbf{B}^{-1}. \tag{A.1}$$

Now, let λ_1, λ_2 and λ_3 be the eigen values of $\mathbf{B}$ and let $\mathbf{T} = p\mathbf{1}$. Let us choose a coordinate system that coincides with the eigen directions of $\mathbf{B}$. Then

$$p = \alpha_0 + \alpha_1\lambda_i + \alpha_2\frac{1}{\lambda_i}, \qquad \text{for} \qquad i = \{1, 2, 3\}, \tag{A.2}$$

which can be rearranged to obtain

$$[\lambda_1 - \lambda_2][\alpha_0 - p + \alpha_1(\lambda_1 + \lambda_2)] = 0, \tag{A.3}$$

$$[\lambda_1 - \lambda_3][\alpha_0 - p + \alpha_1(\lambda_1 + \lambda_3)] = 0, \tag{A.4}$$

$$\alpha_0 - p + \alpha_1\lambda_1 + \frac{\alpha_2}{\lambda_1} = 0, \tag{A.5}$$

The above equations can potentially have at least four different solutions. First, $\lambda_1 = \lambda_2 = \lambda_3 = \lambda$ and $(\alpha_0 - p)\lambda + \alpha_1\lambda^2 + \alpha_2 = 0$, must hold. Second, $\lambda_1 = \lambda_2 \neq \lambda_3$

and

$$\alpha_0 - p + \alpha_1(\lambda_1 + \lambda_3) = 0, \tag{A.6}$$

$$(\alpha_0 - p)\lambda_1 + \alpha_1\lambda_1^2 + \alpha_2 = 0, \tag{A.7}$$

must hold. The other two solutions are cyclic permutations of the above solution. It is possible that for a given α_i, there exist no solutions or many solutions in some other cases.

Here our aim is to find if there exist solution of the form $\mathbf{B} = \lambda\mathbf{1}$ when $\Delta = 0$. In this case, the hydrostatic pressure p has a special form

$$p = \begin{cases} \frac{1}{2\alpha_2}\left[\beta_2 \pm \sqrt{\left(\alpha_1^2 J_3^2 - \alpha_2^2 J_2\right)^2 + 4\alpha_2^3\left(2\alpha_1 - \frac{J_1}{J_3^2}\alpha_2\right)}\right] & \text{, when } \alpha_2 \neq 0, \\ \alpha_0 & \text{, when } \alpha_2 = 0. \end{cases}, \tag{A.8}$$

where $\beta_2 = 2\alpha_2\alpha_0 + \alpha_1^2 J_3^2 + J_2\alpha_2^2$, $\alpha_i = \overline{\alpha}_i(J_1, J_2, J_3)$.

First, let us consider the case when $\alpha_2 = 0$. Then, it follows from (A.8) and (A.5) that $\alpha_1 = 0$. Thus, in this case the value of principal invariants of $\mathbf{B}$ should be such that $\alpha_1 = 0$ and $\alpha_2 = 0$. Since, $\overline{\alpha}_i(J_1, J_2, J_3) = 0$ implies the principal invariants are not independent, it would happen only when the algebraic multiplicity of eigen values of $\mathbf{B}$ is two or three[3]. Also it is worthwhile to note that when $\alpha_2 = 0$ and $\Delta = 0$ then α_1 has to be zero. Thus, we see that if $\Delta = 0$ and $\alpha_2 = 0$ then $\mathbf{B} = \lambda\mathbf{1}$ or $\mathbf{B} = \lambda\mathbf{1} + \lambda_3\mathbf{e}\otimes\mathbf{e}$, where $\mathbf{e}$ is an eigen direction of $\mathbf{B}$, are possible solutions. For example, consider $\overline{\alpha}_1 = 3J_1 - (J_2J_3)^2$ and $\overline{\alpha}_2 = J_1J_2 - 9$ which yields $\alpha_1 = \alpha_2 = 0$ when $\mathbf{B} = \lambda\mathbf{1}$.

[3]Here we do not consider the trivial case for which $\overline{\alpha}_1 = \overline{\alpha}_2 = 0$ identically.

Next, we consider the case when $\alpha_1 = 0$. Noting that for this case

$$p = \begin{cases} \alpha_0 + \frac{\alpha_2}{2}\left[J_2 \pm \sqrt{J_2^2 - 4\frac{J_1}{J_3^2}}\right] & \text{, when } \alpha_2 \neq 0, \\ \alpha_0 & \text{, when } \alpha_2 = 0. \end{cases}, \tag{A.9}$$

there are three solutions for equations (A.3) and (A.4).

Case 1: $\alpha_2 = 0$ which then reduces to the case studied above.

Case 2: $\lambda_1 = \lambda_2 = \lambda_3 = \lambda$. However, for this case $J_2^2 - 4J_1/J_3^2 = -3/\lambda^2 < 0$ and hence the solution is not possible, as otherwise p would not be real. Note that this is not of concern when $\alpha_2 = 0$.

Case 3: $\left[J_2 \pm \sqrt{J_2^2 - 4\frac{J_1}{J_3^2}}\right] = 0$ which again is not possible since $J_1 > 0$.

Thus, as one would expect, this case yields a solution same as the case considered above.

Finally, we solve equations (A.3) through (A.5) given that $\alpha_2 \neq 0$ and $\alpha_1 \neq 0$. Then, there are four possible solutions.

Solution 1: $\lambda_1 = \lambda_2 = \lambda_3 = \lambda$, i.e., $\mathbf{B} = \lambda\mathbf{1}$ where λ is obtained by solving (A.5). It remains to be shown that there exist a solution for this equation. However, this can be studied only for specific constitutive relations.

Solution 2: $\lambda_2 = \lambda_1 \neq \lambda_3$. Then λ_3 and $\lambda\ (= \lambda_1)$ are such that $\alpha_0 - p + \alpha_1(\lambda + \lambda_3) = 0$ and (A.5) holds. Here our interest is in examining whether there exist a solution, $\lambda_3 \neq \lambda$ such that

$$\alpha_1[\lambda + \lambda_3] = \frac{1}{2\alpha_2}\left[\alpha_1^2 J_3^2 + J_2\alpha_2^2 \pm \sqrt{\left(\alpha_1^2 J_3^2 - \alpha_2^2 J_2\right)^2 + 4\alpha_2^3\left(2\alpha_1 - \frac{J_1}{J_3^2}\alpha_2\right)}\right], \tag{A.10}$$

$$\alpha_1\lambda + \frac{\alpha_2}{\lambda} = \frac{1}{2\alpha_2}\left[\alpha_1^2 J_3^2 + J_2\alpha_2^2 \pm \sqrt{\left(\alpha_1^2 J_3^2 - \alpha_2^2 J_2\right)^2 + 4\alpha_2^3\left(2\alpha_1 - \frac{J_1}{J_3^2}\alpha_2\right)}\right], \tag{A.11}$$

where $\alpha_i = \overline{\alpha}_i(J_1, J_2, J_3)$, $J_1 = 2\lambda + \lambda_3$, $J_2 = 2/\lambda + 1/\lambda_3$ and $J_3 = \lambda\sqrt{\lambda_3}$. Equating

equations (A.10) and (A.11) we obtain

$$\lambda_3 = \frac{\alpha_2}{\alpha_1 \lambda} = \frac{\mu}{\lambda}, \tag{A.12}$$

which on substituting in (A.11) we find that it is satisfied identically for any value of λ and μ. Thus, there exist solutions other than the classical $\mathbf{B} = \lambda\mathbf{1}$ when $\mathbf{T} = p\mathbf{1}$ and p is given by (A.8) whenever equation (A.12) has a solution for λ_3. There are examples for both; constitutive equations for which (A.12) has a solution and for which it doesn't. Consider the general Blatz-Ko model (2.94). While it admits solutions of the form $\lambda_1 = \lambda_2 \neq \lambda_3$ when $\mu_2 > 1$ or $\mu_2 < 0$, it doesn't when $0 < \mu_2 < 1$, since for this case the constant, μ $(= 1/\mu_2 - 1) < 0$.

Solution 3 and solution 4 are permutations of the above case, in which $\lambda_1 = \lambda_3 \neq \lambda_2$ and $\lambda_2 = \lambda_3 \neq \lambda_1$ respectively.

For physical reasons, solutions of the form $\mathbf{B} = \lambda\mathbf{1} + \lambda_3 \mathbf{e} \otimes \mathbf{e}$, are not desirable and hence we propose restrictions on the constitutive equation, as outlined in chapter III, which ensures that these solutions are not possible when $\Delta = 0$.

VITA

Saravanan Umakanthan was born on July, 25 1978, in Chennai, a city in the southern state of Tamil Nadu, in India. He completed his high school at Loyola Matriculation Higher Secondary School in April 1995. He received his Bachelor of Technology in civil engineering from the Indian Institute of technology, Madras in July 1999 and his Master of Science in mechanical engineering from Texas A&M University, College Station, in August 2001. The author may be contacted at 27, first cross street, united India colony, Kodambakkam, Tamil Nadu 600024 India and by email: saran@tamu.edu.